“CHANNELING THE GREEN DEAL FOR VENICE”
Action n. 2019-IT-TM-0096-S
CEF Connecting Europe Facility

TECHNICAL- METHODOLOGICAL REPORT

PHASE-1 ACTIVITIES

Activity		**Phase 1**
Task		Meteomarine and hydrogeological characterization of Venice Lagoon
Authors		Marco Guerrini Giorgio Fontolan Andrea Pedroncini, Project Manager
Dissemination Level		Restricted
Status		Final
Due date		
Document Date		11/05/2022
Version Number		1.0

LIST OF CONTENTS

APPENDICES

1 CONTENT

The final goal of the comprehensive set of undergoing activities is to quantify the impact along the Malamocco – Marghera Channel and surrounding areas induced by vessel transits in the Channel, to identify possible solutions aimed at minimizing the erosion processes that are now affecting the tidal flats surrounding the Channel, thus achieving sustainable navigation conditions.

To match this ambitious goal, following Public Tender procedures, the Contract was awarded by Port of Venice to a Consortium led by DHI S.r.l. and formed by DHI A/S, Force Technology, HS Marine S.r.l., Cetena S.p.A. and Around Water.

The present first document, after a brief overview of the methodological approach proposed by the Consortium and now under execution, will focus on the first set of activities; in particular, with reference to the "*Capitolato Tecnico*" the present document includes:

2. *Relazione tecnica metodologica finalizzata alla definizione dell'iter procedurale per lo sviluppo del servizio*
3. *Relazione tecnica di caratterizzazione climatica e idrogeologica del sito;*
4. *Relazione tecnica di caratterizzazione geotecnica del sito;*
5. *Relazione tecnica preliminare per la calibrazione dei parametri di simulazione idrodinamica.*

2 TECHNICAL REPORT ON THE METHODOLOGY FOR THE DEFINITION OF THE SERVICE DEVELOPMENT PROCESS (*RELAZIONE TECNICA METODOLOGICA FINALIZZATA ALLA DEFINIZIONE DELL'ITER PROCEDURALE PER LO SVILUPPO DEL SERVIZIO*)

2.1 Phase 1-HYD: Establishment of meteomarine conditions at lagoon scale

Although the main focus of the study is devoted to the achievement of a sustainable navigation along the Malamocco-Marghera Channel, it is of utmost importance, prior to implement navigation simulations and proper 3D hydrodynamic modelling of the Channel and surrounding areas response to passing vessels, to establish a robust characterization of meteomarine conditions in the Venice lagoon, that can form the basis for the next steps.

In this regard, despite the numerous measurement stations present in the lagoon (wind and tide level in particular, to a by far minor extent currents and waves), the development of an **integrated modelling system (hydrodynamics + waves)** capable of reconstructing, over a sufficiently long time and after proper calibration and validation, the spatial and temporal distribution of the main meteomarine variables of interest at lagoon scale can be considered as a first milestone in the development of the study.

After a complex phase of data collection and interpretation (including the challenging setup of a proper bathymetry for the entire Venice lagoon), an integrated 2D model of the entire lagoon, aiming at establishing, for one representative year, the spatial and temporal distribution of water levels, currents and wave conditions was implemented.

In particular, the hydrodynamic model was developed using the MIKE 21 HD model (HydroDynamics). Water levels measured at the three lagoon inlets were used as boundary conditions, while a distributed map of wind speed and direction over the entire lagoon, established through proper processing of available wind measurement at several stations was used as internal forcing. The contribution from the rivers discharging in the area was also included.

The wave model was developed using the MIKE 21 SW model (Spectral Waves). The distributed map of wind speed and direction mentioned above was used for wave generation inside the lagoon, while the contribution of waves entering from the three inlets was included using the time series from three virtual buoys derived from the Mediterranean Wind Wave Model (MWM), a wind-wave hindcast database jointly developed by DHI and HyMO*Lab* (University of Trieste). Actual water levels in the lagoon were derived from the HD model.

The description of the setup, calibration, validation and production of the integrated modelling system is widely illustrated in Section 5 of the present report.

The results of the integrated modelling system have been extensively processed to derive the required input data for a number of applications that are under development and will be described in the following.

A specific session is dedicated to the geotechnical data collection, analysis and regionalization, that includes the illustration of the factors influencing the erosion threshold of the seabed in the lagoon of Venice and their implications on the development of the 3D model of the Malamocco Marghera

Channel which is under development at the time of issuing the present document and will be finalized in Phase 2 of the Project.

2.2 Phase 1-NAV_A: Execution of preliminary full mission simulations

A preliminary full-mission simulation study was conducted in order to assess the existing Malamocco-Marghera access Channel's capacity for different selected design ships including Cruise (2), Container (3), and Bulk (1) ships. The main objective of this preliminary simulations was to test large vessels and exclude from the very beginning of the study that safe navigation conditions could be achieved for those type of vessels under the existing configuration of the Channel. Groundings have been reported in some cases even without any meteomarine forcing.

2.3 Phase 2 – NAV_A: advanced UKC study along the Malamocco Marghera Channel using NCOS

The one-year long time series of meteomarine conditions along the Channel derived from the 2D model of the lagoon (wind conditions, water levels, tidal currents and waves, in the form of 2D spectral information) have already been used as direct input for the Nonlinear Channel Optimisation Simulator (NCOS). NCOS is used to assess the Channel UKC capacity in quantification of the spatial variations in channel operability for the most important deep-drafted design vessels, considering vessel specific response to local meteomarine conditions, and transit procedures.

Through the NCOS simulations, that are running at the time of issuing the present document, it will be possible to assess the existing capacity of the Channel under its current bathymetric profile through operability assessment of three deep-drafted design vessel classes (one Cruise, one Container and one Bulk) that have been selected in agreement with Port of Venice.

The main outcomes from NCOS simulations will include the following:

- calculation of the annual percentage operability of each design vessel configuration;
- identification of sections of the channel constricting operability for each vessel configuration;
- identification of weather conditions that constrict operability for each vessel configuration;
- determination of the length of safe transit windows and their dependency on maneuvering constraints and UKC;
- determination of maximum draft (m) the port can safely accommodate with no additional dredging;

The detailed analysis of NCOS results will support the proper selection of meteomarine and transit conditions to be simulated with the fast time simulator and with the full mission simulator (Phase 2-B and Phase 2-C below).

2.4 Phase 2-NAV_B: Fast time simulations

The analysis of NCOS results for the existing configuration of the Malamocco-Marghera Channel will allow identifying relevant meteomarine and transit conditions to test with the fast time simulator. The software Simflex, developed by the former Danish Maritime Institute (later merged with FORCE Technology software) will be used to study a given area under different weather conditions repeatedly. It also includes the navigator's different behavioural patterns with regard to manoeuvring the ship. This yields a fast identification of problematic areas or conditions in the early design phase which can reduce the cost significantly when constructing or changing channel layouts.

The main goal of the fast-time simulations for the existing configuration of the Channel is, through systematic analysis of different manoeuvres, also accounting tug support, a complete definition of problematic areas and environmental conditions, and vessels for further testing during the real-time simulations, thus integrating from manoeuvring perspective what NCOS provided from a under keel clearance side. The down time analysis will be based on observed usage of rudder and distance to channel limits combined with statistical occurrence of weather scenarios

The fast-time study will be carried out as per the PIANC Recommendations and will replicated no less than 10 times. Tentatively, 5 vessels will be tested during the fast-time study and each vessel will be tested in three combinations of wind, current and waves.

The fast time model operates under given speed profiles and tracks, that have already been agreed with Port of Venice. The fast time controller induces statistical noise to the plan simulating slightly different behaviour from transit to transit. Repeating the transit 10 times gives some variations and the following statistical analysis will reveal the mean speeds and the variation in the homogeneous regions in the channel.

The role of fast time simulations is even more relevant in Phase 3 of the project, when this agile tool will be ideal to test different configurations of the Malamocco-Marghera Channel, thus supporting the optimization of the candidate solution with respect of sustainable navigation (see Section 2.9)

2.5 Phase 2-NAV_C: Full Mission Simulations

A mathematical and 3D visual model of the Channel, from the Malamocco entrance to the port area, is under development and will form the basis for the session of full mission simulations that will be carried out immediately after the fast time simulations phase.

Following the NCOS and fast-time simulations, a real-time study will be performed in one of Force Technology full-mission simulators.

The goal of the real-time study for the existing configuration of the Channel is twofold: to further study critical vessels and scenarios based on the outcome of the fast-time and NCOS study and to evaluate navigation for the entire length of the Channel, with focus on critical stretches as identified during the fast-time and NCOS study as well as during the preliminary full mission simulations

Simulations will be carried out by experience Captains made available by Force Technology and will account the tug support as well as the navigation in convoy, which is typical in Venice lagoon. It is planned to spend 5 days for the full mission simulations of the existing channel, while 7 days will be dedicated to the final verification of the new layout of the Channel (see Section 2.9).

2.6 Phase 2-HYD_A: Establishment of 3D hydrodynamic model of the Channel and surrounding areas (navigation forcing)

The effect of navigation on the hydrodynamics and morphology of the Malamocco-Marghera Channel and surrounding areas primarily deals with two types of waves induced by passing vessels. Two different types of vessel-generated waves are identified: Primary waves (draw down) and secondary waves (Kelvin wake). Primary waves are bound displacement waves induced by the acceleration of the flow under and around the ship's hull. The secondary wave system consists of diverging and transverse waves in a restricted wedge-shaped region, a Kelvin wake, where the cusp angle is about 19.5^{o} and almost independent of the ship speed. The diverging waves spread on each side of the ship at an acute angle of about +35^{o} relative to the course, whereas the transverse waves move in the same direction as the ship.

Usually, and this is also the case of the MM Channel, primary waves are of far greater importance than secondary (Kelvin) waves.

Primary waves will be simulated using a 3D hydrodynamic model (MIKE 3 HD FM) covering the Channel and surrounding areas. The vessel is introduced to the flow as a moving pressure field boundary condition, where the pressure field is proportional to the draft of the vessel. The hull shape is specified using an independent mesh, which is generally much finer than the mesh resolving the

water body. The numerical model for modelling draw-down, that has previously been successfully validated against physical model tests, will be calibrated against two datasets of measurements:

- wave data measured by CNR in the proximity of “Cassa di Colmata B” between August 2019 and February 2020: a selection of “events” (vessel passages creating significant displacement waves) has already been carried out;
- new wave data from a dedicated campaign (a day when relevant vessel traffic along the Channel is planned) that the Joint Venture is planning to execute.

The propagation of the secondary waves into the tidal flats will be simulated using DHI’s Spectral Wave model MIKE 21 SW. The calibration and validation of the model will benefit from the planned CFD simulations (two vessels, different velocities and water level) that will be carried out by CETENA.

The implementation of the above modelling will make it possible to assess the morphological impact of passing vessels on the nearby tidal flats on the basis of the sediment transport rates and sediment budget calculated during a series of events.

2.7 Phase 2-HYD_A: Establishment of hydrodynamic model of the Channel and surrounding areas (natural forcing)

The same 3D model of the Channel and surrounding areas, developed and calibrated to simulate the effects of the passing vessels on hydrodynamics and morphology of the tidal flats surrounding the Channel is also used to derive, within the same area, the morphological response induced by natural forcing (wind, wave, tide) during a series of events, that will be selected on the basis of the analysis of the one year simulation of meteomarine conditions for the entire lagoon (see Section 3.3).

2.8 Phase 2-SOL: Development of a package of coordinated solutions

The field of analysis moves within a series of needs and constraints of different nature: first of all functional, environmental and economic. The development of the design solution will therefore move within these constraints and needs, alternating phases of study and analysis of the results with moments of confrontation with the Client. The most critical phenomenology, that is the displacement wave, is in fact directly linked to the dimensional relationship between the section of the channel, the submerged hull of the ship and the speed with respect to the water. The displacement wave

represents the most critical aspect of the problem because it cannot have a small-scale solution (therefore simply based on “ordinary” solutions for bank stabilization).

The first step in the definition of the solutions is the proper study of the geometry of the Channel suitable for ensuring the safety of navigation. This activity will be developed with the support of manoeuvre simulations (fast time simulations). Once a “candidate” geometry of the channel will be achieved, the 3D hydrodynamic simulations will be replicated, with special focus on the displacement wave and its potential impact on the morphological response of the tidal flats around the Channel.

Once the “large scale” solutions will be selected, the local stresses in the various project areas will be assessed overall, updating the modelling, and then analysed the local design solutions aimed at preventing the erosion of the tidal flats and Channel banks. In this context, both traditional types of intervention (bank protections) and innovative ones, based on the consolidation of the seabed with seagrass (where the stress level is compatible), "self-sustaining oyster / bio reefs" (optimal in relation to water exchange and nutrient load, as well as adaptive and resilient) will be taken into consideration.

2.9 Phase 3-HYD-NAV-SOL: Validation of proposed solutions

The candidate solution will be finally validated through a replication of the integrated modelling system (3D hydrodynamics /morphological impact) and the execution of additional days of full mission simulations (7).

3 TECHNICAL REPORT ON METEOMARINE AND HYDROGEOLOGY SITE CHARACTERIZATION (*RELAZIONE TECNICA DI CARATTERIZZAZIONE CLIMATICA E IDROGEOLOGICA DEL SITO*)

The assessment of meteomarine conditions for Venice lagoon is an essential stage in the process towards the development of navigation models as well as models simulating induced effects caused by passing vessels in the Malamocco-Marghera Channel.

A well distributed network of measuring stations provides water level and wind observations across the Venice lagoon. Observations are typically publicly available and can be downloaded from open access portals ([1], [2]), however they are limited to point measurements and therefore not suitable for reproducing the complex 2D space variability of meteomarine conditions.

To address this, within Task 1.3, a coupled 2D Hydrodynamics and Spectral Waves (hereinafter HD and SW respectively) model was developed and ran for one representative entire year (see Section 3.3).

The HD model enables the characterization of water level and 2D depth-integrated current field induced by the combination of tides and storm surges. The SW model builds on the water levels provided by the HD model to resolve wave spectral energy equations enabling wave climate computation in the entire lagoon under the effect of space and time varying wind fields as well as of residual waves entering from the three lagoon mouths (Lido, Malamocco and Chioggia).

The year-long generated meteomarine conditions are used to derive representative scenarios for the navigation simulations. For safety reasons the meteomarine conditions must err on the conservative side but, on the other hand, should not feature “extreme” characteristics that would excessively penalise the navigation simulations.

3.1 Lagoon general hydrodynamics aspects

The Venice lagoon, with an area of circa 550Km^2 and a length of 50 km along the South-West/North-East axis, is the larger Italian lagoon. It is located in the northern Adriatic Sea to which it is connected through three main inlets, namely Lido, Malamocco and Chioggia. For this reason, the lagoon is traditionally considered subdivided in three sub-basins separated by two watersheds through which the residual flow is minimum [3]

Broadly speaking, water exchange between lagoon environments and the open sea is controlled by tides, atmospheric forcing on (non-tidal) low frequencies and by the freshwater discharges [4].

The water circulation in the Venice lagoon is mostly triggered by the water level variation at the three inlets and by the resulting propagation of the tidal wave taking place thorough the deeper channels and then extending to the shallow water areas [5] .

The tide system in the northern Adriatic Sea generates a mixed semidiurnal tidal regime which gives rise to a microtidal regime featuring mean tidal range from 50 cm during neap tides to 100 cm during spring tides [4].

It is estimated that the total volume of the lagoon is around $632 \cdot 10^6$ m^3 and the exchange of water through the inlets in each tidal cycle accounts for about a third of the total volume of the lagoon [3]. In regard to this, semi-diurnal constituents (mainly M2 and S2) are reported to be responsible for about 80% of the flow exchange [4].

A complicated topography made of shallower areas, islands and an interconnected network of deeper channels interacts with the general hydrodynamics and the circulation generated by tides and wind is modified by the non-linear interaction with the bottom of the lagoon [5]. These deeper channels are also reported to perform a drainage function, often continuing to flow long after the tide has receded and the marshes are exposed [6].

The tidal exchange of seawater and the freshwater input from river runoff define the brackish characteristics of the lagoon. It has to be noted, however, that the freshwater discharge into the lagoon is relatively low because in the 15th and 16th centuries, Venetians deviated major river flows from the lagoon directly into the Adriatic Sea [4].

The city of Venice being situated on low-lying islands is rather often exposed to flooding events (also commonly known as “acqua alta”) which are typically associated with the superposition of high tides, and wind and/or atmospheric pressure induced high sea-level (i.e. storn surges) [4].

Energetic wind conditions from South-East (i.e. “Scirocco”) blowing along the minor axis of the lagoon are typically responsible of “acqua alta” episodes. Their frequency reaches its maximum in autumn period (November and December) when sea-level setup induced by winds blowing from South-East over the larger Adriatic area coincides with a low atmospheric pressure [7] .

Besides the generation of storm surges and water level set-up, wind energy transfer mechanisms can give raise to moderate sea-states inside the lagoon. North-Easterly wind systems acting along the major lagoon axis, i.e. “Bora”, are typically associated with larger wave generation phenomena inside, owing that to an extended fetch and typically to more sustained wind speeds. Overall, wave penetration through the three inlets is of little importance and is limited to smaller waves of longer period.

3.2 Site meteomarine characterization

3.2.1 Wind field

Wind data obtained from the two main met stations networks operating in Venice lagoon are used in this study, i.e. ISPRA-Venezia [1] and ISPRA-Rete Mareografica Nazionale [8] (see map in Figure 1).

ISPRA-Rete Mareografica Nazionale [8] provide observations at one single met-station (i.e. “Lido Diga Sud”) for a period spanning from 1998 to date allowing for long term wind analysis. However, the lack of additional met stations in the lagoon makes the wind field spatial variation analysis unfeasible.

Conversely, the ISPRA-Venezia [1] network provide shorter timeseries (or with several gaps), but spatially well distributed across the lagoon.

A number of statistical indices, namely mean value, 95th and 98th percentile for wind speed at 10 m above MSL, were derived from observation at “Lido Diga Sud” for the period 1998 to 2021. These indices can be considered as a proxy variable for the yearly variation of the wind field energy and are instrumental in the selection of the year to be simulated as described in Section 3.3.

Figure 1. *Venice lagoon met-station networks: ISPRA-Venezia* [1] *(light blue pins) and ISPRA-Rete Mareografica Nazionale (yellow point)* [8]*.*

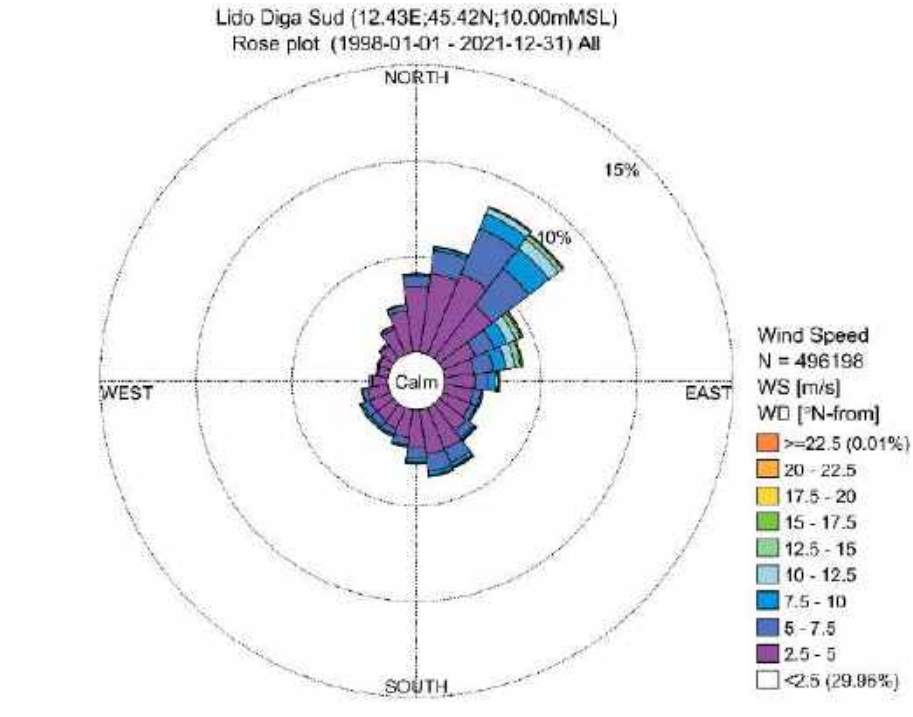

Figure 2."Lido Diga Sud" wind rose for the period 1998-2021

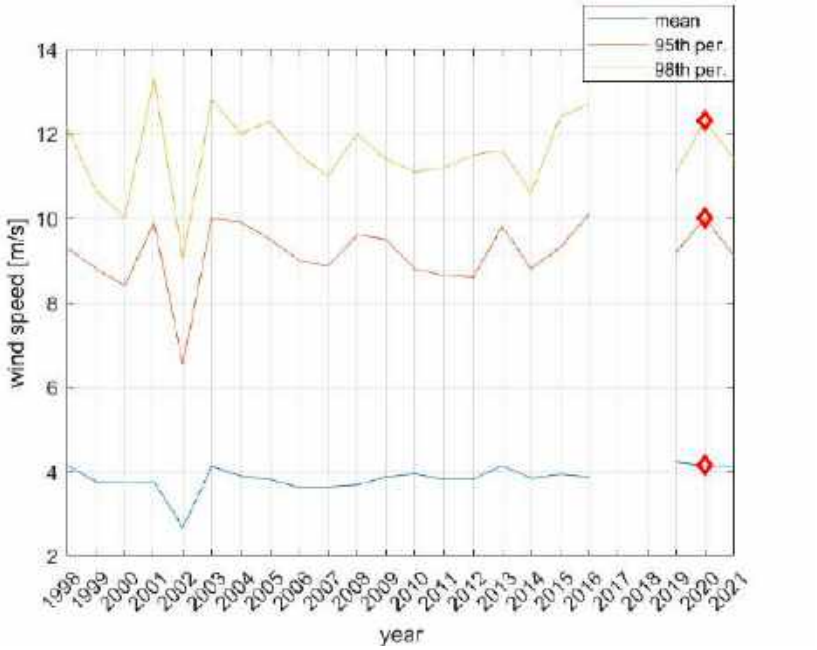

Figure 3. Wind statistics at "Lido Diga Sud" for the period 1998-2021.

Table 1. Wind statistics for the period 1998-2021 at "Lido Diga Sud" station. Highlighted the chosen year for model simulations, i.e. year 2020.

Year	Mean [m/s]	95th percentile [m/s]	98th percentile [m/s]
1998	4.15	9.30	12.17
1999	3.76	8.81	10.65
2000	3.74	8.40	10.00
2001	3.75	9.90	13.30
2002	2.67	6.54	9.05
2003	4.12	10.00	12.80
2004	3.89	9.90	12.00
2005	3.81	9.50	12.30
2006	3.62	9.00	11.50
2007	3.64	8.86	11.00
2008	3.68	9.60	12.00
2009	3.87	9.50	11.40
2010	3.94	8.80	11.10
2011	3.81	8.65	11.20
2012	3.81	8.60	11.50
2013	4.14	9.80	11.60
2014	3.84	8.80	10.60
2015	3.93	9.30	12.40
2016	3.87	10.10	12.70
2017	N/A	N/A	N/A
2018	N/A	N/A	N/A
2019	4.22	9.20	11.10
2020	4.15	10.00	12.30
2021	4.13	9.10	11.40

Observed wind time series at 10m above MSL for the year 2020 were downloaded for six met stations (Figure 4, Table 2) available from ISPRA-Venezia data portal [1]. Data were quality controlled and cross-correlated to investigate the wind field spatial variability.

Table 2. Met-station coordinates from ISPRA – Venezia portal [1]

Station	Long [°E]	Lat [°N]
Grassabò	12.529878	45.521456
Lido Meteo	12.382950	45.430150
San Giorgio in Alga	12.294947	45.425169
Malamocco Diga Nord	12.341625	45.334450
Petta de Bò	12.241781	45.266422
Chioggia Diga Sud	12.312767	45.228547

Figure 4 shows wind roses for the six met stations available inside Venice Lagoon, from which a marked wind field space dependency can be appreciated.

A more detailed view of wind roses for the six met stations can be found in Figure 5 to Figure 10.

In general, Venice lagoon shares a similar wind system to the Northern Adriatic Sea, that is wind from north-easterly and south-easterly directional sectors also known as “Bora” and “Scirocco” respectively.

“Bora” wind shows larger magnitude in terms of wind speed and blows from a direction roughly parallel to the major lagoon axis giving rise to more energetic wave conditions. “Scirocco” wind, blowing roughly perpendicular to the lagoon major axis is regarded as the main cause of storm surges on Northern Adriatic Sea and in turn in Venice Lagoon [5].

Frequency of occurrence tables for all met stations (10m wind speed vs direction) are presented in Appendix A.

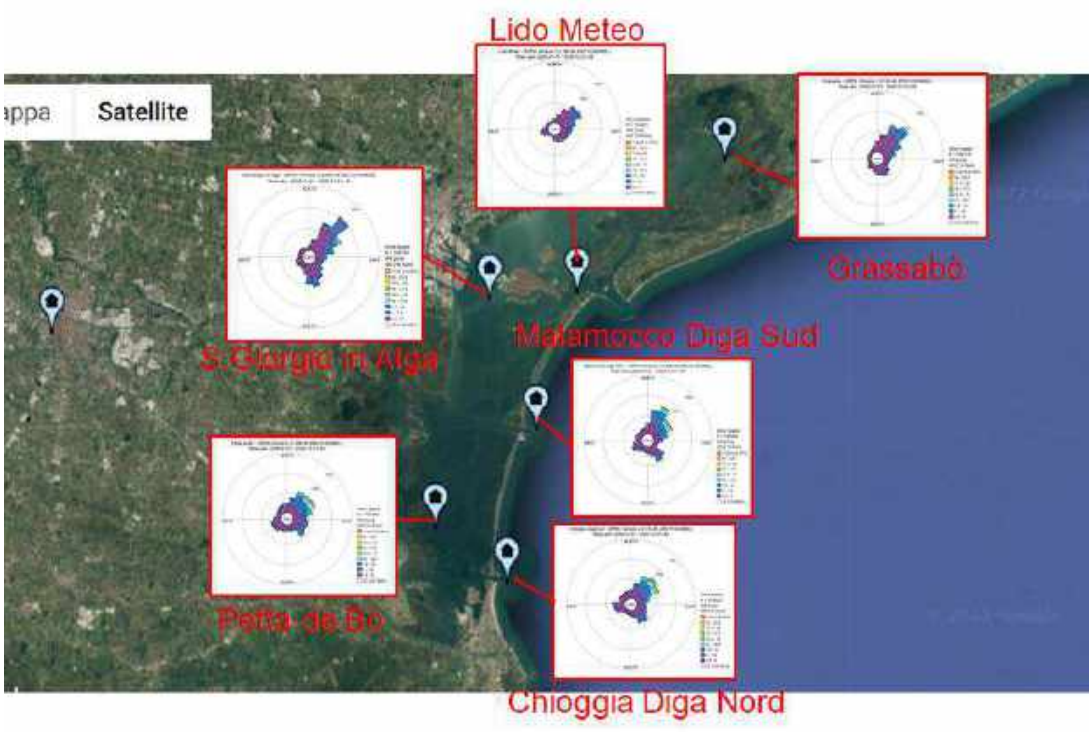

Figure 4.Venice lagoon met-stations wind roses for the year 2020.

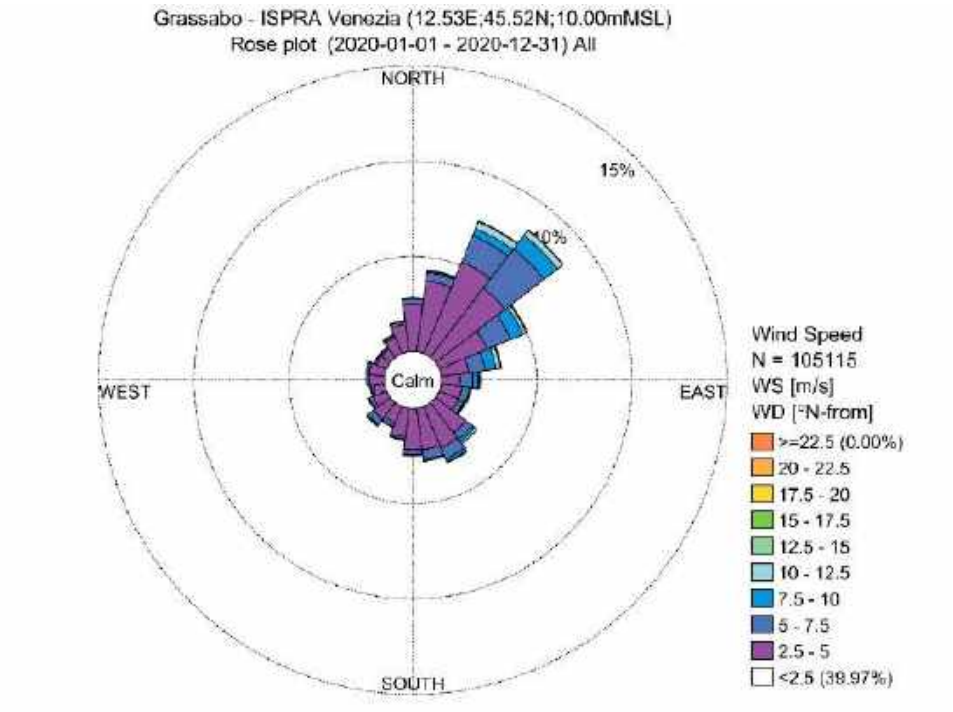

Figure 5. Grassabò met station wind rose: 10m above MSL wind speed vs direction

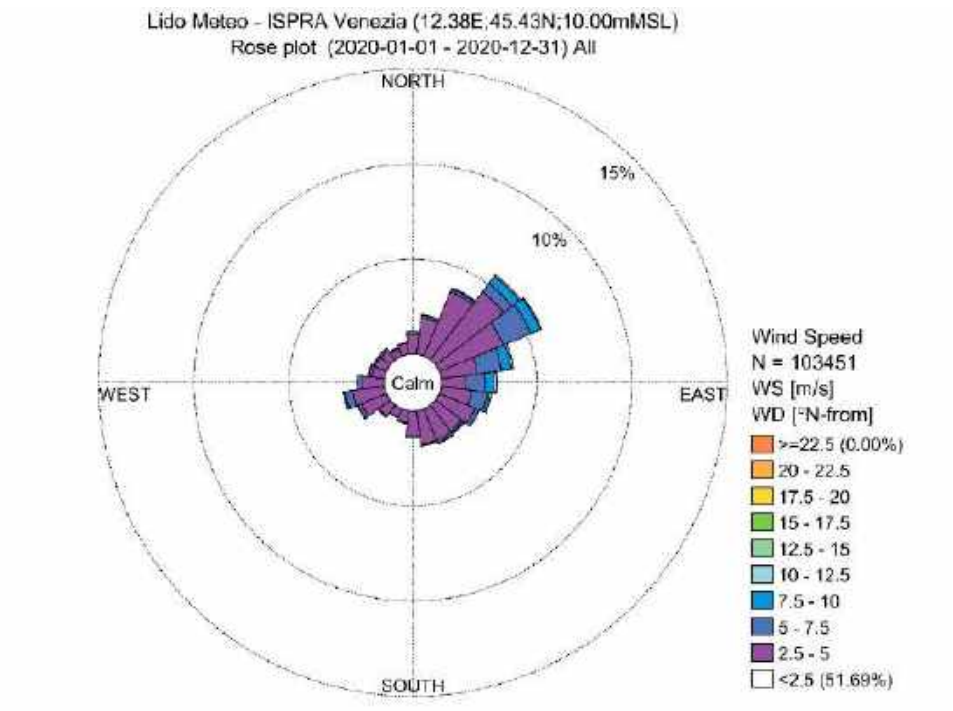

Figure 6. Lido meteo met station wind rose: 10m above MSL wind speed vs direction

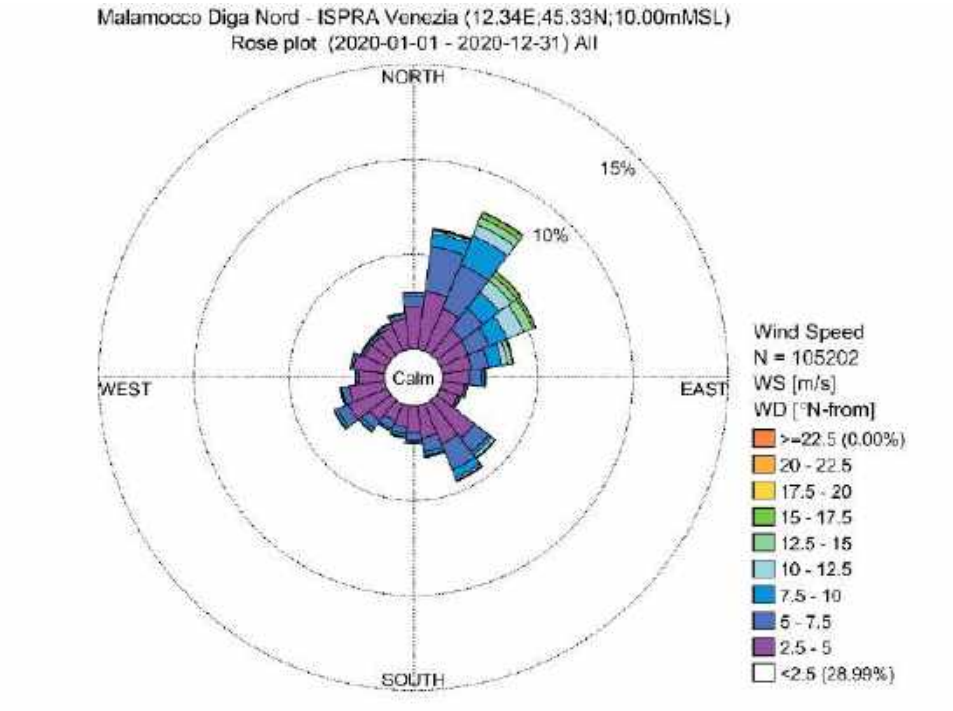

Figure 7. Malamocco Diga Nord met station wind rose: 10m above MSL wind speed vs direction

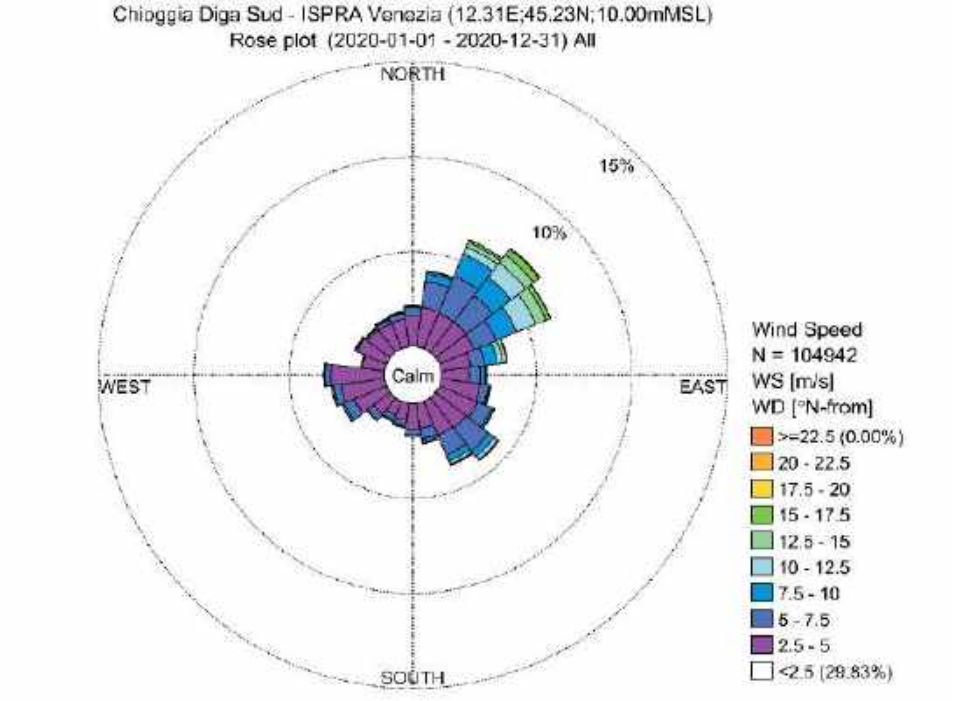

Figure 8. Chioggia Diga Sud met station wind rose: 10m above MSL wind speed vs direction

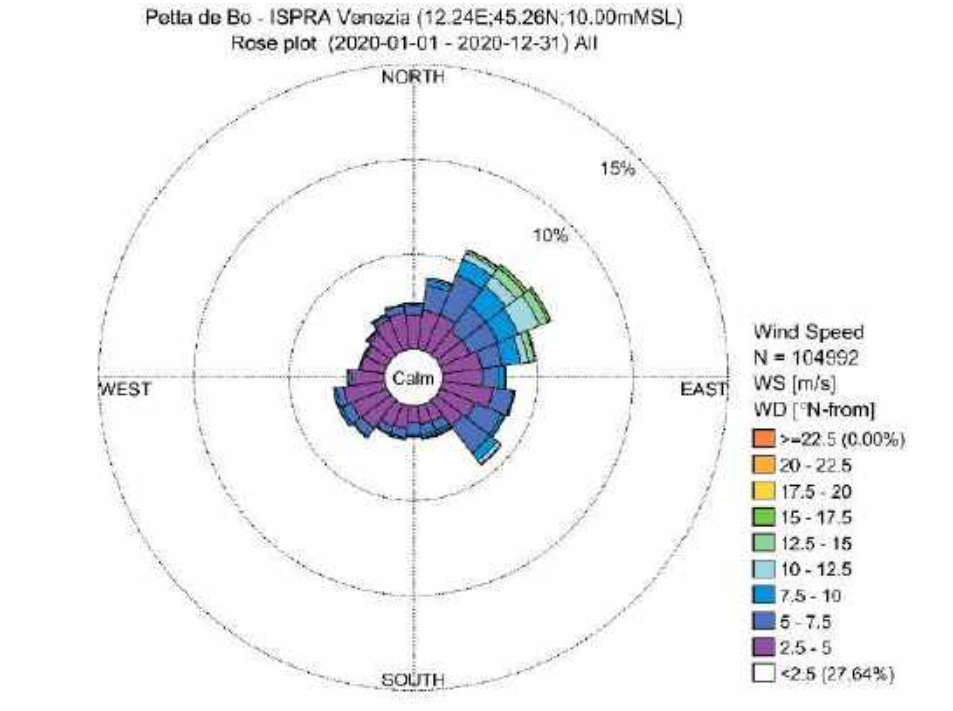

Figure 9. Petta de Bò met station wind rose: 10m above MSL wind speed vs direction

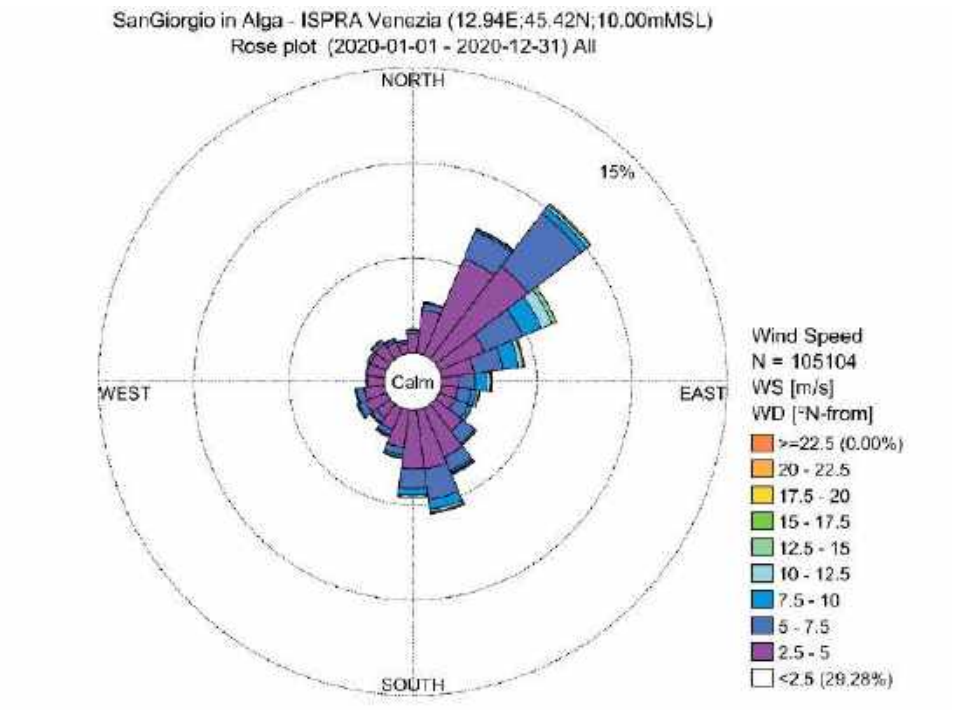

Figure 10. S. Giorgio in Alga met station wind rose: 10m above MSL wind speed vs direction

3.2.2 Wave field

The main mechanism giving rise to waves inside the lagoon is the energy transfer between wind and water surface. Due to the contained geographical fetch (i.e. limited by the lagoon area) waves are typically characterised by short periods. Nonetheless, waves of longer periods generated in the northern Adriatic Sea can propagate into the lagoon through the three inlets. To account for this, the SW model is forced at the three open boundaries by wave timeseries extracted from MWM (Appendix E**)**

MWM is a high-resolution historical database of hindcast wind and wave conditions in the Mediterranean Sea. The database, produced through state-of-the-art wind and wave models, is the result of a joint research project between DHI and HyMO*Lab* (Hydrodynamics and Met-Ocean Laboratory of the Department of Engineering and Architecture of the University of Trieste, Italy), and it consists of hourly data, beginning in 1979, obtained from a last-generation modelling chain. The meteorological model used by MWM is the WRF-ARW model, one of the most widely recognized and state-of-the-art non-hydrostatic meteorological models. The resolution of the WRF model is 0.1°, while CFSR/CFSv2 global datasets (Climate Forecast System Reanalysis /Analysis), produced and published by NCEP (National Centre for Environmental Predictions) provide the boundary and initial conditions.

MWM performances are validated against satellite observations covering several areas within the Mediterranean Sea (Figure 12). Results relative to the comparison in the northern Adriatic Sea area of MWM modelled data against observations from missions Geosat, Envisat and Jason 2 are illustrated in Figure 13 **-** Figure 15**.**

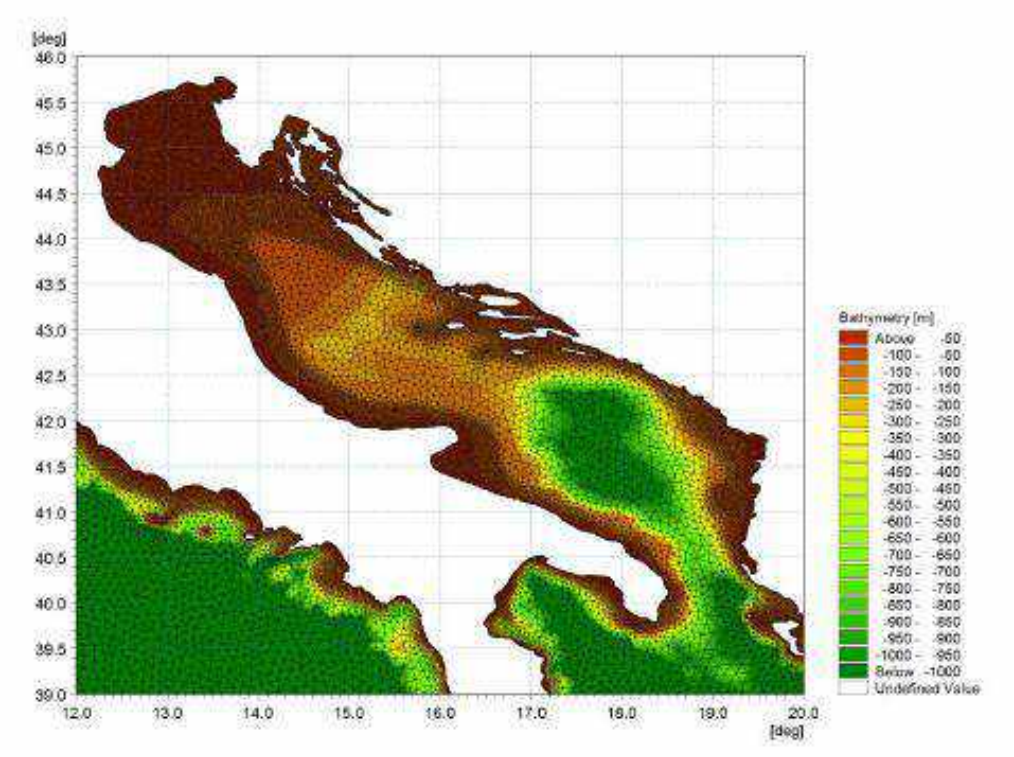

Figure 11. MWM mesh and bathymetry in the Adriatic Sea

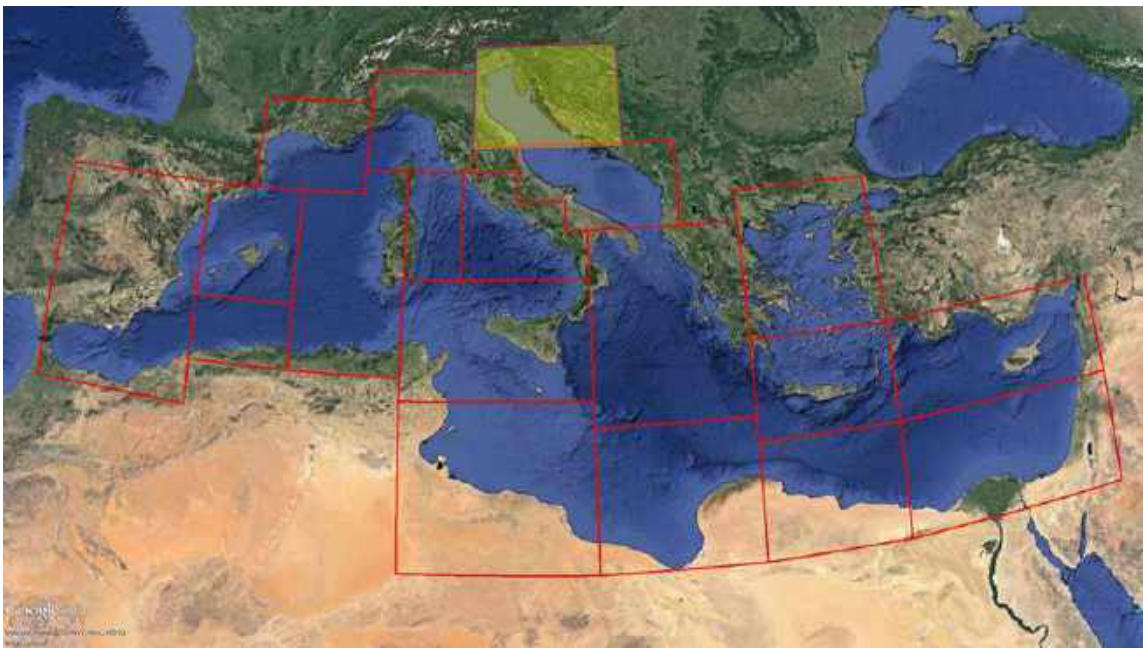

Figure 12. Image of macro areas used for MWM model validation. Highlighted in light yellow the northern Adriatic Sea area related to the satellite observation used in the MWM validation.

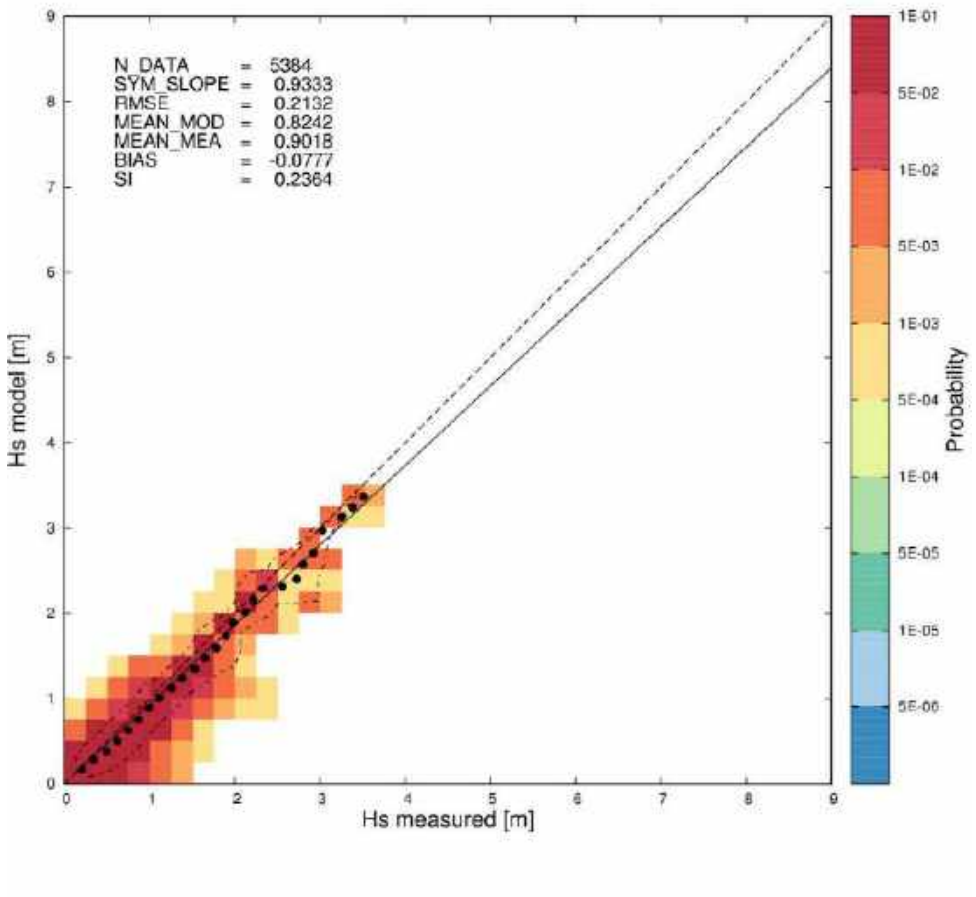

Figure 13. MWM simulated significant wave height (Hs) vs Jason 2 mission satellite observations

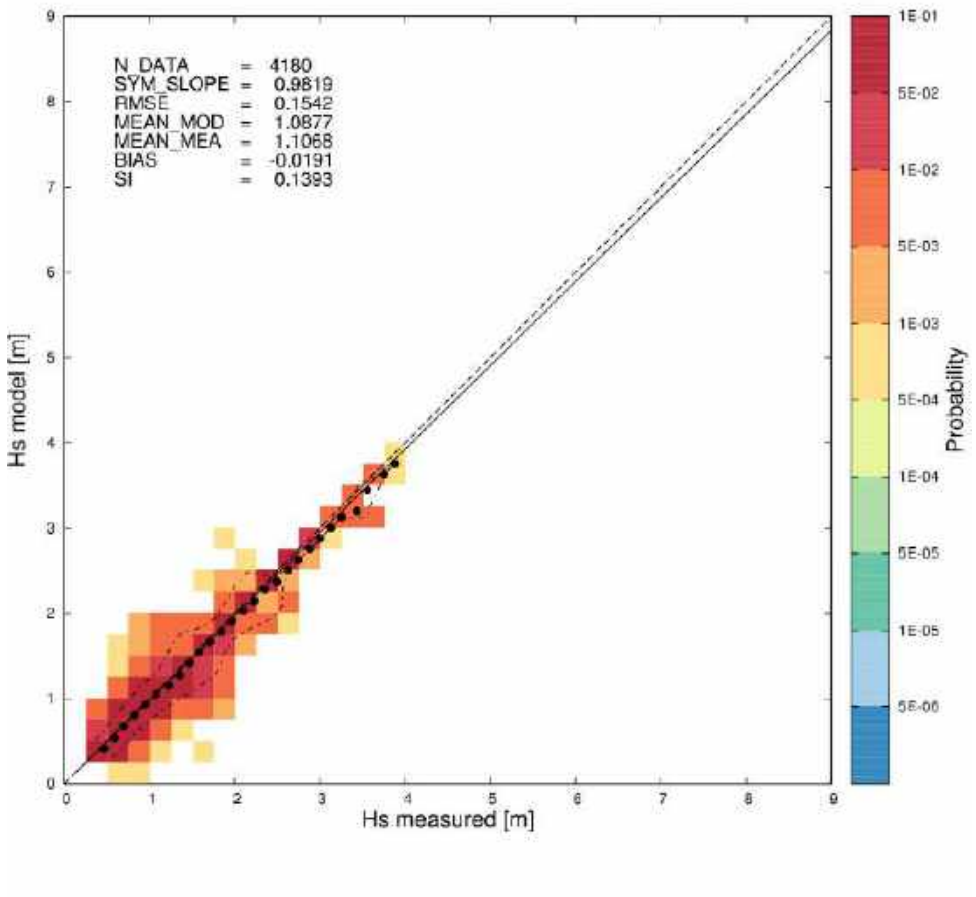

Figure 14. MWM simulated significant wave height (Hs) vs Geosat mission satellite observations

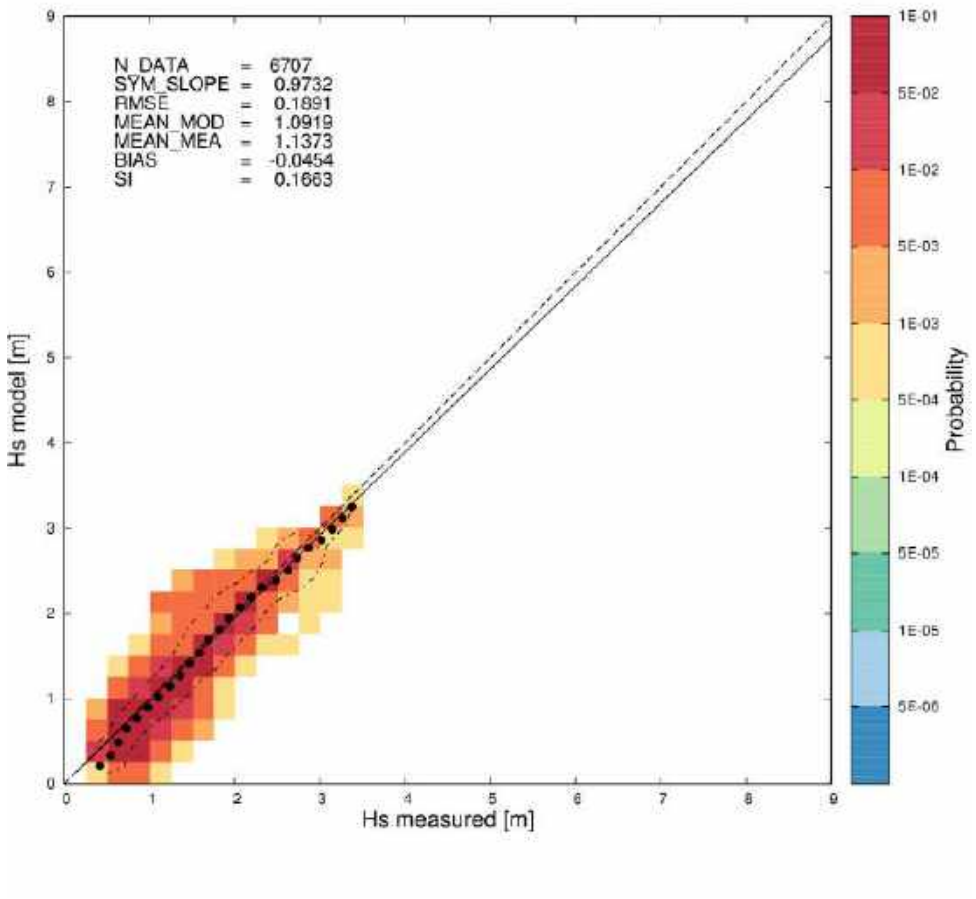

Figure 15. MWM simulated significant wave height (Hs) vs Envisat mission satellite observations

Wave data for a period spanning 41 year (1979-2020) was extracted from the MWM model at the three inlets and are hereafter presented in Figure 16 - Figure 18 and Table 3- Table 5 in the form of wave roses and scatter tables.

Figures display a similar wave climate trend at the three inlets with a noticeable predominant direction from East and South-East sectors. Typically, about 70% of significant wave heights (H_s) are below 0.5m reaching maximum values of 3.13 m, 3.12 m and 3.11 m for Lido, Malamocco and Chioggia, respectively.

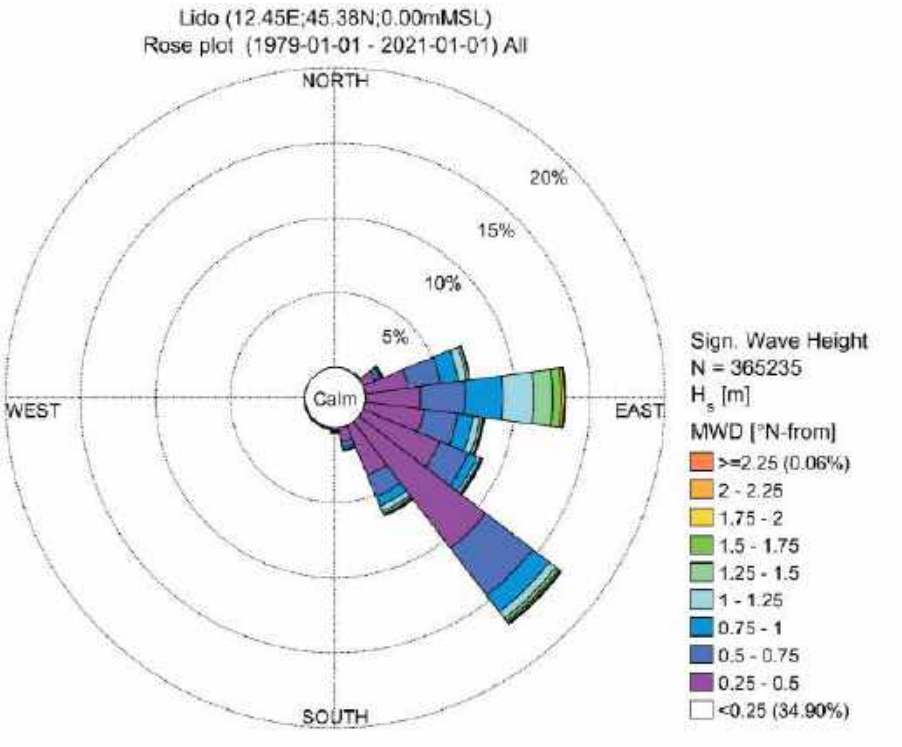

Figure 16. Lido inlet wave rose (1979 -2020) – MWM model.

Table 3. Scatter table of Significant Wave Height (Hs) vs Mean Wave Direction (MWD) from MWM data extracted at Lido inlet.

Lido (12.45E;45.38N;0.00mMSL)
Frequency of Occurrence [%] (1979-01-01 - 2021-01-01) All
H_s [m] - Sign. Wave Height

MWD [°N-from] - Mean Wave Direction

	[0-0.25[	[0.25-0.5[	[0.5-0.75[	[0.75-1[	[1-1.25[	[1.25-1.5[	[1.5-1.75[	[1.75-2[	[2-2.25[	[2.25-2.5[	[2.5-2.75[	[2.75-3[	[3-3.25[	[3.25-3.5[	Total	Accum
[337.5-352.5[	0.008	0.007	0.002	-	-	-	-	-	-	-	-	-	-	-	0.016	100.000
[322.5-337.5[	0.007	0.008	0.001	-	-	-	-	-	-	-	-	-	-	-	0.016	99.982
[307.5-322.5[	0.009	0.007	0.000	-	-	-	-	-	-	-	-	-	-	-	0.016	99.966
[292.5-307.5[	0.013	0.015	-	-	-	-	-	-	-	-	-	-	-	-	0.028	99.950
[277.5-292.5[	0.013	0.023	0.001	-	-	-	-	-	-	-	-	-	-	-	0.037	99.922
[262.5-277.5[	0.024	0.039	0.002	-	-	-	-	-	-	-	-	-	-	-	0.065	99.885
[247.5-262.5[	0.060	0.059	0.018	0.002	-	-	-	-	-	-	-	-	-	-	0.139	99.820
[232.5-247.5[	0.097	0.079	0.030	0.003	0.000	-	-	-	-	-	-	-	-	-	0.209	99.681
[217.5-232.5[	0.066	0.055	0.025	0.003	0.001	-	0.000	-	-	-	-	-	-	-	0.174	99.595
[202.5-217.5[	0.074	0.106	0.030	0.004	0.001	0.000	-	-	-	-	-	-	-	-	0.215	99.395
[187.5-202.5[	0.120	0.115	0.040	0.015	0.001	-	-	-	-	-	-	-	-	-	0.310	99.170
[172.5-187.5[	0.328	0.221	0.064	0.049	0.012	0.003	0.001	-	-	-	-	-	-	-	0.707	98.850
[157.5-172.5[	1.259	0.933	0.203	0.159	0.055	0.012	0.003	0.001	-	-	-	-	-	-	2.637	98.154
[142.5-157.5[	4.557	3.615	1.325	0.655	0.354	0.176	0.095	0.045	0.021	0.005	0.001	-	0.001	-	11.125	95.517
[127.5-142.5[	13.315	10.649	3.955	1.401	0.544	0.238	0.144	0.076	0.031	0.022	0.008	0.003	0.001	-	30.379	84.392
[112.5-127.5[	8.906	5.574	2.009	0.627	0.212	0.103	0.050	0.028	0.008	0.005	0.001	0.001	-	-	14.704	54.013
[97.5-112.5[	3.963	3.966	2.263	1.056	0.497	0.191	0.070	0.042	0.011	0.005	0.003	0.001	-	-	11.727	39.309
[82.5-97.5[	5.094	3.692	2.385	2.503	2.099	1.247	0.591	0.176	0.036	0.009	0.002	0.000	-	-	18.564	27.582
[67.5-82.5[	1.962	2.875	2.200	1.203	0.574	0.172	0.055	0.008	-	-	-	-	-	-	8.979	9.018
[52.5-67.5[	0.306	0.521	0.380	0.124	0.061	0.015	0.006	0.001	-	-	-	-	-	-	1.776	0.038
[37.5-52.5[	0.068	0.079	0.050	0.014	0.005	0.001	-	-	-	-	-	-	-	-	0.219	0.262
[22.5-37.5[	0.015	0.019	0.005	0.003	-	-	-	-	-	-	-	-	-	-	0.042	0.043
[7.5-22.5[	0.000	0.001	0.001	0.001	-	-	-	-	-	-	-	-	-	-	0.003	0.001
[-7.5-7.5[	0.000	0.001	0.000	-	-	-	-	-	-	-	-	-	-	-	0.001	0.000
Total	34.997	33.108	16.035	7.946	4.383	2.158	1.025	0.536	0.137	0.046	0.012	0.005	0.001	-	100.000	-
Accum	34.997	68.005	84.041	91.987	96.371	98.529	99.554	100.000	100.000	100.000	100.000	100.000	100.000	100.000	-	-

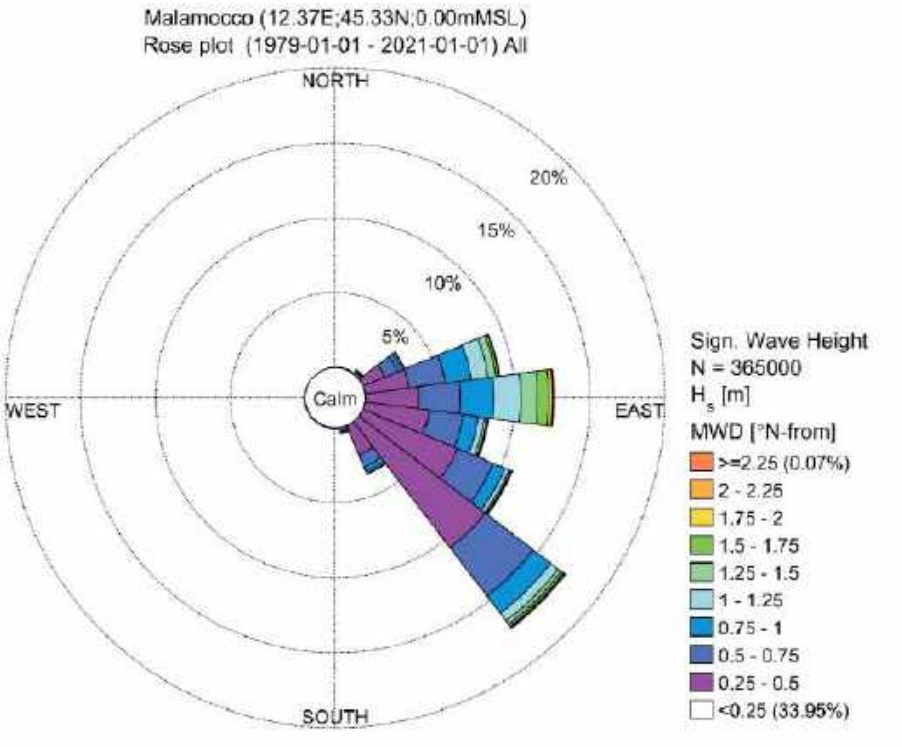

Figure 17. Malamocco inlet wave rose (1979 -2020) – MWM model.

Table 4. Scatter table of Significant Wave Height (Hs) vs Mean Wave Direction (MWD) from MWM data extracted at Malamocco inlet.

Malamocco (12.37E;45.33N;0.00mMSL)
Frequency of Occurrence [%] (1979-01-01 - 2021-01-01) All
H_s [m] - Sign. Wave Height

MWD [°N-from] - Mean Wave Direction

	[0-0.25[	[0.25-0.5[	[0.5-0.75[	[0.75-1[	[1-1.25[	[1.25-1.5[	[1.5-1.75[	[1.75-2[	[2-2.25[	[2.25-2.5[	[2.5-2.75[	[2.75-3[	[3-3.25[	[3.25-3.5[	Total	Accum
[337.5-352.5[	0.016	0.007	0.001	-	-	-	-	-	-	-	-	-	-	-	0.025	100.000
[322.5-337.5[	0.015	0.009	0.000	-	-	-	-	-	-	-	-	-	-	-	0.025	99.974
[307.5-322.5[	0.014	0.009	0.001	-	-	-	-	-	-	-	-	-	-	-	0.023	99.949
[292.5-307.5[	0.010	0.012	0.000	-	-	-	-	-	-	-	-	-	-	-	0.023	99.926
[277.5-292.5[	0.011	0.013	-	-	-	-	-	-	-	-	-	-	-	-	0.025	99.897
[262.5-277.5[	0.011	0.029	0.001	-	-	-	-	-	-	-	-	-	-	-	0.041	99.871
[247.5-262.5[	0.016	0.047	0.005	0.000	-	-	-	-	-	-	-	-	-	-	0.068	99.833
[232.5-247.5[	0.016	0.049	0.005	-	-	-	-	-	-	-	-	-	-	-	0.069	99.765
[217.5-232.5[	0.016	0.045	0.005	0.000	0.000	-	-	-	-	-	-	-	-	-	0.067	99.696
[202.5-217.5[	0.041	0.062	0.004	0.000	-	-	-	-	-	-	-	-	-	-	0.107	99.629
[187.5-202.5[	0.052	0.059	0.006	-	-	-	-	-	-	-	-	-	-	-	0.117	99.507
[172.5-187.5[	0.068	0.084	0.009	0.002	0.000	-	-	-	-	-	-	-	-	-	0.213	99.390
[157.5-172.5[	0.160	0.258	0.109	0.025	0.004	0.001	-	-	-	-	-	-	-	-	0.761	99.177
[142.5-157.5[	2.805	3.134	0.865	0.515	0.155	0.056	0.016	0.005	0.001	0.000	-	-	-	-	8.556	98.416
[127.5-142.5[	19.300	10.611	4.036	1.459	0.550	0.277	0.136	0.052	0.032	0.020	0.006	0.003	0.001	-	36.669	89.860
[112.5-127.5[	7.098	6.830	2.567	0.843	0.286	0.125	0.059	0.030	0.014	0.005	0.004	0.001	-	-	17.899	61.422
[97.5-112.5[	4.053	4.333	2.265	1.022	0.398	0.174	0.083	0.045	0.015	0.009	0.002	0.001	-	-	12.372	43.522
[82.5-97.5[	3.104	3.569	2.765	2.232	1.796	1.153	0.709	0.287	0.086	0.017	0.005	0.001	-	-	15.715	31.150
[67.5-82.5[	2.251	2.965	2.642	1.759	1.125	0.523	0.179	0.052	0.009	0.001	-	-	-	-	11.304	15.436
[52.5-67.5[	0.510	1.682	0.980	0.359	0.150	0.047	0.015	0.003	-	-	-	-	-	-	3.525	4.133
[37.5-52.5[	0.093	0.207	0.092	0.036	0.016	0.002	0.001	0.001	-	-	-	-	-	-	0.435	0.608
[22.5-37.5[	0.019	0.038	0.016	0.015	0.001	-	-	-	-	-	-	-	-	-	0.053	0.158
[7.5-22.5[	0.015	0.015	0.009	0.002	0.000	-	-	-	-	-	-	-	-	-	0.044	0.085
[-7.5-7.5[	0.003	0.014	0.000	0.001	-	-	-	-	-	-	-	-	-	-	0.041	0.041
Total	33.950	33.013	16.164	8.602	4.947	2.964	1.216	0.511	0.137	0.050	0.017	0.005	0.001	-	100.000	-
Accum	33.950	66.963	83.149	91.751	96.698	99.662	99.878	99.989	99.926	99.976	99.993	99.998	100.000	100.000	-	-

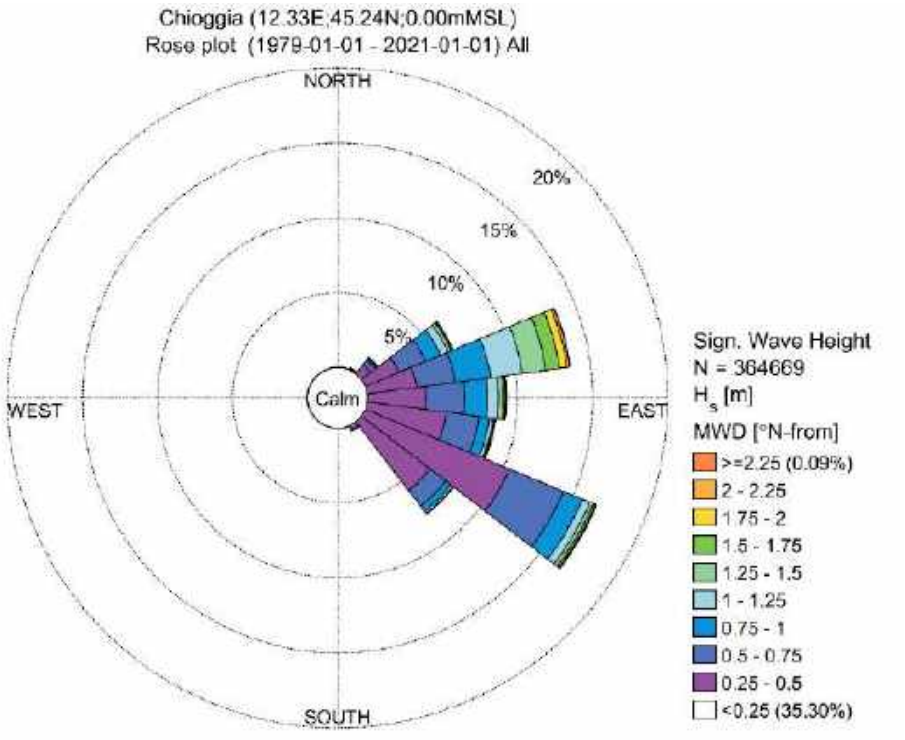

Figure 18. Chioggia inlet wave rose (1979 -2020) – MWM model.

Table 5. Scatter table of Significant Wave Height (Hs) vs Mean Wave Direction (MWD) from MWM data extracted at Chioggia inlet.

Chioggia (12.33E;45.24N;0.00mSL)
Frequency of Occurrence [%] (1979-01-01 - 2021-01-01) All
H_s [m] - Sign. Wave Height

MWD [°N-from] - Mean Wave Direction

	[0-0.25[	[0.25-0.5[	[0.5-0.75[	[0.75-1[	[1-1.25[	[1.25-1.5[	[1.5-1.75[	[1.75-2[	[2-2.25[	[2.25-2.5[	[2.5-2.75[	[2.75-3[	[3-3.25[	[3.25-3.5[	Total	Accum
[332.5-352.5[	0.015	0.015	0.001	-	-	-	-	-	-	-	-	-	-	-	0.032	100.000
[322.5-337.5[	0.013	0.012	0.001	-	-	-	-	-	-	-	-	-	-	-	0.027	99.968
[307.5-322.5[	0.018	0.023	0.000	-	-	-	-	-	-	-	-	-	-	-	0.041	99.942
[292.5-307.5[	0.022	0.018	0.001	-	-	-	-	-	-	-	-	-	-	-	0.041	99.900
[277.5-292.5[	0.022	0.037	-	-	-	-	-	-	-	-	-	-	-	-	0.059	99.859
[262.5-277.5[	0.032	0.037	0.001	-	-	-	-	-	-	-	-	-	-	-	0.070	99.794
[247.5-262.5[	0.026	0.033	0.000	-	-	-	-	-	-	-	-	-	-	-	0.059	99.724
[232.5-247.5[	0.021	0.017	0.000	-	-	-	-	-	-	-	-	-	-	-	0.038	99.664
[217.5-232.5[	0.018	0.018	0.000	0.000	-	-	-	-	-	-	-	-	-	-	0.037	99.626
[202.5-217.5[	0.017	0.013	0.001	-	-	-	-	-	-	-	-	-	-	-	0.032	99.589
[187.5-202.5[	0.017	0.018	0.000	-	-	-	-	-	-	-	-	-	-	-	0.035	99.557
[172.5-187.5[	0.032	0.030	0.002	-	-	-	-	-	-	-	-	-	-	-	0.063	99.522
[157.5-172.5[	0.048	0.054	0.012	0.002	-	-	-	-	-	-	-	-	-	-	0.115	99.459
[142.5-157.5[	0.515	0.330	0.089	0.011	0.001	-	-	-	-	-	-	-	-	-	1.025	99.344
[127.5-142.5[	10.720	5.789	1.321	0.434	0.170	0.044	0.017	0.001	-	-	-	-	-	-	18.479	98.319
[112.5-127.5[	10.512	10.381	3.814	1.360	0.527	0.250	0.152	0.059	0.052	0.000	0.004	0.001	-	-	27.109	79.840
[97.5-112.5[	5.164	5.836	2.310	0.853	0.336	0.099	0.047	0.021	0.013	0.000	0.004	0.001	-	-	13.783	52.641
[82.5-97.5[	3.486	3.821	2.477	1.930	0.736	0.305	0.115	0.056	0.032	0.006	0.006	0.001	0.001	-	12.748	38.858
[67.5-82.5[	2.740	3.304	2.693	2.379	2.124	1.586	0.822	0.508	0.177	0.038	0.013	0.002	0.001	-	16.308	26.110
[52.5-67.5[	1.302	2.433	1.913	1.074	0.636	0.241	0.097	0.032	0.007	0.000	-	-	-	-	7.602	9.802
[37.5-52.5[	0.265	0.759	0.415	0.136	0.008	0.022	0.009	0.009	0.001	-	-	-	-	-	1.678	2.200
[22.5-37.5[	0.055	0.058	0.049	0.018	0.010	0.001	-	-	-	-	-	-	-	-	0.226	0.341
[7.5-22.5[	0.030	0.028	0.011	0.006	0.006	-	-	-	-	-	-	-	-	-	0.081	0.115
[-7.5-7.5[	0.015	0.014	0.004	0.001	-	-	-	-	-	-	-	-	-	-	0.034	0.034
Total	35.295	32.592	15.118	7.661	4.406	2.551	1.359	0.873	0.350	0.056	0.027	0.005	0.001	-	100.000	-
Accum	35.295	67.890	83.008	90.669	95.056	97.615	98.974	99.846	99.910	99.967	99.993	99.999	100.000	100.000	-	-

3.2.3 Water levels

The mixed semidiurnal tidal regime generates water level variation in the range of 50 cm and 100 cm during neap and spring tides respectively. These water levels are invariably occurring throughout the years and therefore do not represent, as is, a hazard with regard to flooding of Venice city and other sensitive low-lying areas in the lagoon.

The nature of the meteorological phenomena is instead chaotic and more difficult to predict. Typically, sustained south-easterly wind system can generate water level set-up which is the main responsible for the, locally called, “acqua alta” events.

The value of 110 cm above ZMPS at “Punta della Salute” tide gauge is historically used as the water level threshold for identifying “acqua alta” episodes. Throughout the years, due to a global scale variation of meteorological conditions,” the number of “acqua alta” episodes ranged, on average, from 5 events for the 1984-2011 period to 6.5 for the 2011-2018 period and to 6 events

from 2019 onwards. The largest water level value ever recorded dates back to 4th of November 1966 when a 194 cm above ZMPS was observed at the “Punta della Salute” tide gauge [9].

In general water levels generated in the northern Adriatic Sea show a small difference at the three tide gauges situated at the three inlets both in terms of phase and total range. In this regard, a more detailed description is provided in Section 5.1.3.3 .

3.2.4 Tributary flow rates

The current Venice Lagoon layout is a remnant of the old lagoonal belt that used to rim the northern Adriatic coast. Until the 16th century the fluvial deposition was responsible of a progressive sedimentary infilling, causing water surfaces reduction and canals deactivation. To prevent further silting of the lagoon during the 16th and 17th centuries the lagoon was involved in an extensive programme of artificial river diversions that lasted almost two centuries and brought to a change in the paths of Po, Brenta, Bacchiglione, Marzenego, Sile, Piave, Livenza and minor rivers [10].

Whitin this study the main eleven lagoon tributaries were taken into account.

The averaged flow rates over eleven years (2000-2010) were derived from Zirino et al [11] and are illustrated in Table 6.

Figure 19. Location of the eleven mass point sources assimilated into the model.

Table 6. Coordinates of the eleven mass point sources (UTM-33 map).

Station	Easting [m]	Northing [m]	Flow rate [m^3/s]
Silone	297957.7775	5043961.082	3.0509
Osellino Tessera	291015.3821	5040946.148	1.4155
Osellino Rotte	287113.564	5037435.345	1.0509
Lusore	283279.6995	5037112.727	2.7709
Nav. Brenta	281179.2103	5032867.427	4.1027
Canale Lova	280643.0638	5024111.68	1.1945
Novissimo	277595.176	5015251.035	3.4582
Montalbano	281002.1474	5011402.192	0.4845
Cuori	280536.5756	5008626.533	2.5645
Zero	294905.7314	5044053.254	3.2782
Dese	294469.4179	5043523.444	2.5073

Carniello et al. [12] describe a flow rate through each inlet in the range of 4000~6000 m^3/s. In this regard the tributaries flow rates account, on average, for a 0.5% of the total lagoon rate of mass balance over a tidal cycle and therefore their contribution to the general circulation in the lagoon is expected to be negligible.

The implementation of tributaries into the model is discussed in Section 5.1.3.4.

3.3 Identification of the representative year

The general lagoon hydrodynamics is driven from a combination of tide, wind and pressure driven water levels (storm surges) and waves. Tides are bound to astronomical traction forces and therefore are invariably occurring throughout the years.

In this regard, the energy transfer mechanisms between the wind field and the water surface are the main responsible for deviations from predictable water levels generated by tides. It follows that the wind field acting upon the lagoon is the key parameter setting the basis for the year selection criterion.

The selection must fulfil two main requirements. The first requirement is tied to the objective of the study, i.e. the representative year must be chosen among periods characterised by “conservative but not extreme” meteomarine conditions from an energetic perspective.

Figure 3 and Table 1 show that the year 2020 exhibits “above average” wind conditions from an energetic perspective. From a quality control standpoint 2020 is also the year for which lesser measurement gaps occurred.

The second requirement is the actual availability of observed data needed for generating model inputs for the relevant year-long simulation. In fact, although the main parameter for the representative year selection is the wind field, the 2D model requires a larger set of data encompassing several hydraulic and meteorological conditions, specifically:

- wind (and pressure) field distribution over the entire lagoon;
- time series of water level conditions at the three model inlets (tide and storm surge);
- lagoon tributaries flow rates;
- wave conditions at the three model inlets.

These conditions are commonly known as model boundary conditions (Section 5.1.3).

A secondary constraint in the year selection is related to the water levels observed in the lagoon.

The lagoon hydrodynamics is strongly affected from larger scale dynamics propagating from the northern Adriatic Sea into the lagoon through the three inlets of Lido, Malamocco and Chioggia.

In this regard, following the same selection criterion applied for the wind parameter, the water level observations inside the lagoon for the reference year should not exhibit extreme values.

It must be noted that the M.O.S.E. mobile barriers system became operational in 2020 reducing the number of extreme high-water events inside the Venice lagoon.

Historically, the main station for water level references in the Venice lagoon is “Punta della Salute” tide gauge. The measuring station detected only two events of high-waters above 110 cm ZMPS occurred throughout the year 2020 with the larger one reaching 139 cm ZMPS (Figure 20).

As a term of comparison, Figure 21 show about six high-water events above the 110 cm ZMPS threshold detected by a mareograph outside the lagoon (i.e., “Malamocco Diga Nord”), in line with the average number of high-water events per year as reported by Volpe et. al [9] between 2011 and 2018.

It is worth being mentioned that the ZMPS vertical datum sits 23.56 cm below the ordnance datum IGM42 and 32 cm below the current MSL tidal datum.

The concurrent availability of water level timeseries with a limited number of extreme high-waters events and “above average” wind field, makes the year 2020 the definitive choice for the representative year to simulate.

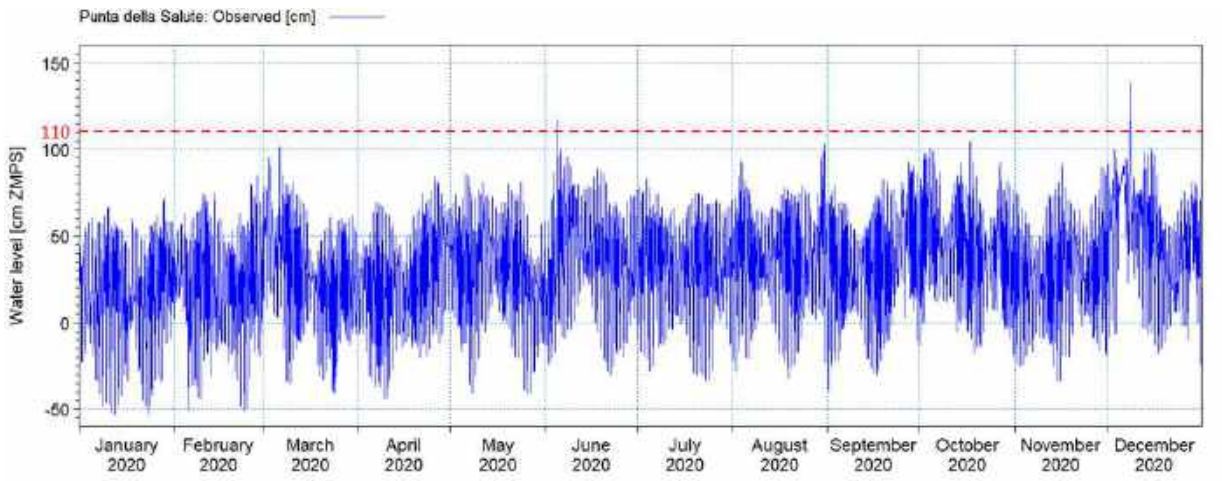

Figure 20. Water level timeseries at “Punta della Salute” tide gauge. In red dashed line the 110 cm ZMPS threshold defining extreme high-water events.

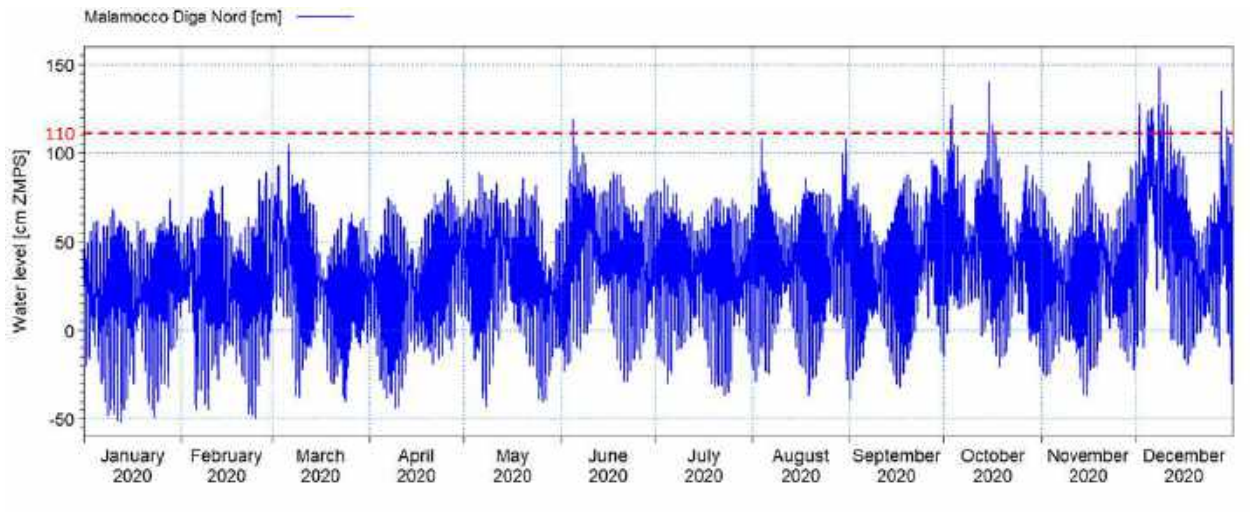

Figure 21. Water level timeseries at "Malamocco Diga Nord" tide gauge. In red dashed line the 110 cm ZMPS threshold defining extreme high-water events.

4 TECHNICAL REPORT ON GEOTECHNICS SITE CARACTERIZATION (*RELAZIONE TECNICA DI CARATTERIZZAZIONE GEOTECNICA DEL SITO*)

4.1 Factors influencing the erosion threshold of the sea-bed in the Lagoon of Venice

Amos et al. ([13], [14]) provides a description of two surveys undertaken in Venice Lagoon during the summer of 1998 and the subsequent winter using two benthic annular flumes: Sea Carousel and Mini Flume. Interpolated plots of the distribution of erosion threshold throughout Venice lagoon are shown in Figure 22 (A and B) for summer and winter, respectively.

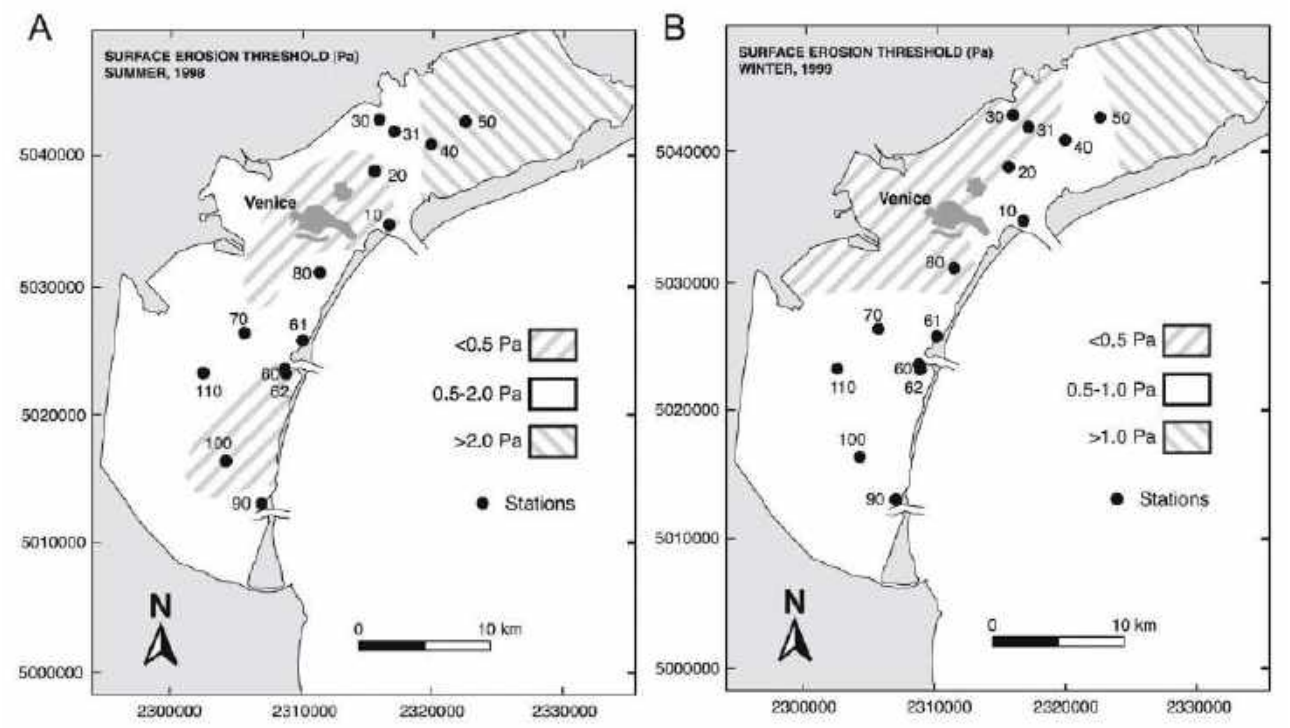

Figure 22. The sites occupied during the summer (A) and winter (B) surveys of Amos et al. [13]. Also shown are the regions of surface erosion threshold (τ_c) interpolated across the entire lagoon. Notice that in both periods, the highest threshold is found in the northern lagoon, and the lowest in a broad region around the city of Venice (after Amos et al., [14]).

The summer thresholds were significantly higher (t_c =1.10 ± 0.69 Pa) than winter ones (t_c = 0.66 ± 0.27 Pa). Highest strengths were in the northern lagoon and the lowest were in the central and southern lagoon. The inter-tidal region exhibited the highest strengths (Figure 23).

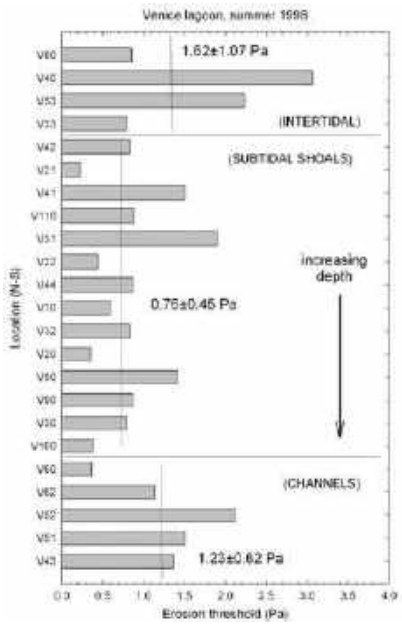

Figure 23. Surface erosion thresholds for the summer survey plotted against relative depth. Notice that erosion threshold peaks in the inter-tidal region (1.62 ± 1.07 Pa) and in the channels (1.23 ± 0.62 Pa) and is least in the sub-tidal muddy shoals (0.76± 0.45 Pa) (After Amos et al., [14]).

A secondary peak in strength was found in the deepest stations, and the lowest strengths were associated with the sub-tidal muddy shoals.

Regions of low strength (<0.5 Pa) appeared to coincide with regions of high boat activity; that is around Venice and where bottom fishing for *Tapes Phillipinarum* (the Manilla clam) is intense.

The greatest heterogeneity (or patchiness) was found amongst intertidal stations (τ_c = 1.62 ± 1.07 Pa) and was greater during summertime than winter. Highest erosion thresholds were found in the inter-tidal region during summer and were strongly influenced by seabed habitat type and depth. The lowest thresholds were associated with ‘‘bare’’ subtidal mud shoals (τ_c =0.76 ± 0.45 Pa) followed by the channel margin sand shelly bottoms (τ_c =1.23 ± 0.62 Pa).

During winter, there was much less variation in threshold with water depth. The highest thresholds were again in the northern lagoon (τ_c =0.71 ± 0.32 Pa) and lowest in the central and southern lagoon

(τ_c =0.57 ± 0.11 Pa). There was a weak inverse relationship between erosion threshold and friction coefficient suggesting that poorly consolidated materials were of greater resistance. This supports the fact that stability is largely brought about by low-density biofilms and bio-stabilisation.

Winter data from the Venice experiment suggest low bio-stabilization. Considering the almost stable bed condition, a simple first best fit regression of the bed shear stress (t_c) as a function of bed density (ρ_b) was proposed by Amos et al. [13] as follows:

$$\tau_{cp} = 5.44 \cdot 10^{-4} (\rho_b) - 0.28 \text{ Pa} \quad (1)$$

Where t_{cp} is a predicted value of surface strength due to bed density. Since the relationship resulted from low biostabilisation condition, the relationship is interpreted as neutral stability, as it is expressed only in term of bed density. Biostabilisation should add to the strength, bioturbation should reduce it.

The biostabilization Index (BI) can be obtained by:

$$BI\ (\%) = 100\ (\tau_c / \tau_{cp}) \quad (2)$$

An important derivation of the analysis by Amos et al. [13] in summarized in Fig. 3, which illustrates the data derived from Sea Carousel over the lifetime of its use, also considering a large variability of wet bulk densities, also not found in the Lagoon of Venice. The ‘‘solid’’ region refers to ρ_b > 1400 kg/m^3 and all the examples from Venice Lagoon fall within this region.

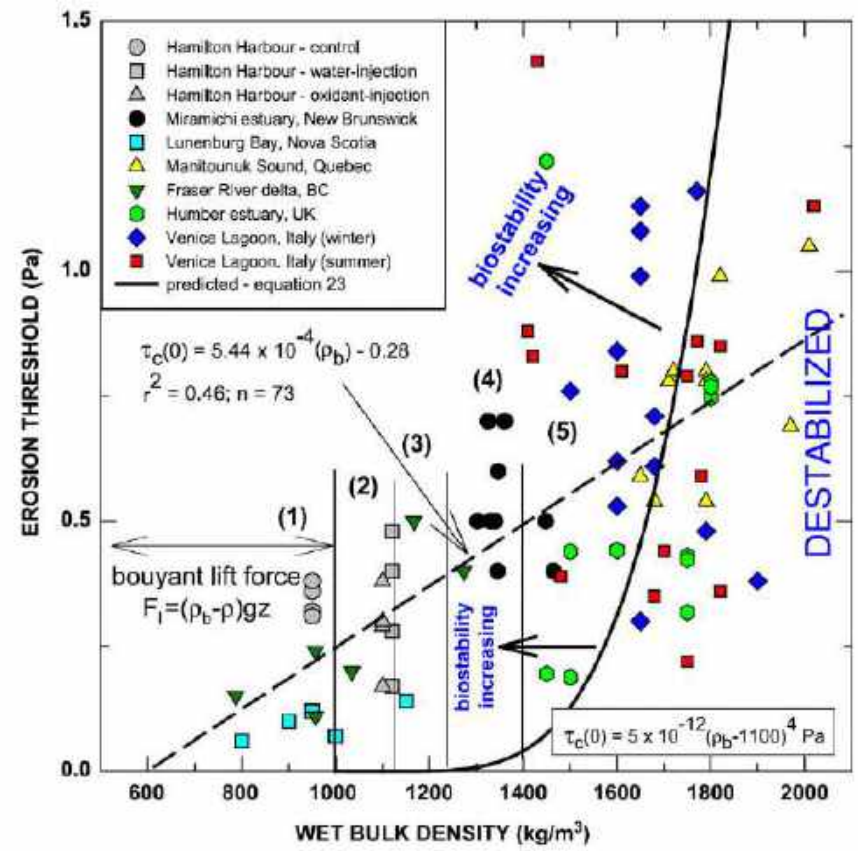

Figure 24 *A detailed scattergram of surface sediment erosion threshold stress and wet sediment bulk density for a wide range of sites monitored using Sea Carousel. The best-fit regression line of all data is shown as the dotted line (see Eq. 1). Five regions are illustrated: (1) buoyant (gassy) beds; (2) mobile fluid muds; (3) dense fluid muds; (4) stiff mud (solid, 10 years old); and (5) hard mud (solid, 100 years old) following van Rijn (1993). The solid line (Eq. 3) attempts to satisfy the laboratory analyses of sediment behaviour at the liquid limit (ρ_b ~ 1100 kg/m^3) and the assumption that the erosion threshold of silica (ρ = 2650 kg/m^3) may be considered as infinite. The curve was fitted to data from Canadian Arctic, hence neutral. On the basis of this fit, regions of disturbance and biostabilization may be defined (After Amos et al., [13]).*

The trends in Figure 24 may be examined more rigorously by the following arguments: (1) Neutral bed strength should go to zero at 1100 kg/m^3 bed density, since this value represents the onset of stationary fluid muds; (2) bed strength should approach infinity as $\rho_b \rightarrow$ 2600 kg/m^3, as this reflects solid rock; and (3) a neutral relationship (bed density vs. critical shear stress) needs to consider neutral material (nor bioturbated, nor biostabilized), as those coming from the Arctic (triangle symbol, Quebec).

A neutral relationship has been fitted by iteration to fit the two density limits and pass through the Arctic data. This relationship has the form:

$$\tau_c = 5 \cdot 10^{-12} (\rho_b - 1100)^4 \text{ Pa} \quad (3)$$

where all units are SI.

This power function is reported as a solid curve in Figure 24. Data falling towards the left of the line are interpreted as biostabilized, and those falling to the right are considered disturbed (perhaps bioturbated).

These conditions can be associated to the different values of critical shear stress found during the experiment, as synthesized in Figure 25.

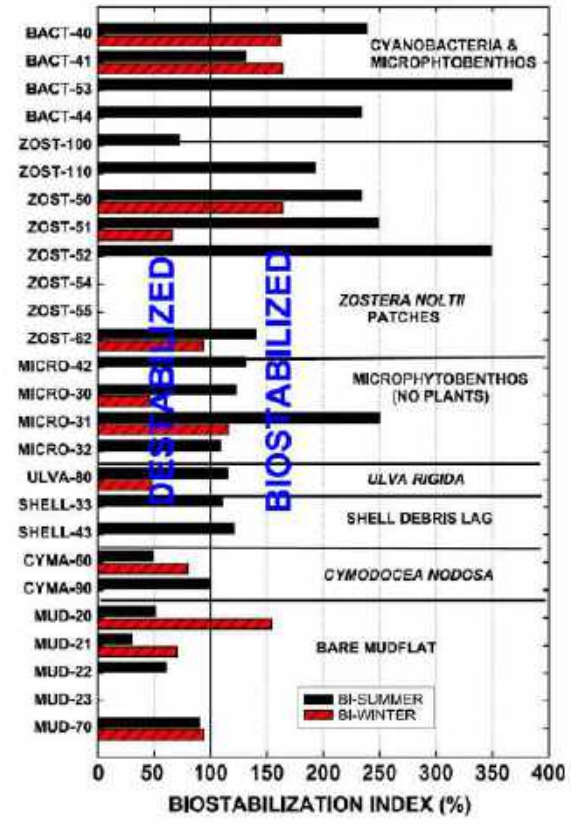

Figure 25. The Biostabilization Index from Sea Carousel measured during summer (August) 1998. The sites have been clustered and ranked into principal bed types according to their ability to stabilize their substrate: (1) filamentous cyanobacteria (2) Zoostera noltii (3) surficial microphytobenthos [(4) shelly lag (5) Ulva rigida (6) Cymodocea nodosa and (7) sublittoral bare mud. The plot is subdivided into biostabilized (BI>100%) and destabilized regions (BI < 100%) and shows that the lagoon bed is more stabilized during the summer, and perhaps even destabilized during the winter (After Amos et al., [13]).

The highest BI (486%) was found in northern Venice Lagoon at a site dominated by filamentous cyanobacteria (BI = 244%). Intermediate biostabilization was evident at sites occupied by *Zoostera nolti* (BI = 206%) and on mudflats dominated by surface microphytobenthos (BI = 153%). Low biostabilization was found at sites occupied by *Ulva rigida* (BI = 115%), shell debris (BI = 111%) and *Cymodocea nodosa* (BI = 74%). Finally, bare mudflats appeared to be destabilized (BI = 58%) and of low strength.

Mean erosion rates (E_m) found by Amos et al. [13] [14] at a given stress were higher in Venice than those reported in other studies and were best simulated by the expression:

$$E_m = \chi \tau_s^{\beta} \qquad \text{kg/m}^2\text{/s} \qquad (4)$$

where the mean summer and winter values of χ and β were 0.0029 and 0.99, and 0.0012 and 2.13, respectively. This expression lacks a critical value, and thus, it should be used only in cases where the flow exceeds the appropriate erosion threshold.

Erosion rate (E) was better expressed as a function of excess bed shear stress than absolute stress. The summer form is:

$$E = 9.46 \cdot 10^{-4} (\tau_0 - \tau_{crit,z})^{0.87} \quad \text{kg/m}^2\text{/s} \qquad (5)$$

The mean wintertime erosion rate is defined by:

$$E = 6.02 \cdot 10^{-3} (\tau_0 - \tau_{crit,z})^{1.23} \quad \text{kg/m}^2\text{/s} \qquad (6)$$

These functions are lagoon-averaged and hence generally applicable within Venice lagoon. Erosion resistance ($\tau_{crit,z}$) increased as a power function of depth of burial (z) in the form:

$\tau_{crit,z} = 1.74\ z^{0.09}$ for the northern and central lagoon, and in the form:
$\tau_{crit,z} = 1.27\ z^{0.10}$ for the southern lagoon.

4.2 Possible implication/applications

The results of the only experiments on bed erosion threshold conducted in the Venice Lagoon (and more broadly in a lagoon as a whole) are crucial for a correct modeling approach, because the erosive effects caused by hydrodynamic forcings are typically simplified using a single mean value of threshold bottom shear stress for cohesive bed erosion, set at 0.7 Pa.

Petti et al. [15], in assessing the siltation processes of tidal channels in the Marano-Grado Lagoons used two different types of sediment for the computational approach: a granular sediment with a mean diameter set equal to 180 μm and a cohesive one with a mean diameter set equal to 30 μm, according to the available grainsize dataset (Figure 26). To assign the threshold bed shear stress they carried out a scrupulous work of comparison, by means of morphological similarity, with the critical shear stress values determined by Amos et al. [13]. Authors adopted a morphological similarity criterion, considering representative mean values for the critical erosion shear stress, chosen from the available measurements by Amos et al. [13], ranging from 0.7 Pa to 1.8 Pa, with the addition of a new category, related to anthropogenic stressors (Figure 27):

- Marshes and highest intertidal flats, wet only by the high tide, with the highest critical shear stress (1.8 Pa);
- Permanently submerged lowest mudflats and subtidal flats, with the mean critical shear stress already adopted in the Venice Lagoon (0.7 Pa);
- Tidal flats occupied by the seagrass in patches that covered 20–60% of the sea-bed, assumed partially stabilized with a critical shear stress of 1.2 Pa. The increased threshold is also justified by the test results by Thompson et al. [16].
- the last new category refers to the mudflats that are subject to greater mobility of the cohesive sediment. This class is characterized by a lower critical erosion value, set equal to 0.5 Pa. It refers, for example, to areas used for shellfish farming, where the resuspension of sediments is comparable to that induced by the wave motion during storm conditions.

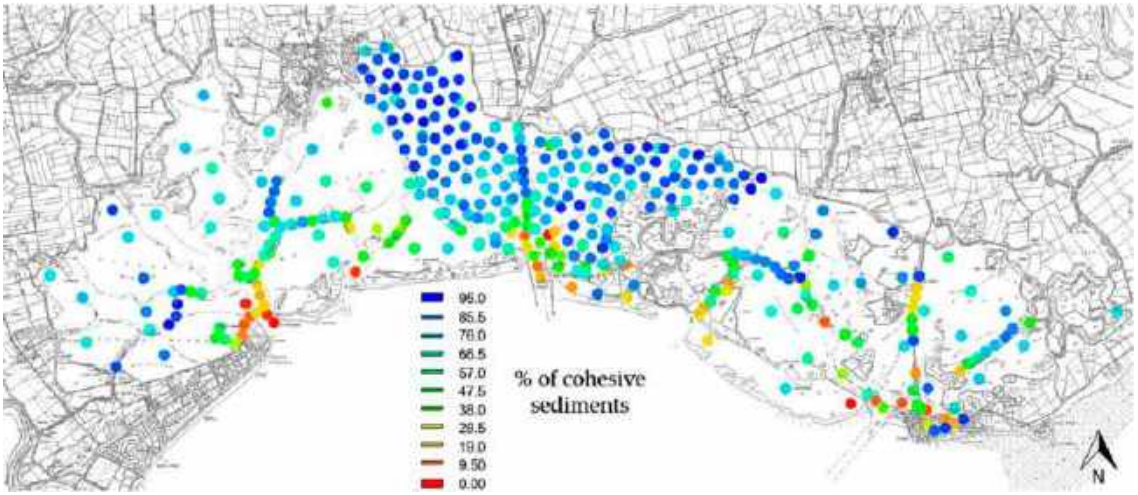

Figure 26. Sediment samples and grainsize data used for the definition of the bed shear stress in the hydrodynamic simulation of the Marano and Grado Lagoons (after Petti et al., [15])

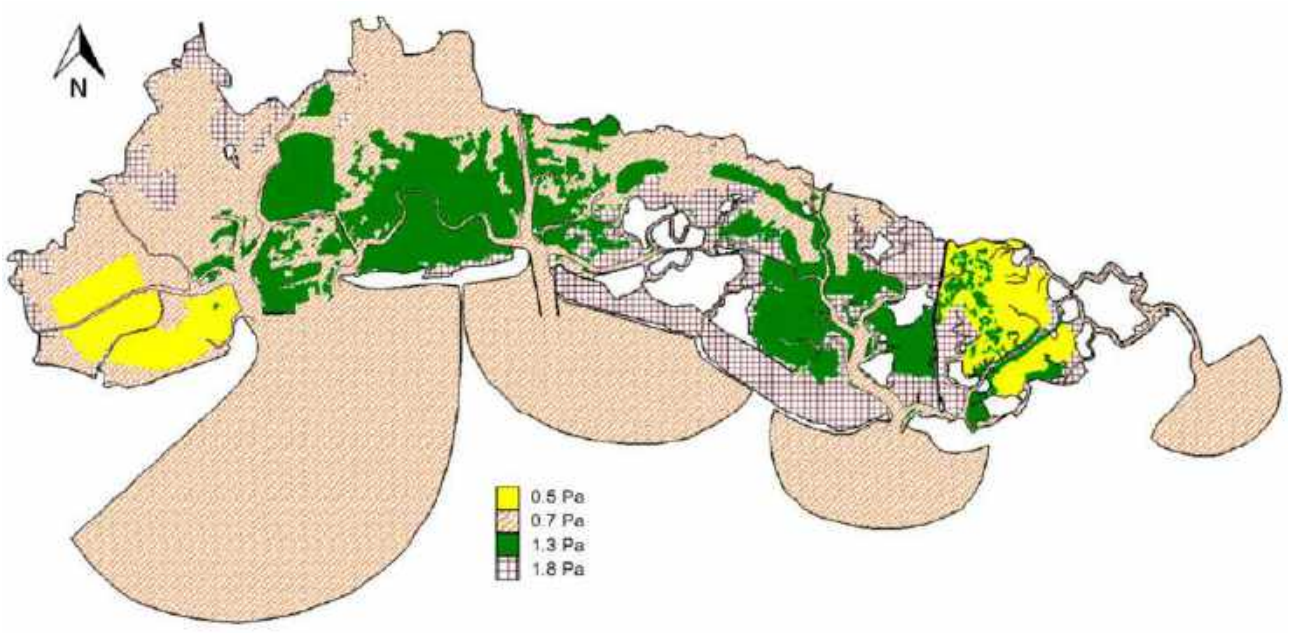

Figure 27. Different distribution of the bed shear stress assumed for the hydrodynamic simulation of the Marano and Grado Lagoons (after Petti et al., [15])

4.3 Data to use

Petti et al. [15]'s approach could be employed for the specific modeling of the simulation to be undertaken for assessing the effects of various Malamocco-Marghera channel designs and marine traffic on the surrounding intertidal and subtidal muddy flats.

In light of the findings of Amos et al. [13] [14] and their available dataset (summarized in Table 7) , we need to gather additional data to improve the reconstruction of the bed shear stress distribution as a mandatory input for modeling:

Table 7. Summary of the sea-bottom characteristics for critical shear stress assessment (after Amos et al. [13] [14]. See Figure 22 for the reference sample points. (C.n. = Cymodocea nodosa; U.r. = Ulva rigida; d50 = median in microns).

sample	characteristics	others	ρb (kg/m3) Summer	ρb (kg/m3) Winter	d50 Summer	d50 Winter	τc Summer	τc Winter	τc average
20	bare mudflat		1763	1803	28	16	0.35	1.08	
21	bare mudflat		1843		33	20	0.22	1.13	
22	bare mudflat		1840		33		0.44		
70	bare mudflat	large ship effect	1720	1710	58	28	0.59	0.61	0.63
10	Cymodocea nodosa cover		1975						
60	Cymodocea nodosa cover	shelly sand with C.n.+U.r.	1865	1728	74	21	0.36	0.53	
62	Cymodocea nodosa cover	shelly sand with C.n.+U.r.			81	39			
90	Cymodocea nodosa dense mat		2100				0.86		0.58
33	high intertidal flat		1833		20		0.79		
40	high intertidal flat		1672	1672	22	26	3.06	0.84	
53	high intertidal flat		1630		16		2.23		
80	high intertidal flat	Ulva rigida	1865	1960	30	16	0.85	0.38	1.36
30	microphytobenthos		1705		23	46	0.80	0.3	
31	microphytobenthos		1909	1718		19	1.90	0.76	
32	microphytobenthos						0.83		
42	microphytobenthos				22		0.83		0.90
50	Zoostera noltii 20-60%		1630	1691	10	24	1.42	0.99	
51	Zoostera noltii 20-60%			1857		23	1.51	0.48	
52	Zoostera noltii 20-60%						2.12		
53	Zoostera noltii 20-60%		1630		16		2.23		
61	Zoostera noltii 20-60%		1992				1.13	0.62	
100	Zoostera noltii 20-60%		1495		21		0.39		
110	Zoostera noltii 20-60%		1352		23		0.88		1.18
41	not specified			1824	21	36	1.51	1.16	
43	not specified						1.37		
44	not specified		1820		32		0.86		
71	not specified					19		0.71	1.12

1) detailed grainsize distribution of the sediments
2) information on the bulk density of sediments, or its relationship with grainsize, if available from literature, possibly in the same or similar environment
3) detailed distribution of sea grass

4) information on clam fishing activity and concessions, as a fundamental forcing able to induce significant changes in the geotechnical parameters of the sea-bed.

Herein a synthesis of the collected information and available data.

1. Grain size distribution

For the lagoon of Venice, a large grainsize dataset is available. The first sedimentological map is referred to Barillari & Rosso [17] and Barillari [18], and reported using the Shepard [19] classification (Figure 28).

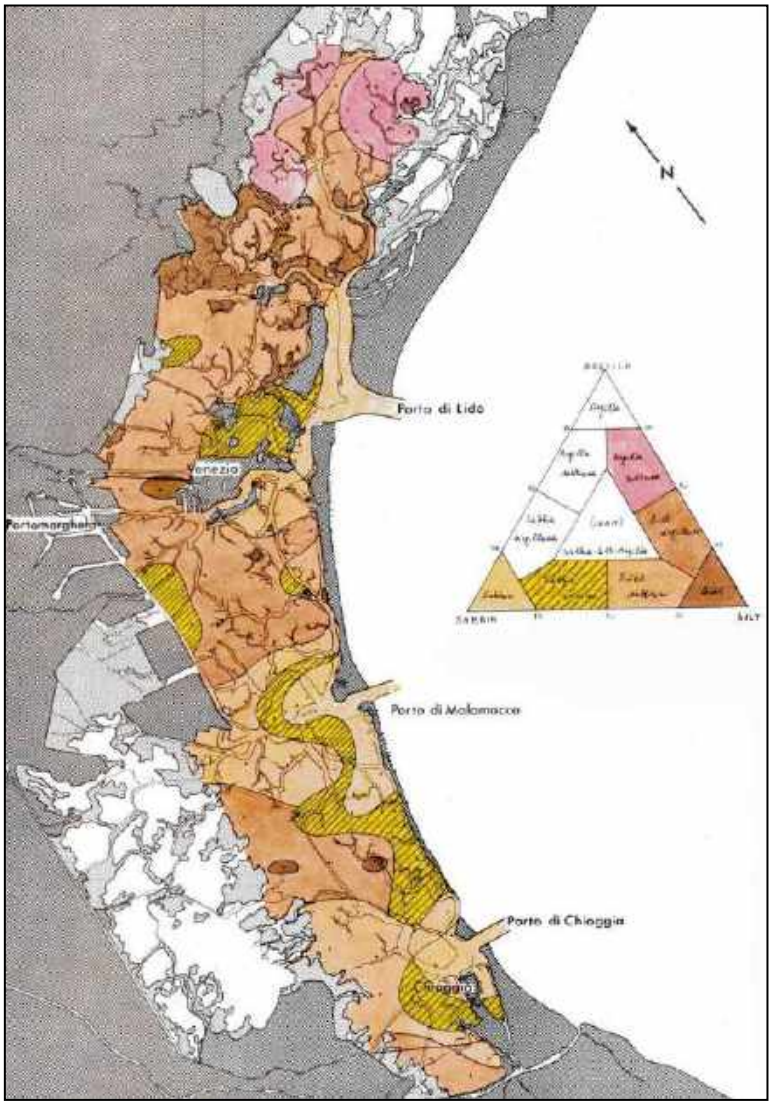

Figure 28. Sedimentological map of the Venice Lagoon. The classification is according to Shepard [19] (after Barillari & Rosso [17]; Barillari [18]).

Successive available samples, as well sediment distributions are reported and compared by Molinaroli et al. [20]. Information reported by Molinaroli et al. [20]refer to a different dataset for the 1970s samples. The oldest dataset is referred to as “GM70”, i.e. samples from the first campaign carried out in 1976-78 by the “Sezione Geo-Mineralogica” of Venice Ca' Foscari University, resulting in a total of 162 samples. The second set of samples was collected in the year 2002 by CNR-ISMAR, referred to as “UI00”, resulting in a total of 140 samples.

Data have been used for the *Atlante della Laguna di Venezia* and are available in the WebGis http://www.atlantedellalaguna.it.

In Figure 29 the complete available dataset is reported as synthetic maps compiled from the WebGis, which include also a third intermediate collection dated 1983-84.

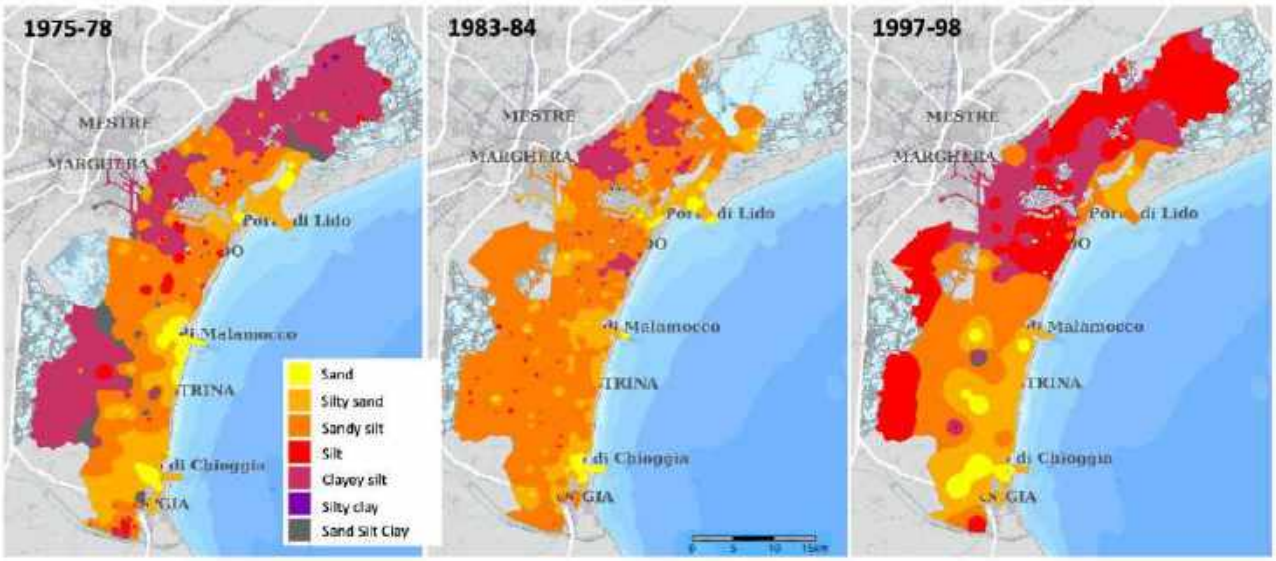

Figure 29. Sedimentological map of the Venice Lagoon. The classification is according to Shepard [19] (redrawn from http://www.atlantedellalaguna.it; Molinaroli et al., [20]).

The main results of a detailed GIS-based comparison of bathymetry, grain-size and morphology from data collected in 1970 and 2000 can be derived by the residuals of the sand contents (Figure 30). Molinaroli et al. [20] synthesized as follows:

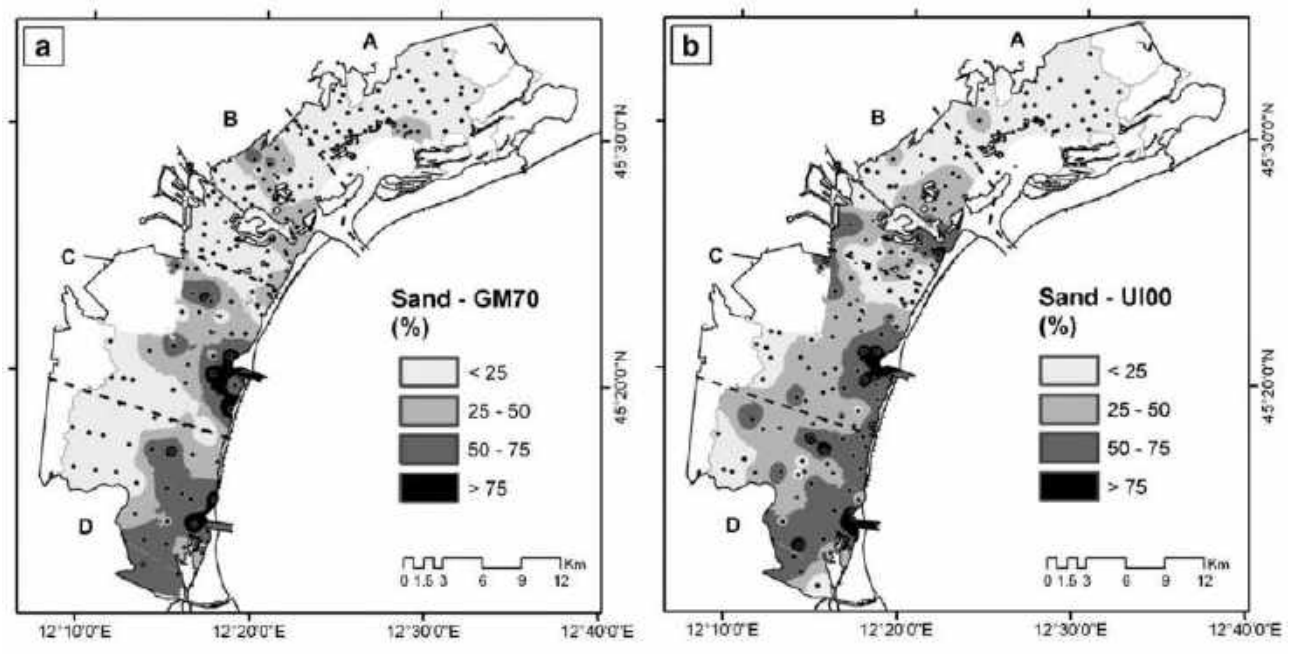

Figure 30. Changes in spatial distribution of sand in the 1970s and in the 2000s (after Molinaroli et al., [20]). A: Treporti sub-basin, B: Lido sub-basin, C: Malamocco sub-basin, D: Chioggia sub-basin).

1) The Lagoon of Venice is not a single lagoon, but rather is subdivided into four sub-basins: changes occurring during the 30-year period are specific to each sub-basin due to variations in sediment input, erosion versus deposition, hydrodynamic energy and land-use.
2. There has been a general reduction in the frequency of depths of −0.60/−0.80 m, combined with a general increase in frequency of elevations of −1.00/−1.20 m in sub-basins of Lido and Chioggia, and up to −1.80 m in Malamocco sub-basin. This shift has caused a flattening of the lagoonal morphology with a concomitant transition from intertidal flats to subtidal flats (~30 km^2) and from subtidal flats to open lagoon conditions (~60 km^2).
2) The recorded deepening of tidal flats (by approximately 20 cm) is to be ascribed more to decreased sediment supply, disappearance of seagrass and clam fishing than to the relative sea level. Changes in the bathymetry and grain size distribution of the central and southern basins of the Lagoon of Venice are probably due to changes in tidal currents, bed shear stress from wind waves and fetch length.
3) More than 50% of the lagoon experienced erosion in the 30-year period, only 25% remaining stable. Comparison of sediment types shows that all basins experienced depletion of the fine-

grained sediments (<22 μm), and a shift in sedimentary facies from lower to higher energy patterns.

4) On the basis of detailed grain-size analyses, the paucity of ~8 μm particles in the frequency distribution roughly separates the population into two classes: sortable silts and aggregated fine silty clays.

The newest dataset concerning the grainsize distribution of lagoon sediments, is reported by Zonta et al. [21], and is assumed as the reference data to use for the modeling purposes.

Dataset consists of sediment cores collected at 380 sites distributed throughout the shallow areas of the lagoon (Figure 31) in early 2008.

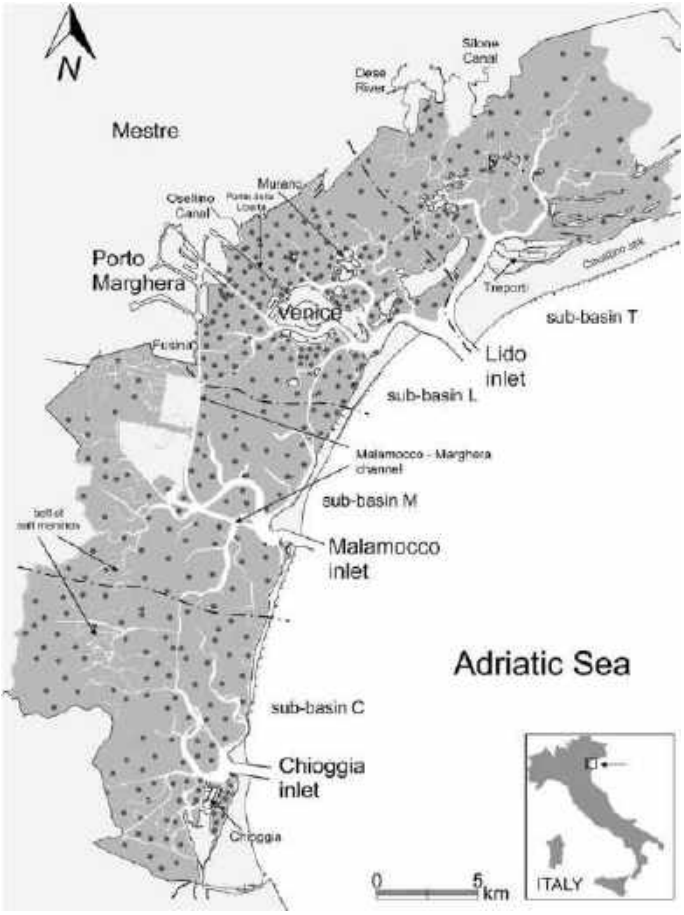

Figure 31. Location of the sediment samples collected in the 2008 campaign (after Zonta et al., [21]). Broken lines depict sub-basin (T, L, M, C) boundaries.

The large number of sampling sites ensured coverage of at least one site per 2 km^2. 50 cm-long cores were collected in each site and sectioned into five depth intervals named: A (0–5 cm), B (5–10 cm), C (10–20 cm), D (20–30 cm) and E (30–50 cm).

Sediment particle size distribution in the Venice Lagoon reflects the presence of two gradients: the first is generated by the three inlets and is characterised by a fining of sediment from the inlet toward the inner lagoon; the second is due to the greater supply of finer sediment to the northern sub-basins from the freshwater tributaries, resulting in a coarsening of particle diameters from the northern sub-basin of Treporti (T) towards the southern sub-basin of Chioggia (C). These gradients are observed in both buried and surface sediments. However, in a majority of sites, strong depletion of finer particles was observed in the surface (ca. 10 cm) sediment layer with respect to the deeper ones (Figure 32 and Figure 33). This occurs in all four sub-basins, including the Treporti sub-basin, which is more “pristine” and less affected by the impact of anthropogenic activities.

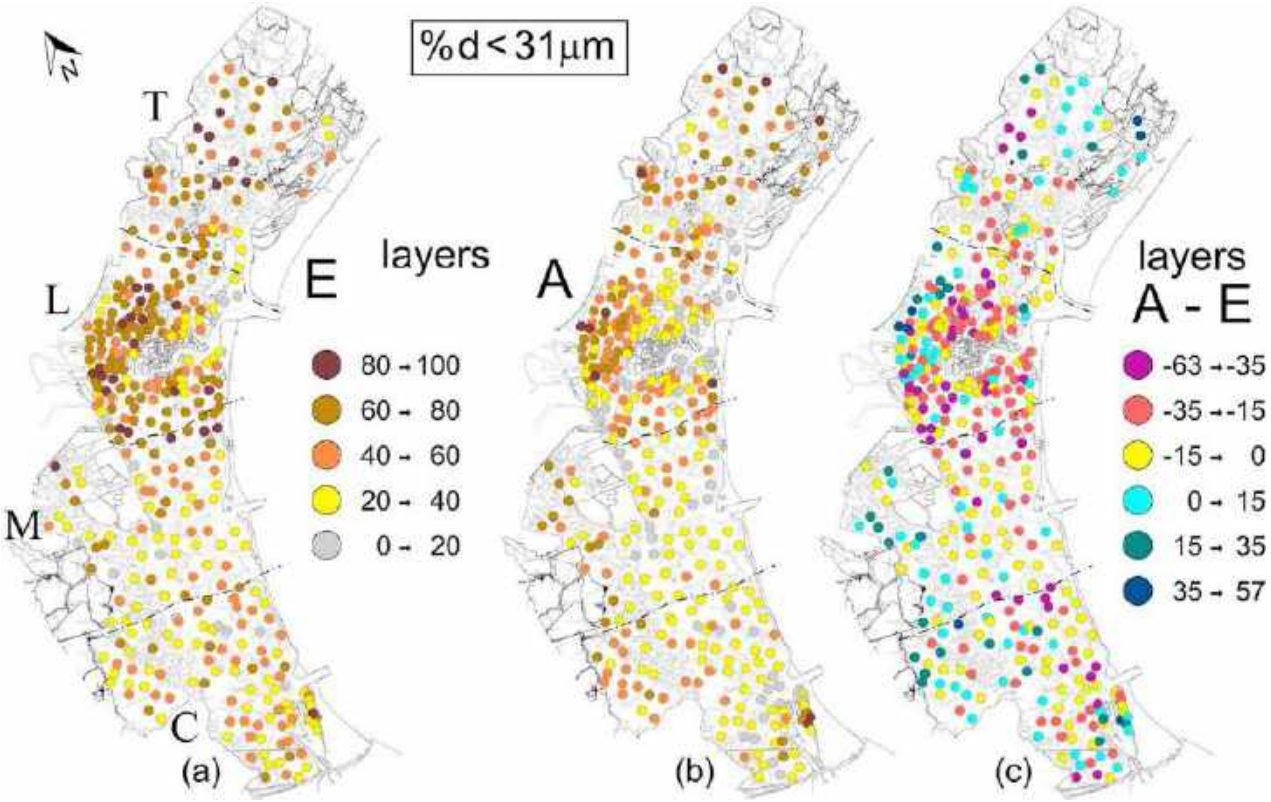

Figure 32. Spatial distribution of fine mud (d < 31 mm fraction, in %) in a) the deepest layer E (30-50 cm), and b) the surface layer A (0-5 cm), for all 380 sampling sites. c) Differences between fine mud percentage in layer A and E (after Zonta et al., [21]).

Relative depletion of finer particles in the surface layer occurred in all settings, but was particularly evident in moderately erosional and stable conditions, which together account for 70% of sites. The corresponding areas are chiefly responsible for the deficit of finer particles in the lagoon, which is progressively changing to a more marine, flatter and deeper system, with the loss of typical morphological structures linked to the estuarine complexity, such as salt marshes, secondary channels and tidal creeks, and the general loss of finer particles toward the Adriatic Sea (Figure 34)

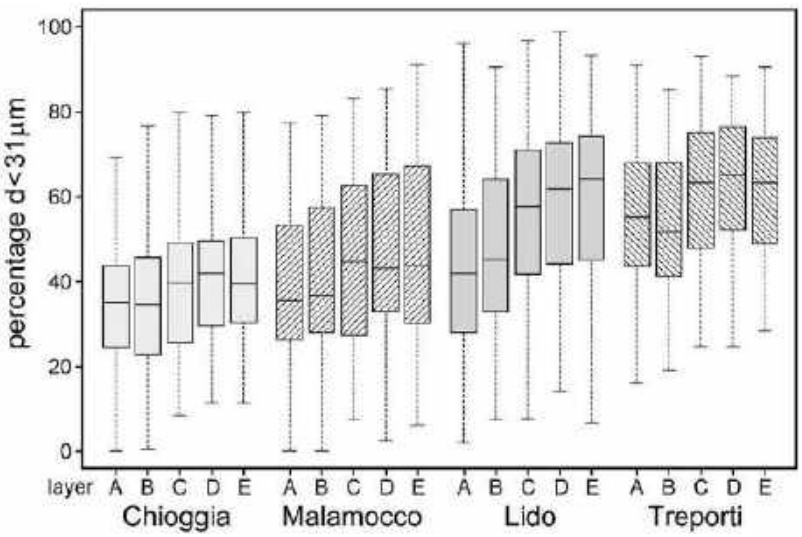

Figure 33. Box-plot of medians and percentiles (25% and 75%) of fine mud (d < 31 mm fraction, in %) in the five layers (A-E) for the four sub-basins (after Zonta et al., [21]).

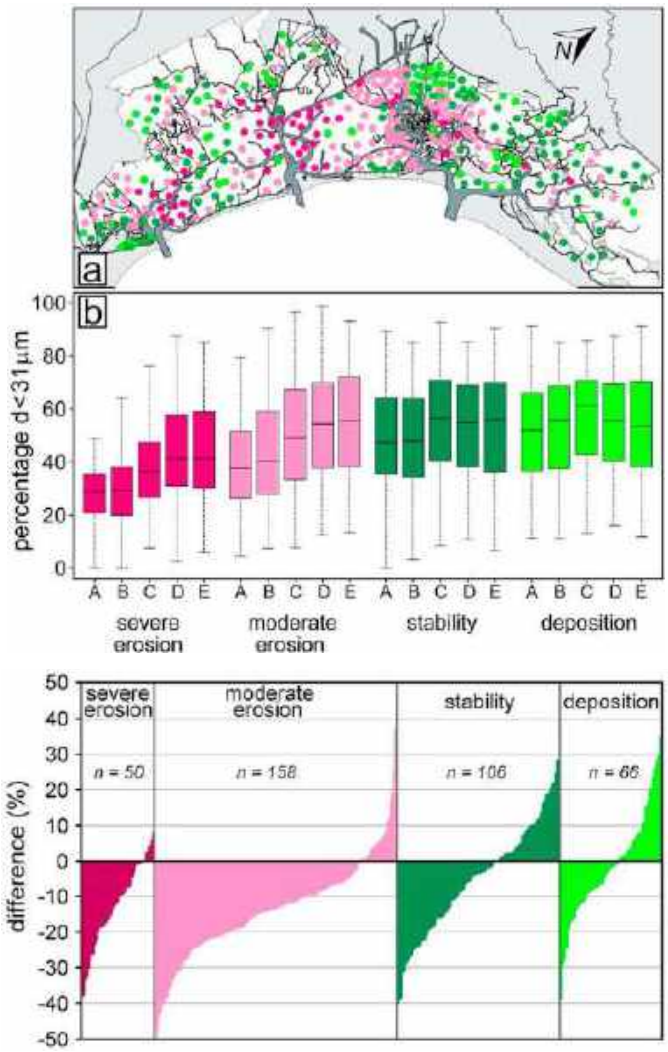

Figure 34. a) Subdivision of sampling sites into four classes of erosional/depositional conditions in accordance with Sarretta et al. [22]; b) Box plot of medians and percentiles (25% and 75%) of fine mud (d < 31 mm fraction) in the five layers (A-E), subdivided in accordance with erosional - depositional conditions. Lower scheme: differences in mean fine mud content (d < 31 mm) between deep layers (D and E) and upper layers (A and B). Data are grouped into four classes of erosional/depositional conditions and plotted in ascending order within each group. Negative values correspond to a coarsening effect in the upper sediment layers. (After Zonta et al., [21]).

The diminution of fine particle content in the upper sediment layers in stable and particularly in depositional sites is a worrying trend. This is a signal that sediments are being affected by the altered environmental conditions (increased hydrodynamics and fewer finer particles in the water column), which result in the formation of coarser sediments and may trigger substantial modifications in areas of the lagoon that still maintain sediment typical of transitional environments.

2) Information on the bulk density of sediments, or its relationship with grainsize

A reliable relationship between bulk density and grainsize in a similar environment (Po delta lagoons) is reported by Zonta et al. [23]. Advantage in the use of these relationship is that bulk density is derived by CT scan, the same procedure used by Amos et al. [13]. In such a way, the dataset of grainsize by Zonta et al. [21] can be converted in bulk density, thus obtaining a theoretical bed shear stress, using Eq. 3. Data can be then controlled for the presence of the other constraints, as fishing concession (thus reducing the shear stress) or sea-grasses, that tend to increase the same parameter.

5) Detailed distribution of sea grass

Dataset on sea grass distribution has been furnished by Port Authority. Other information is available in http://www.atlantedellalaguna.it. Maps constructed using the GIS layer (e.g. Figure 35) can be superimposed to the sediment information dataset, for the parameterization of the physical properties of the sea-bed.

Figure 35. Distribution of sea grass in the northern Lagoon of Venice (GIS layer furnished by the Port Authority).

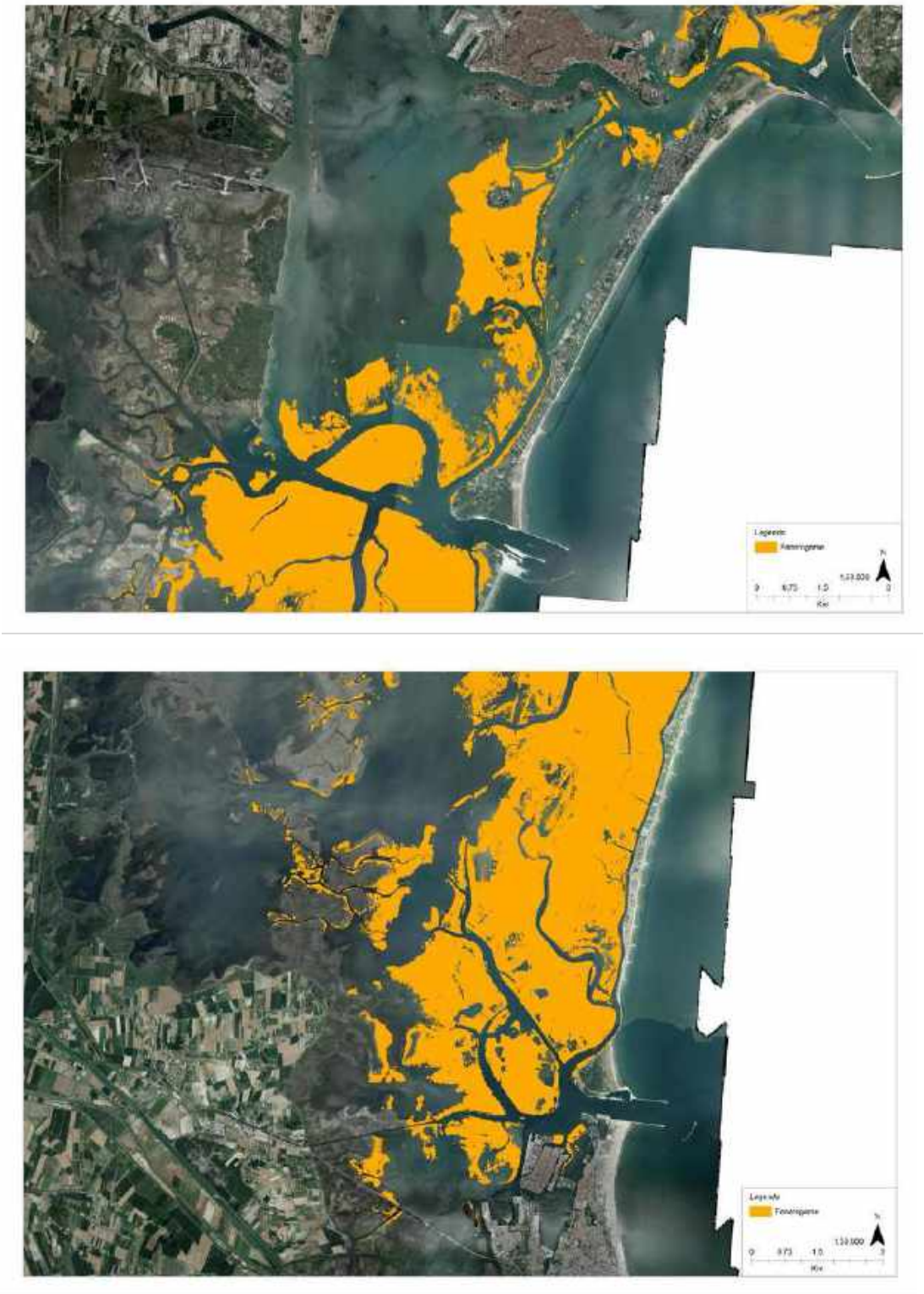

Figure 36. Distribution of sea grass in the central and southern Lagoon of Venice (GIS layer furnished by the Port Authority).

If it is necessary to discriminate among the different species, the latest dataset (2010) available in http://www.atlantedellalaguna.it reports the distribution of the various species of *Zoostera* and *Cymodocea* (Phanerogams) (Figure 37).

6) Information on clam fishing activity and concessions

This information is already available as inserted in the Morphological Plan. The updated reference document is *Piano d'Uso delle Aree in Concessione per la Venericoltura* by San Servolo s.r.l. (Pessa et al. [24]) which reports the details of the old and new concession, easily transferable in GIS for the superimposition with the sediment GIS layers. An example of the map reporting the concessions is given in Figure 38.

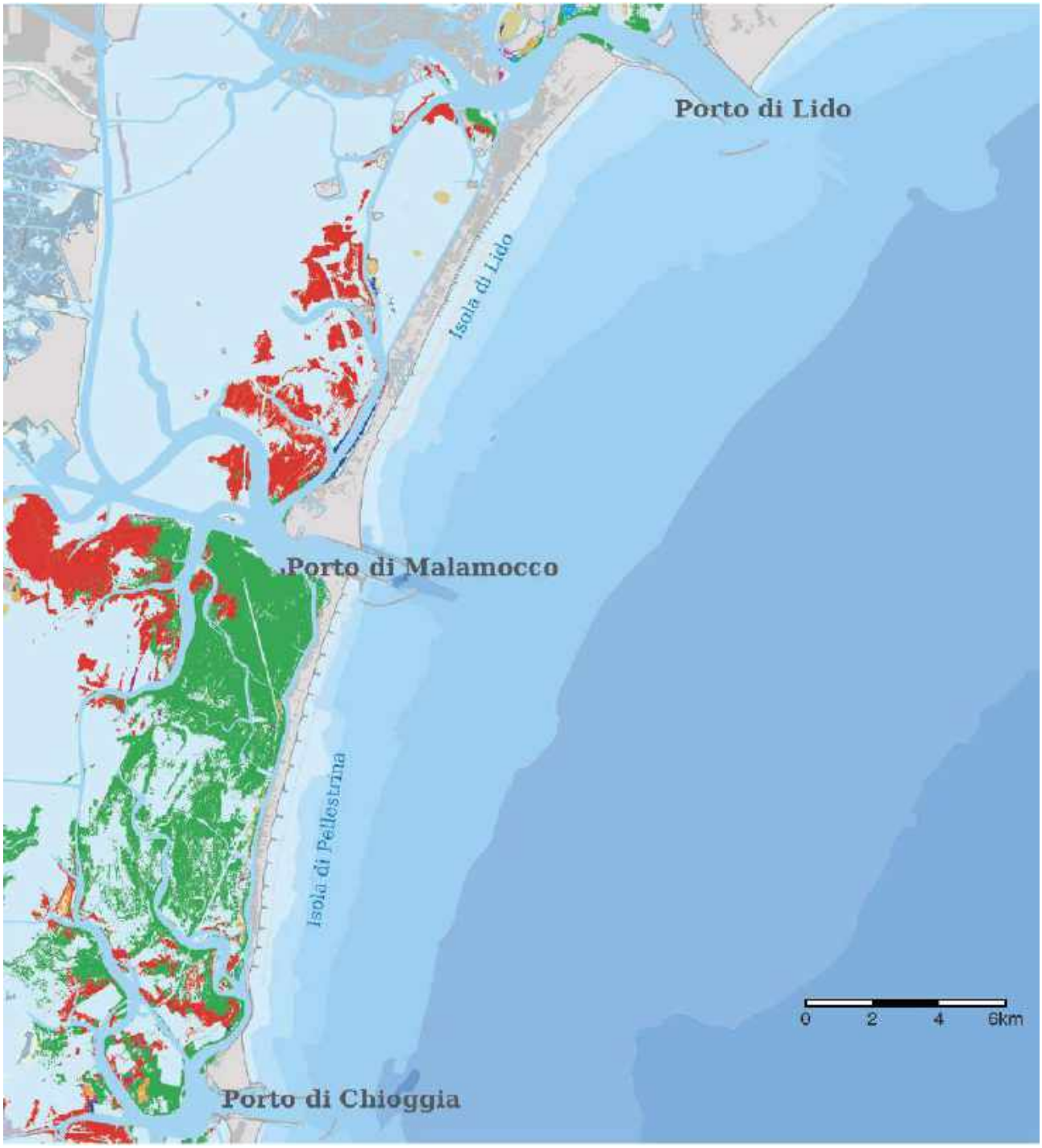

Figure 37. *Distribution of sea grass (2010) as reported in the WebGis at http://www.atlantedellalaguna.it. The green layer is Cymodocea nodosa, the red one is Zoostera marina.*

Figure 38. *Central Lagoon: differences between the surfaces of the required concessions (April 2018) and those of May 2015 (red contour) are shown in the colors of the map. The areas to abandon are shaded in yellow, and the areas of new demand are shaded in green (after Piano d'Uso delle Aree in Concessione per la Venericoltura, [24]).*

5 PRELIMINARY TECHNICAL REPORT ON HYDODYNMIC MODEL PARAMETER CALIBRATION (RELAZIONE TECNICA PRELIMINARE PER LA CALIBRAZIONE DEI PARAMETRI DI SIMULAZIONE IDRODINAMICA)

5.1 2D model development

The MIKE 21 Flow Model is a modelling system for 2D free-surface depth-integrated flows developed and maintained by DHI. The model system is based on the numerical solution of the two-dimensional (2D) incompressible Reynolds averaged Navier-Stokes equations subject to the assumptions of Boussinesq and of hydrostatic pressure. The model is applicable for the simulation of hydraulic and environmental phenomena in lakes, estuaries, bays, coastal areas, and seas, wherever stratification can be neglected. The model can be used to simulate a wide range of hydraulic and related items, including tidal exchange and currents and storm surges.

The hydrodynamic (HD) module is the basic module in the MIKE 21 Flow Model. It simulates water level variations and flows in response to a variety of forcing functions in lakes, estuaries, and coastal regions. The effects and facilities include:

- Bottom shear stress
- Wind shear stress
- Barometric pressure gradients
- Sources and sinks (e.g. rivers, intake and outlets from power plants)
- Flooding and drying
- Momentum dispersion
- Tidal potential
- Coriolis force
- Precipitation/Evaporation
- Ice coverage
- Wave radiation stresses

The model uses a flexible mesh (FM) based on unstructured triangular or quadrangular elements and applies a finite volume numerical solution technique.

For further details, see Appendix C.

The **MIKE 21 SW** model is developed, supported and maintained by DHI. Like other modules included in the flexible mesh series of MIKE by DHI, the wave model is based on an unstructured, cell-centered finite volume method and uses an unstructured mesh in geographical space. This approach, which has been available from DHI now for more than two decades and which is thus fully matured, gives the maximum degree of flexibility, and allows the model resolution to be varied and optimized according to requirements in various parts of the model domain.

MIKE 21 SW is DHI's state-of-the-art third generation spectral wind-wave model. The model simulates the growth, decay and transformation of wind-generated waves and swells in offshore and coastal areas.

MIKE 21 SW includes two different formulations:

- Fully spectral formulation
- Directional decoupled parametric formulation

The fully spectral formulation is based on the wave action conservation equation, as described in e.g. Komen et al (1994) and Young (1999). The parametrization of the source terms for wind input and dissipation terms (swell dissipation and whitecapping) are available in two formulations, i.e. Modified WAM Cycle 4 and Ardhuin et al. [25]. The directional decoupled parametric formulation is based on a parameterization of the wave action conservation equation. The parameterization is made in the frequency domain by introducing the zeroth and first moment of the wave action spectrum. The basic conservation equations are formulated in either Cartesian coordinates for small-scale applications or polar spherical coordinates for large-scale applications.

The discretization of the governing equation in geographical and spectral space is performed using cell-centered finite volume method. In the geographical domain, an unstructured mesh technique is used. The time integration is performed using a fractional step approach where a multi-sequence explicit method is applied for the propagation of wave action.

Due to its unique unstructured flexible mesh technique, MIKE 21 SW is particularly suited for simultaneous, i.e. in one single model domain, wave modelling at regional scale and at local scale.

Coarse spatial resolution is used for the regional part of the mesh and a higher resolution is applied in more shallow water environment at the coastline, around structures, etc.

MIKE 21 SW includes the following physical phenomena:

- Wave growth by action of wind
- Non-linear wave-wave interaction (quadruplet and triad-wave interactions)
- Dissipation due to white capping
- Dissipation due to bottom friction
- Dissipation due to depth-induced wave breaking
- Refraction and shoaling due to depth variations and currents
- Wave-current interaction
- Effect of time-varying water depth and currents
- Effect of ice coverage on the wave field
- Wave diffraction
- Wave reflection
- Influence of structures (like piers, wind turbine foundations, WEC, TEC)

Main computational features of MIKE 21 are:

- Source functions based on state-of-the-art 3rd generation formulations
- Fully spectral and directionally decoupled parameterized formulation
- In-stationary and quasi-stationary solutions
- Optimal degree of flexibility in describing bathymetry and ambient flow conditions using depth-adaptive and boundary-fitted unstructured mesh
- Coupling with hydrodynamic flow model for modelling of wave-current interaction and time-varying water depth
- Flooding and drying in connection with time-varying water depths
- Water-structure interaction module

- Parallelized using OpenMP and MPI techniques

For further details, see Appendix D.

The model utilizes a series of input which can be largely summarized in:

- Bathymetry: the sea bottom topographic description,
- Mesh: an unstructured grid for which governing equation are resolved at each node,
- Boundary conditions: a series of natural forcing providing boundary values to the system of differential equations resolved in the computational domain.

Furthermore, the model allows also for implementation of fixed structure as well as mobile barriers. Ponte della Libertà piers are accounted for as sub-grid structures using a drag-law to capture the increasing resistance imposed by the piers as the flow speed increases.

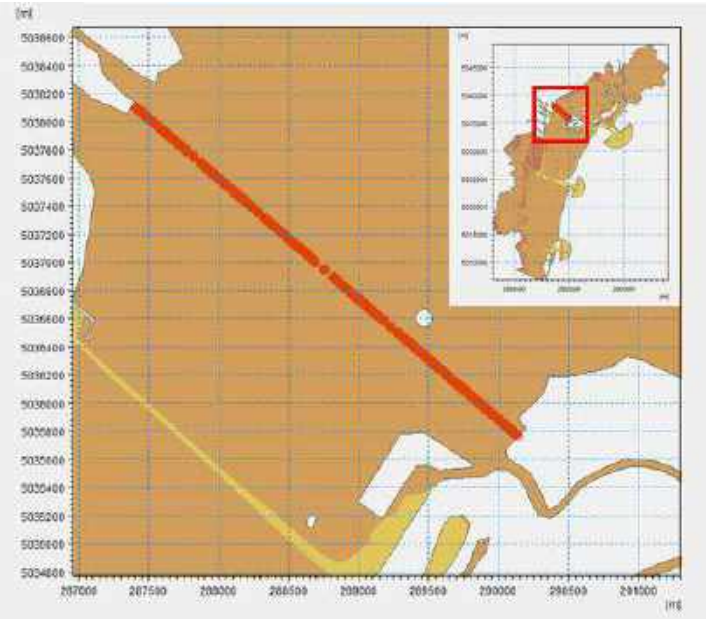

Figure 39. Ponte della libertà bridge piers model schematization.

The M.O.S.E. barriers are implemented in the model as a system of three gates structures whose operating time windows can be supplied as input to the model.

The operating time windows were derived by screening through observed water level timeseries inside and outside the lagoon identifying clear high-water events cut-off. For these periods the M.O.S.E. system was assumed to be operating.

The information derived by such analysis does not allow to differentiate barrier operating windows among the three inlets and therefore the scenario of partial closure of the lagoon is not accounted for, i.e. the three gates simultaneously raise and fall.

In absence of detailed information on the type of closure procedure the governing law passed to the model is of “Boolean” type, hence the three gates instantly close and open.

The M.O.S.E. closing period thereby derived are listed in Table 8.

Table 8. M.O.S.E. operating windows implemented in the model.

Closure window	Start time	End time
1	03/10/2020 08:10:00	03/10/2020 14:40:00
2	15/10/2020 07:00:00	15/10/2020 13:20:00
3	16/10/2020 07:10:00	16/10/2020 13:30:00
4	02/12/2020 05:20:00	02/12/2020 13:20:00
5	04/12/2020 22:05:00	06/12/2020 18:50:00
6	09/12/2020 03:50:00	09/12/2020 18:30:00
7	10/12/2020 04:15:00	10/12/2020 11:50:00
8	11/12/2020 04:20:00	11/12/2020 10:45:00
9	12/12/2020 04:00:00	12/12/2020 10:35:00
10	28/12/2020 06:00:00	28/12/2020 23:40:00
11	30/12/2020 04:10:00	30/12/2020 12:40:00
12	31/12/2020 06:00:00	30/12/2020 13:00:00

5.1.1 Bathymetry

The Venice lagoon is characterised by a complex network of channels intersecting a rapidly varying topographic system composed of shallow waters and tidal flat.

This overall complex bathymetric set-up contributes to generate a unique hydrodynamics inside the lagoon driven by wind and tides modified by the non-linear interaction with the bottom of the lagoon [5].

The presence of many islands and semi-submerged areas (called “barene”) increase the complexity of the circulation pattern [5].

Moreover, Venice lagoon throughout his history underwent radical morphological evolution mostly due to anthropogenic activities, in particular the excavation works carried out at the three inlets to cater for modern navigation requirements [26].

For this study it was not made available a single topographic survey covering the entire lagoon, thus several surveys carried out at different periods and related to different areas of the lagoon were instead used.

The resulting “hybrid” bathymetry was quality controlled from a qualitatively perspective, focussing mostly along adjacent and intersecting survey areas. A more quantitively quality control procedure was not possible due to the survey campaigns carried out in different periods and in an environment characterised by a marked morphodynamic processes.

Bathymetric surveys employed in this study are listed in Table 9.

Table 9. List of bathymetric datasets employed in the model

Source	Dataset number	Survey(s) date	Horizontal resolution [m]	Vertical datum	Area
Autorità di Sistema Portuale del Mare Adriatico Setten-trionale [27]	1	2002	1	IGM42	Figure 40
Provveditorato (Ex Magistrato delle Acque) [28]	2	2018	~100	IGM42	Figure 41
Autorità di Sistema Portuale del Mare Adriatico Setten-trionale [27]	3	2017 - 2021	1	IGM42	Figure 42
Consiglio Na-zionale delle Ricer-che [29]	4	2013	1	IGM42	Figure 43

As a general criterion for dataset selection, where possible the most recent survey was used, exceptions made for dataset (4) which provides a finer description for channels within the area covered by dataset (2).

Broadly speaking, dataset (1) was used as underling dataset for the entire lagoon and was cleaned up from overlaps with dataset (2) in the central part of the Lagoon and dataset (4) wherever bathymetric data for channels were available.

Dataset (3) is made of a number of surveys carried out between 2017 and 2021 including surveys taking place after 2021 dredging operations, and therefore of relevance for simulating navigation scenarios. Dataset (3) stretch from the Malamocco-Marghera channel, through Canale Vittorio Emanuele III, Canale della Giudecca up to Lido inlet.

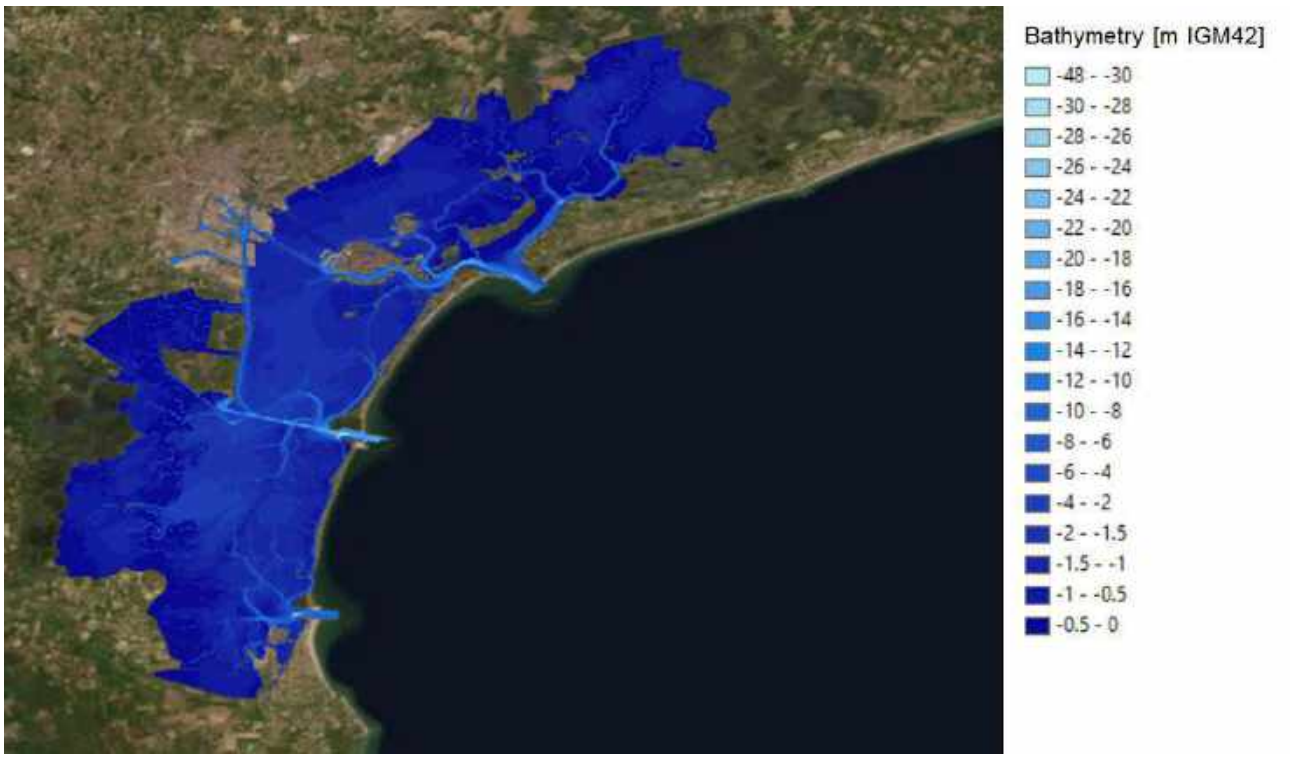

Figure 40. Bathymetry dataset (1).

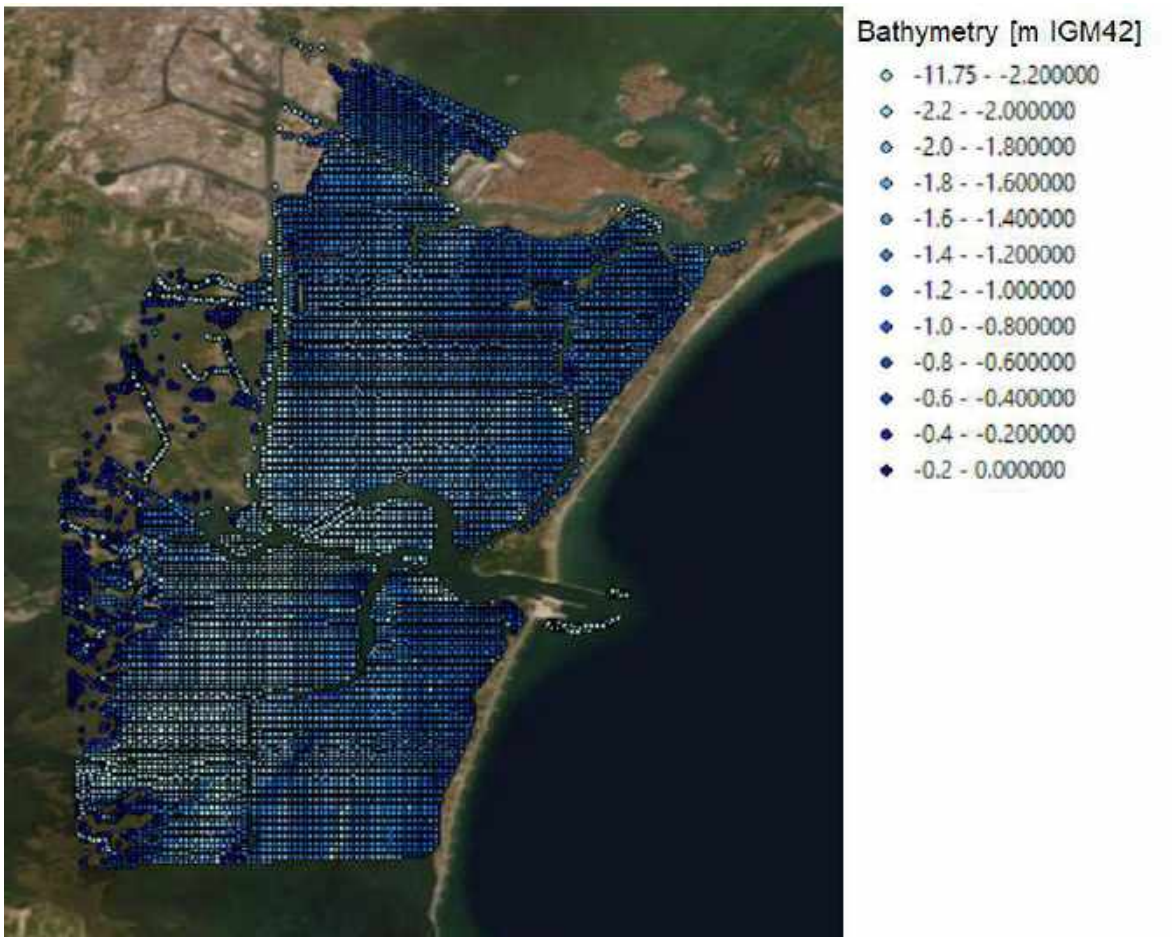

Figure 41. Bathymetry dataset (2)(colour scale values were chosen to highlight shallower areas)

Figure 42. Bathymetry dataset (3).

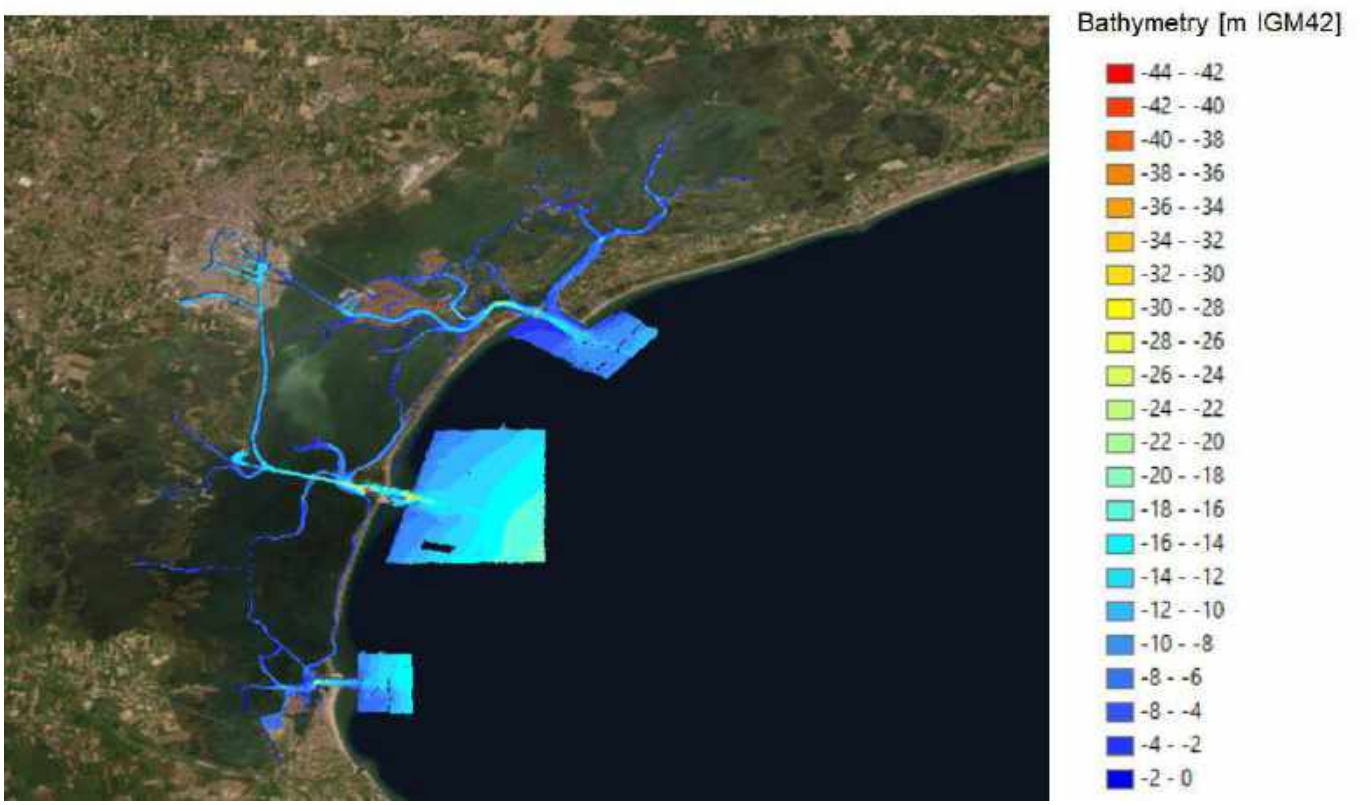

Figure 43. Bathymetry dataset (4)

5.1.2 Model Mesh

The lagoon topography complexity as described in Section 5.1.1 is transferred to the coupled model by interpolating it to an unstructured mesh.

The model mesh is composed of triangular elements for the shallow water areas (including tidal flats and “barene”) and quadrangular elements for channels enabling a more accurate resolution of flow field with marked bidirectional features.

The optimal trade-off between the mesh size and computational effort was achieved by running a number of mesh convergence tests.

The total mesh comprises 49493 nodes and a combination of 81500 triangular and quadrangular elements.

In the process of the defining the final mesh structure previous studies in the lagoon environment were taken into consideration. The final mesh is comparable to the model described by Carniello et al. [12] with 35000 nodes and 67000 total elements. Other studies such as Umgiesser et al. [5] describe a model mesh with a reduced number of elements and nodes (4359 and 7842 respectively)

without incurring in model results deteriorations. Feola et al. [30] applies a mesh of double size circa (i.e., 83600 nodes and 160000 elements) although the total counting accounts for a wider area enclosing the northern Adriatic Sea.

Broadly speaking, each model described in the forementioned publications pursue different objectives, simulates different period and avails of different computational resources, hence an absolute fair comparison is not possible.

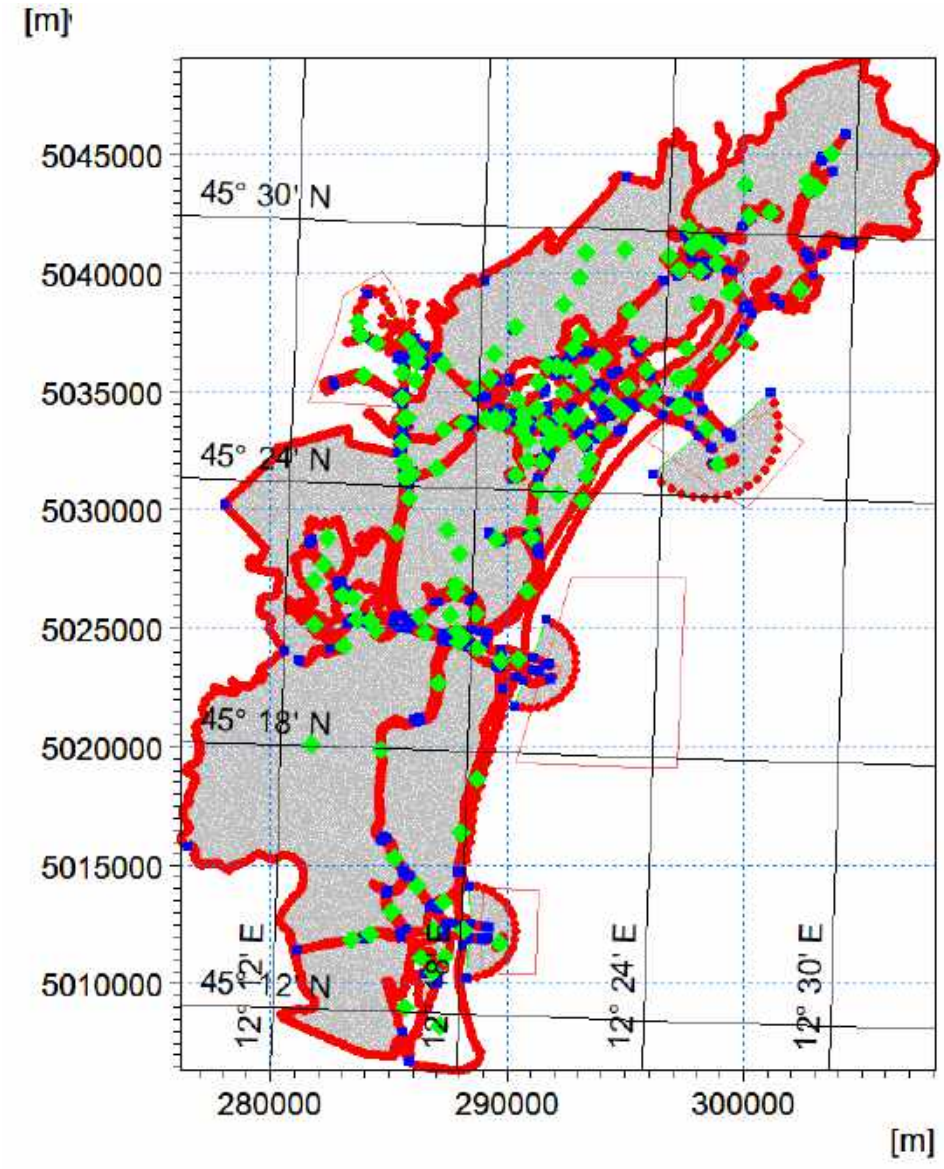

Figure 44. Optimised model mesh: 49493 nodes, 81500 elements.

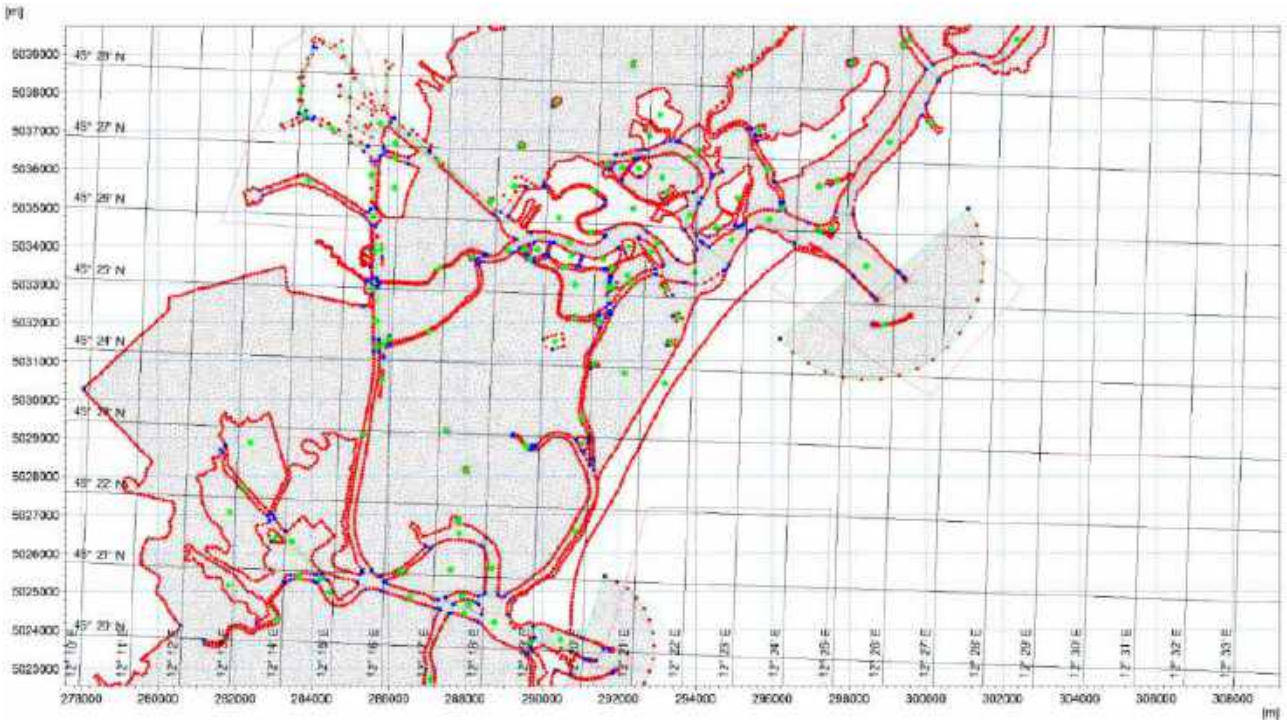

Figure 45. Mesh detail of the central lagoon area.

Figure 46. Mesh details: northern lagoon area.

Figure 47. Mesh details: central lagoon area.

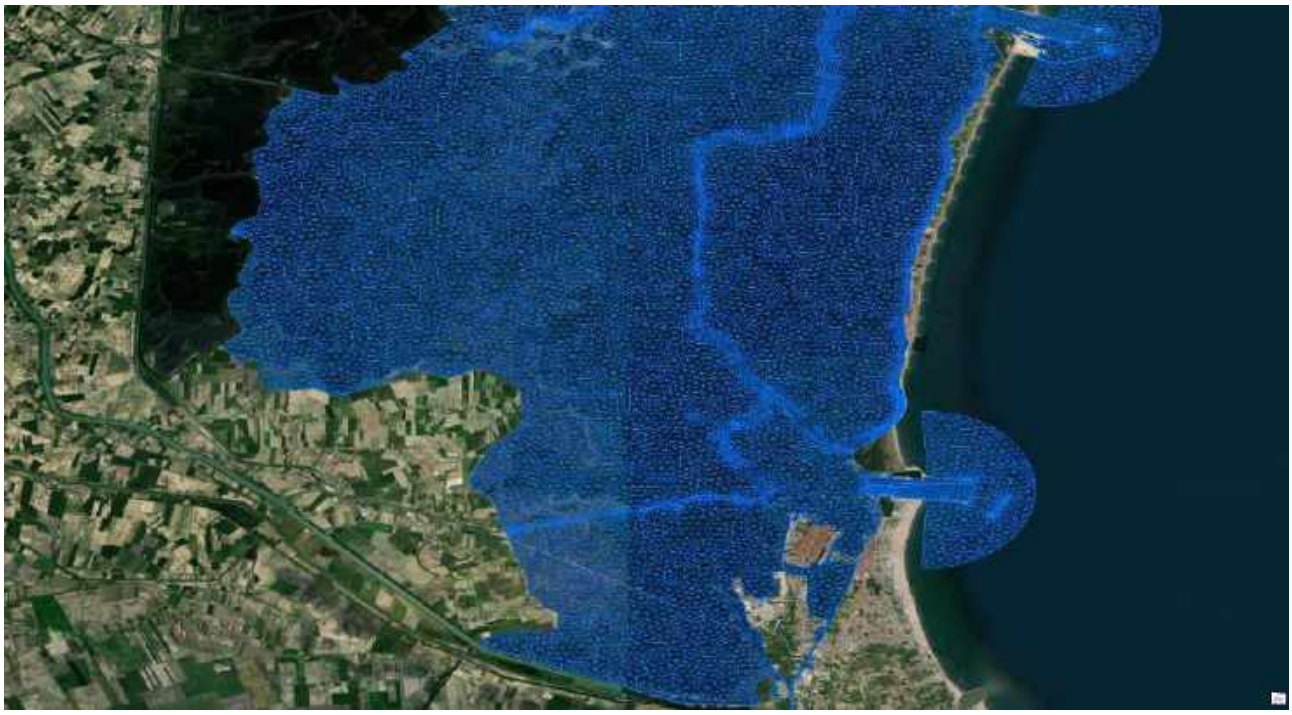

Figure 48. Mesh details: southern lagoon area.

Figure 49. Mesh details: channels network in and around Venice city.

5.1.3 Model boundary conditions and forcing

5.1.3.1 Wind forcing

Given the wind field spatial variability discussed in Section 3.2.1 and its relative importance in connection to the energy transfer mechanisms responsible for waves generation inside the Venice lagoon, a 2D (spatially and temporally varying) wind field was generated starting from the six single-point time series using the well-established Thiessen polygons methodology. The methodology consists of generating N sub-domains, with N equal to the number of observation points available and attributing to each subdomain the wind timeseries measurements from the corresponding met station.

5.1.3.2 Waves

Wave data extracted for the year 2020 from the MWM model at the three inlets are hereafter presented in Figure 50 - Figure 52 and Table 10 - Table 12 in the form of wave roses and scatter tables.

It is worth mentioning that the year 2020 represents a sub-set of the parent time series presented in Section 3.2.2 covering the period from 1979 to 2020. In relation to this, the yearly wave roses do not show appreciable variation with respect to the parent wave roses in terms of directionality (i.e. East and South east as main directional sectors) and overall frequency of occurrence. Typically, about 70% of significant wave heights (H_s) are below 0.5m reaching maximum values of 2.49 m, 2.44 m and 2.25 m for Lido, Malamocco and Chioggia, respectively.

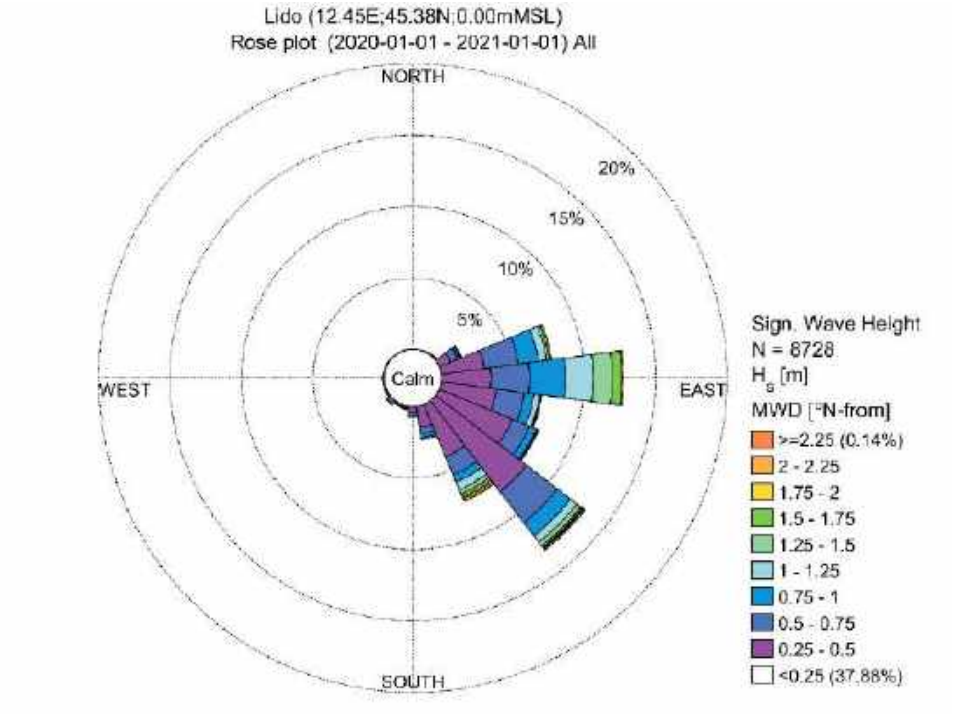

Figure 50. Wave rose from MWM data extracted at Lido inlet (2020).

Table 10. Scatter table of Significant Wave Height (Hs) vs Mean Wave Direction (MWD) from MWM data extracted at Lido inlet.

Lido (12.45E,45.38N,0.00mMSL)
Frequency of Occurrence [%] (2020-01-01 - 2021-01-01) All
H_s [m] - Sign. Wave Height

MWD [°N-from] - Mean Wave Direction

	[0-0.25[	[0.25-0.5[	[0.5-0.75[	[0.75-1[	[1-1.25[	[1.25-1.5[	[1.5-1.75[	[1.75-2[	[2-2.25[	[2.25-2.5[	[2.5-2.75[	[2.75-3[	Total	Accum
[337.5-352.5[	-	0.011	0.011	-	-	-	-	-	-	-	-	-	0.023	100.000
[322.5-337.5[	0.011	0.024	-	-	-	-	-	-	-	-	-	-	0.046	99.977
[307.5-322.5[	0.011	0.023	-	-	-	-	-	-	-	-	-	-	0.034	99.931
[292.5-307.5[	-	0.069	-	-	-	-	-	-	-	-	-	-	0.080	99.897
[277.5-292.5[	0.011	0.069	-	-	-	-	-	-	-	-	-	-	0.080	99.828
[262.5-277.5[	-	0.126	0.011	-	-	-	-	-	-	-	-	-	0.137	99.748
[247.5-262.5[	0.046	0.069	0.046	-	-	-	-	-	-	-	-	-	0.160	99.610
[232.5-247.5[	0.057	0.057	0.080	-	-	-	-	-	-	-	-	-	0.195	99.450
[217.5-232.5[	0.080	0.332	0.046	-	-	-	-	-	-	-	-	-	0.458	99.255
[202.5-217.5[	0.080	0.137	0.057	-	-	-	-	-	-	-	-	-	0.275	98.797
[187.5-202.5[	0.126	0.103	0.092	0.046	-	-	-	-	-	-	-	-	0.367	98.522
[172.5-187.5[	0.390	0.436	0.206	0.092	-	-	-	-	-	-	-	-	1.123	98.155
[157.5-172.5[	1.272	1.489	0.470	0.275	0.115	0.011	-	-	-	-	-	-	3.632	97.033
[142.5-157.5[	5.133	3.964	1.386	0.536	0.564	0.368	0.241	0.126	0.172	0.023	-	-	12.477	93.401
[127.5-142.5[	13.829	5.052	2.727	1.167	0.573	0.321	0.126	0.046	0.080	0.115	-	-	27.005	80.923
[112.5-127.5[	6.656	5.645	1.395	0.493	0.092	0.080	0.011	-	-	-	-	-	13.371	53.918
[97.5-112.5[	4.411	3.918	1.959	0.676	0.390	0.080	0.046	0.023	-	-	-	-	11.503	40.548
[82.5-97.5[	3.747	3.472	2.704	2.488	1.959	1.295	0.696	0.103	0.023	-	-	-	16.489	29.044
[67.5-82.5[	2.337	3.099	2.406	1.409	0.596	0.183	0.160	-	-	-	-	-	10.128	12.556
[52.5-67.5[	0.344	0.871	0.538	0.126	0.103	0.069	-	-	-	-	-	-	2.051	2.428
[37.5-52.5[	0.137	0.069	0.011	0.046	-	0.011	-	-	-	-	-	-	0.275	0.367
[22.5-37.5[	-	0.023	0.004	-	-	-	-	-	-	-	-	-	0.057	0.092
[7.5-22.5[	-	0.011	-	-	-	-	-	-	-	-	-	-	0.011	0.034
[-7.5-7.5[	-	0.023	-	-	-	-	-	-	-	-	-	-	0.023	0.023
Total	37.878	31.920	14.081	7.358	4.411	2.360	1.283	0.298	0.275	0.137	-	-	100.000	-
Accum	37.878	69.798	83.879	91.236	95.646	98.006	99.290	99.588	99.863	100.000	100.000	100.000	-	-

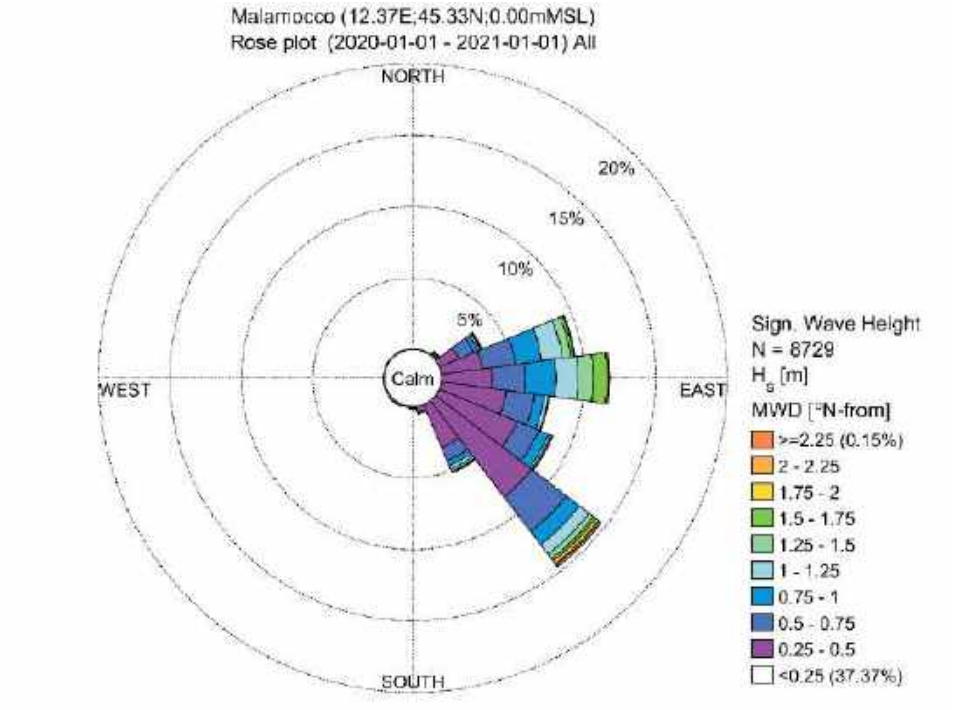

Figure 51. Wave rose from MWM data extracted at Malamocco inlet (2020).

Table 11. Scatter table of Significant Wave Height (Hs) vs Mean Wave Direction (MWD) from MWM data extracted at Malamocco inlet (2020).

Malamocco (12.37E;45.33N;0.00mMSL)
Frequency of Occurrence [%] (2020-01-01 - 2021-01-01) All
H_s [m] - Sign. Wave Height

MWD [°N-from] - Mean Wave Direction

	[0-0.25[	[0.25-0.5[	[0.5-0.75[	[0.75-1[	[1-1.25[	[1.25-1.5[	[1.5-1.75[	[1.75-2[	[2-2.25[	[2.25-2.5[	[2.5-2.75[	[2.75-3[	Total	Accum
[337.5-352.5[	0.011	0.023	-	-	-	-	-	-	-	-	-	-	0.034	100.000
[322.5-337.5[	0.023	0.069	0.011	-	-	-	-	-	-	-	-	-	0.103	99.966
[307.5-322.5[	-	0.023	-	-	-	-	-	-	-	-	-	-	0.023	99.863
[292.5-307.5[	0.023	0.080	-	-	-	-	-	-	-	-	-	-	0.103	99.840
[277.5-292.5[	0.023	0.046	-	-	-	-	-	-	-	-	-	-	0.069	99.737
[262.5-277.5[	-	0.092	-	-	-	-	-	-	-	-	-	-	0.092	99.668
[247.5-262.5[	0.046	0.057	0.034	-	-	-	-	-	-	-	-	-	0.137	99.576
[232.5-247.5[	0.011	0.069	-	-	-	-	-	-	-	-	-	-	0.080	99.439
[217.5-232.5[	0.080	0.140	-	-	-	-	-	-	-	-	-	-	0.220	99.358
[202.5-217.5[	0.046	0.160	-	-	-	-	-	-	-	-	-	-	0.206	99.139
[187.5-202.5[	0.069	0.057	-	-	-	-	-	-	-	-	-	-	0.126	98.933
[172.5-187.5[	0.115	0.103	0.069	-	-	-	-	-	-	-	-	-	0.286	98.797
[157.5-172.5[	0.367	0.378	0.149	-	-	-	-	-	-	-	-	-	0.894	98.511
[142.5-157.5[	2.664	3.276	0.985	0.378	0.263	0.183	0.057	0.023	0.023	-	-	-	8.054	97.617
[127.5-142.5[	14.584	5.469	3.059	1.146	0.848	0.412	0.195	0.229	0.115	0.149	-	-	29.224	89.564
[112.5-127.5[	6.508	5.900	1.927	0.756	0.183	0.103	0.046	-	-	-	-	-	15.603	60.339
[97.5-112.5[	4.170	4.617	1.993	0.676	0.298	0.023	0.023	0.023	-	-	-	-	11.823	44.736
[82.5-97.5[	4.044	3.553	2.291	2.188	1.512	1.077	0.915	0.149	0.069	-	-	-	15.809	32.913
[67.5-82.5[	3.001	2.875	2.371	1.844	1.466	0.867	0.286	0.083	-	-	-	-	12.453	17.104
[52.5-67.5[	0.630	1.479	1.145	0.321	0.160	0.080	0.069	-	-	-	-	-	3.884	4.651
[37.5-52.5[	0.172	0.137	0.126	0.069	0.023	0.011	0.011	-	-	-	-	-	0.550	0.766
[22.5-37.5[	0.046	0.023	0.023	0.011	-	-	-	-	-	-	-	-	0.103	0.218
[7.5-22.5[	0.011	0.023	-	0.011	-	-	-	-	-	-	-	-	0.046	0.115
[-7.5-7.5[	0.046	0.023	-	-	-	-	-	-	-	-	-	-	0.069	0.069
Total	37.370	31.710	13.885	7.401	4.754	2.497	1.524	0.504	0.206	0.149	-	-	100.000	-
Accum	37.370	69.080	82.966	90.365	95.120	97.617	99.141	99.645	99.851	100.000	100.000	100.000	-	-

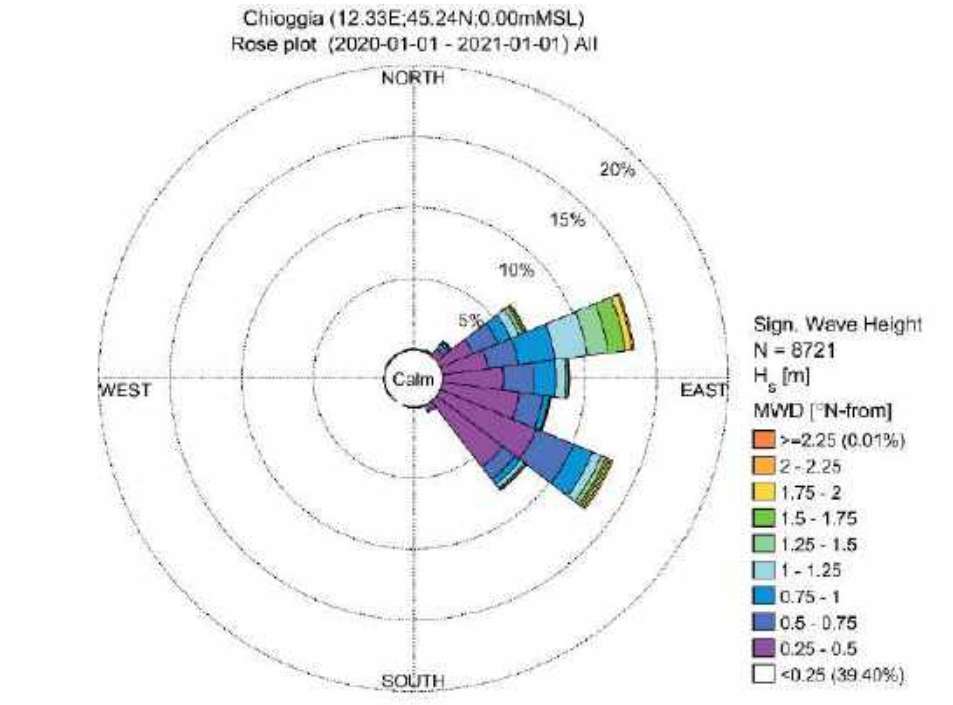

Figure 52. Wave rose from MWM data extracted at Chioggia inlet (2020).

Table 12. Scatter table of Significant Wave Height (Hs) vs Mean Wave Direction (MWD) from MWM data extracted at Chioggia inlet.

Chioggia (12.33E;45.24N;0.00mSL)
Frequency of Occurrence [%] (2020-01-01 - 2021-01-01) All
H_s [m] - Sign. Wave Height

MWD [°N-from] - Mean Wave Direction

	[0-0.25[	[0.25-0.5[	[0.5-0.75[	[0.75-1[	[1-1.25[	[1.25-1.5[	[1.5-1.75[	[1.75-2[	[2-2.25[	[2.25-2.5[	[2.5-2.75[	[2.75-3[	Total	Accum
[337.5-352.5[	-	0.046	0.023	-	-	-	-	-	-	-	-	-	0.069	100.000
[322.5-337.5[	0.011	0.024	0.023	-	-	-	-	-	-	-	-	-	0.069	99.931
[307.5-322.5[	0.023	0.092	-	-	-	-	-	-	-	-	-	-	0.115	99.862
[292.5-307.5[	0.080	0.080	-	-	-	-	-	-	-	-	-	-	0.161	99.748
[277.5-292.5[	0.069	0.023	-	-	-	-	-	-	-	-	-	-	0.092	99.587
[262.5-277.5[	0.046	0.069	-	-	-	-	-	-	-	-	-	-	0.115	99.495
[247.5-262.5[	0.057	0.080	-	-	-	-	-	-	-	-	-	-	0.138	99.381
[232.5-247.5[	0.103	0.069	-	-	-	-	-	-	-	-	-	-	0.172	99.243
[217.5-232.5[	0.057	0.023	-	-	-	-	-	-	-	-	-	-	0.080	99.071
[202.5-217.5[	0.055	-	-	-	-	-	-	-	-	-	-	-	0.069	98.991
[187.5-202.5[	0.011	0.046	-	-	-	-	-	-	-	-	-	-	0.057	98.922
[172.5-187.5[	0.023	0.023	-	-	-	-	-	-	-	-	-	-	0.046	98.865
[157.5-172.5[	0.033	0.080	-	-	-	-	-	-	-	-	-	-	0.103	98.819
[142.5-157.5[	0.413	0.539	0.069	-	-	-	-	-	-	-	-	-	1.021	98.716
[127.5-142.5[	12.476	5.858	1.101	0.459	0.321	0.126	0.080	-	-	-	-	-	20.411	97.695
[112.5-127.5[	10.996	7.253	2.909	1.445	0.654	0.344	0.183	0.183	0.161	-	-	-	24.088	77.285
[97.5-112.5[	4.747	5.455	1.674	0.413	0.057	0.069	-	-	-	-	-	-	12.416	53.216
[82.5-97.5[	4.197	4.296	2.190	1.468	0.688	0.172	0.057	0.023	0.023	-	-	-	13.083	40.799
[67.5-82.5[	3.715	5.222	2.156	2.591	2.270	1.479	1.193	0.482	0.138	0.011	-	-	17.257	27.715
[52.5-67.5[	1.653	2.468	1.392	0.952	0.631	0.287	0.149	0.115	0.011	-	-	-	8.187	10.458
[37.5-52.5[	0.447	0.619	0.436	0.172	0.080	0.023	0.023	0.011	-	-	-	-	1.812	2.270
[22.5-37.5[	0.149	0.046	0.046	0.046	0.023	-	-	-	-	-	-	-	0.310	0.459
[7.5-22.5[	0.011	0.023	0.023	0.011	-	-	-	-	-	-	-	-	0.069	0.149
[-7.5-7.5[	0.011	0.046	0.023	-	-	-	-	-	-	-	-	-	0.080	0.080
Total	39.399	30.513	12.484	7.556	4.724	2.503	1.686	0.814	0.533	0.011	-	-	100.000	-
Accum	39.399	69.912	82.396	89.952	94.657	97.166	98.842	99.656	99.989	100.000	100.000	100.000	-	-

5.1.3.3 Water levels

ISPRA-Venezia [1] provides continuous observation of water level at several stations. The observation from three stations located at the inlets were used to derive water level boundary conditions input to the model.

Figure 53. In red circles the three water level stations used to derive model boundary conditions.

Table 13. Inlet tide gauges coordinates.

Station	Long [°E]	Lat [°N]
Meda Bocca Lido	12.414564	45.426744
Malamocco Diga Nord	12.341625	45.334450
Chioggia Diga Sud	12.312767	45.228547

The time series of measured water levels for the entire year 2020 are shown in Figure 54.
Little water level variability across the three inlets is noticeable from the signal close up in Figure 55, attributing most of the water level variability inside the lagoon to internal basin mechanisms peculiar to the Venice lagoon.

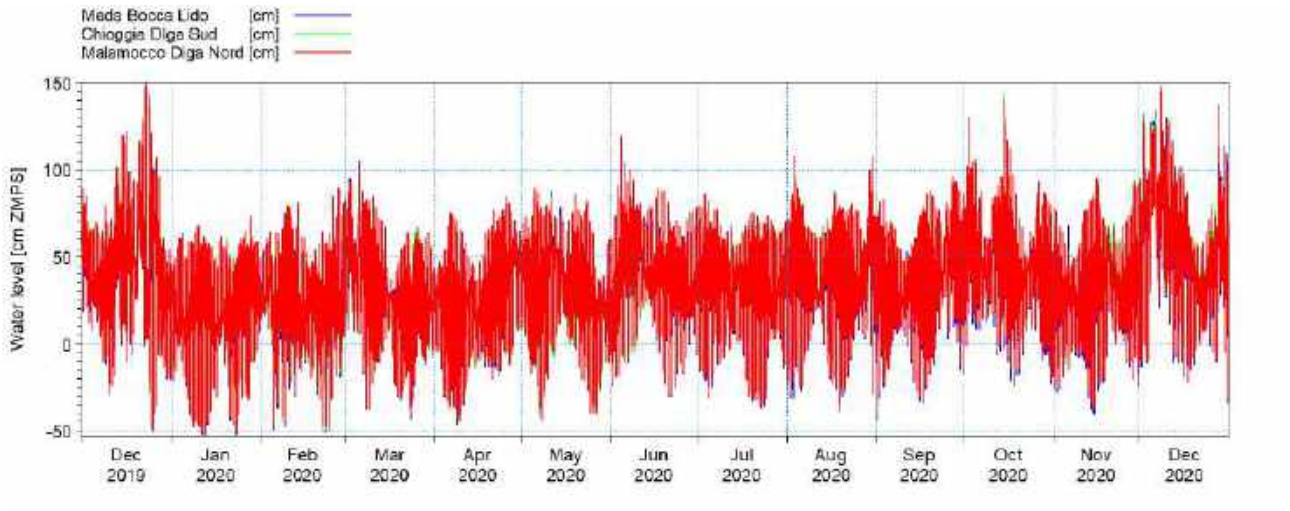

Figure 54. Water elevation measurements at the three inlets.

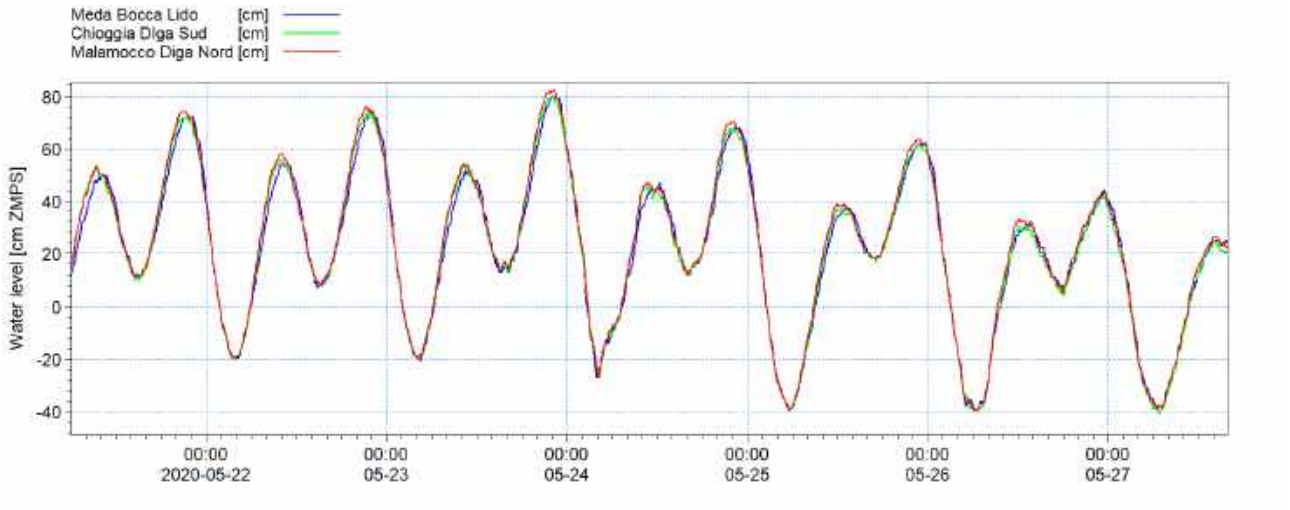

Figure 55. Detail of water elevation measurements at the three inlets.

5.1.3.4 Mass sources

Flow rates contributing to the mass balance of the Venice Lagoon were integrated into the model as mass point sources boundary conditions. A total of eleven sources were considered applying stationary flow rate values derived from Zirino et al. [11] as described in Section 3.2.4

5.2 HD model calibration and validation

To ensure that the model set-up in conjunction with the input so far described (i.e., boundary conditions, bathymetry and mesh) is capable of closely reproducing hydrodynamics parameters within the lagoon domain, a calibration task was undertaken.

Model water levels outputs were compared against a number of water level observations derived from two main networks of tide gauges operating in the Venice lagoon, i.e. “ISPRA-Venezia” [1] and “Città di Venezia” [2] (Figure 56).

Figure 56. Tide gauges used for model calibration and validation. In red stations from “ISPRA-Venezia”, in yellow stations from “Città di Venezia”.

The period chosen for the calibration was selected among the two-weeks time window for which tides were the main drivers of the circulation patterns inside the lagoon (i.e., small to negligible storm surge effects). This period thereby selected goes from 29-Jun-2020 to 16-Jul-2020.

The two-weeks window is typically a representative period that allows to simulate at least one neap and one spring tide cycle but at the same time to keep relatively low the computational burden for the calibration task allowing for several tests to be run.

In line with other authors [5] [30], calibration tests were run with the objective of minimising relevant fitting quality indices (i.e., RMSE and BIAS) by sweeping through a number of combinations of Manning's M number for the channels and shallow waters.

The Manning's M number is the model parameter accounting for bottom frictions and therefore affecting flow energy loss. It must be noted that the Manning M number ($m^{1/3}/s$) implemented in the MIKE 21 model is the reciprocal value of the Manning´s n often found in literature [32]. Table 14 illustrates the list of tests run.

Table 14. List of Manning's M number combinations tested for model calibration. Highlighted the test returning optimised fitting quality indices.

Test No.	Shallow waters: Manning's M [$m^{1/3}/s$]	Channels: Manning's M [$m^{1/3}/s$]
01	32	32
02	30	30
03	40	40
04	32	52
05	**42**	**52**
06	30	42
07	30	52

Based on DHI experience, built on previous Venice lagoon modelling projects, no additional distinctions were made with regard to the Manning's M number within the "Shallow waters" areas.

It is worth to be noticed that some authors applied for the lagoon environment a further differentiation for bottom friction values within mud flat areas such as "shallow water", "barene" and areas with distributed vegetation [5]. Conversely, Feola et al. [30] applies a single Strickler coefficient for the entire domain.

Figure 57 shows the Manning's M number distribution map used in this study.

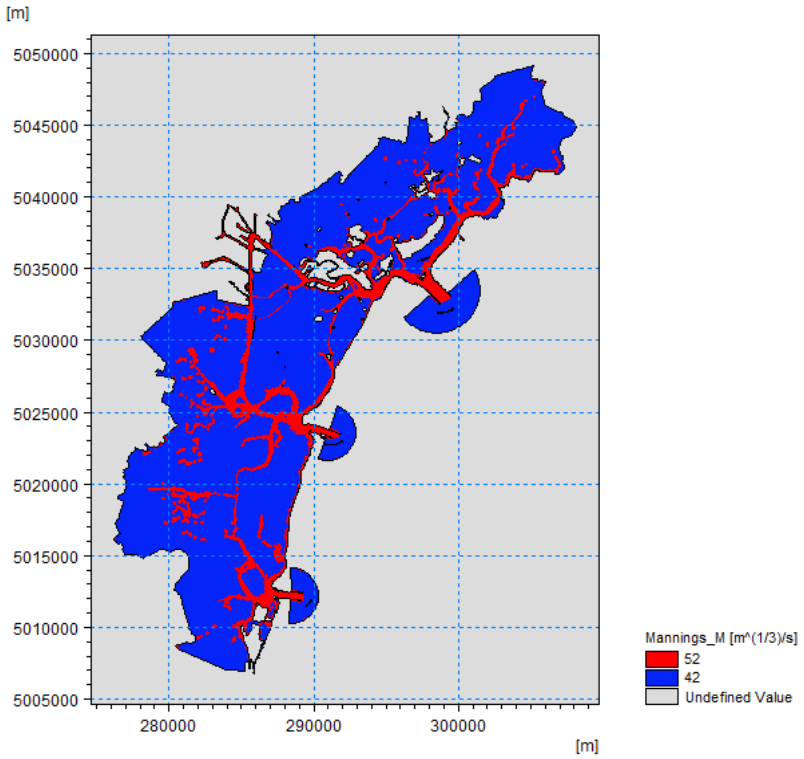

Figure 57. Manning's M number distribution map.

For the sake of conciseness only outputs relative to test 05, which return the most accurate results, are shown thereafter.

As a term of comparison, Figure 58 shows the calibration improvement obtained from test 01 to test 05 for the reference tide gauge at "Punta della Salute".

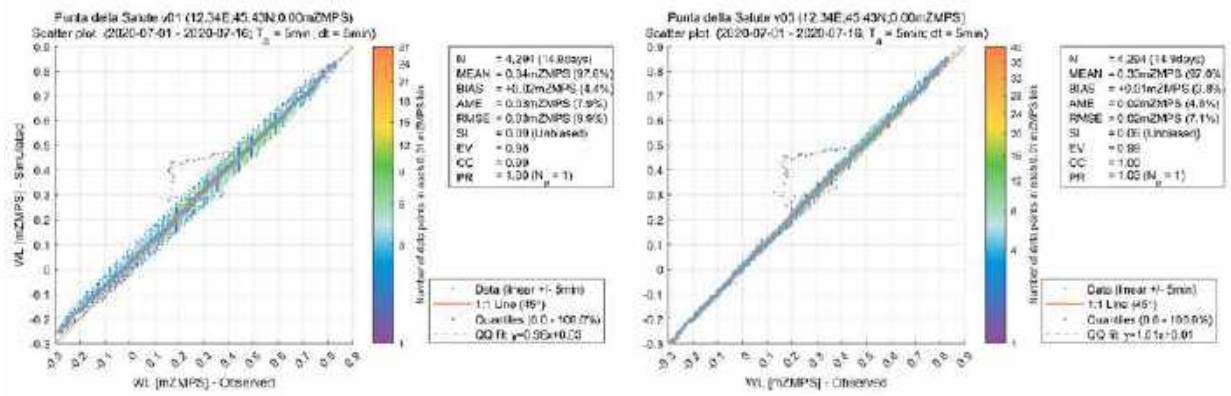

Figure 58. Calibration quality indices for initial test 01 (left) and test 05 (right).

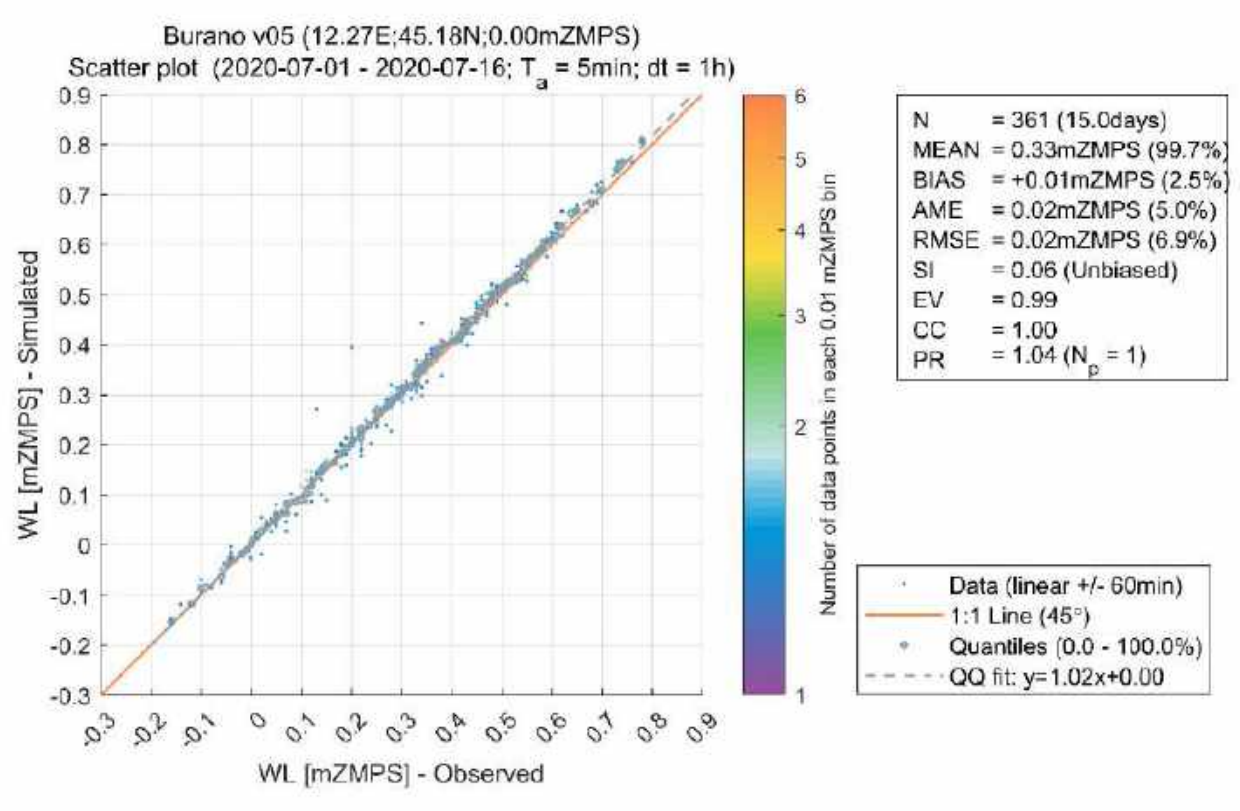

Figure 59. Burano calibration station: QQ plot and fitting quality indices.

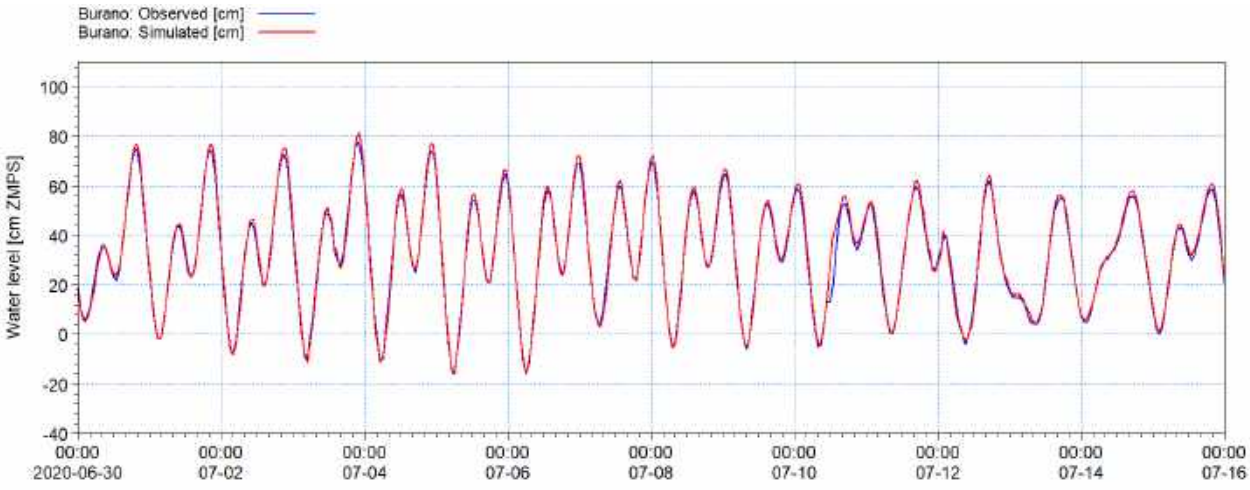

Figure 60. Burano calibration station: Time series comparison.

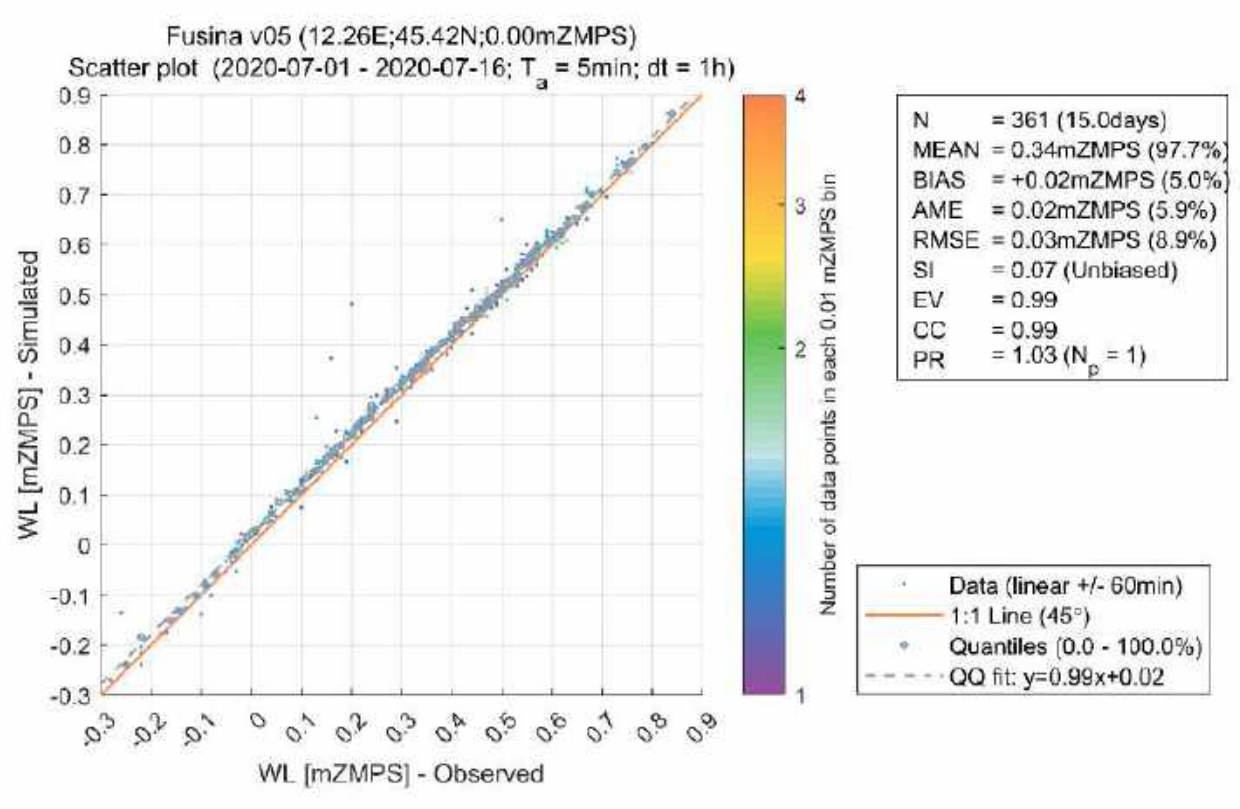

Figure 61. Fusina calibration station: QQ plot and fitting quality indices.

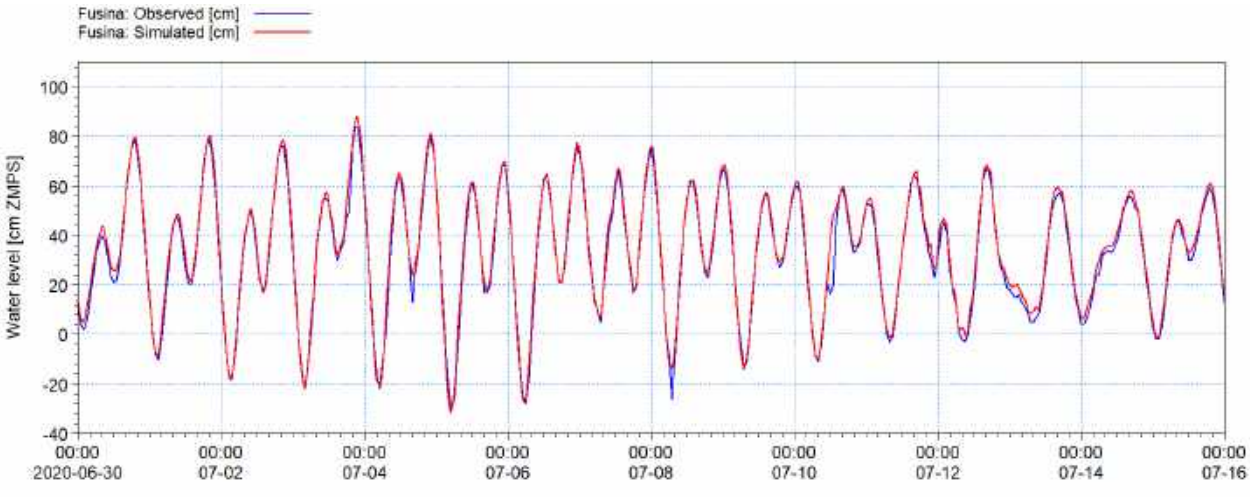

Figure 62. Fusina calibration station: Time series comparison.

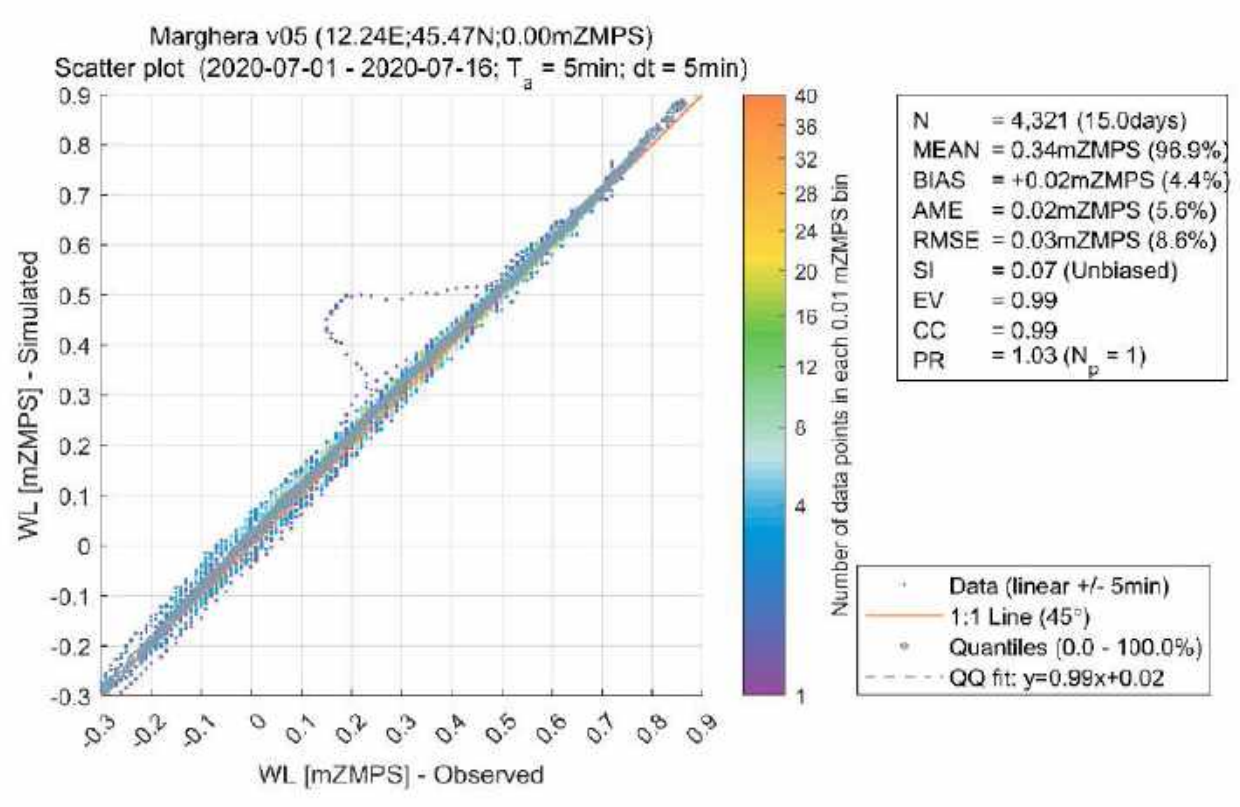

Figure 63. Marghera calibration station: QQ plot and fitting quality indices.

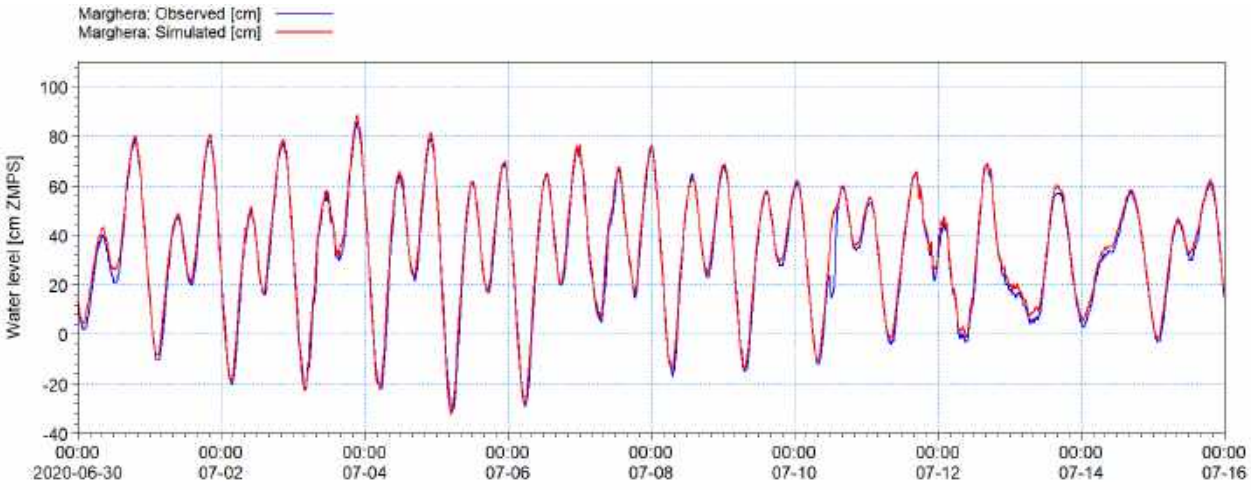

Figure 64. Marghera calibration station: Time series comparison.

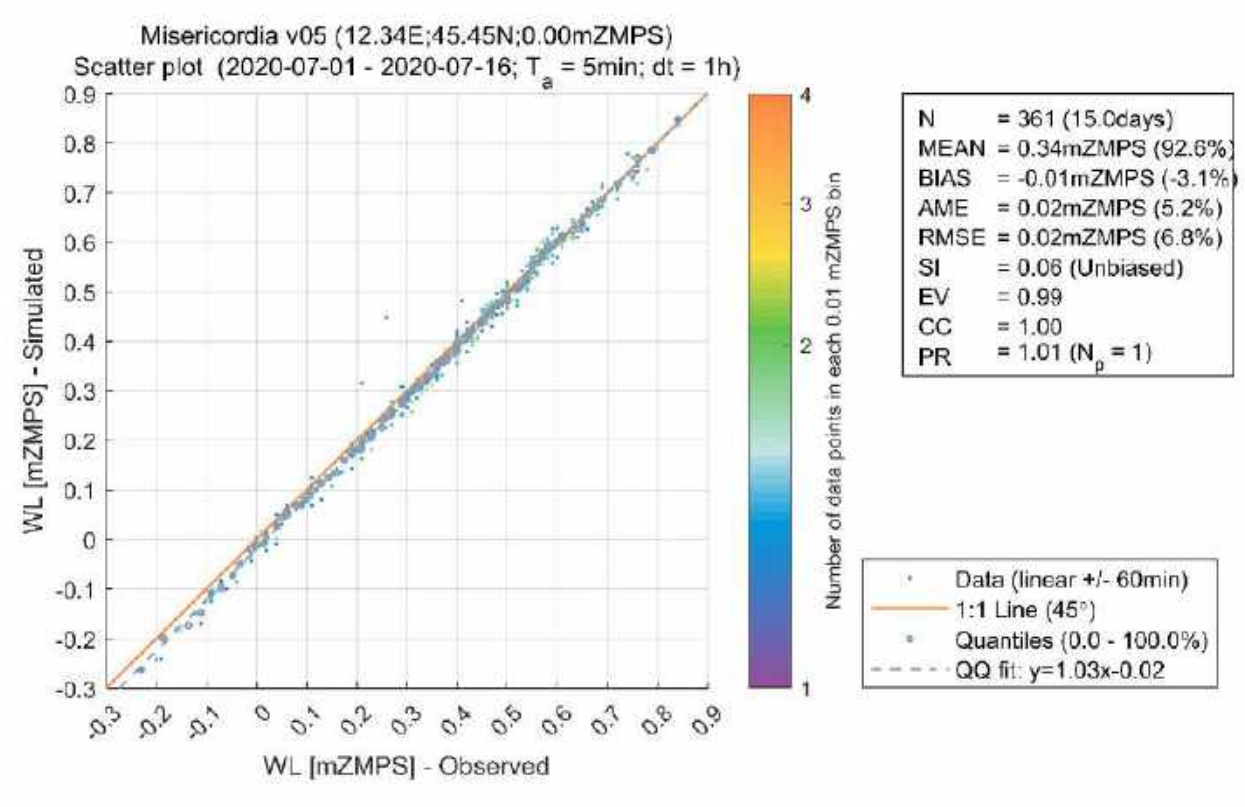

Figure 65. Misericordia calibration station: QQ plot and fitting quality indices.

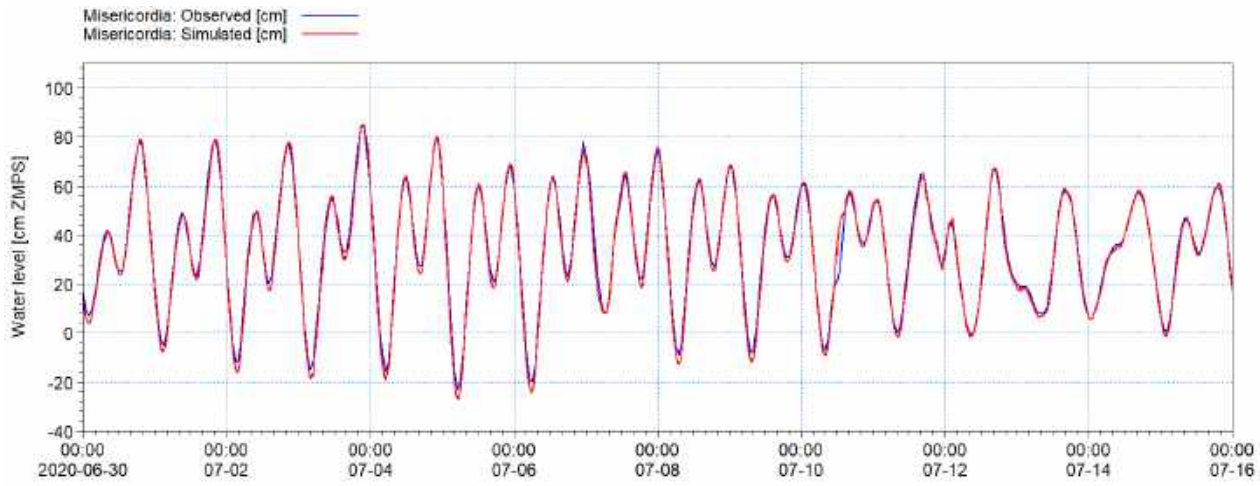

Figure 66. Misericordia calibration station: Time series comparison.

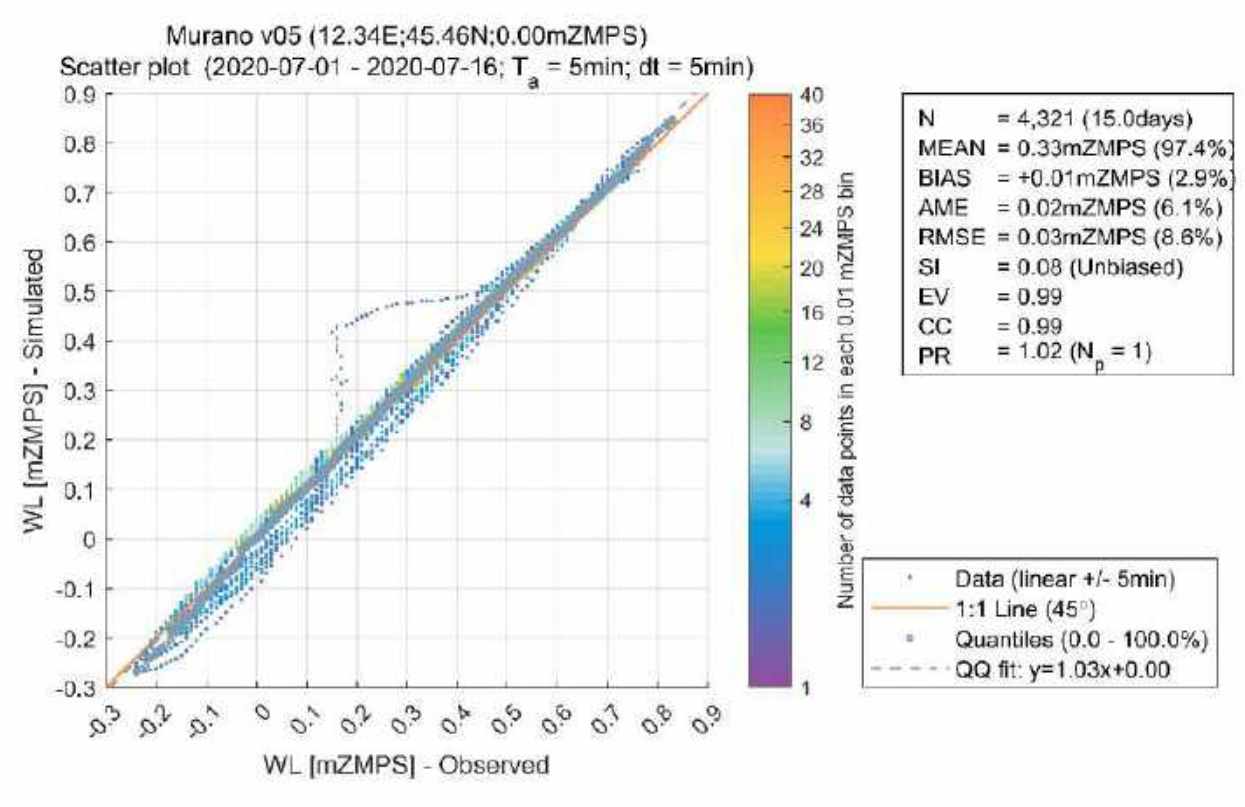

Figure 67.. Murano calibration station: QQ plot and fitting quality indices.

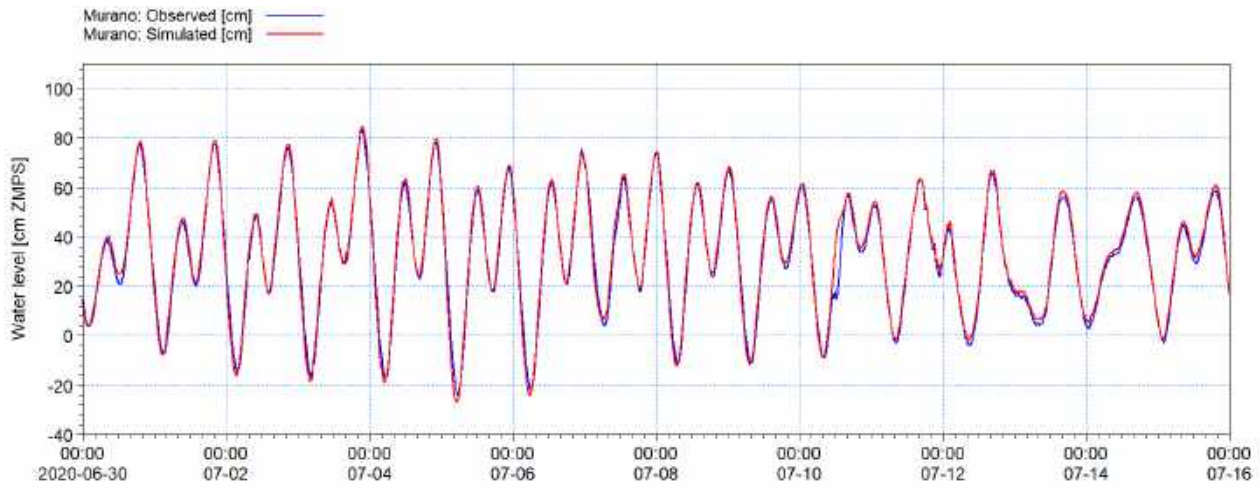

Figure 68. Murano calibration station: Time series comparison.

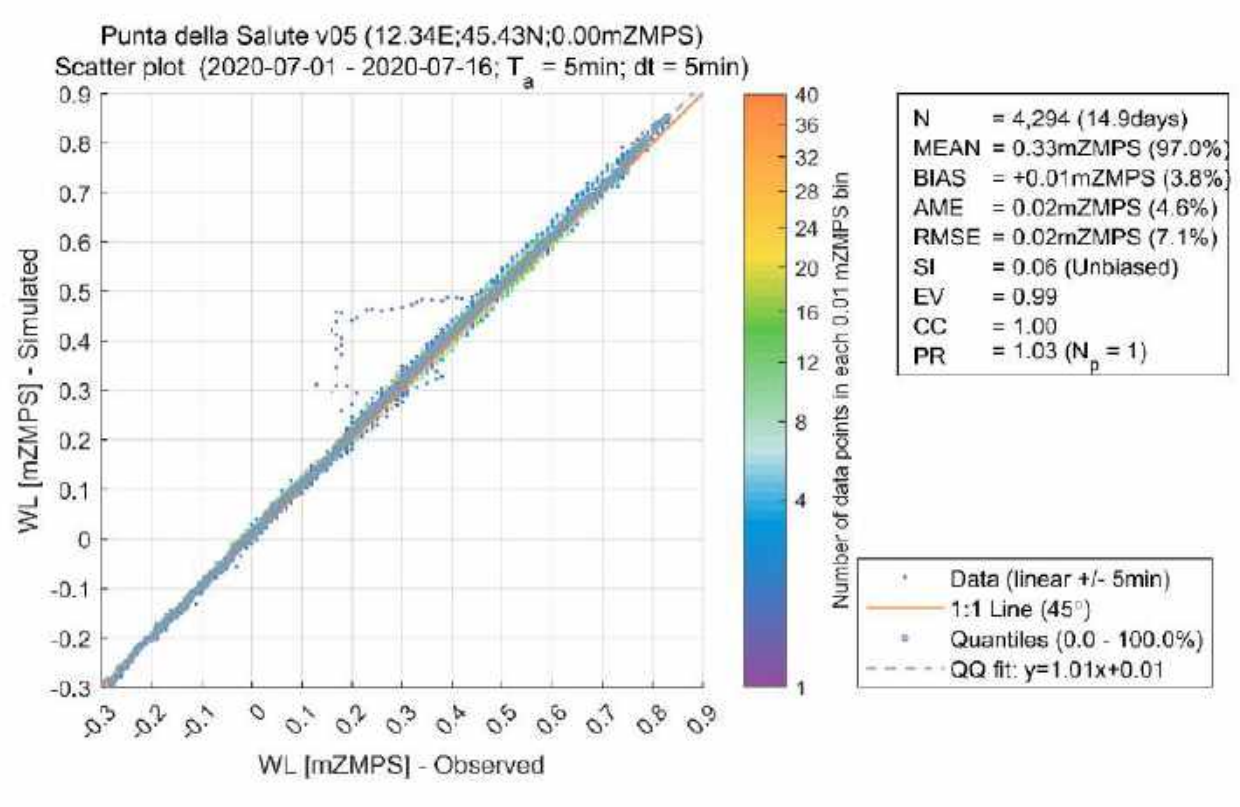

Figure 69. Punta della Salute calibration station: QQ plot and fitting quality indices.

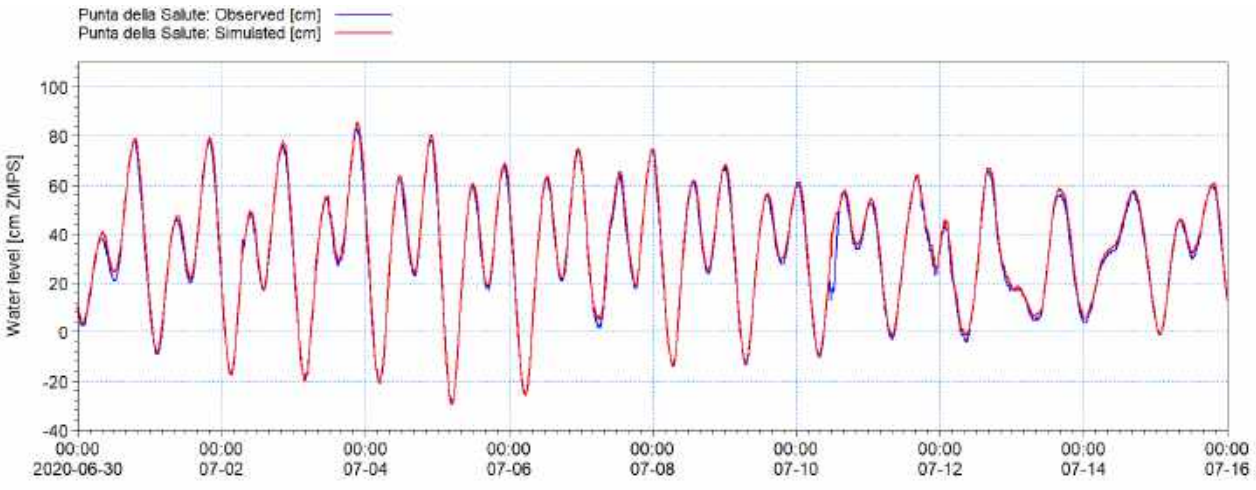

Figure 70. Punta della Salute calibration station: Time series comparison.

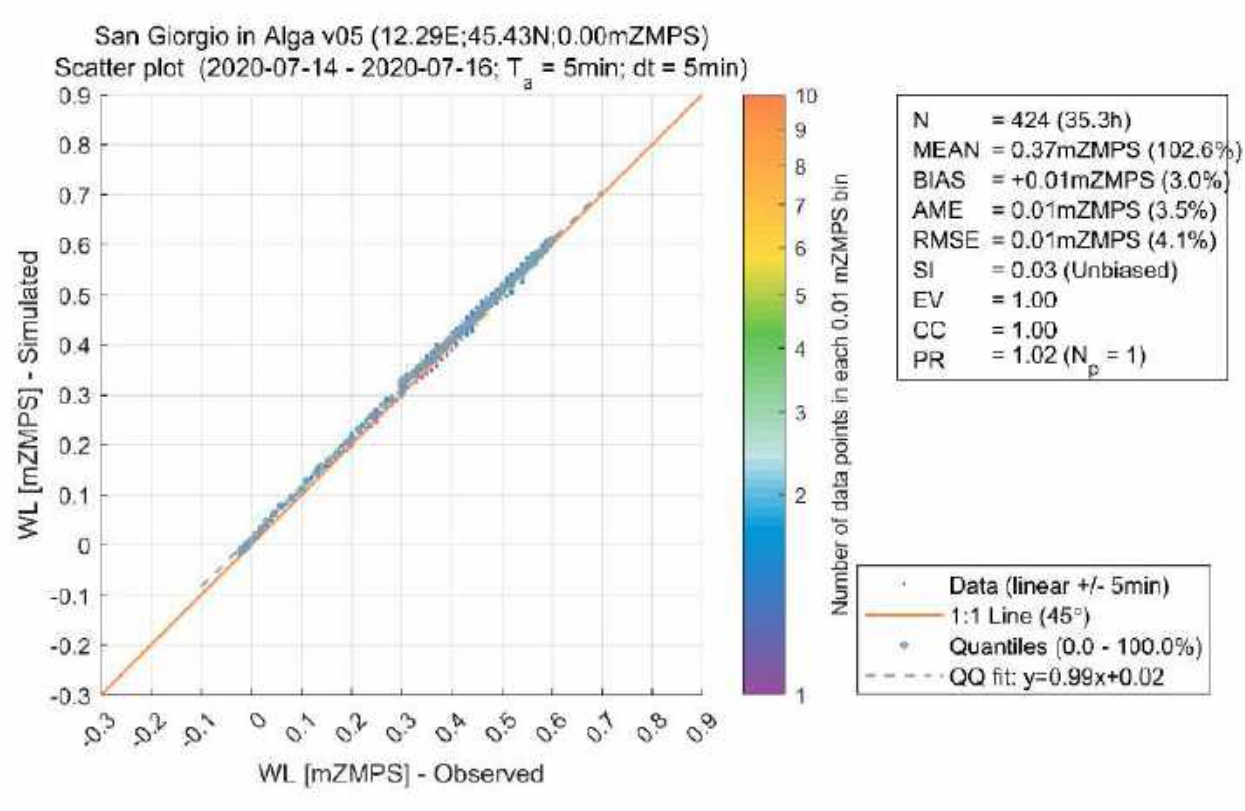

Figure 71. San Giorgio in Alga calibration station: QQ plot and fitting quality indices.

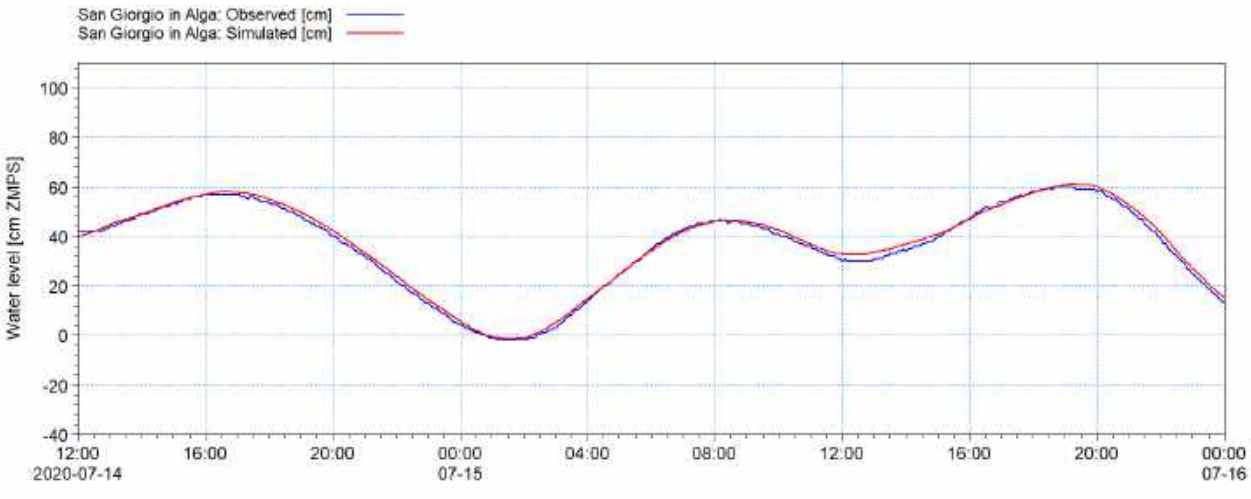

Figure 72. San Giorgio in Alga calibration station: Time series comparison.

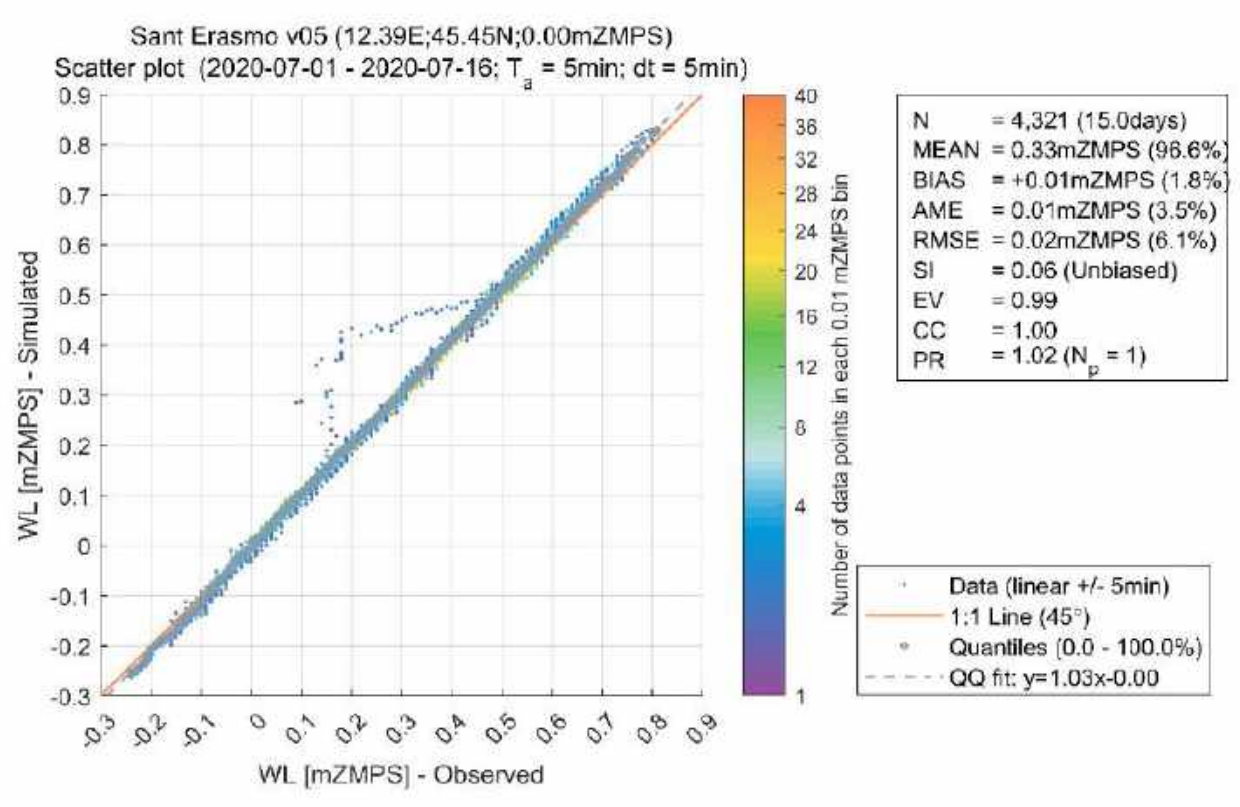

Figure 73. Sant Erasmo calibration station: QQ plot and fitting quality indices.

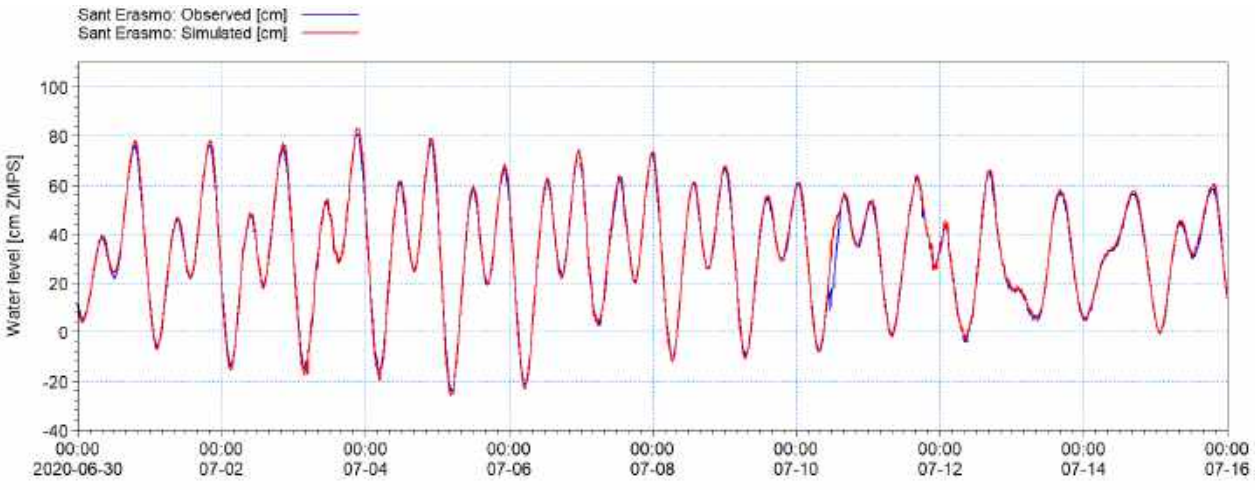

Figure 74. Sant Erasmo calibration station: Time series comparison.

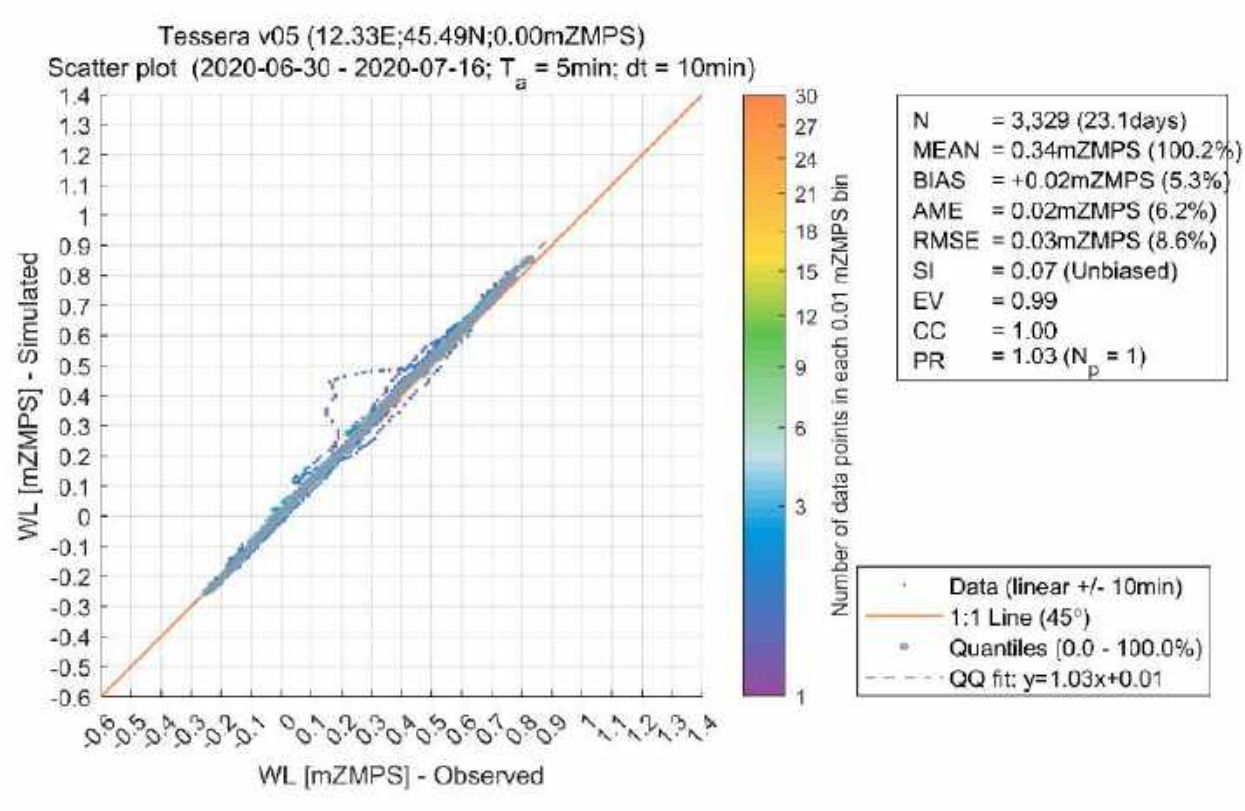

Figure 75. Tessera calibration station: QQ plot and fitting quality indices.

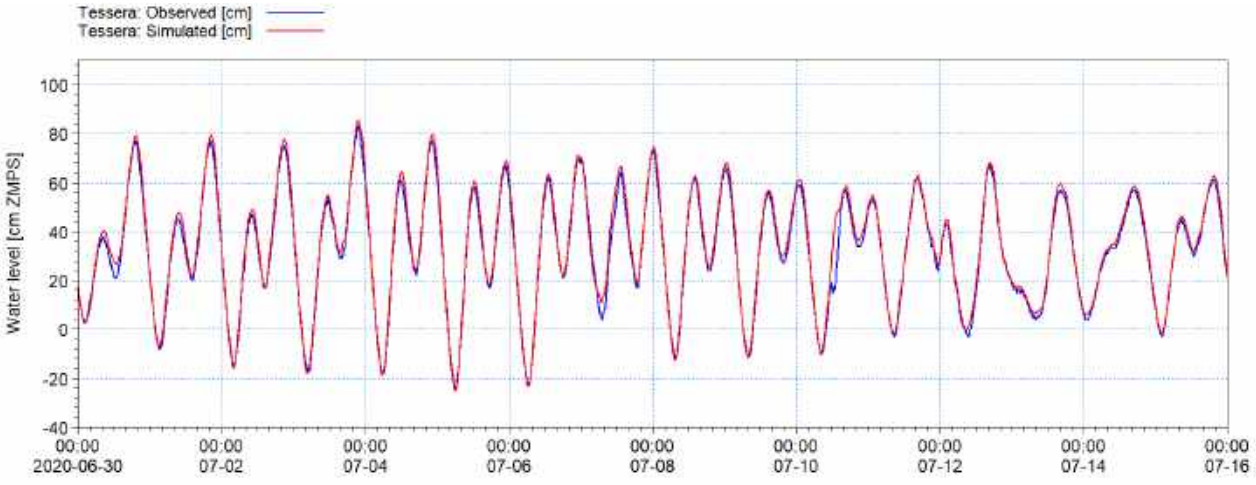

Figure 76. Tessera calibration station: Time series comparison.

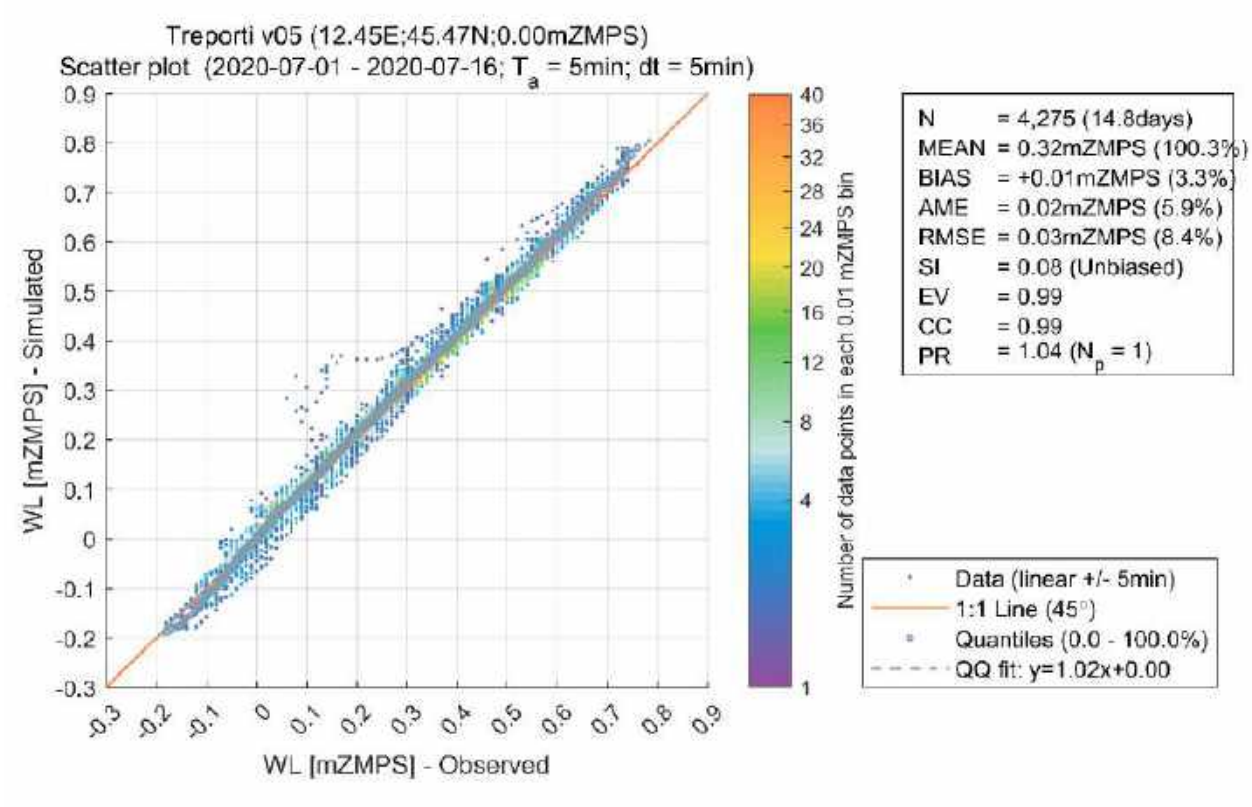

Figure 77. Treporti calibration station: QQ plot and fitting quality indices.

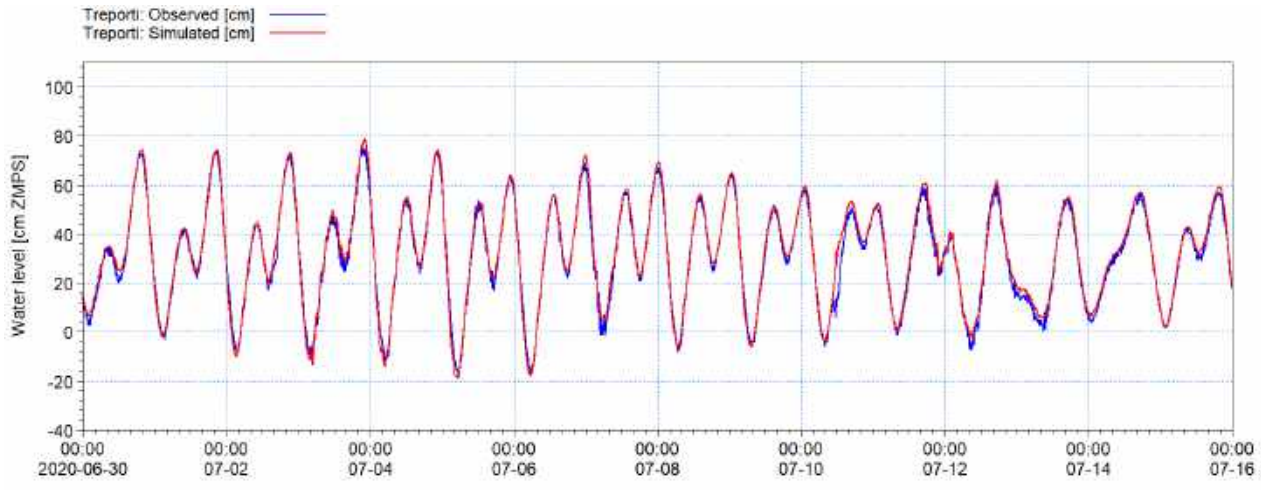

Figure 78. Treporti calibration station: Time series comparison.

Overall, plots for all stations show a remarkable agreement between measured and simulated values.

RMSE and BIAS values for all stations are on average about 2-3 cm and less than 2cm respectively, CC values are all in around 1. The mathematical definition of fitting quality indices is reported in Appendix B.

As shown in Figure 72, for the selected calibration period, only two days of measurements are available at the “San Giorgio in Alga” tide gauge; nonetheless quality fitting and comparison plots are shown for the sake of completeness.

Table 15. Computed RMSE and BIAS indices at all stations for test 05.

Station	RMSE [cm]	BIAS [cm]	CC
Burano	2.33	0.84	1.00
Fusina	3.12	1.74	0.99
Marghera	3.03	1.56	0.99
Misericordia	2.47	-1.14	1.00
Murano	2.95	0.99	0.99
Punta della salute	2.44	1.32	1.00
San Giorgio in Alga	2.44	1.32	1.00
Sant Erasmo	2.08	0.61	1.00
Tessera	2.94	1.83	0.99
Treporti	2.70	1.06	0.99
Average	2.65	1.24	0.995

The average values of the fitting quality indices computed are comparable to values illustrated in Ferrarin et al. [33] reporting RMSE, BIAS and CC averaged over several tide gauges in the lagoon of 3.1 cm, 0.8 cm, 0.993 respectively.

The model proves to correctly reproduce all features of the water level signal propagation, i.e. phase, range and values of high and low waters.

Sporadically, a few points laying out the main bisector line can be found in the QQ-fit plots. These points are generated from a single event occurring during the first flood tide of 10th of July. The

tide gauges show an abrupt deviation from typical water level cycles that cannot be reproduced by a 2D model on a relatively large scale such as the Venice lagoon.

To ensure the model robustness, the calibration was followed by a validation carried out for a different period spanning from 01-Dec-2020 to 16-Dec-2020. This period was chosen among two-weeks periods in 2020 which showed at least one event above 110cm ZMPS. The rational beyond this was to ensure the model performance would not deteriorate when simulating “high water” events.

Results in terms of water level timeseries comparison (i.e., observed vs simulated) are shown from Figure 79 to Figure 88 for the very same stations discussed in the calibration exercise.

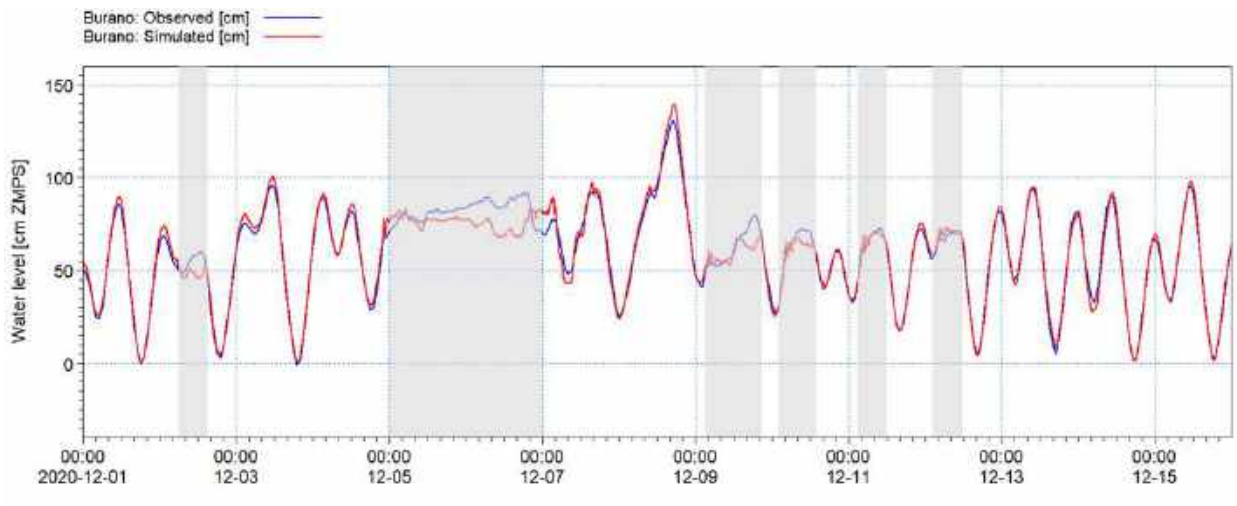

Figure 79. Burano validation station: Time series comparisons. In grey M.O.S.E operating windows.

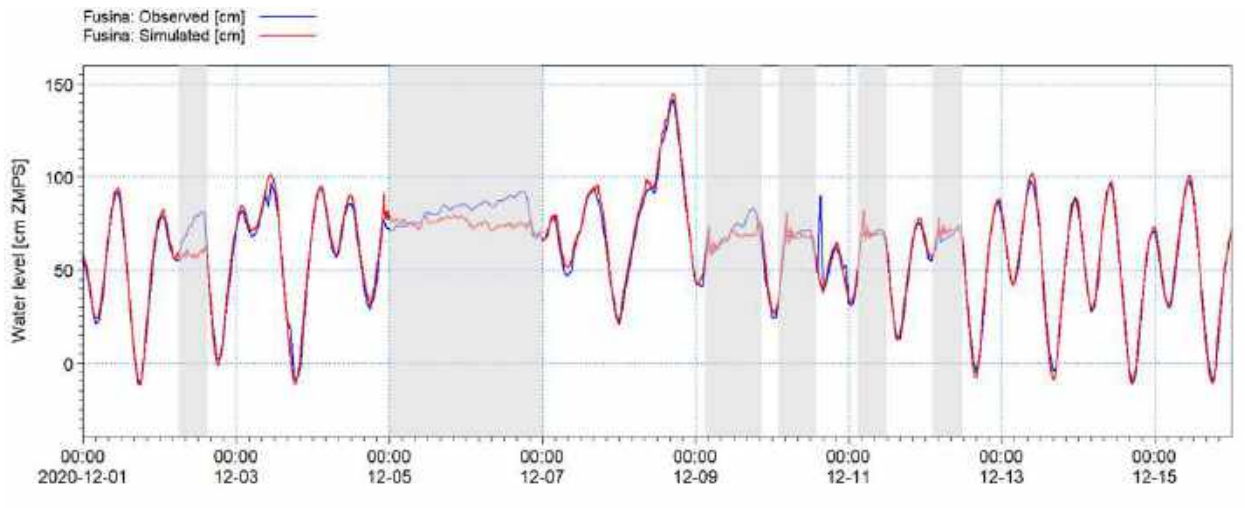

Figure 80. Fusina validation station: Time series comparisons. In grey M.O.S.E operating windows.

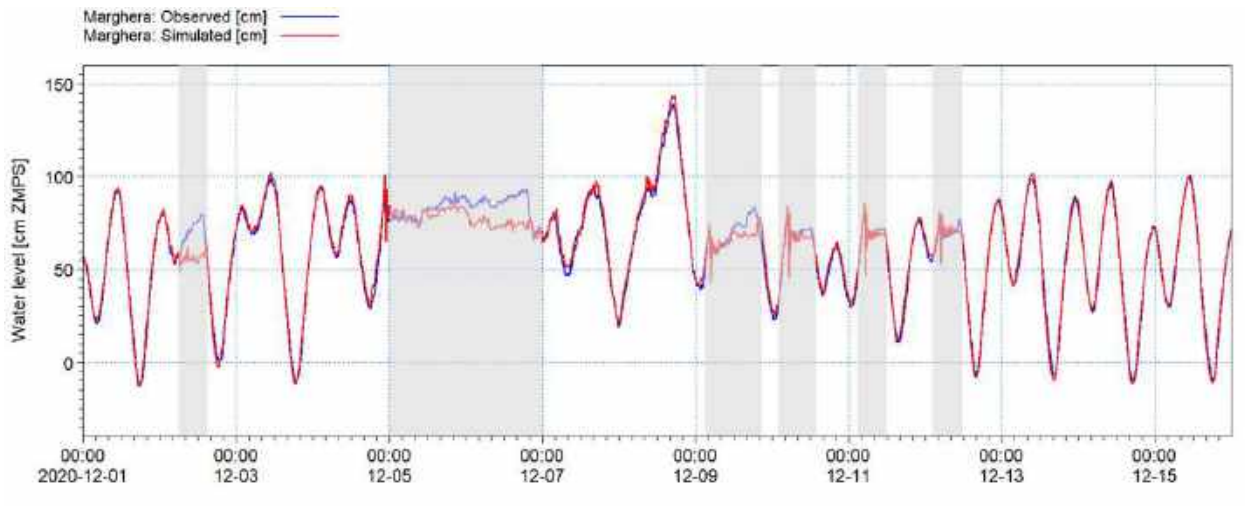

Figure 81. Marghera validation station: Time series comparisons. In grey M.O.S.E operating windows.

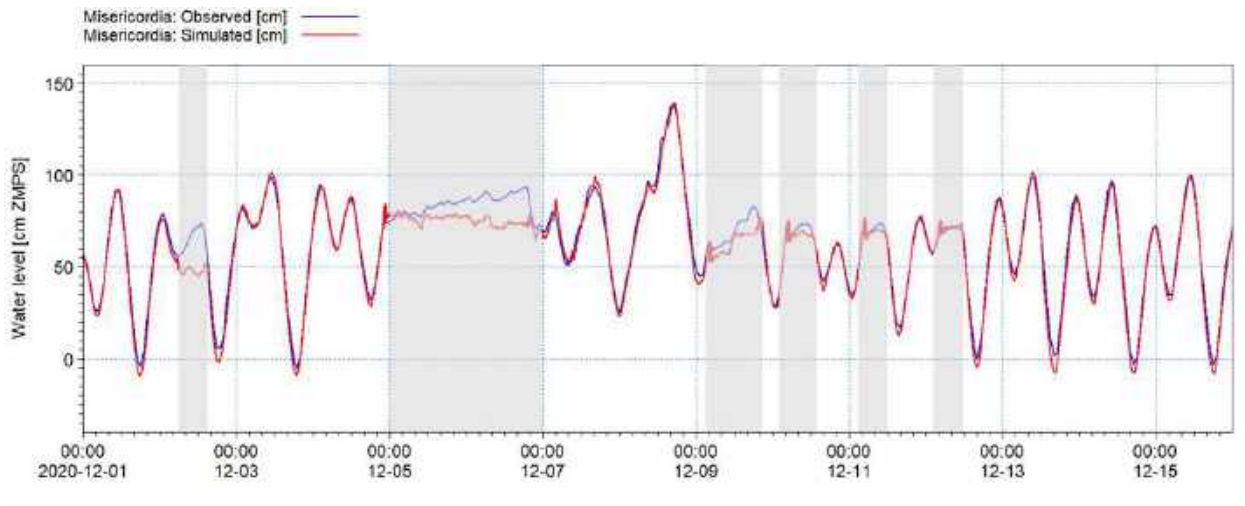

Figure 82. Misericordia validation station: Time series comparisons. In grey M.O.S.E operating windows.

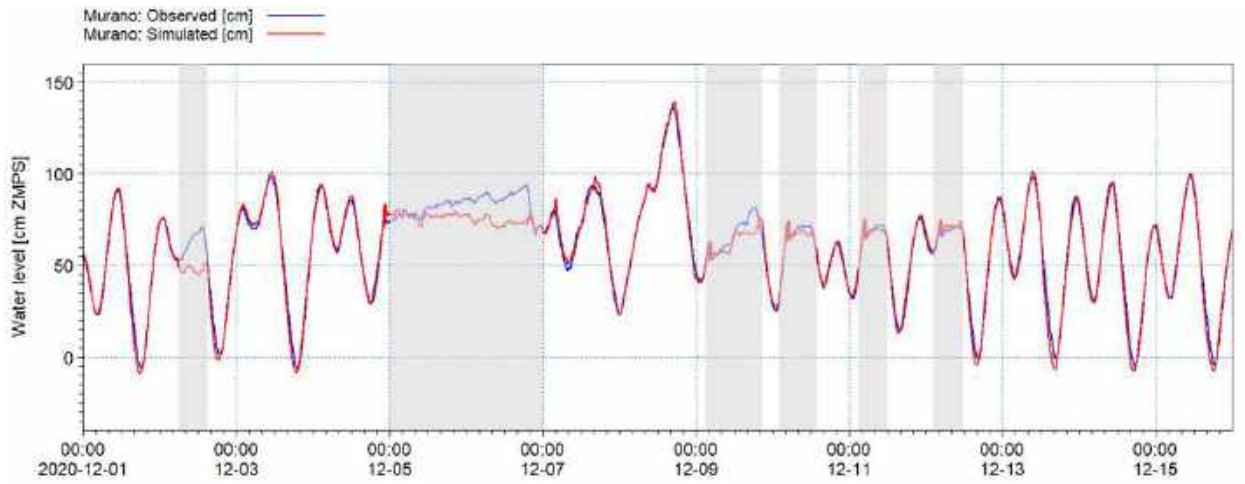

Figure 83. Murano validation station: Time series comparisons. In grey M.O.S.E operating windows.

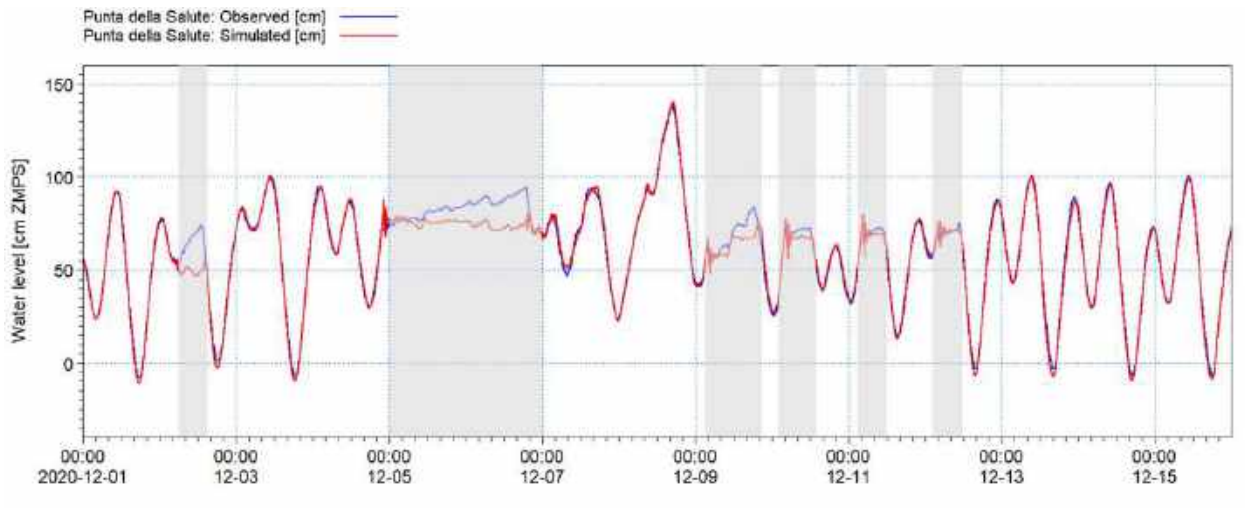

Figure 84. Punta della Salute validation station: Time series comparisons. In grey M.O.S.E operating windows.

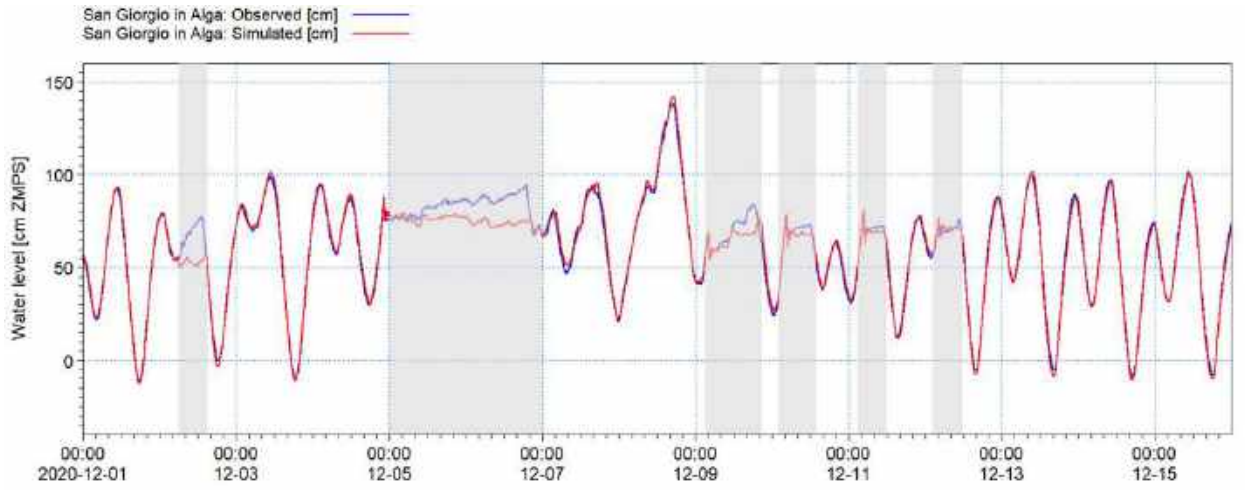

Figure 85. San Giorgio in Alga validation station: Time series comparisons. In grey M.O.S.E operating windows.

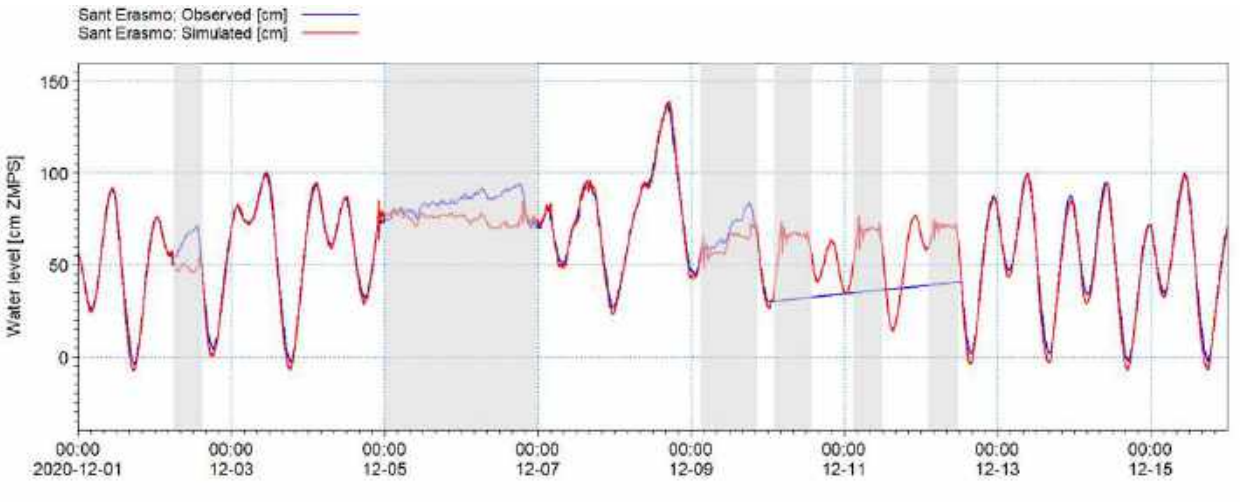

Figure 86. Sant' Erasmo validation station: Time series comparisons. In grey M.O.S.E operating windows.

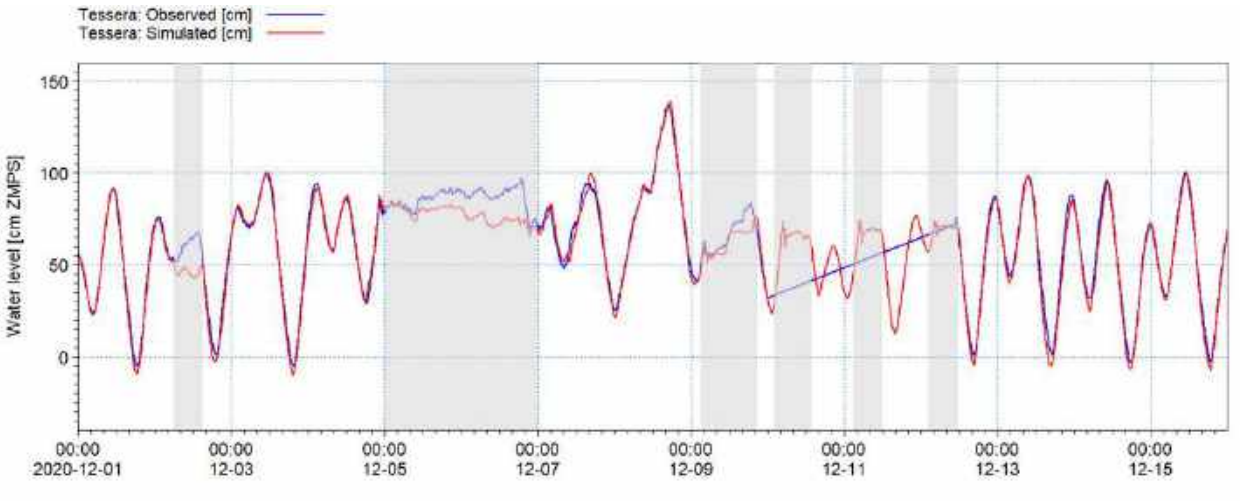

Figure 87. Tessera validation station: Time series comparisons. In grey M.O.S.E operating windows.

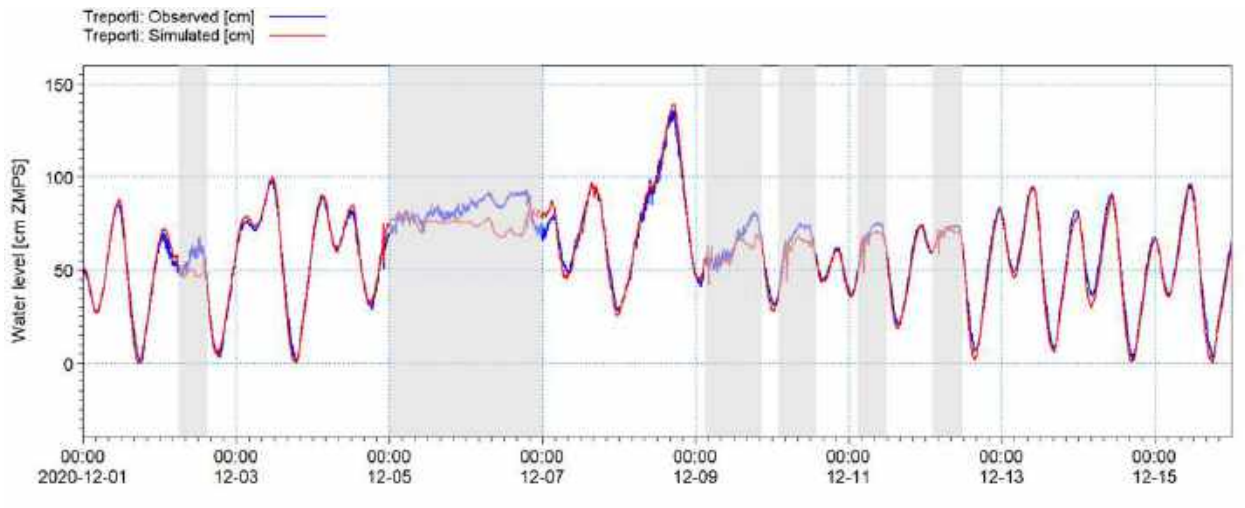

Figure 88. Treporti validation station: Time series comparisons. In grey M.O.S.E operating windows.

The time series comparisons show some evident discrepancies. These discrepancies occur only during the M.O.S.E operation. In fact, notwithstanding the implementation of the M.O.S.E. barriers at the three inlets as discussed in Section 5.1, it is unfeasible and out of the scope of this model, to reproduce exactly the law governing the rise and fall of barriers at each inlet, especially for events when the M.O.S.E operated by partially closing off only one or two inlets.

Moreover, a substantial inflow is expected through the narrow gaps in-between barriers during the M.O.S.E. operative windows. This effect is not accounted for in the model.

In this regard the calculation of fitting quality indices for the validation period was deemed not to be significant as the discrepancies would invalidate the analysis.

Nonetheless, the visual inspection of the timeseries comparisons confirm the robustness of the model.

5.3 SW model calibration and validation

SW model calibration was achieved by tuning the two main parameters responsible for energy dissipation, i.e. bottom friction and white capping.

Bottom friction was implemented by tuning the Nikuradse roughness parameter, whereas white capping parameters were adjusted based on DHI experience in similar studies.

Wave measurements are very scarce in the lagoon, for this study calibration and validation data were retrieved from available literature.

Carniello et al. [12] describes a number of wave model tests run for a combination of wind conditions and water level. Wind conditions refer to the two most significant meteorological forcing scenarios for Venice lagoon, i.e. “Bora” (represented by wind blowing from 45° N) and “Scirocco” (represented by wind blowing from 135° N).

The combination of wind condition and water level tested are described in Table 16.

Table 16. List of scenario tested in Carniello et al. [ref:Carniello].

Test	Wind direction [blowing from]	Wind Speed	Water level
01	45 °N	10 m/s	0 m MSL
02	45 °N	15 m/s	0.5 m MSL
03	135 °N	8 m/s	0.5 m MSL
04	45 °N	10 m/s	0.5 m MSL
05	135 °N	5 m/s	0 m MSL

Model results and measurements at two points inside the lagoon, i.e. 1BF and 2BF (Figure 89), are available in the publication from Table 1 to Table 5.

Similar combinations of wind conditions and water levels as illustrated in Table 16 were reproduced in the SW model with the objective of enabling comparison of model outputs against measurements reported in the publication.

Specifically, the SW model was calibrated against test 01 and test 02, and subsequently validated against test 03, 04 and 05. For all tests, wind conditions were kept stationary for the entire duration of the simulations until wave field reached stationarity too.

Table 17 illustrates simulated values against observed values for spectral wave height (Hm0) parameter. The observed values were averaged over time to return a single value representative of the scenarios simulated in the publication.

Figure 89. Wave observations point location from Carniello et al. [12].

Table 17. List of Hm0 measured and simulated values for scenarios illustrated in Table 16.

Validation test	Point	Hm0 [m] - measu-red	Hm0 - simula-ted	Publication reference table [ref Carniello]
Test 01	2BF	0.50	0.47	**Table 1**
Test 02	2BF	0.77	0.78	Table 2
Test 03	2BF	0.43	0.24	Table 3
Test 04	1BF	0.19	0.25	Table 4
Test 05	1BF	0.04	0.01	Table 5

In general, the SW model shows to be capable of reproducing wave height values for both measurement points far apart in the lagoon. An exception is made for test 03 which leads to an underestimation of simulated wave height under “Scirocco” wind conditions.

It must be noted, however, that for test 02 measured Hm0 drops to a 56% with respect to measured Hm0 in test 03. Test 02 simulates a “Bora” event with more than double in value (i.e., 15m/s) wind speed applied with respect to test 03 (i.e., 8 m/s) and, given the directional sector, with a considerable lager fetch. It would be expected a larger drop in energy transfer and hence a more pronounced reduction in spectral wave height. This misalignment could be due to the teat assumption of keeping the wind stationary for a number of hours, which is an unrealistic condition.

5.4 HD model results

The calibration and validation tasks ensured that the model is capable of closely reproducing general hydrodynamics inside the lagoon.

Similar to the calibration task, an additional analysis was carried out for a period going from 01-Jan-2020 to 01-Oct-2020 with the objective of producing fitting quality indices (simulated vs observed values) for all tide gauges discussed in Section 5.2. Figure 90 to Figure 99 show the outcome of such analysis. It must be noted that, since the M.O.S.E. barriers operational windows are not known, the analysis was run for the nine-month period excluding the last three months of the year for which the M.O.S.E. system was operating. This allows to avoid time windows giving rise to excessive discrepancies between the simulated and observed values which would partially invalidate the calculation of the statistical indices. Lastly, some tide gauges show a shorter time window used for comparisons due to unavailability of observed data.

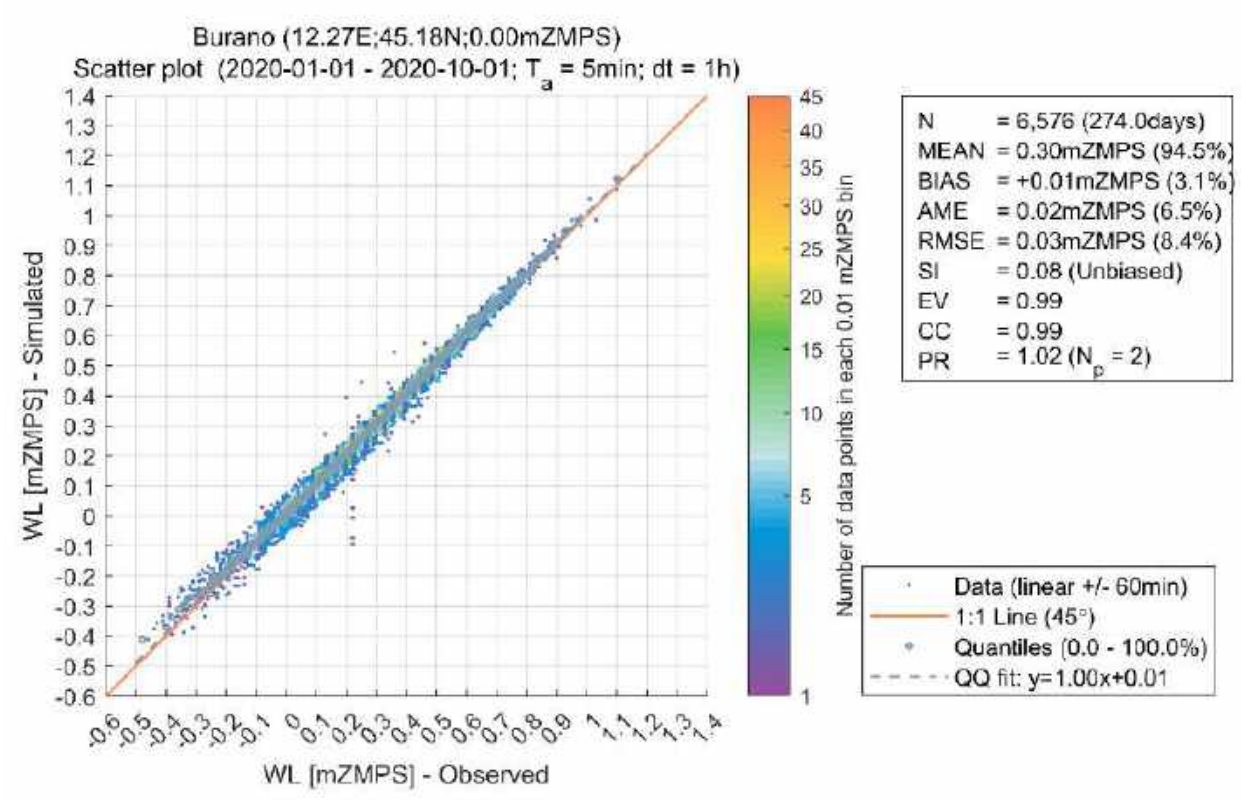

Figure 90. Burano results analysis: QQ plot and fitting quality indices.

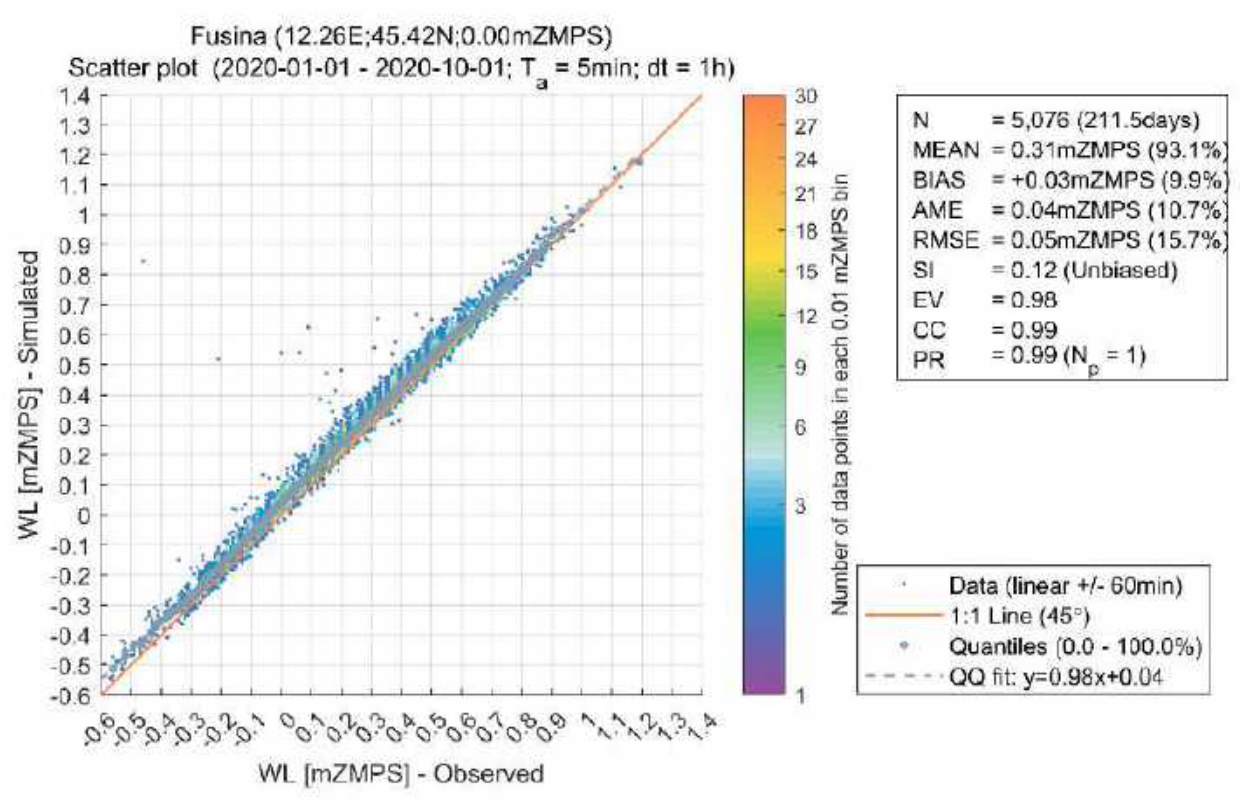

Figure 91. Fusina results analysis: QQ plot and fitting quality indices.

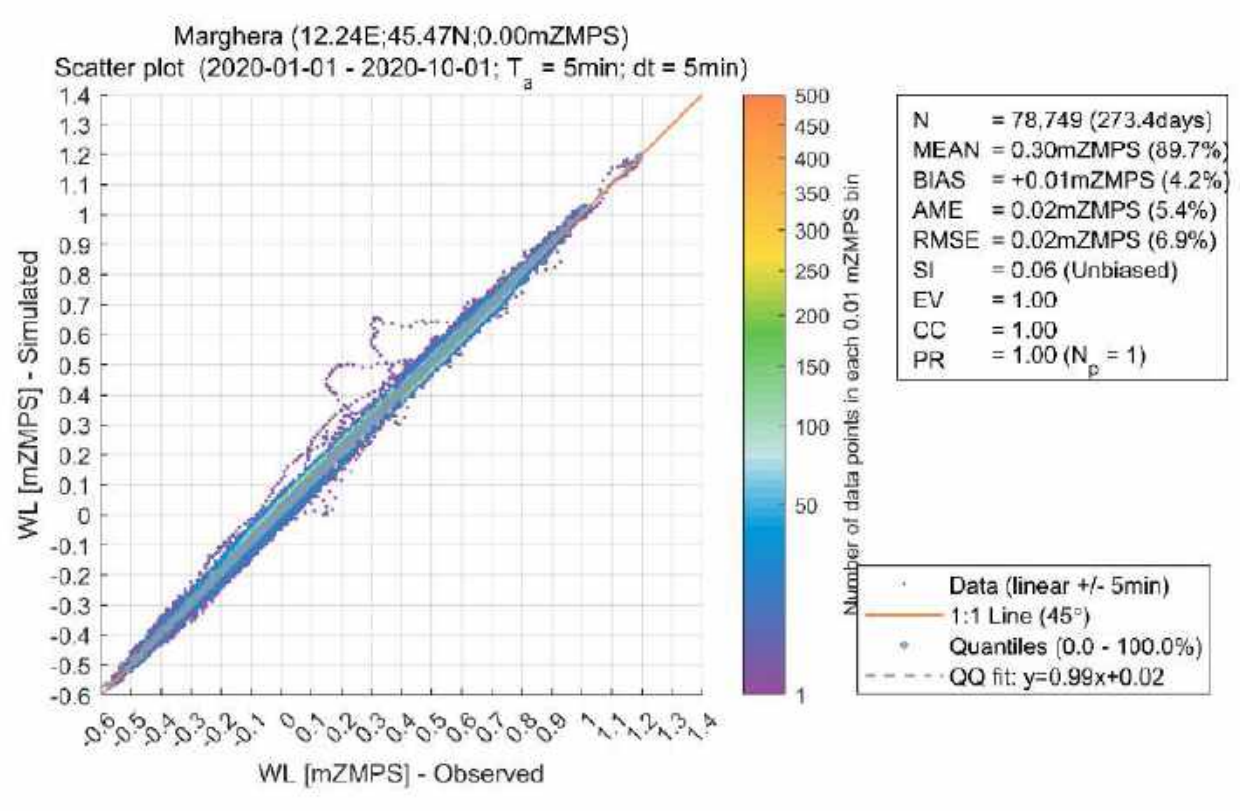

Figure 92. Marghera results analysis: QQ plot and fitting quality indices.

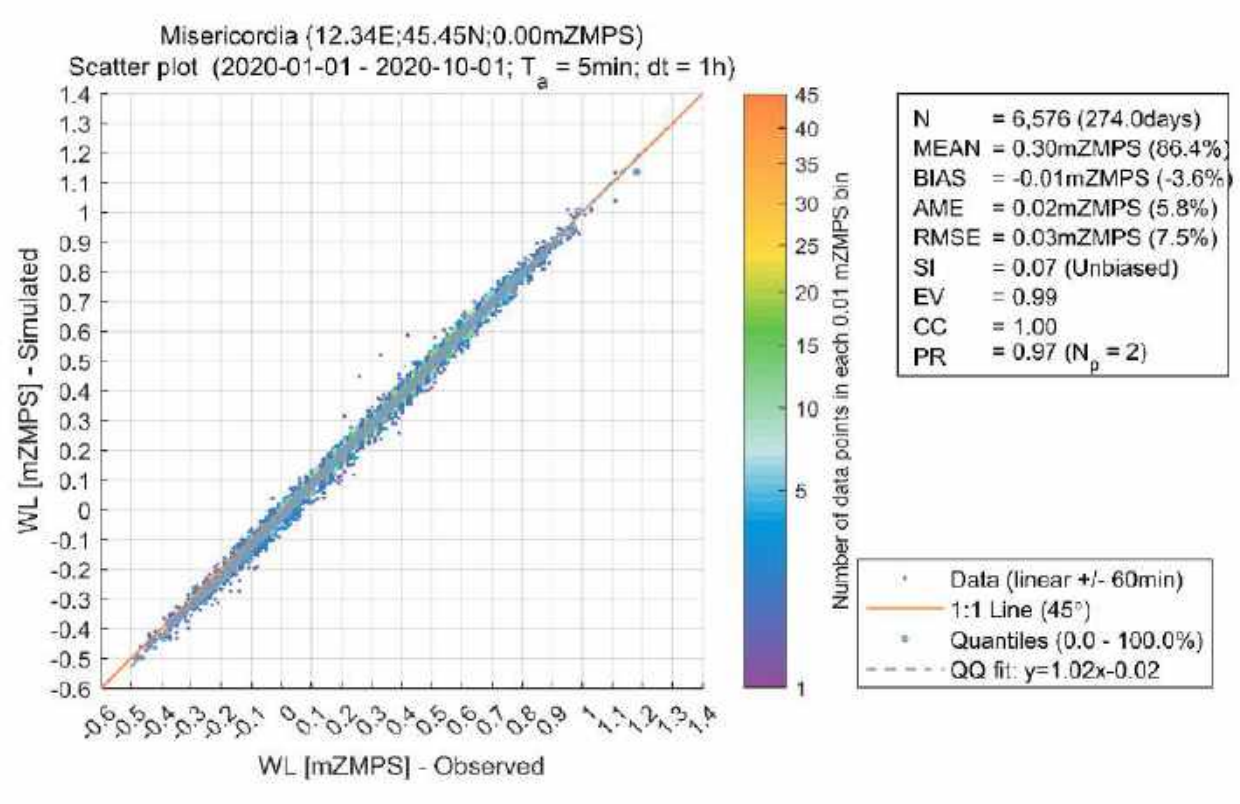

Figure 93. Misericordia results analysis: QQ plot and fitting quality indices.

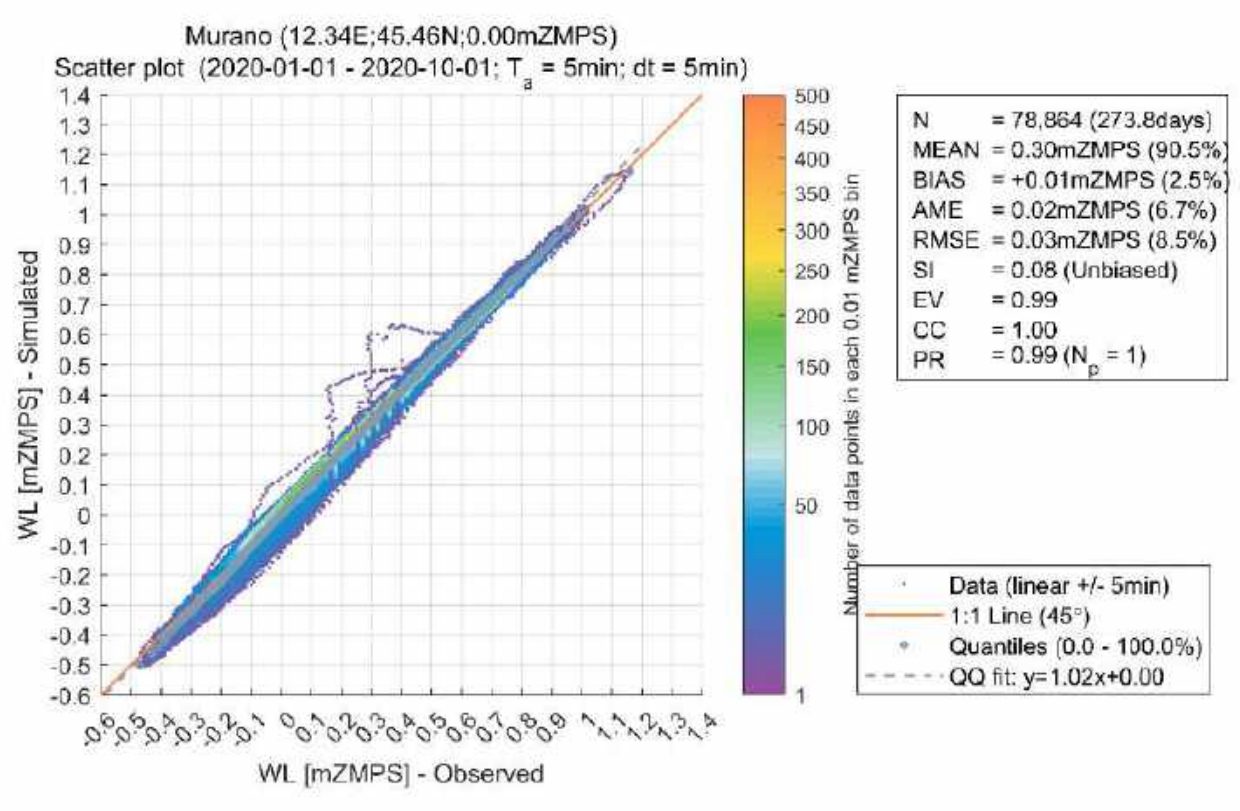

Figure 94. Murano results analysis: QQ plot and fitting quality indices.

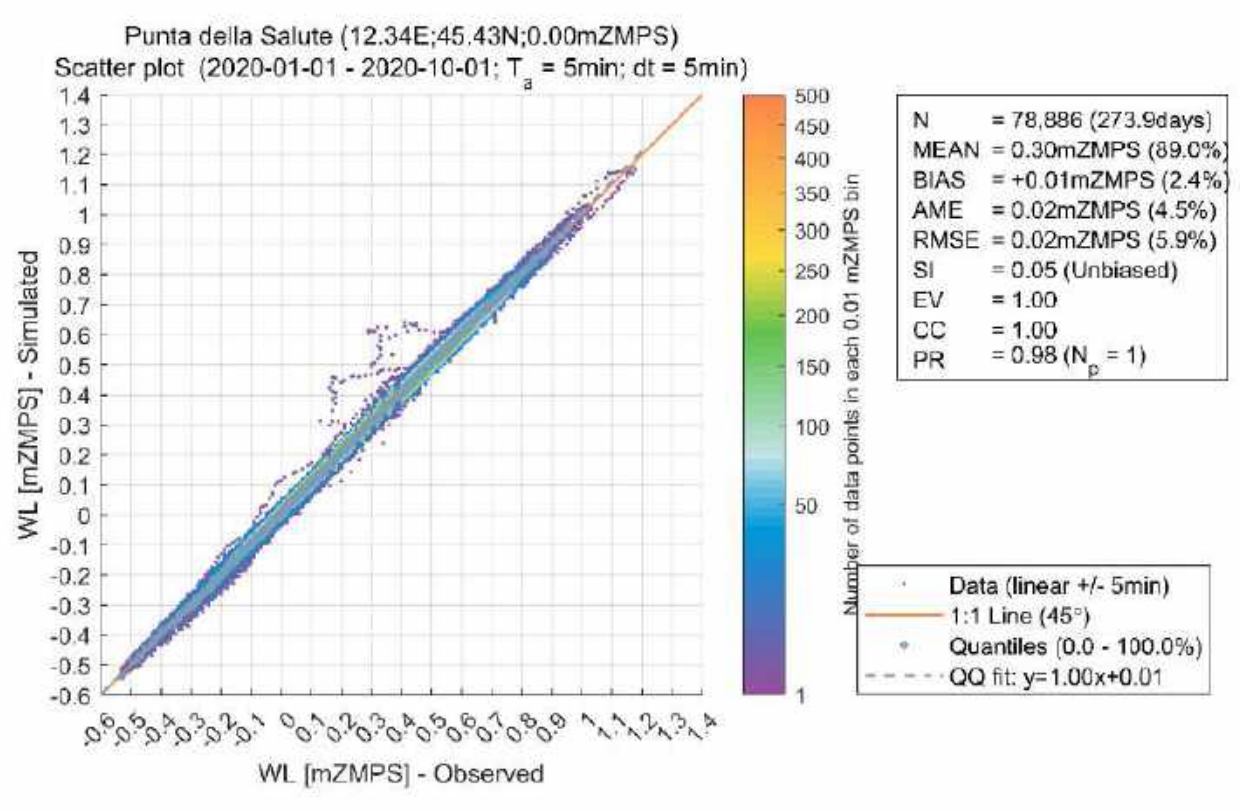

Figure 95. Punta della Salute results analysis: QQ plot and fitting quality indices.

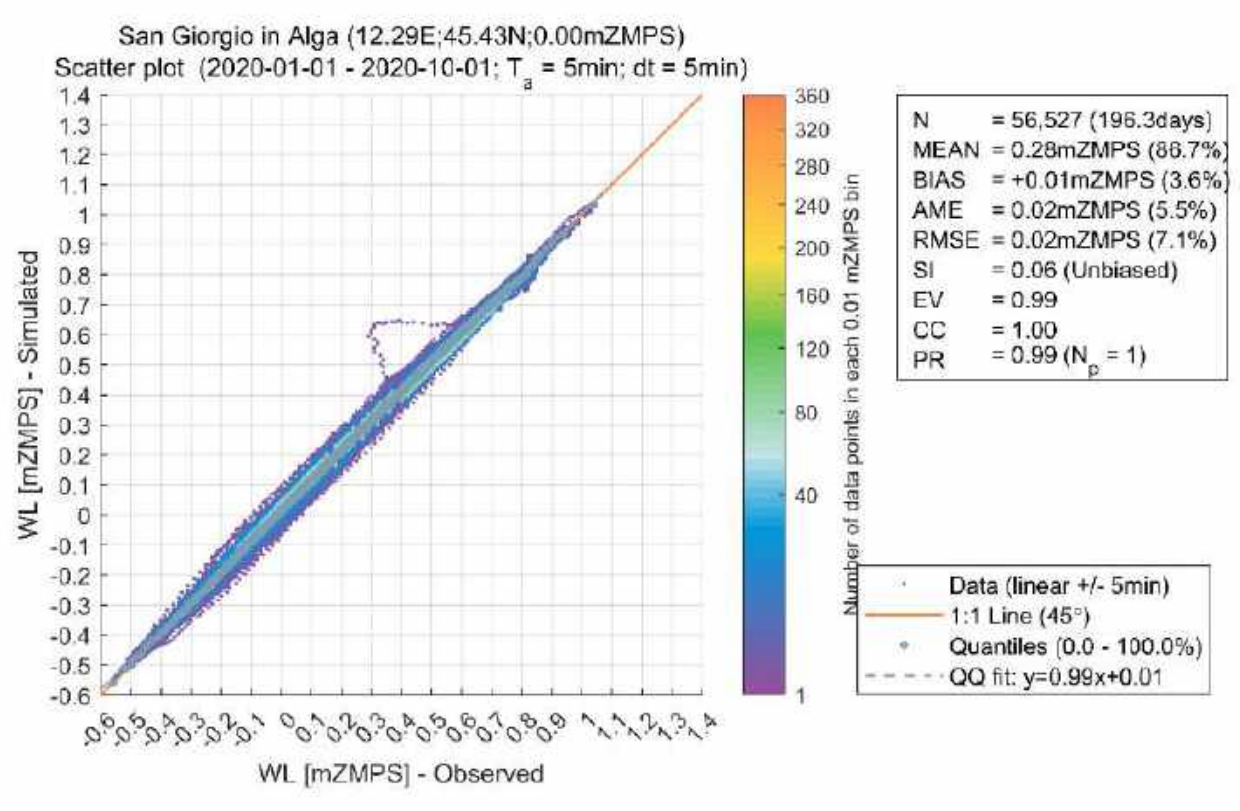

Figure 96.. San Giorgio in Alga results analysis: QQ plot and fitting quality indices.

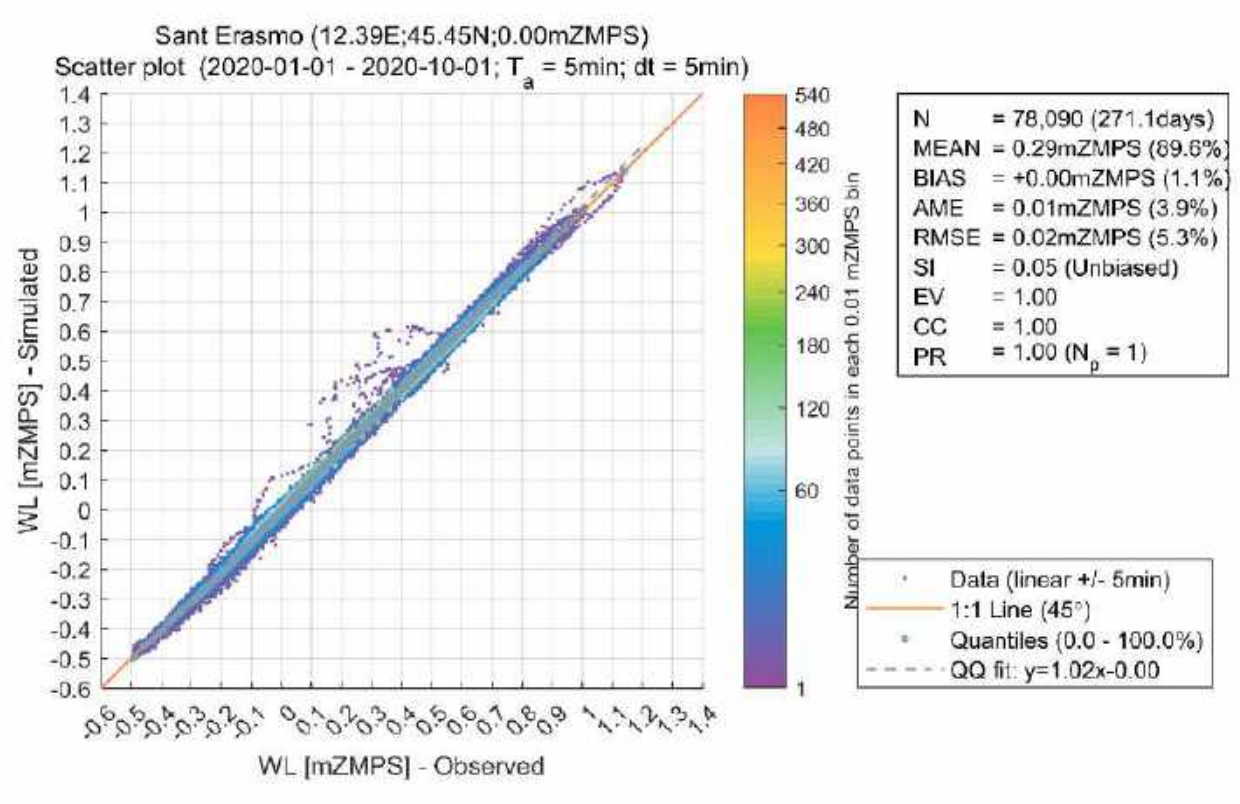

Figure 97. Sant Erasmo results analysis: QQ plot and fitting quality indices.

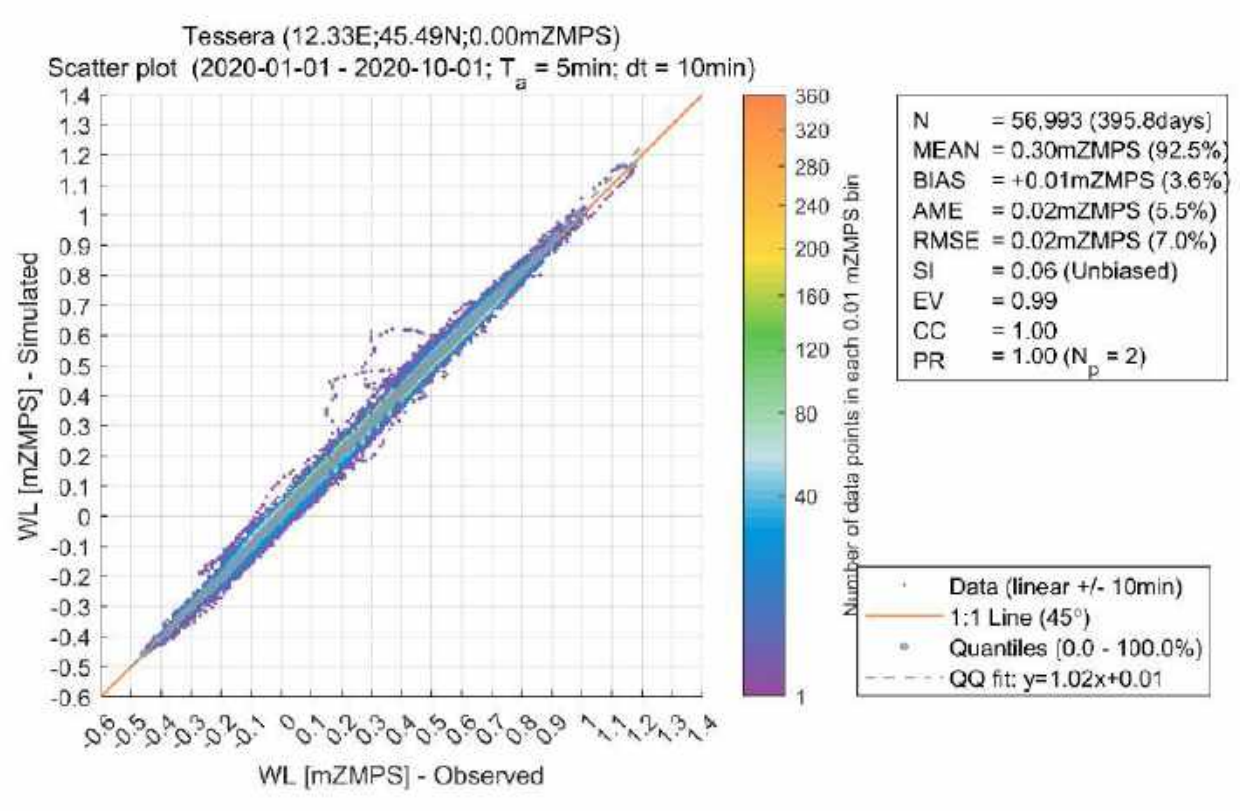

Figure 98. Tessera results analysis: QQ plot and fitting quality indices.

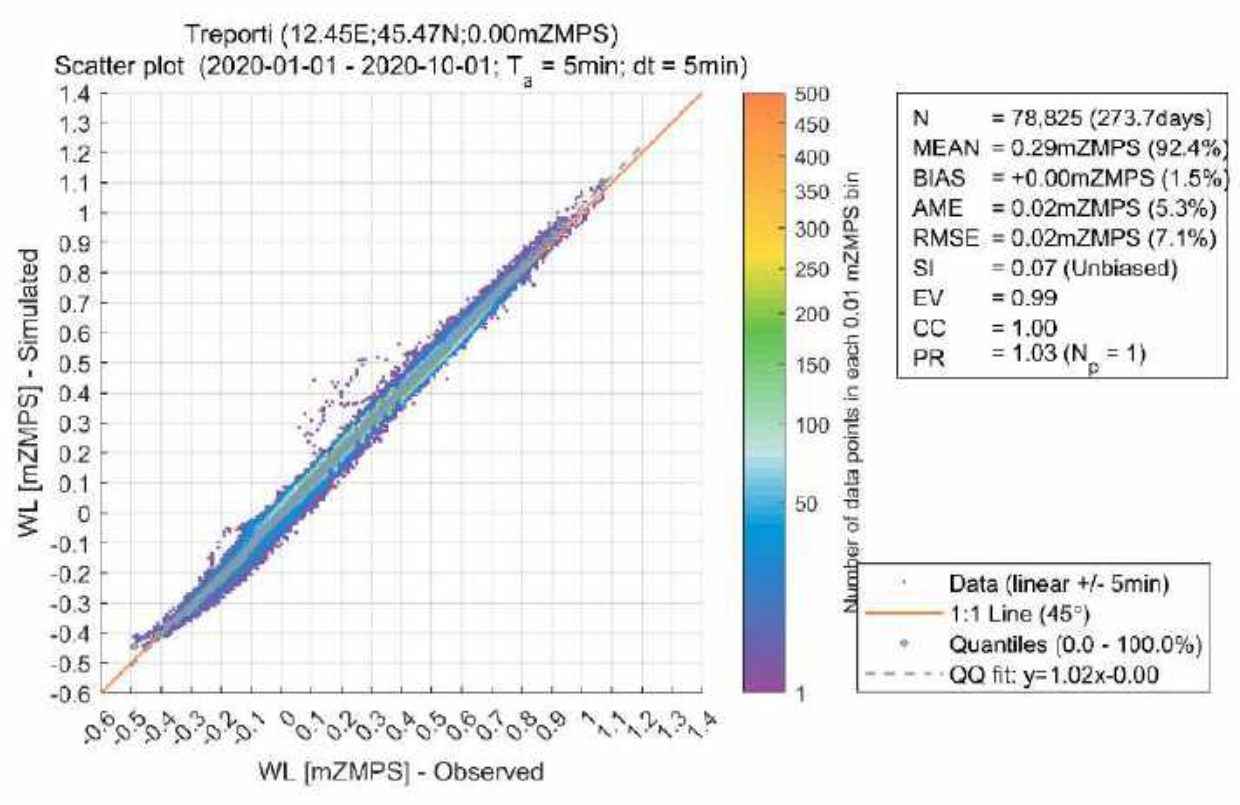

Figure 99.Treporti results analysis: QQ plot and fitting quality indices.

Figure 55 shows that the water levels observed at the three inlets which were used as model water level boundary conditions, do not exhibit significant differences. The water level distribution across the lagoon thus is due to the basin response mechanisms inclusive of wind forcing.

As an example, Figure 100 and Figure 101 shows respectively a single instance of high water occurring at 26-Apr-2020 00:10:00 and low water occurring at 30-Apr-2020 09:00:00.

Typical flow fields generated at mid-flood (21-Apr-2020 18:50:00) and mid-ebb (21-Apr-2020 01:00:00) conditions are illustrated in Figure 102 and Figure 104.

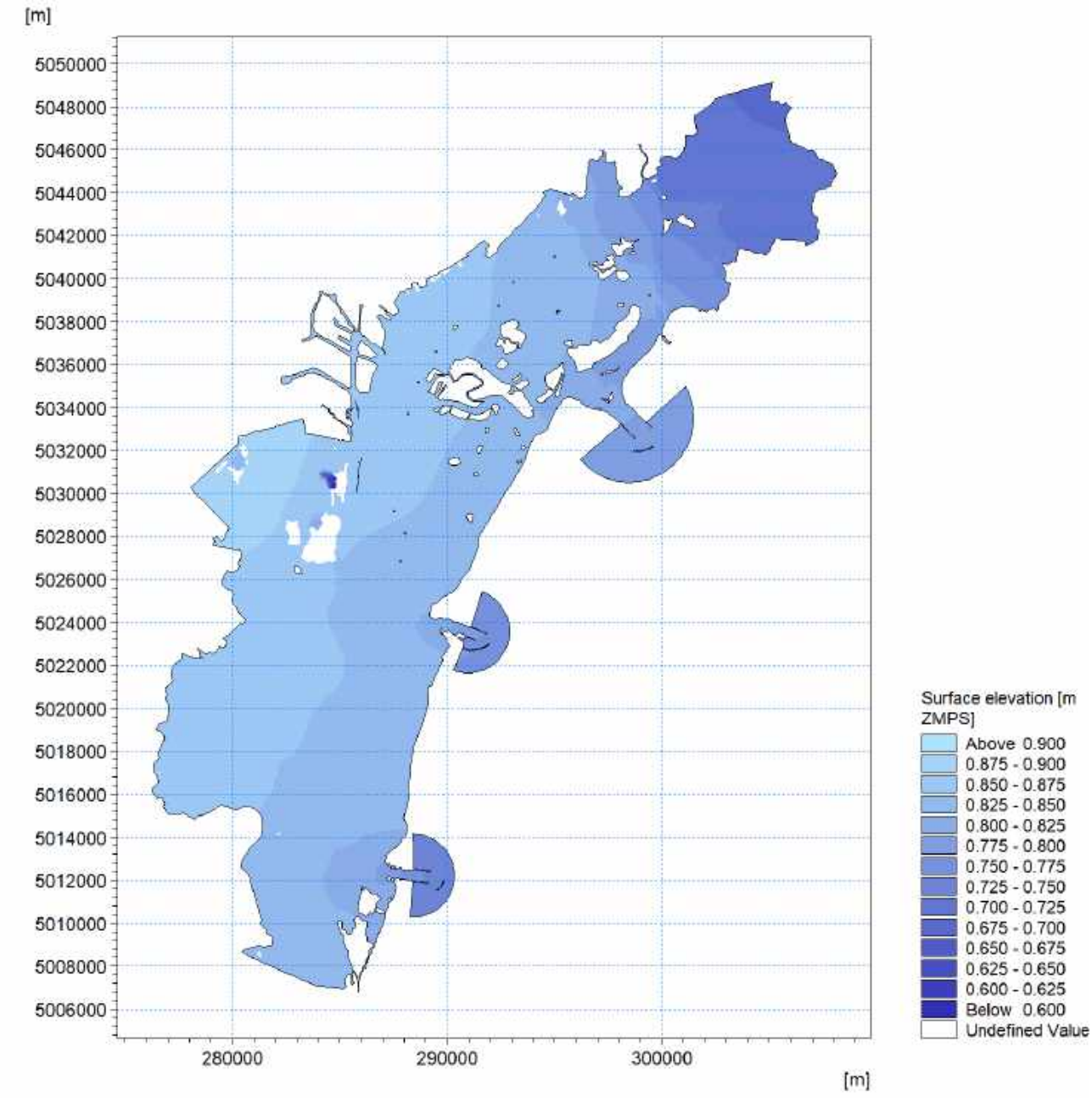

Figure 100. Water level distribution corresponding to a high-water event at 26-Apr-2020 00:10:00.

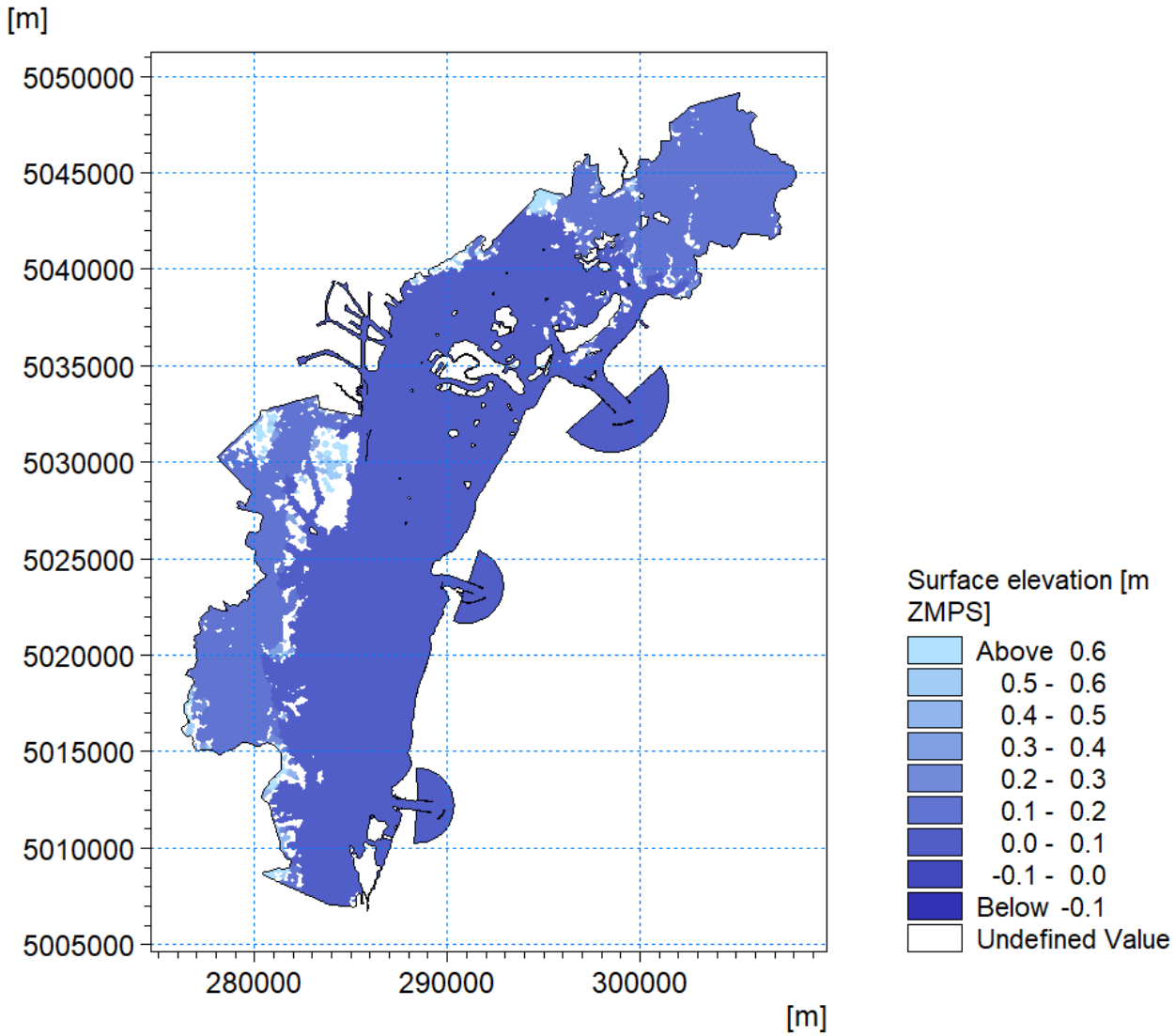

Figure 101. Water level distribution corresponding to a low-water event at 30-Apr-2020 09:00:00.

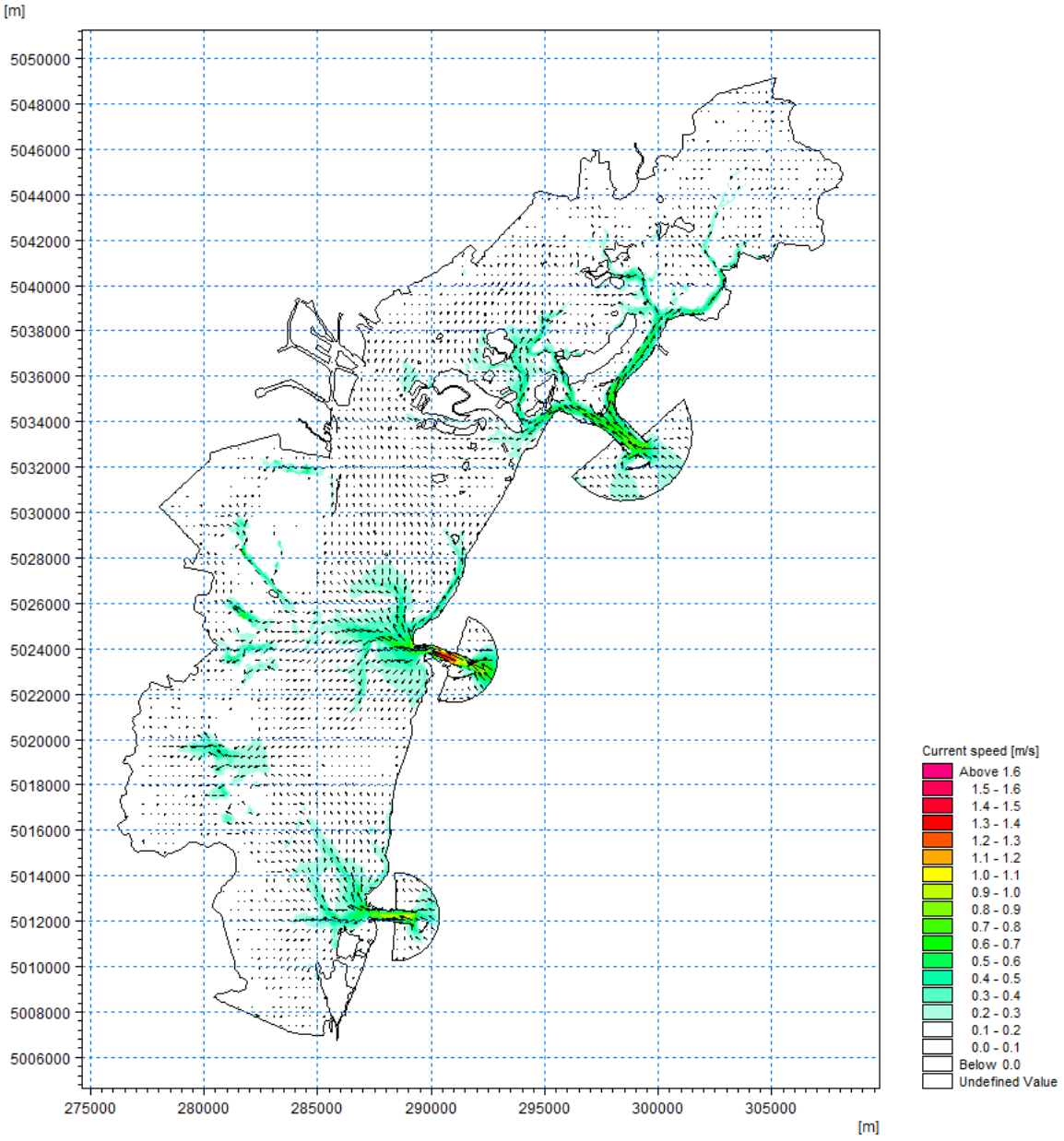

Figure 102. Typical current field at mid-flood tide (21-Apr-2020 18:50:00).

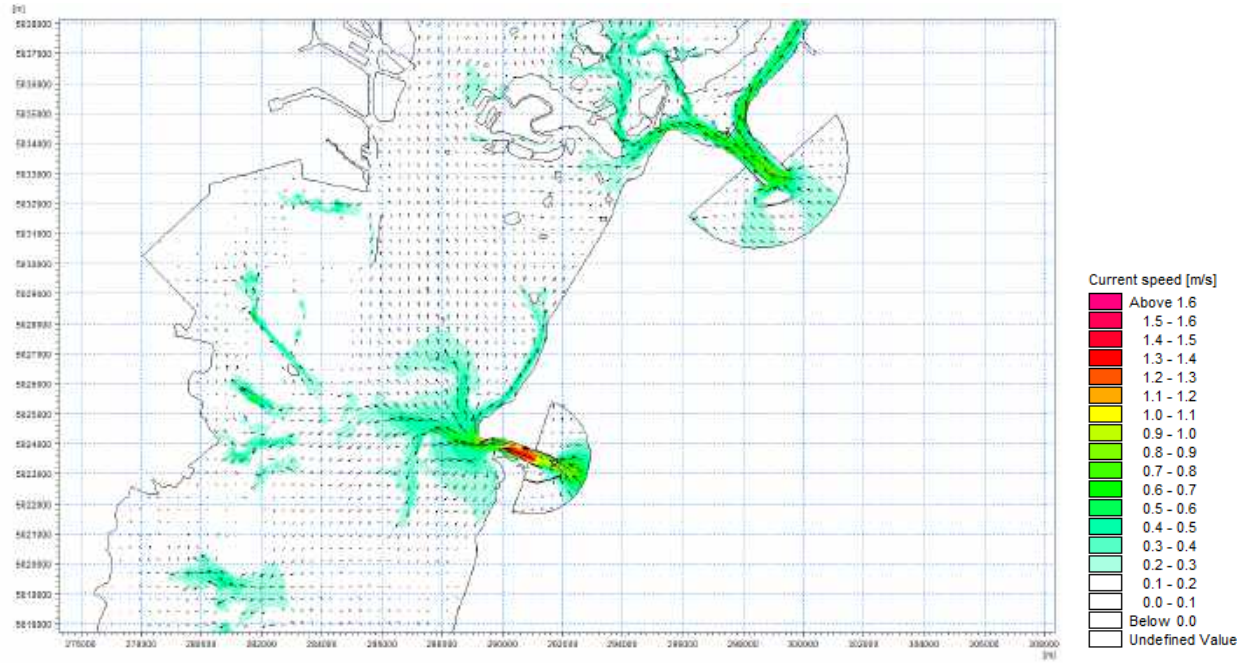

Figure 103. Close up of the central part of the Lagoon at mid-flood tide (21-Apr-2020 18:50:00).

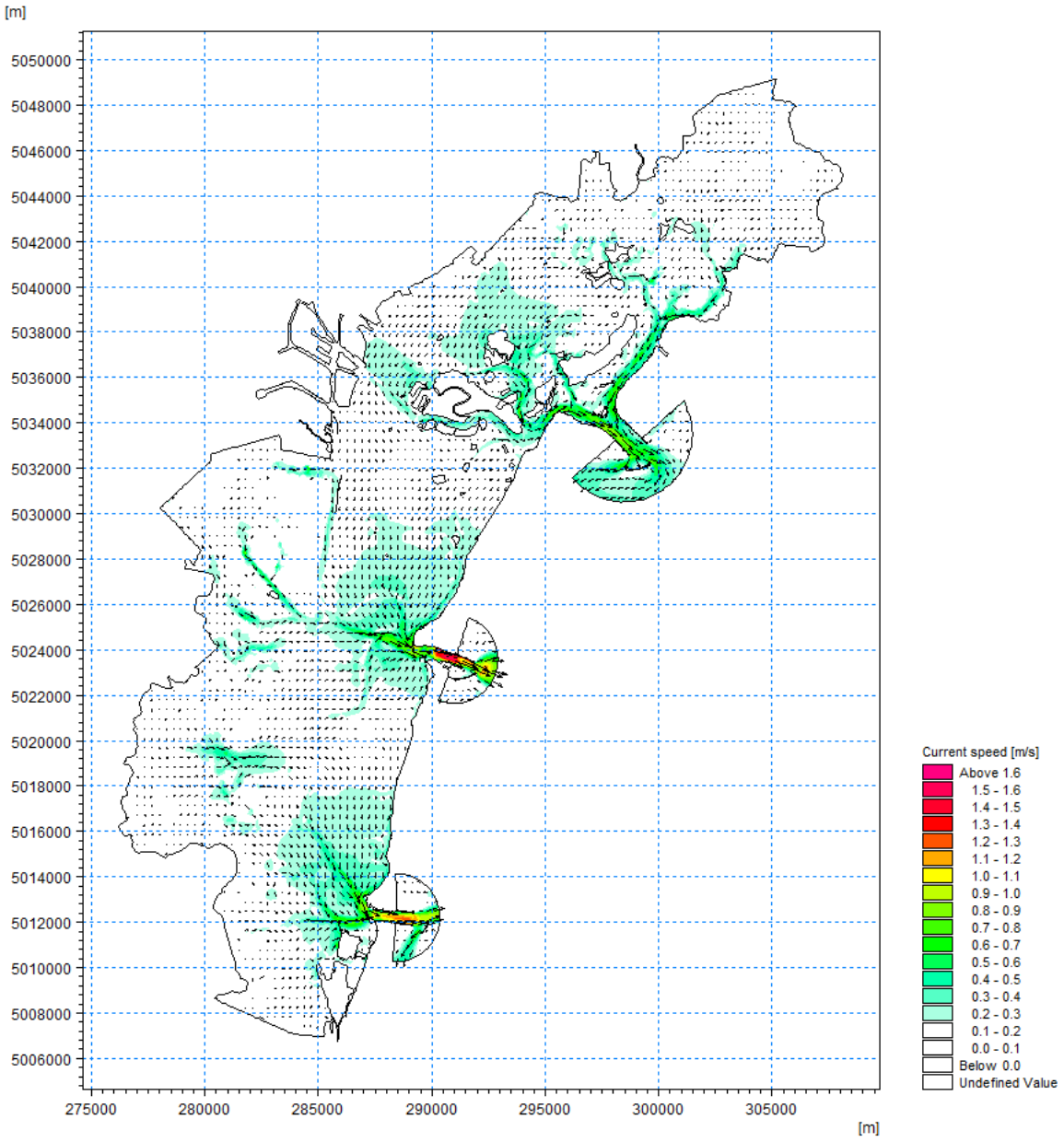

Figure 104. Typical current field at mid-ebb tide (21-Apr-2020 01:00:00).

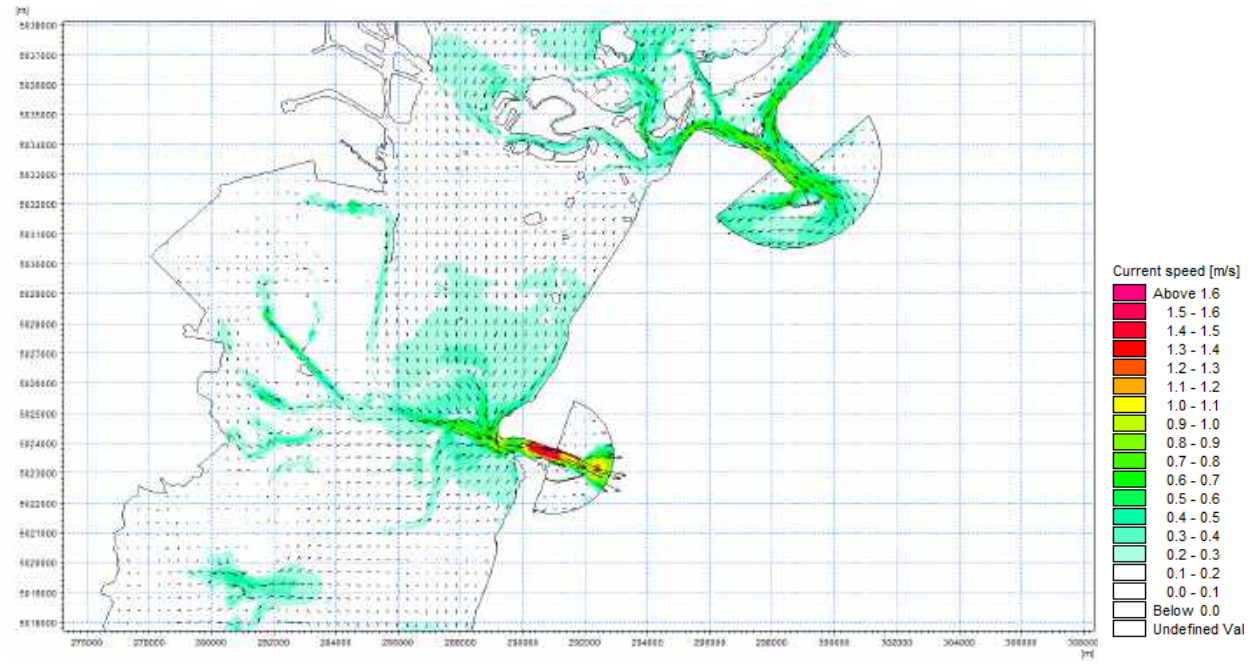

Figure 105.Close up of the central part of the Lagoon at mid-ebb tide (21-Apr-2020 01:00:00).

Flow speed 50th, 90th and 98th percentiles were computed for the entire simulated period to provide a more comprehensive picture of the overall flow field distribution inside the lagoon (Figure 106 to Figure 108).

The percentiles maps, as one would expect, show larger current speed magnitude in the main lagoon channels departing from lagoon openings reaching maximum values through the inlets.

Regardless the percentile, Malamocco inlet typically shows larger flow speed values reaching a maximum value of 1.7 m/s for the 98th percentile, whit Lido and Chioggia inlets reaching maximum values of 1.1 m/s and 1.2 m/s respectively.

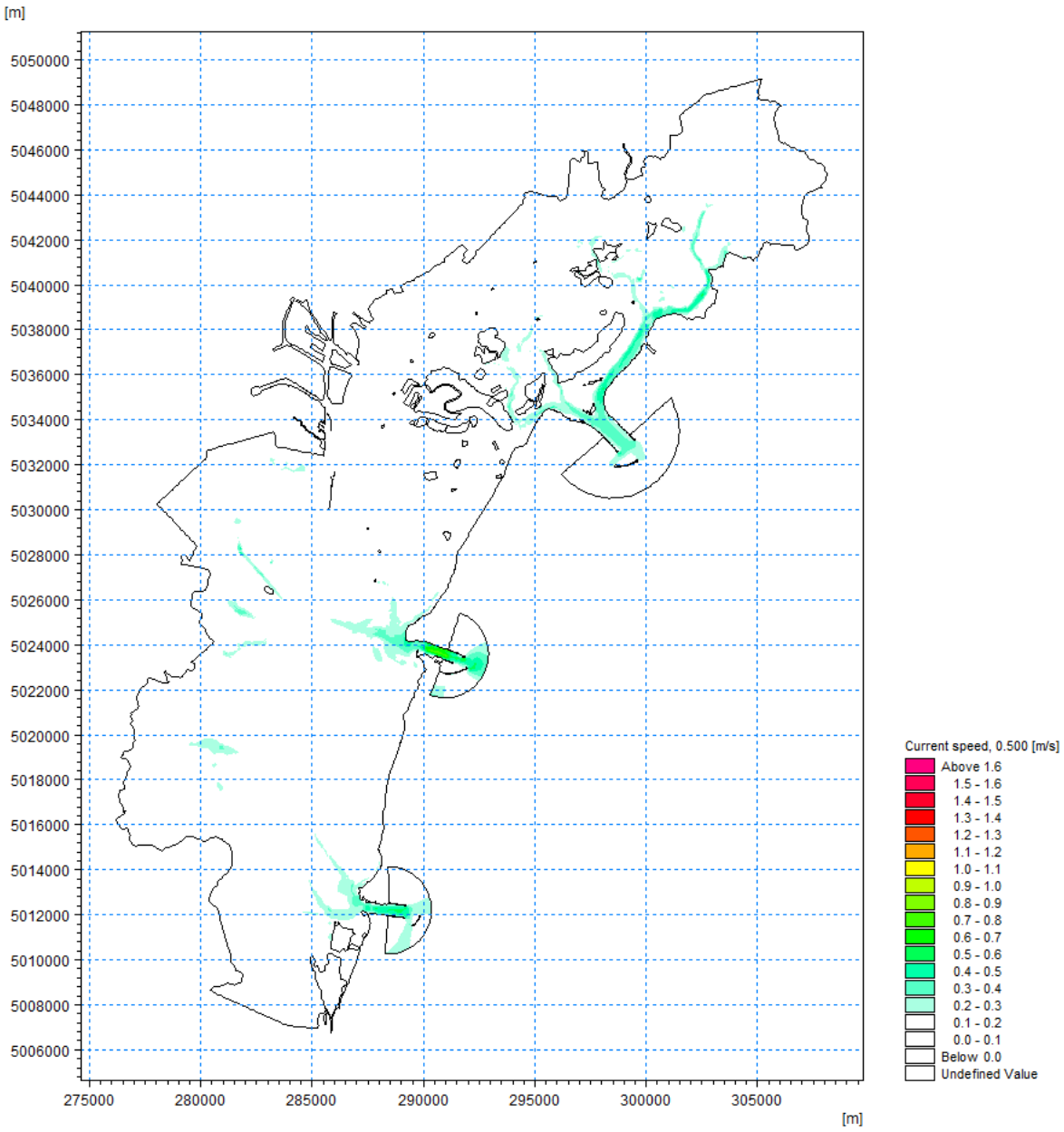

Figure 106. Flow field: 50th percentile map.

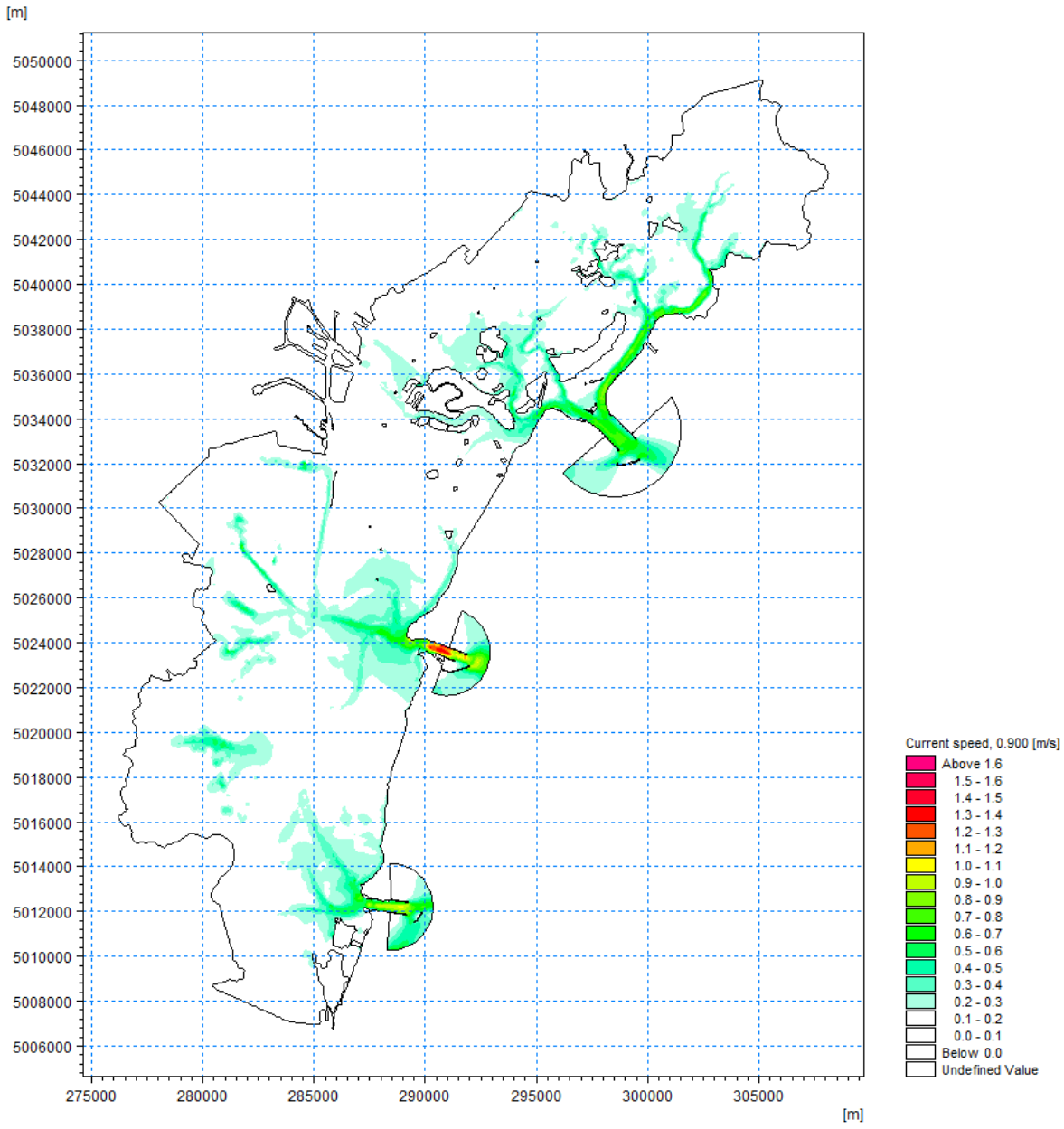

Figure 107. Flow field: 90th percentile map.

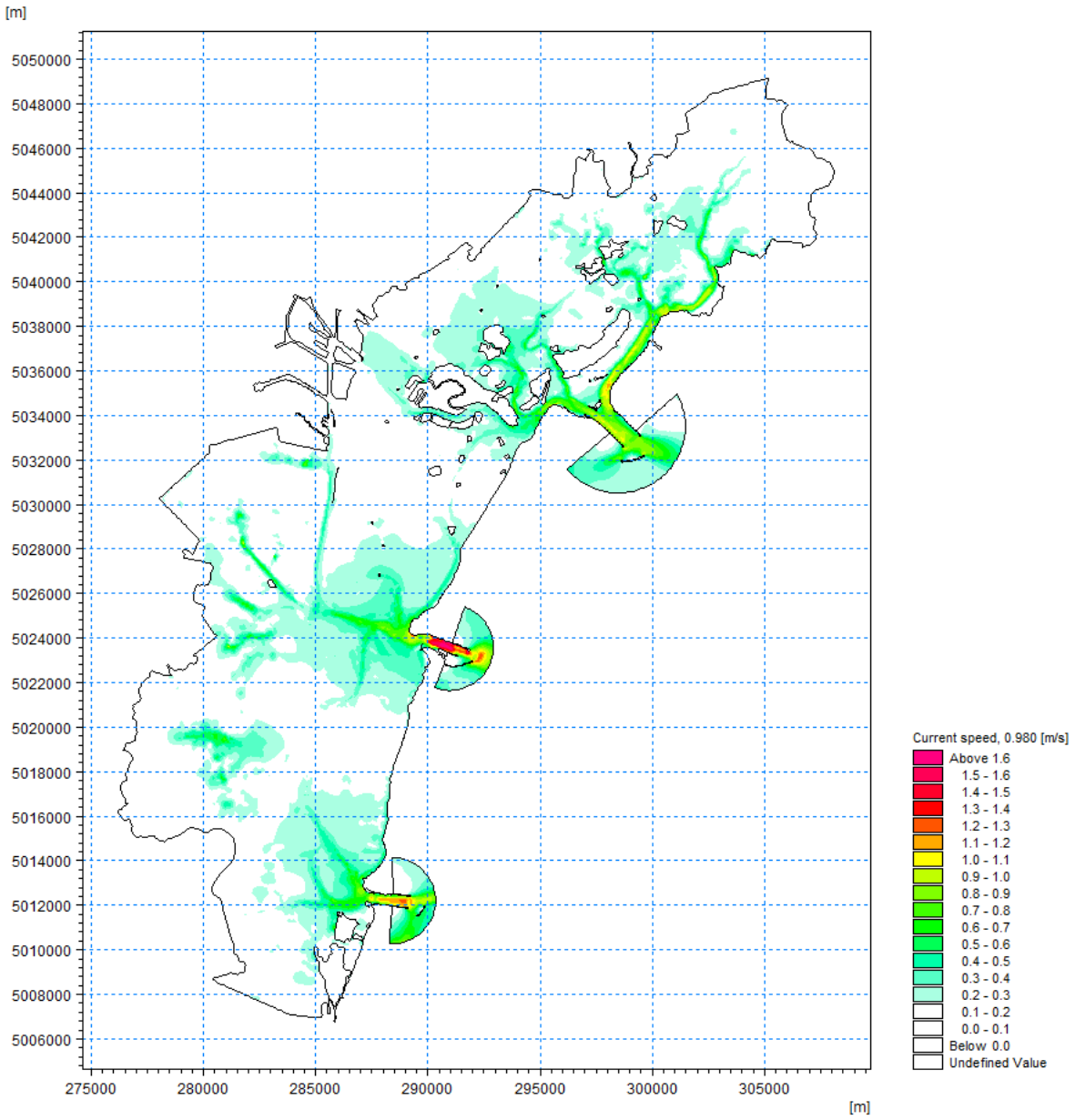

Figure 108. Flow field: 98th flow percentile map.

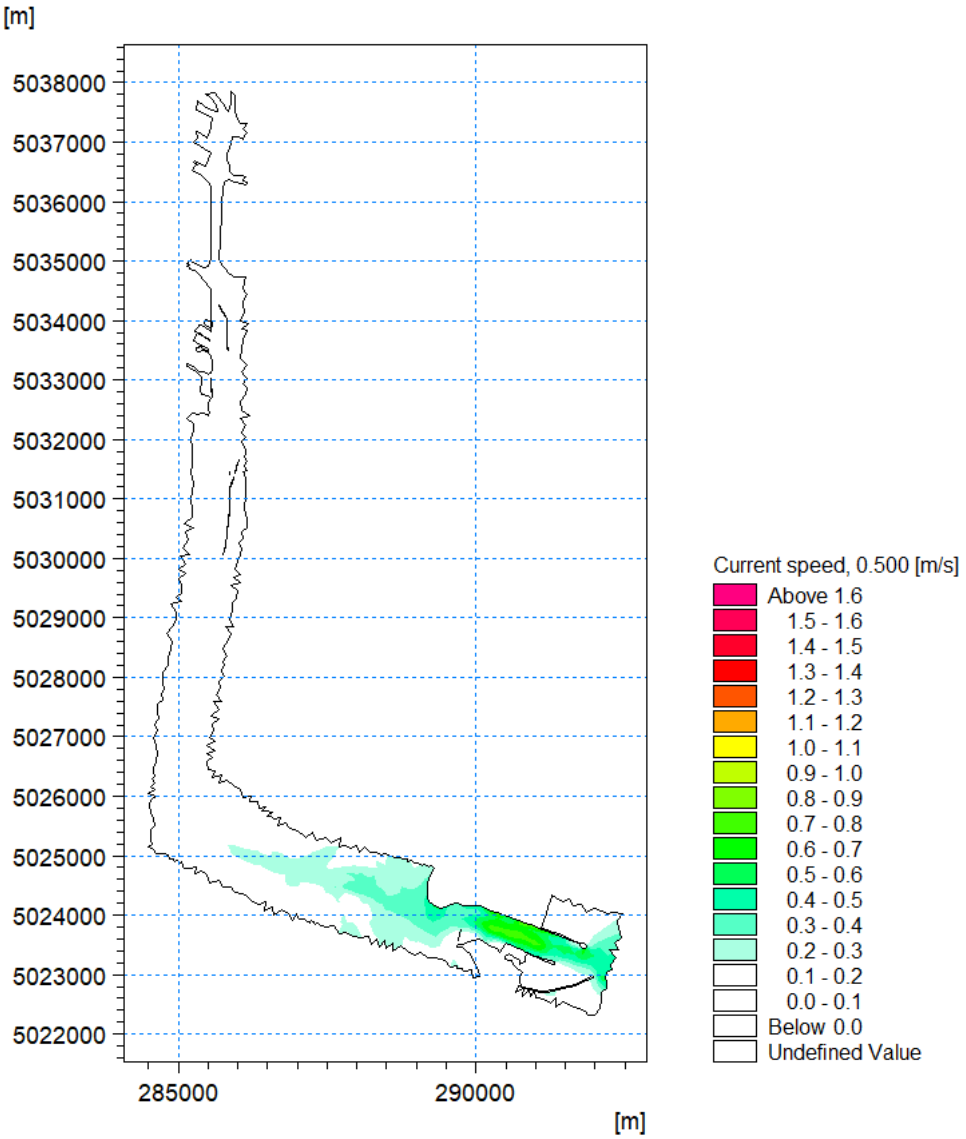

Figure 109. Flow field: 50th percentile map in the Malamocco-Marghera channel.

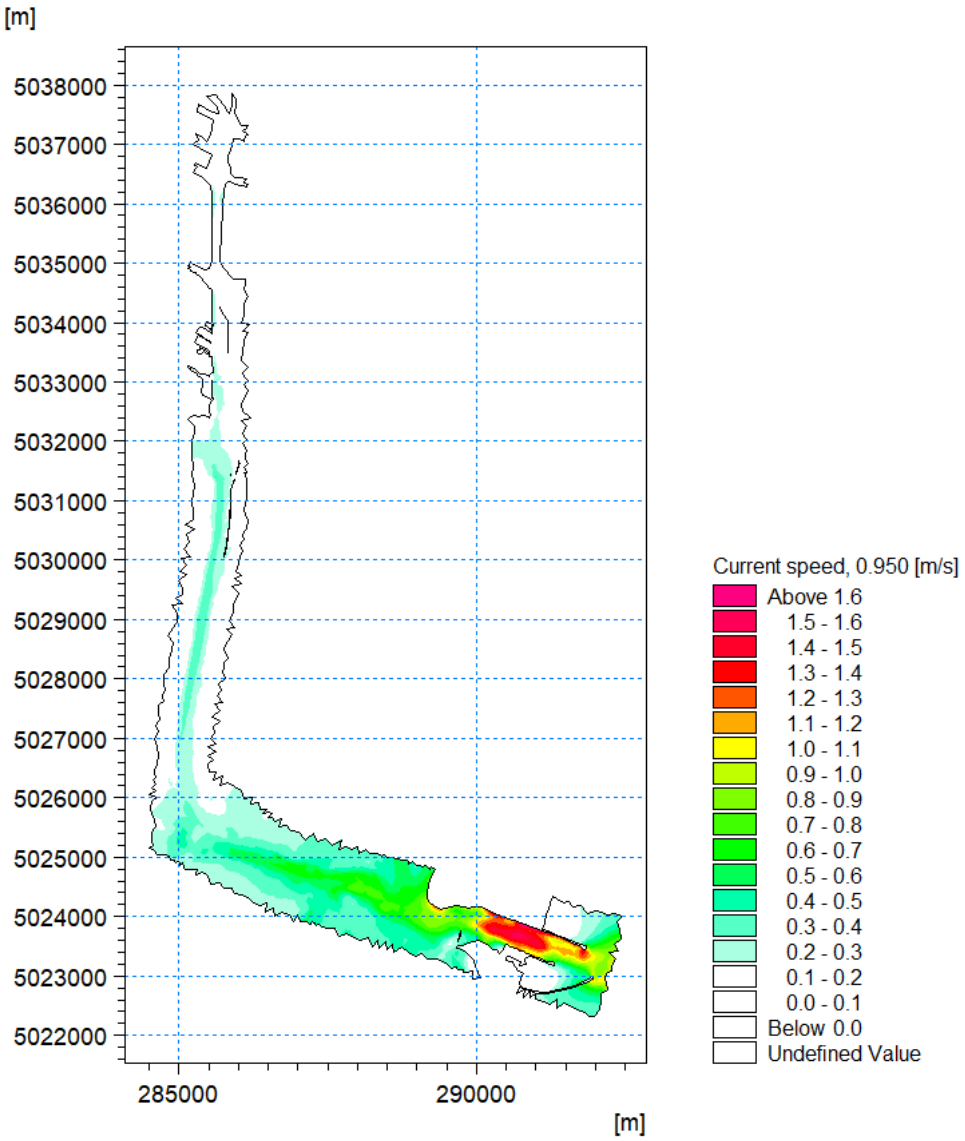

Figure 110. Flow field: 95th percentile map in the Malamocco-Marghera channel.

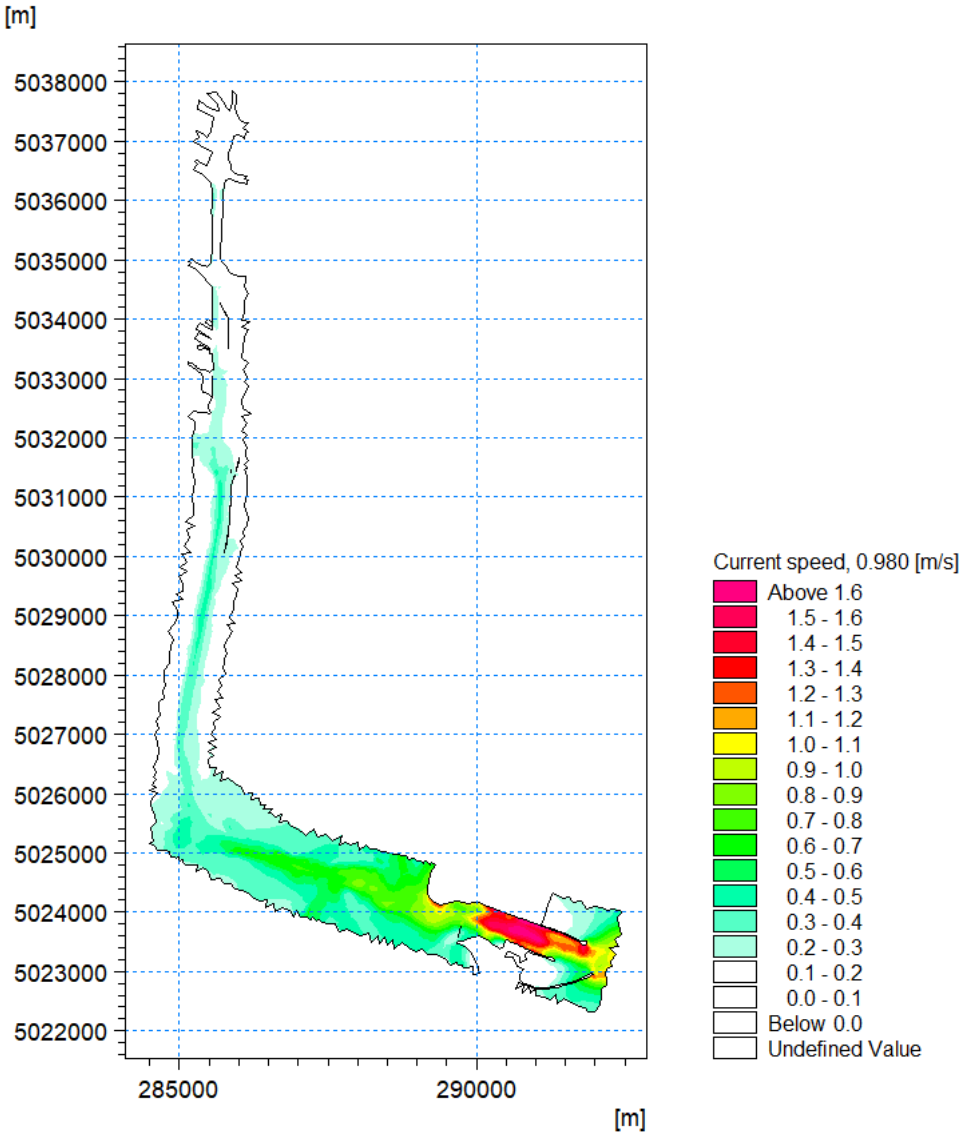

Figure 111. Flow field: 98th percentile map in the Malamocco-Marghera channel.

5.5 SW model results

As mentioned in Section 3.2.2 waves inside Venice lagoon are mostly generated through wind-water surface energy transfer mechanisms. These wind-waves are typically characterised by short periods and their growth is influenced by the magnitude and persistence of the wind system blowing over the lagoon as well as by the fetch extent.

For Venice lagoon the fetch represents the main limiting factor to wave growth, with “Bora” winds blowing parallel to the major lagoon axis and giving rise, typically, to more energetic sea-states.

A second limiting factor is the total water depth over which waves can propagate, which represents a key element in a marked tidal environment such as the Venice Lagoon.

In this regard the wave climate inside the lagoon is a result of a complex energy balance between wind energy gain and depth-induced breaking energy loss.

For that reason, Scirocco wind events during high waters, despite acting upon a reduced fetch, could occasionally give rise to sea states comparable to “Bora” events occurring at low water tide stage.

Generally, longer period waves propagating from Northern Adriatic Sea through the inlets are of little interest in relation to the overall wave climate inside the lagoon and they are only relevant in limited areas around the inlets.

Figure 112 and Figure 113 show significant wave height maps for a typical “Bora” and “Scirocco” events occurring at 26-Mar-2020 11:30:00 and at 04-Dec-20 22:00:00, respectively.

To gain a more comprehensive insight of the overall wave climate inside the lagoon, statistics of wave height distribution in the lagoon accounting for the 50^{th},90^{th} and 98^{th} percentiles are computed (Figure 114 to Figure 116).

Typically, larger waves are found in the southern portion of the lagoon, i.e. between Malamocco and Chioggia inlet, owing that to the larger fetch along the major lagoon axis during wind events from North-East direction.

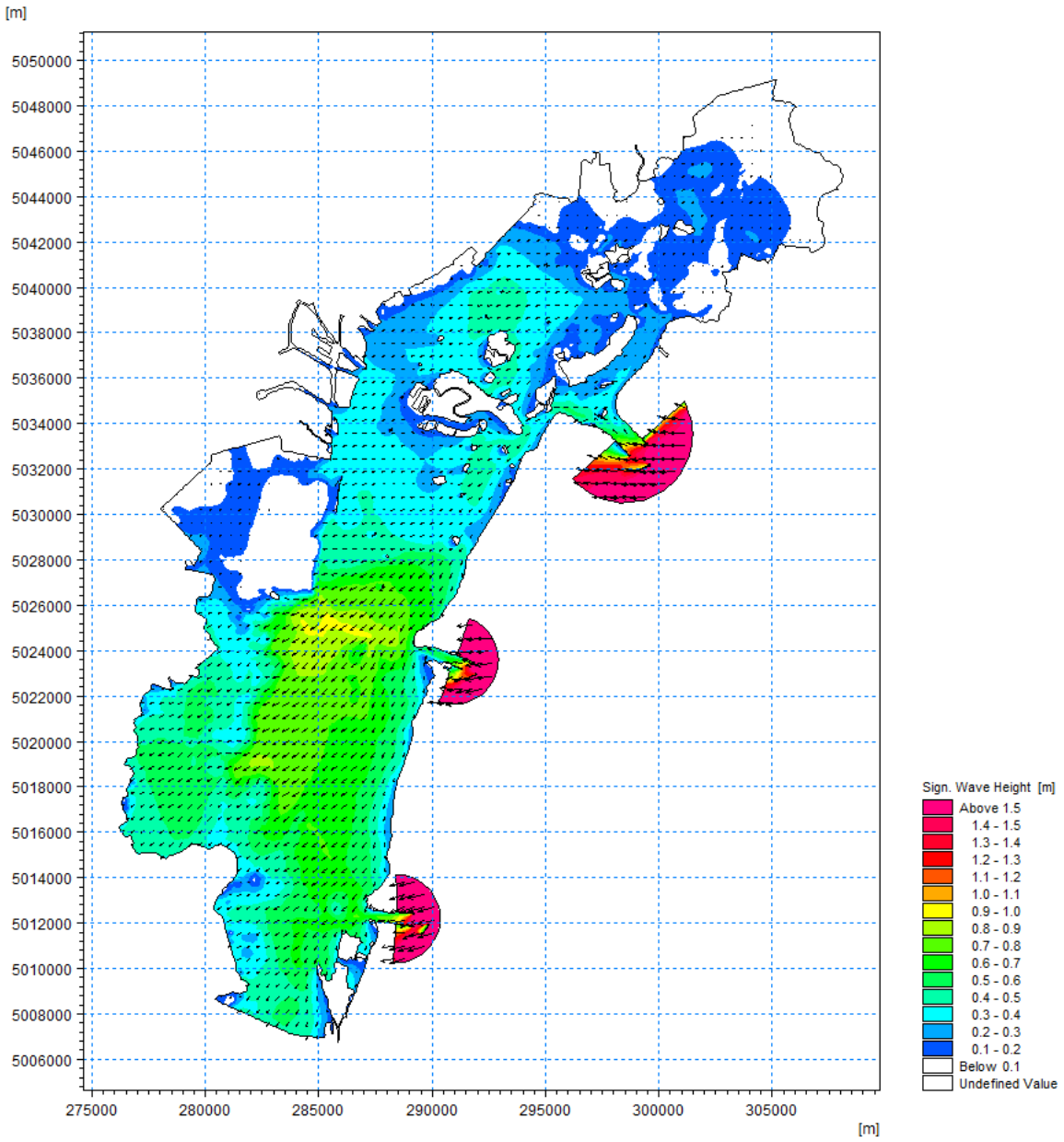

Figure 112. Wave height distribution during a "Bora" event (26-Mar-2020 11:30:00).

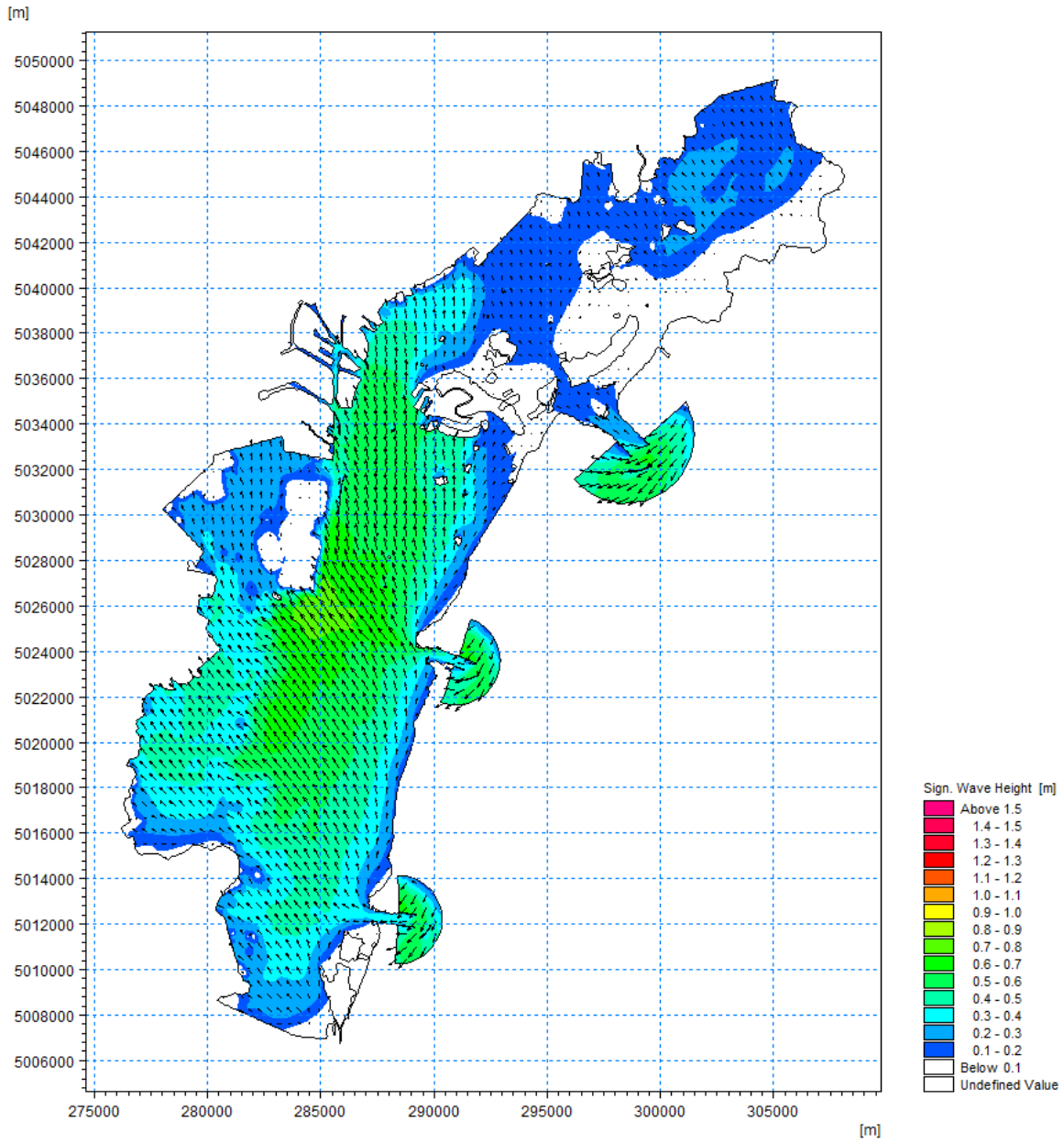

Figure 113. Wave height distribution during a "Scirocco" event (04-Dec-20 22:00:00).

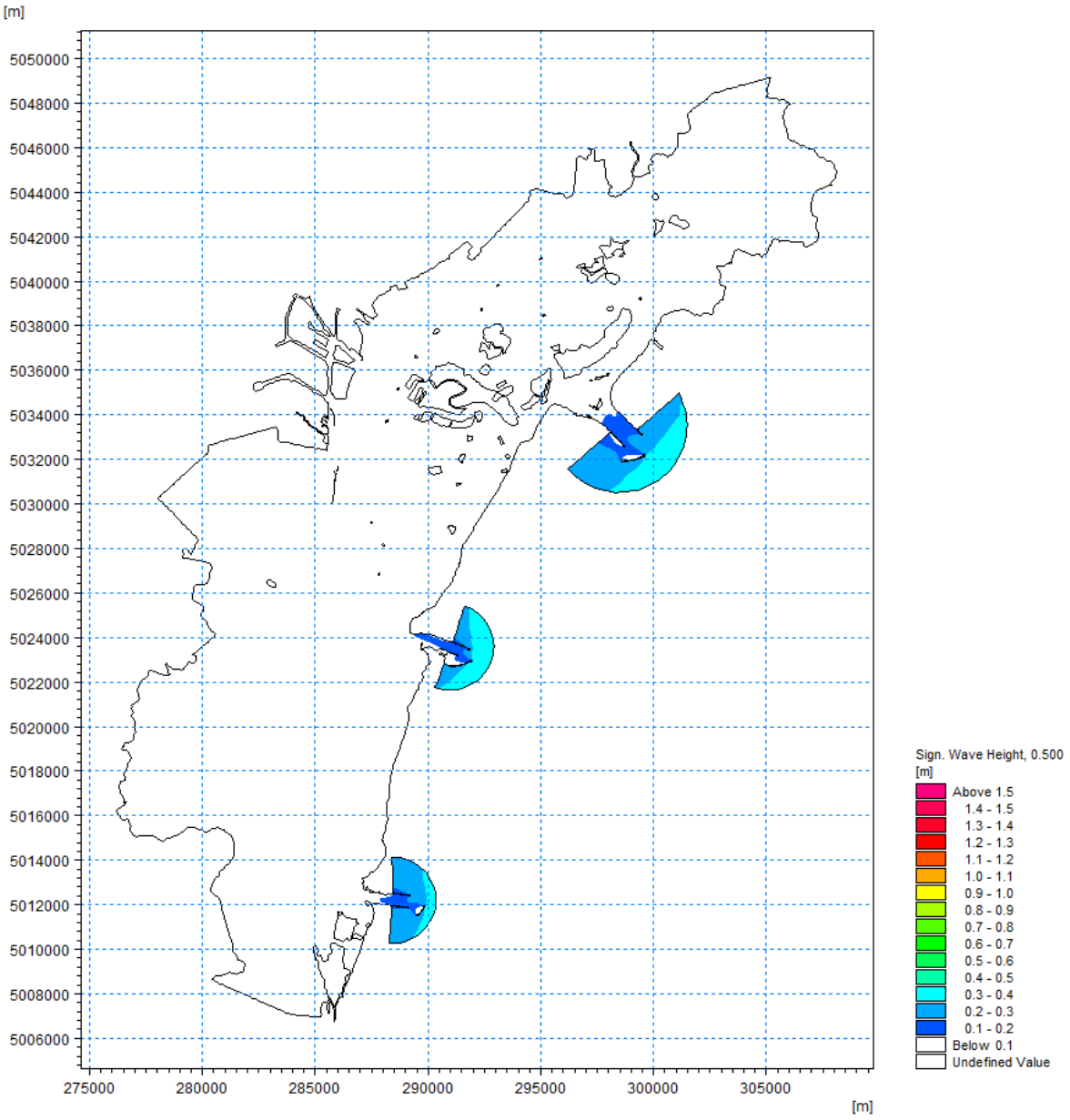

Figure 114. Wave height 50th percentile map.

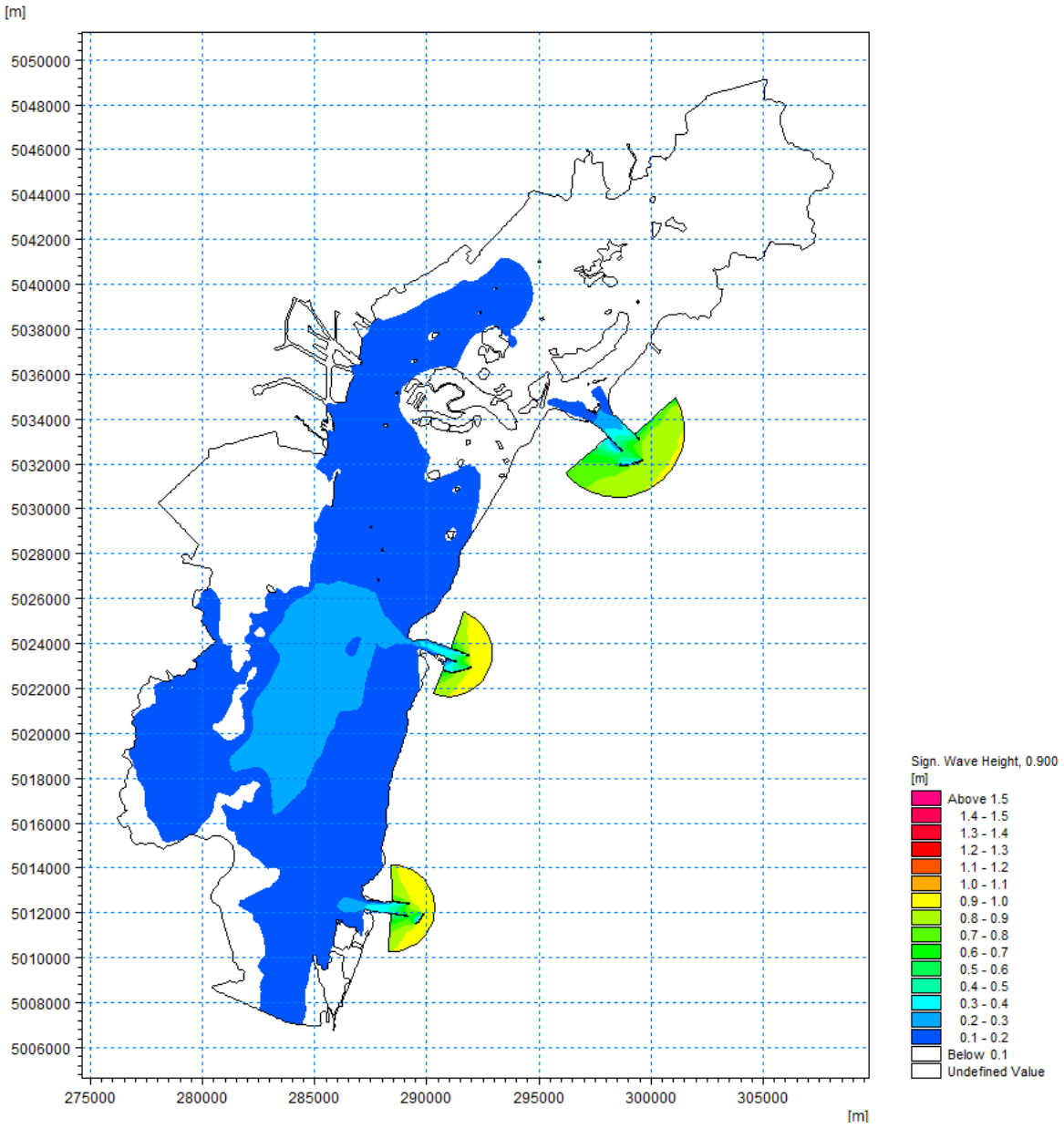

Figure 115. Wave height 90th percentile map.

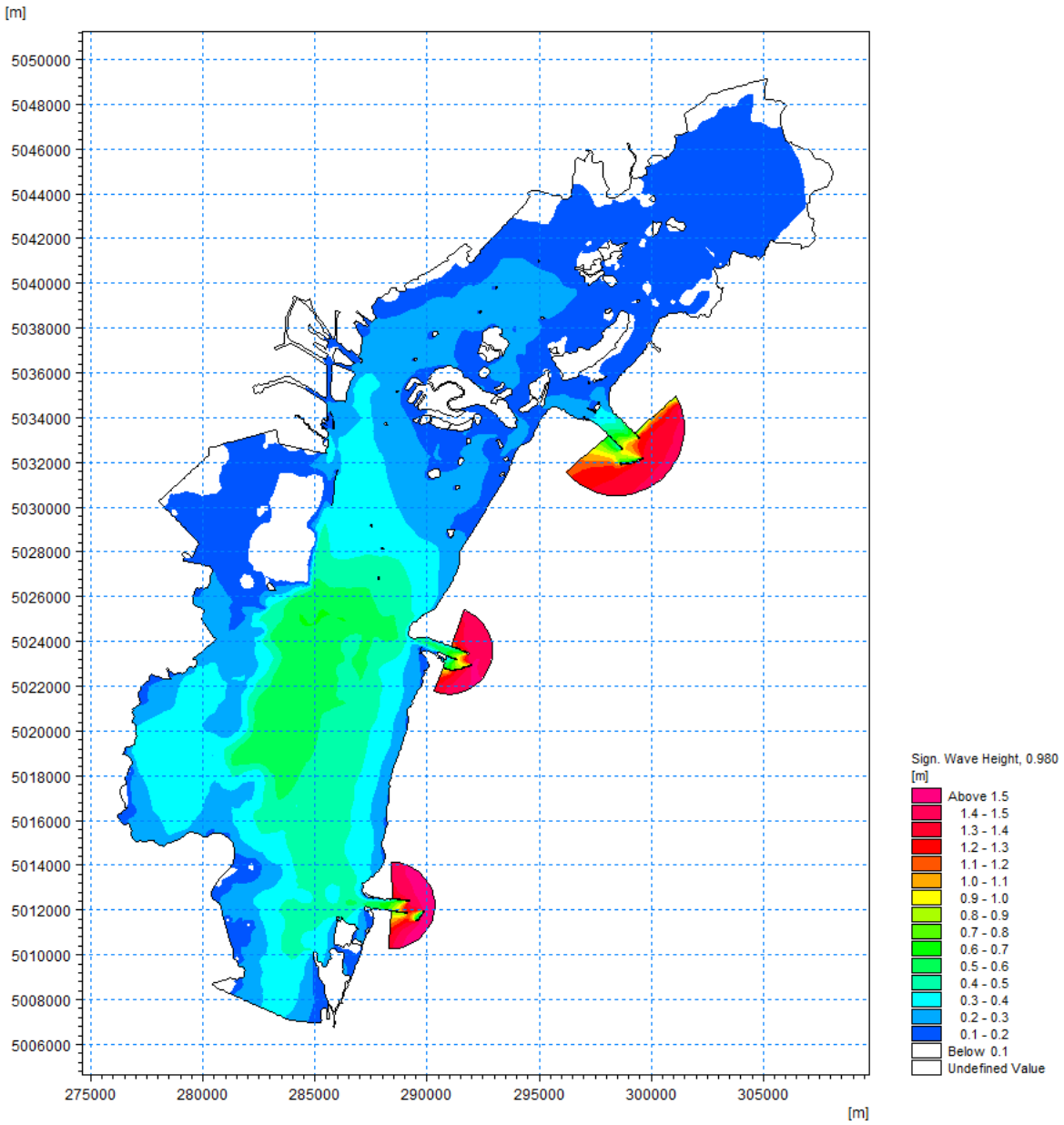

Figure 116. Wave height 98th percentile map.

5.6 2D model output data feed process

The 2D hydrodynamics model is the first link of a modelling chain comprising 3D hydrodynamics/morphological models and navigation simulators. In this regard, the main objectives of the coupled HD and SW model can be summarised as:

- to provide a validated set of boundary conditions for a 3D a hydrodynamics/morphological model describing sediment transport rates under natural (undisturbed) conditions for the central part of the lagoon including the Malamocco-Marghera channel and surrounding shallow water areas,
- the same 3D model will be forced by hydrodynamic fields generated by passing vessels enabling the comparison to undisturbed sediment transport phenomena occurring in the area subject of the study,
- to provide meteomarine conditions to under keel clearance (UKC) simulations performed in NCOS environment,
- to set the basis for navigation scenarios utilised by Fast Time simulations.

Broadly speaking, the main outputs of the model are 2D fields of:

- Wind: speed and direction;
- Water levels;
- Currents: depth integrated current speed and direction;
- Wave spectral integral parameters: Significant wave height (Hs), Peak period (Tp), Mean Period (T01), Zero Crossing Period (T02), Mean Wave Direction (MWD), Directional Standard Deviation (DSD).

The 2D model also allows for computation of sea-state spectral energy content in the frequency-direction space. A series of points were selected along a representative vessel navigation track (Figure 96) and, as an example, typical spectra for point 79 under a “Bora” and “Scirocco” conditions are illustrated in Figure 97 and Figure 98.

The knowledge of the wave energy distribution will enable the computation of the vessel frequency response for the selected project fleet in the upcoming navigation tasks (i.e. NAV tasks in the project Phase 2 e 3).

Figure 117. Close up of model point spectrum output locations along a representative vessel track at San-Leonardo bend.

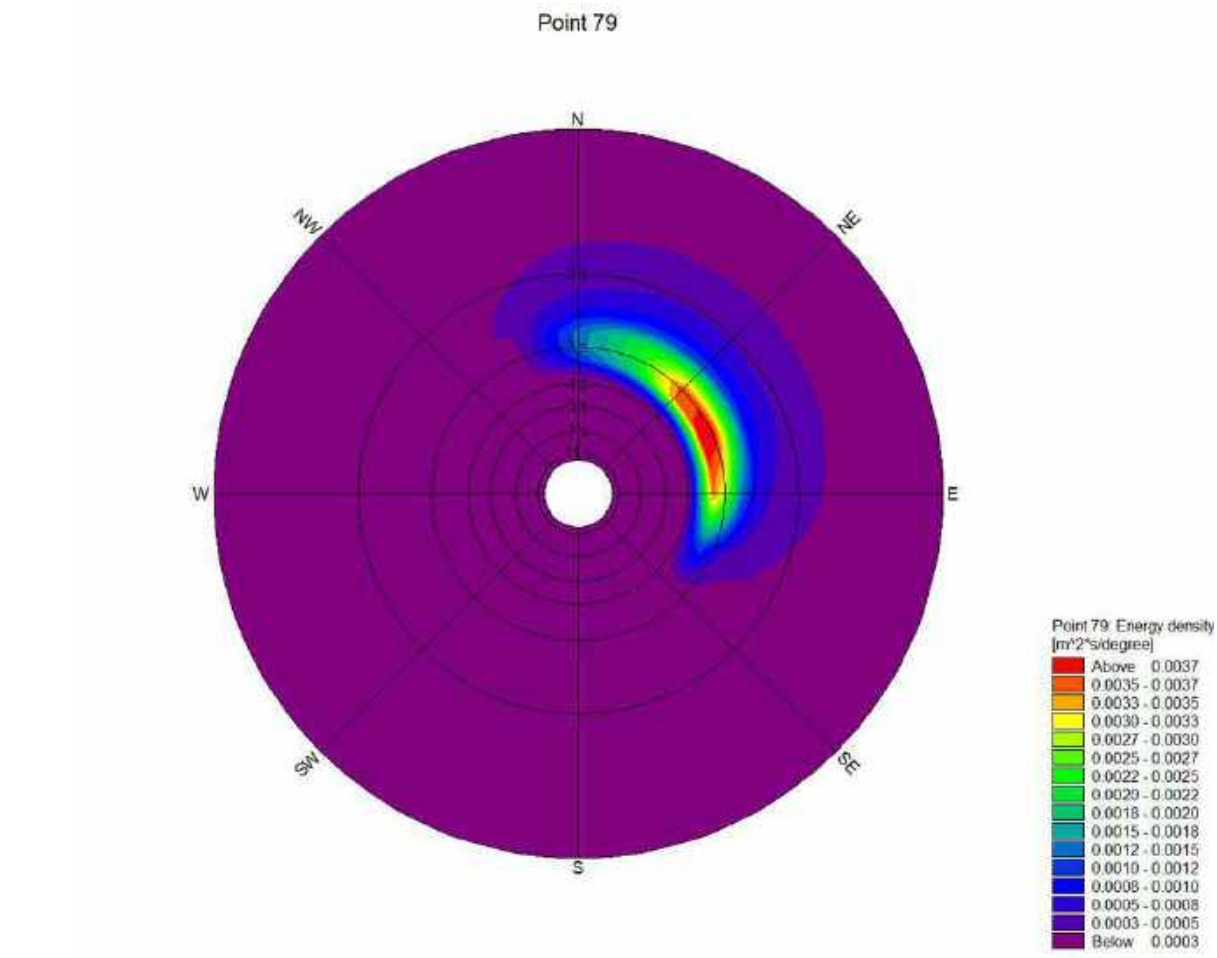

Figure 118. Sea-state energy density distribution at Point 79 for a "Bora" event (26-Mar-2020 11:30:00).

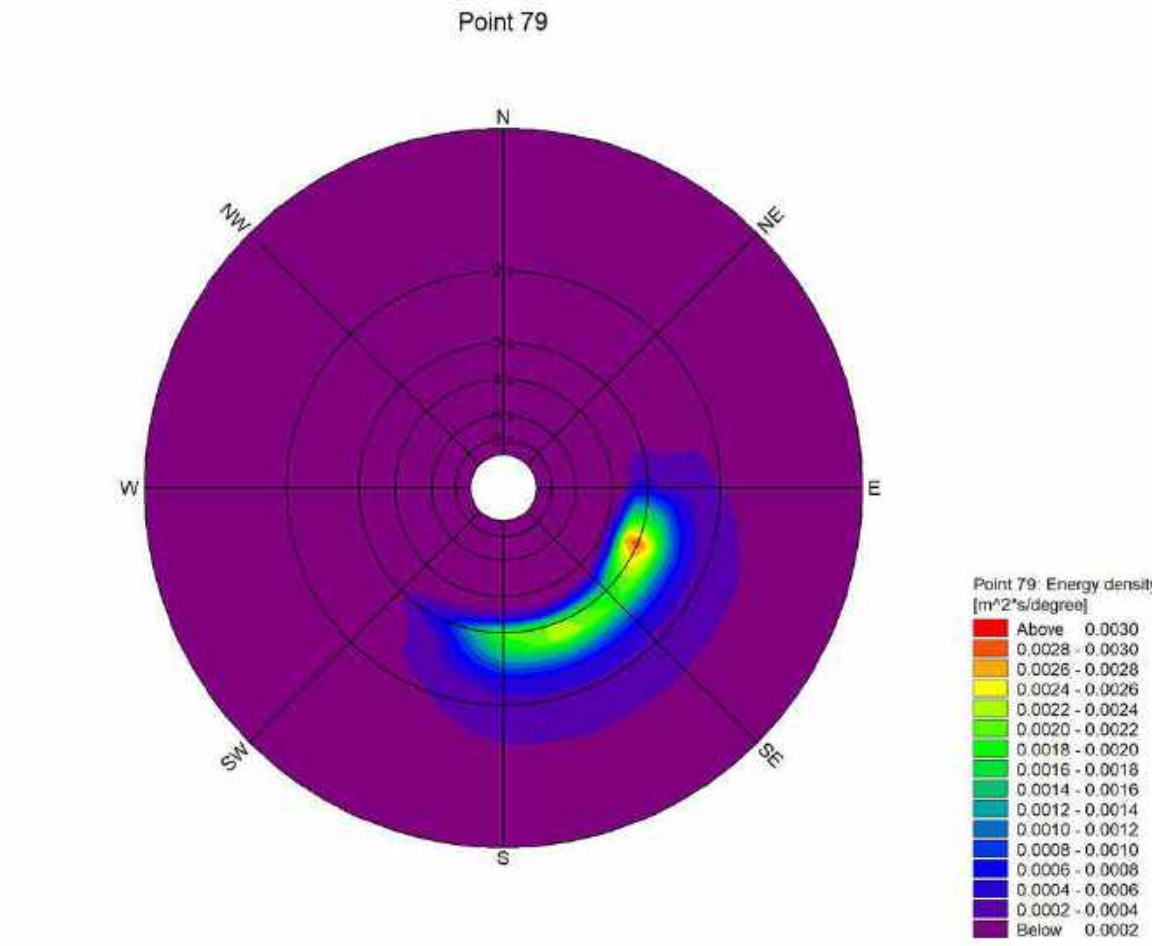

Figure 119. Sea-state energy density distribution at Point 79 for a "Scirocco" event (04-Dec-2020 22:00:00).

6 BIBLIOGRAPHY

[1] «ISPRA-Venezia,» [Online]. Available: https://www.venezia.isprambiente.it/.

[2] «Città di Venezia,» [Online]. Available: https://www.comune.venezia.it/it/content/dati-dalle-stazioni-rilevamento.

[3] C. Solidoro, D. Melaku Canu, A. Cucco e G. Umgiesser, «A partition of the Venice Lagoon based on physical properties and analysis of general circulation,» *Journal of Marine Systems,* 2004.

[4] M. Gacic, I. Mancero Mosquera, V. Kovacevic, A. Mazzoldi, V. Cardin, F. Arena e G. Gelsi, «Temporal variations of water flow between the Venetian lagoon and the open sea,» *Journal of Marine Systems,* 2004.

[5] G. Umgiesser, D. Melaku, A. Cucco e C. Solidoro, «A finite element model for the Venice Lagoon. Development, set up, calibration and validation,» *Journal of Marine Systems,* 2004.

[6] L. D'Alpaos e A. Defina, «Mathematical modeling of tidal hydrodynamics in shallow lagoons: A review of open issues and applications to the Venice lagoon,» 2007.

[7] A. Tomasin e R. Frasetto, «Cyclogenesis and Forecast of Dramatic Water Elevations in Venice,» *Marine Forecasting,* vol. 25, pp. 427-438, 1979.

[8] «ISPRA - La Rete Mareografica Nazionale,» [Online]. Available: https://mareografico.it/?session=0S2135586704UTF84716578A&syslng=ita&sysmen=-1&sysind=-1&syssub=-1&sysfnt=0. [Consultato il giorno 2021].

[9] V. Volpe, A. Pedroncini, F. Rameni, A. Guarnieri, M. Lomazzi, G. Barusolo e S. Libardo, *La previsione e i sistemi di decisione per la protezione del territorio: il caso della sala operativa decisionale del sistema MOSE,* Coast, 2019.

[10] A. Bondesan e P. Furlanetto, «Artificial fluvial diversions in the mainland of the Lagoon of Venice during the 16th and 17th centuries inferred by historical cartography analysis,» *Géomorphologie : Relief, Processus, Environnement,* vol. 18, pp. 175-200, 2012.

[11] A. Zirino, C. Neira, H. Elwany e F. Maicu, «Salinity and its variability in the Lagoon of Venice, 2000–2009,» *Advances in Oceanography and Limnology,* 2014.

[12] L. Carniello, A. Defina, S. Fagherazzi e L. D'Alpaos, «A combined wind wave–tidal model for the Venice lagoon, Italy,» *Journal of Geophysical Research,* vol. 110, 2005.

[13] C. Amos, A. Bergamasco, G. Umgiesser, S. Cappucci, D. Cloutier, L. DeNat, M. Flindt, M. Bonardi e S. Cristante, «The stability of tidal flats in Venice lagoon – the results of in-situ measurements using two benthic, annular flumes,» *Journal Marine Systems,* 2004.

[14] C. Amos, G. Umgiesser, C. Ferrarin, C. Thompson, R. Whitehouse, T. Sutherland e A. Bergamasco, «The erosion rates of cohesive sediments in Venice lagoon, Italy.,» *Continental Shelf Research,* 2010.

[15] M. Petti, S. Bosa e S. Pascolo, «Lagoon Sediment Dynamics: A Coupled Model to Study a Medium-Term Silting of Tidal Channels.,» *Water,* 2018.

[16] C. Thompson, C. Amos e G. Umgiesser, «A comparison between fluid shear stress reduction by halophytic plants in Venice Lagoon, Italy and Rustico Bay, Canada - analyses of in situ measurements.,» *Journal of Marine Systems,* pp. 293-308, 2004.

[17] A. Barillari e A. Rosso, «Prime notizie sulla distribuzione dei sedimenti superficiali nel bacino settentrionale della Laguna Veneta.,» in *Memorie di Biogeografia Adriatica suppl.*, 1976.

[18] A. Barillari, «Distribuzione dei sedimenti superficiali nel bacino meridionale della laguna di Venezia.,» 1981.

[19] F. Shepard, «Nomenclature based on sand-silt-clay ratios.,» *Journal of Sedimentary Research,* vol. 24, pp. 151-158, 1954.

[20] E. Molinaroli, S. Guerzoni, A. Sarretta, M. Masiol e P. M., «Thirty-year changes (1970 to 2000) in bathymetry and sediment texture recorded in the Lagoon of Venice sub-basins, Italy,» *Marine Geology,* vol. 258, pp. 115-125, 2009.

[21] R. Zonta, M. Botter, D. Cassin, L. Bellucci, R. Pini e J. Dominik, «Sediment texture and metal contamination in the Venice Lagoon (Italy): A snapshot before the installation of the MOSE system.,» *Estuarine Coastal and Shelf Science,* vol. 205, pp. 131-151, 2018.

[22] A. Sarretta, S. Pillon, E. Molinaroli, S. Guerzoni e G. Fontolan, «Sediment budget in the Lagoon of Venice.,» *Continental Shelf Research,* vol. 30, pp. 934-949, 2010.

[23] R. Zonta, G. Fontolan, D. Cassin e J. Dominik, «X-ray computed tomography as a tool for screening sediment cores: an application to the lagoons of the Po River Delta (Italy).,» *MDPI Journal of Marine Science and Engineering,* 2021.

[24] G. Pessa, D. Fischetti e S. A., «Piano d'uso delle aree in concessione per la venericoltura.,» San Servolo s.r.l. Servizi Metropolitani di Venezia, Gestione Risorse Lagunari., 2018.

[25] F. Ardhuin, R. Magne, A. Babanin e A. Roland, «Semiempirical Dissipation Source Functions for Ocean Waves. Part I: Definition, Calibration, and Validation,» *Journal of Physical Oceanography,* 2010.

[26] L. D'Alpaos, «L'evoluzione morfologica della Laguna di Venezia attraverso la lettura di alcune mappe storiche e delle sue carte idrografiche,» Comune di Venezia, 2010.

[27] «Autorità di Sistema Portuale del Mare Adriatico Settentrionale,» [Online]. Available: https://www.port.venice.it/it/autorita-portuale-di-venezia.html. [Consultato il giorno 2022].

[28] «Provveditorato Interregionale per le Opere Pubbliche per il Veneto, Trentino Alto Adige e Friuli Venezia Giulia - Ex Magistrato alle Acque - Venezia,» [Online]. Available: http://provveditoratovenezia.mit.gov.it/index.html. [Consultato il giorno 2022].

[29] «Consiglio Nazionale delle Ricerche,» [Online]. Available: https://www.cnr.it/. [Consultato il giorno 2022].

[30] A. Feola, F. Cacciatore, R. Brusà Boscolo e B. Matticchio, «An Integrated Approach for Evaluating the Restoration of the Salinity Gradient in Transitional Waters: Monitoring and Numerical Modeling in the Life Lagoon Refresh Case Study,» *Environments,* 2022.

[31] L. Carniello, D. Defina e L. D'Alpaos, «Morphological evolution of the Venice lagoon: Evidence from the past and trend for the future,» *Journal of Geophysical Research,* vol. 114, 2009.

[32] DHI, «MIKE21 Flow Model HD - Hydrodynamic and Transport module - Scientific Documentation,» 2022. [Online]. Available: https://manuals.mikepoweredbydhi.help/2022/Coast_and_Sea/MIKE_21_Flow_FM_Scientific_Doc.pdf.

[33] C. Ferrarin, A. Cucco, G. Umgiesser, D. Bellafiore e C. L. Amos, «Modelling fluxes of water and sediment between Venice Lagoon and the sea,» *Continental Shelf Research,* 2010.

APPENDICES

APPENDIX A
WIND MEASURMENTS: FREQUENCY OF OCCURRENCE

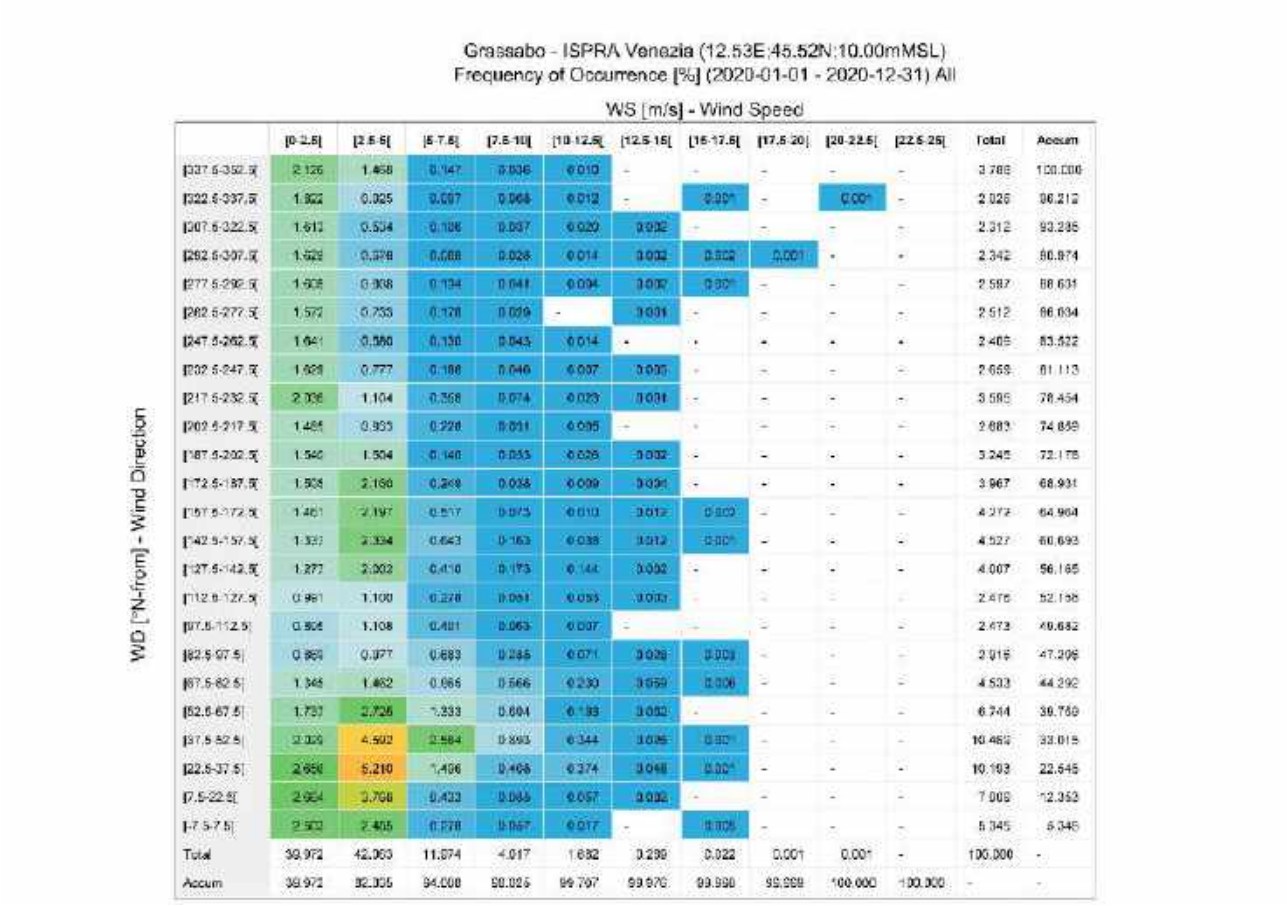

Grassabo - ISPRA Venezia (12.53E 45.52N 10.00mMSL)
Frequency of Occurrence [%] (2020-01-01 - 2020-12-31) All

WS [m/s] - Wind Speed

WD [°N-from] - Wind Direction

	[0-2.5[	[2.5-5[	[5-7.5[	[7.5-10[	[10-12.5[	[12.5-15[	[15-17.5[	[17.5-20[	[20-22.5[	[22.5-25[	Total	Accum
[337.5-352.5[	2.126	1.458	0.147	0.036	0.010	-	-	-	-	-	3.786	100.000
[322.5-337.5[	1.902	0.025	0.007	0.004	0.012	-	0.001	-	0.001	-	2.026	96.212
[307.5-322.5[	1.611	0.504	0.106	0.037	0.020	0.032	-	-	-	-	2.312	93.285
[292.5-307.5[	1.529	0.378	0.068	0.026	0.014	0.032	0.002	0.001	-	-	2.342	90.974
[277.5-292.5[	1.908	0.308	0.134	0.041	0.094	0.007	0.001	-	-	-	2.597	88.631
[262.5-277.5[	1.572	0.755	0.126	0.009	-	0.001	-	-	-	-	2.512	86.034
[247.5-262.5[	1.641	0.560	0.130	0.043	0.014	-	-	-	-	-	2.405	83.522
[232.5-247.5[	1.628	0.777	0.186	0.046	0.037	0.030	-	-	-	-	2.668	81.113
[217.5-232.5[	2.036	1.104	0.358	0.074	0.023	0.001	-	-	-	-	3.595	78.454
[202.5-217.5[	1.486	0.935	0.228	0.011	0.035	-	-	-	-	-	2.693	74.859
[187.5-202.5[	1.540	1.504	0.140	0.053	0.026	0.002	-	-	-	-	3.245	72.176
[172.5-187.5[	1.508	2.166	0.268	0.038	0.009	0.001	-	-	-	-	3.987	68.931
[157.5-172.5[	1.461	2.197	0.517	0.075	0.010	0.012	0.000	-	-	-	4.272	64.944
[142.5-157.5[	1.321	2.334	0.643	0.163	0.038	0.012	0.001	-	-	-	4.527	60.673
[127.5-142.5[	1.277	2.002	0.410	0.173	0.144	0.002	-	-	-	-	4.007	56.146
[112.5-127.5[	0.991	1.100	0.228	0.091	0.095	0.003	-	-	-	-	2.476	52.138
[97.5-112.5[	0.906	1.108	0.481	0.063	0.007	-	-	-	-	-	2.673	49.662
[82.5-97.5[	0.869	0.977	0.683	0.285	0.071	0.029	0.003	-	-	-	2.916	47.296
[67.5-82.5[	1.348	1.462	0.986	0.566	0.230	0.059	0.006	-	-	-	4.533	44.292
[52.5-67.5[	1.737	2.726	1.333	0.604	0.188	0.052	-	-	-	-	6.744	39.759
[37.5-52.5[	2.009	4.502	2.564	0.893	0.344	0.085	0.001	-	-	-	10.464	33.015
[22.5-37.5[	2.656	5.210	1.496	0.468	0.274	0.048	0.001	-	-	-	10.193	22.645
[7.5-22.5[	2.664	3.708	0.433	0.085	0.057	0.002	-	-	-	-	7.009	12.352
[-7.5-7.5[	2.502	2.405	0.278	0.057	0.017	-	0.005	-	-	-	5.345	5.345
Total	39.972	42.063	11.874	4.017	1.682	0.299	0.022	0.001	0.001	-	100.000	-
Accum	39.972	82.035	94.008	98.025	99.707	99.976	99.998	99.999	100.000	100.000	-	-

Figure 120. Grassabò met station scatter table (frequency of occurrence): 10m above MSL wind speed vs direction

Lido Meteo - ISPRA Venezia (12.38E;45.43N;10.00mMSL)
Frequency of Occurrence [%] (2020-01-01 - 2020-12-31) All

WS [m/s] - Wind Speed

WD [°N-from] - Wind Direction

	[0-2.5[	[2.5-5[	[5-7.5[	[7.5-10[	[10-12.5[	[12.5-15[	[15-17.5[	[17.5-20[	[20-22.5[	[22.5-25[	Total	Accum
[337.5-352.5[	2.548	0.594	0.030	0.003	-	-	-	-	-	-	3.175	100.000
[322.5-337.5[	2.220	0.409	0.076	0.015	0.001	-	-	-	-	-	2.719	96.825
[307.5-322.5[	1.934	0.516	0.123	0.029	0.003	-	-	-	-	-	2.602	94.106
[292.5-307.5[	1.562	0.558	0.083	0.040	0.003	-	-	-	-	-	2.346	91.505
[277.5-292.5[	1.240	0.668	0.101	0.014	0.005	-	-	-	-	-	2.028	89.159
[262.5-277.5[	1.535	1.144	0.236	0.037	0.015	0.001	-	-	-	-	2.969	87.063
[247.5-262.5[	2.378	1.093	0.363	0.066	0.029	0.005	-	-	-	-	4.255	84.095
[232.5-247.5[	2.358	1.417	0.186	0.032	0.003	-	-	-	-	-	3.698	79.840
[217.5-232.5[	1.401	0.742	0.020	0.012	-	-	-	-	-	-	2.284	76.140
[202.5-217.5[	1.254	0.469	0.031	0.004	-	-	-	-	-	-	1.763	73.856
[187.5-202.5[	1.578	0.541	0.046	0.004	-	-	-	-	-	-	2.268	72.093
[172.5-187.5[	2.259	1.328	0.067	0.006	0.008	0.031	-	-	-	-	3.698	69.825
[157.5-172.5[	2.818	1.766	0.077	0.026	0.003	-	-	-	-	-	4.790	66.127
[142.5-157.5[	3.051	1.768	0.161	0.054	-	-	-	-	-	-	5.040	61.337
[127.5-142.5[	2.592	1.723	0.116	0.041	-	-	-	-	-	-	4.311	56.297
[112.5-127.5[	1.904	2.061	0.229	0.014	0.043	-	-	-	-	-	3.786	51.986
[97.5-112.5[	1.102	1.809	0.821	0.147	0.093	0.032	-	-	-	-	3.774	48.200
[82.5-97.5[	1.376	1.328	0.927	0.449	0.158	0.025	-	-	-	-	4.293	44.426
[67.5-82.5[	1.460	1.927	1.269	0.524	0.110	0.006	-	-	-	-	5.296	40.133
[52.5-67.5[	1.866	3.548	1.566	0.539	0.069	-	-	-	-	-	7.691	34.837
[37.5-52.5[	3.122	4.509	0.558	0.468	0.037	-	-	-	-	-	8.752	27.146
[22.5-37.5[	4.074	3.866	0.156	0.068	0.003	-	-	-	-	-	7.967	18.393
[7.5-22.5[	4.006	1.927	0.188	0.024	-	-	-	-	-	-	6.145	10.426
[-7.5-7.5[	3.067	1.055	0.110	0.015	0.001	-	-	-	-	-	4.272	4.272
Total	51.665	37.377	7.059	2.856	0.581	0.042	-	-	-	-	100.000	-
Accum	51.665	89.042	96.721	99.577	99.958	100.000	100.000	100.000	100.000	100.000	-	-

Figure 121. Lido meteo met station scatter table (frequency of occurrence): 10m above MSL wind speed vs direction

SanGiorgio in Alga - ISPRA Venezia (12.94E;45.42N;10.00mMSL)
Frequency of Occurrence [%] (2020-01-01 - 2020-12-31) All

WS [m/s] - Wind Speed

WD [°N-from] - Wind Direction

	[0-2.5[	[2.5-5[	[5-7.5[	[7.5-10[	[10-12.5[	[12.5-15[	[15-17.5[	[17.5-20[	[20-22.5[	[22.5-25[	Total	Accum
[337.5-352.5[	1.103	0.509	0.108	0.048	0.014	-	-	-	-	-	1.831	100.000
[322.5-337.5[	1.238	0.747	0.172	0.049	0.018	0.002	-	-	-	-	2.226	98.169
[307.5-322.5[	1.356	1.015	0.221	0.029	0.032	0.004	-	-	-	-	2.552	95.943
[292.5-307.5[	1.278	0.911	0.154	0.010	-	0.001	-	-	-	-	2.354	93.391
[277.5-292.5[	1.741	0.823	0.077	0.015	0.001	-	-	-	-	-	2.757	91.037
[262.5-277.5[	1.733	0.843	0.106	0.026	0.002	-	-	-	-	-	2.709	88.280
[247.5-262.5[	1.170	1.056	0.356	0.076	0.010	0.005	0.005	-	-	-	2.751	85.571
[232.5-247.5[	0.950	1.166	0.428	0.092	0.010	0.002	0.001	-	-	-	2.635	82.821
[217.5-232.5[	0.805	0.895	0.348	0.069	0.012	-	-	-	-	-	2.185	80.186
[202.5-217.5[	0.995	1.250	0.297	0.059	0.032	0.015	0.003	-	-	-	2.678	78.001
[187.5-202.5[	1.443	2.002	0.396	0.139	0.025	0.008	0.003	-	-	-	4.016	75.323
[172.5-187.5[	1.490	3.076	1.061	0.351	0.091	0.022	0.020	-	-	-	6.111	71.312
[157.5-172.5[	1.229	3.131	1.641	0.502	0.163	0.072	0.005	-	-	-	6.749	65.201
[142.5-157.5[	0.898	2.780	0.782	0.126	0.049	0.071	-	-	-	-	4.707	58.453
[127.5-142.5[	0.667	1.792	0.604	0.088	0.025	0.024	-	-	-	-	3.399	53.745
[112.5-127.5[	0.518	0.886	0.761	0.229	0.010	0.010	-	-	-	-	2.412	50.347
[97.5-112.5[	0.603	0.878	0.723	0.276	0.149	0.034	0.002	-	-	-	2.765	47.935
[82.5-97.5[	0.726	0.950	0.814	0.819	0.214	0.037	0.001	0.001	-	-	3.362	45.180
[67.5-82.5[	0.851	1.700	1.518	0.847	0.257	0.067	0.001	-	-	-	5.270	41.786
[52.5-67.5[	1.136	2.576	2.167	1.076	0.618	0.233	0.012	-	-	-	7.807	36.515
[37.5-52.5[	2.008	5.123	3.620	0.380	0.177	0.063	-	-	-	-	12.369	28.712
[22.5-37.5[	2.336	5.527	1.514	0.123	0.052	0.001	0.003	-	-	-	9.555	16.403
[7.5-22.5[	1.742	2.310	0.350	0.057	0.010	0.001	-	-	-	-	4.471	6.848
[-7.5-7.5[	1.140	0.960	0.166	0.046	0.070	0.002	-	-	-	-	2.377	2.377
Total	29.276	44.115	18.545	6.344	1.982	0.705	0.091	0.001	-	-	100.000	-
Accum	29.276	73.390	91.936	97.280	99.245	99.949	99.999	100.000	100.000	100.000	-	-

Figure 122. San Giorgio in Alga met station scatter table (frequency of occurrence): 10m above MSL wind speed vs direction

Malamocco Diga Nord - ISPRA Venezia (12.34E;45.33N;10.00mMSL)
Frequency of Occurrence [%] (2020-01-01 - 2020-12-31) All

WS [m/s] - Wind Speed

WD [°N-from] - Wind Direction

	[0-2.5[	[2.5-5[	[5-7.5[	[7.5-10[	[10-12.5[	[12.5-15[	[15-17.5[	[17.5-20[	[20-22.5[	[22.5-25[	Total	Accum
[337.5-352.5[	1.269	1.514	0.264	0.079	0.013	0.004	-	-	-	-	3.236	100.000
[322.5-337.5[	1.311	1.355	0.188	0.049	0.022	0.006	-	-	-	-	2.941	96.764
[307.5-322.5[	1.563	1.256	0.126	0.074	0.044	0.034	0.002	-	-	-	3.100	93.821
[292.5-307.5[	1.928	1.306	0.140	0.065	0.010	0.002	0.001	-	-	-	3.448	90.713
[277.5-292.5[	1.488	1.705	0.146	0.025	0.001	-	-	-	-	-	3.374	87.265
[262.5-277.5[	1.110	1.339	0.184	0.047	0.009	-	-	0.001	-	-	2.700	83.891
[247.5-262.5[	1.253	1.929	0.367	0.060	0.018	0.005	-	-	0.001	-	3.643	81.191
[232.5-247.5[	1.207	2.205	0.571	0.170	0.035	0.005	0.002	-	-	-	4.207	77.548
[217.5-232.5[	0.866	1.390	0.606	0.191	0.043	0.007	-	-	-	-	3.121	73.342
[202.5-217.5[	0.847	0.990	0.443	0.104	0.017	0.001	-	-	-	-	2.402	70.221
[187.5-202.5[	0.947	1.156	0.339	0.167	0.055	0.020	0.002	-	-	-	2.688	67.819
[172.5-187.5[	1.089	1.409	0.444	0.106	0.029	0.008	0.005	-	-	-	3.089	65.131
[157.5-172.5[	1.260	1.705	0.757	0.201	0.065	0.023	0.017	0.001	-	-	4.045	62.042
[142.5-157.5[	1.902	2.265	1.493	0.442	0.129	0.049	0.029	-	-	-	5.735	57.997
[127.5-142.5[	1.883	2.529	0.936	0.262	0.199	0.051	-	-	-	-	5.290	52.262
[112.5-127.5[	1.148	1.004	0.108	0.009	0.045	-	-	-	-	-	2.333	46.972
[97.5-112.5[	1.122	1.106	0.139	0.029	0.013	0.002	-	-	-	-	2.499	44.640
[82.5-97.5[	1.212	1.493	0.601	0.167	0.029	0.029	0.003	-	-	-	3.494	42.145
[67.5-82.5[	0.963	1.535	0.501	0.743	0.291	0.253	0.082	-	-	-	4.768	38.650
[52.5-67.5[	0.902	1.809	1.196	0.997	0.943	0.615	0.155	0.020	-	-	6.337	33.882
[37.5-52.5[	1.060	1.701	1.328	1.087	0.793	0.335	0.050	0.013	-	-	6.620	27.545
[22.5-37.5[	1.008	2.431	2.496	1.856	0.832	0.406	0.282	0.037	-	-	9.035	20.925
[7.5-22.5[	1.227	3.377	2.279	0.992	0.140	0.070	0.044	0.001	-	-	7.640	11.890
[-7.5-7.5[	1.769	2.760	0.567	0.126	0.024	0.003	-	-	-	-	4.249	4.249
Total	28.994	40.450	18.720	7.535	3.569	1.799	0.855	0.077	0.001	-	100.000	-
Accum	28.994	69.444	88.164	95.699	97.268	99.066	99.922	99.999	100.000	100.000	-	-

Figure 123. Malamocco Diga Nord met station scatter table (frequency of occurrence): 10m above MSL wind speed vs direction.

Petta de Bo - ISPRA Venezia (12.24E;45.26N;10.00mMSL)
Frequency of Occurrence [%] (2020-01-01 - 2020-12-31) All

WS [m/s] - Wind Speed

WD [°N-from] - Wind Direction

	[0-2.5[	[2.5-5[	[5-7.5[	[7.5-10[	[10-12.5[	[12.5-15[	[15-17.5[	[17.5-20[	[20-22.5[	[22.5-25[	Total	Accum
[337.5-352.5[	1.223	1.922	0.356	0.091	0.021	0.007	-	-	-	-	3.619	100.000
[322.5-337.5[	1.563	1.764	0.234	0.068	0.025	0.006	-	-	-	-	3.690	96.381
[307.5-322.5[	1.709	1.416	0.162	0.063	0.015	0.003	-	-	-	-	3.369	92.691
[292.5-307.5[	1.536	1.223	0.106	0.040	-	0.002	-	0.001	-	-	2.907	89.313
[277.5-292.5[	1.508	1.059	0.083	0.021	0.002	-	0.001	0.001	-	0.001	2.885	86.407
[262.5-277.5[	1.628	1.745	0.186	0.036	0.015	0.003	-	-	-	-	3.676	83.522
[247.5-262.5[	1.667	2.309	0.372	0.139	0.020	0.013	-	-	-	-	4.445	79.845
[232.5-247.5[	1.516	2.047	0.541	0.145	0.053	0.010	-	-	-	-	4.253	75.400
[217.5-232.5[	1.222	1.898	0.522	0.089	0.034	-	-	-	-	-	3.766	71.153
[202.5-217.5[	0.944	1.315	0.378	0.068	0.021	-	-	-	-	-	2.726	67.388
[187.5-202.5[	0.705	1.221	0.476	0.097	0.030	0.011	-	-	-	-	2.534	64.662
[172.5-187.5[	0.563	0.912	0.591	0.118	0.012	0.006	-	-	-	-	2.202	62.097
[157.5-172.5[	0.619	0.978	0.568	0.148	0.070	0.035	0.005	-	-	-	2.419	59.895
[142.5-157.5[	0.783	1.010	0.524	0.130	0.086	0.063	0.007	-	-	-	2.622	57.476
[127.5-142.5[	0.895	1.729	1.797	0.493	0.260	0.046	-	-	-	-	5.168	54.854
[112.5-127.5[	0.923	1.900	1.499	0.184	0.031	0.007	-	-	-	-	4.626	49.686
[97.5-112.5[	1.124	2.002	1.061	0.073	0.019	0.007	0.005	-	-	-	4.980	45.059
[82.5-97.5[	1.154	2.104	0.687	0.247	0.044	0.030	0.011	-	-	-	4.537	40.080
[67.5-82.5[	1.108	2.073	1.116	0.958	0.496	0.335	0.041	0.005	-	-	6.129	35.551
[52.5-67.5[	0.952	1.886	1.693	1.164	1.201	0.460	0.158	0.011	-	-	7.234	29.423
[37.5-52.5[	1.035	1.927	1.642	1.349	0.663	0.520	0.193	0.004	-	-	7.018	22.189
[22.5-37.5[	1.066	2.073	2.284	0.881	0.374	0.154	0.042	-	-	-	6.870	15.172
[7.5-22.5[	1.014	2.071	1.308	0.293	0.104	0.030	0.002	-	-	-	4.931	8.290
[-7.5-7.5[	1.002	1.790	0.512	0.161	0.022	0.002	-	-	-	-	3.467	3.467
Total	27.640	40.744	18.800	7.977	3.468	1.782	0.466	0.022	-	0.001	100.000	-
Accum	27.640	68.384	87.185	94.261	97.729	99.511	99.977	99.999	99.999	100.000	-	-

Figure 124. Petta de Bò met station scatter table (frequency of occurrence): 10m above MSL wind speed vs direction.

Chioggia Diga Sud - ISPRA Venezia (12.31E;45.23N;10.00mMSL)
Frequency of Occurrence [%] (2020-01-01 - 2020-12-31) All

WS [m/s] - Wind Speed

WD [°N-from] - Wind Direction	[0-2.5[	[2.5-5[	[5-7.5[	[7.5-10[	[10-12.5[	[12.5-15[	[15-17.5[	[17.5-20[	[20-22.5[	[22.5-25[	Total	Accum
[337.5-352.5[	1.200	1.478	0.266	0.066	0.034	0.007	0.001	-	-	-	3.070	100.000
[322.5-337.5[	1.245	1.427	0.216	0.064	0.050	0.006	-	-	-	-	3.032	96.930
[307.5-322.5[	1.448	1.402	0.170	0.048	0.013	0.025	-	-	-	-	3.106	93.898
[292.5-307.5[	1.367	1.589	0.082	0.027	-	0.032	0.003	-	-	-	3.686	90.792
[277.5-292.5[	1.900	1.197	0.058	0.019	0.032	-	-	-	-	-	3.227	87.093
[262.5-277.5[	2.466	2.021	0.287	0.062	0.015	0.031	-	-	-	-	5.882	83.866
[247.5-262.5[	1.630	2.266	0.426	0.096	0.014	-	-	-	-	-	4.447	78.203
[232.5-247.5[	1.238	1.848	0.561	0.131	0.015	-	-	-	-	-	3.793	73.756
[217.5-232.5[	0.933	1.111	0.386	0.054	0.001	-	-	-	-	-	2.484	69.963
[202.5-217.5[	0.818	0.830	0.265	0.062	0.018	-	-	-	-	-	1.993	67.480
[187.5-202.5[	0.813	0.907	0.256	0.100	0.038	-	-	-	-	-	2.115	65.586
[172.5-187.5[	1.063	1.402	0.251	0.043	0.007	0.041	-	-	-	-	2.807	63.390
[157.5-172.5[	0.849	1.334	0.564	0.146	0.047	0.027	0.014	-	-	-	3.106	60.583
[142.5-157.5[	0.951	1.915	1.155	0.349	0.190	0.059	0.024	-	-	-	4.653	57.475
[127.5-142.5[	1.009	2.021	1.519	0.360	0.234	0.071	-	-	-	-	5.215	52.822
[112.5-127.5[	1.096	2.176	0.804	0.126	0.032	0.007	0.001	-	-	-	4.232	47.606
[97.5-112.5[	1.083	2.074	0.437	0.084	0.031	0.008	0.000	-	-	-	3.717	43.374
[82.5-97.5[	0.960	1.490	0.575	0.263	0.092	0.041	0.009	-	-	-	3.340	39.657
[67.5-82.5[	1.216	1.569	0.718	0.686	0.289	0.210	0.037	-	-	-	4.734	36.306
[52.5-67.5[	1.216	1.082	1.266	1.171	1.075	0.677	0.235	0.030	-	-	7.542	31.574
[37.5-52.5[	1.283	2.037	1.739	1.227	0.947	0.546	0.365	0.066	-	-	8.211	24.031
[22.5-37.5[	1.150	2.036	2.100	1.261	0.418	0.247	0.139	0.012	-	-	7.365	15.820
[7.5-22.5[	1.091	2.093	1.376	0.429	0.098	0.058	0.011	-	-	-	5.155	8.456
[-7.5-7.5[	1.112	1.511	0.451	0.089	0.032	0.003	-	-	-	-	3.300	3.300
Total	29.830	40.777	15.893	6.989	3.882	1.883	0.837	0.111	-	-	100.000	-
Accum	29.830	70.607	86.499	93.488	97.370	99.253	99.089	100.000	100.000	100.000	-	-

Figure 125. Chioggia Diga Sud met station scatter table (frequency of occurrence): 10m above MSL wind speed vs direction.

APPENDIX B
Fitting quality indices

Abbreviation	Description	Definition
N	Number of data (synchronized)	–
MEAN	Mean of Y data, Mean of X data	$\frac{1}{N}\sum_{i=1}^{N} Y_i = \overline{Y}$, $\frac{1}{N}\sum_{i=1}^{N} X_i = \overline{X}$
STD	Standard deviation of Y data Standard deviation of X data	$\sqrt{\frac{1}{N-1}\sum_{i=1}^{N}(Y-\overline{Y})^2}$, $\sqrt{\frac{1}{N-1}\sum_{i=1}^{N}(X-\overline{X})^2}$
BIAS	Mean difference	$\frac{1}{N}\sum_{i=1}^{N}(Y-X)_i = \overline{Y}-\overline{X}$
AME	Absolute mean difference	$\frac{1}{N}\sum_{i=1}^{N}(\lvert Y-X\rvert)_i$
RMSE	Root mean square difference	$\sqrt{\frac{1}{N}\sum_{i=1}^{N}(Y-X)_i^2}$
SI	Scatter index (unbiased)	$\frac{\sqrt{\frac{1}{N}\sum_{i=1}^{N}(Y-X-\mathrm{BIAS})_i^2}}{\frac{1}{N}\sum_{i=1}^{N}\lvert X_i\rvert}$
EV	Explained variance	$\frac{\sum_{i=1}^{N}(X_i-\overline{X})^2-\sum_{i=1}^{N}[(X_i-\overline{X})-(Y_i-\overline{Y})]^2}{\sum_{i=1}^{N}(X_i-\overline{X})^2}$
CC	Correlation coefficient	$\frac{\sum_{i=1}^{N}(X_i-\overline{X})(Y_i-\overline{Y})}{\sqrt{\sum_{i=1}^{N}(X_i-\overline{X})^2\sum_{i=1}^{N}(Y_i-\overline{Y})^2}}$
QQ	Quantile-Quantile (line slope and intercept)	Linear least square fit to quantiles
PR	Peak ratio (of N_{peak} highest events)	$\mathrm{PR}=\frac{\sum_{i=1}^{N_{peak}}Y_i}{\sum_{i=1}^{N_{peak}}X_i}$

APPENDIX C
HD model short description

MIKE
Powered by DHI

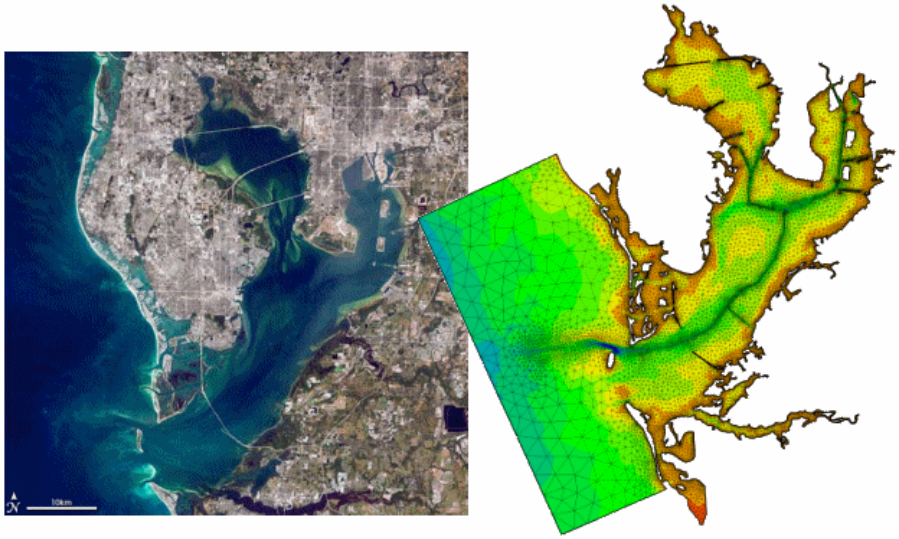

MIKE 21 & MIKE 3 Flow Model FM

Hydrodynamic Module

Short Description

The expert in WATER ENVIRONMENTS

DHI headquarters
Agern Allé 5
DK-2970 Hørsholm
Denmark

+45 4516 9200 Telephone
+45 4516 9333 Support
+45 4516 9292 Telefax

mike@dhigroup.com
www.mikepoweredbydhi.com

MIKE213_HD_FM_Short_Description_.docx / AJS/EBR/NHP / 2021-08-11

MIKE 21 & MIKE 3 Flow Model FM

The Flow Model FM is a comprehensive modelling system for two- and three-dimensional water modelling developed by DHI. The 2D and 3D models carry the same names as the classic DHI model versions MIKE 21 & MIKE 3 with an 'FM' added referring to the type of model grid - Flexible Mesh.

The modelling system has been developed for complex applications within oceanographic, coastal and estuarine environments. However, being a general modelling system for 2D and 3D free-surface flows it may also be applied for studies of inland surface waters, e.g. overland flooding and lakes or reservoirs.

MIKE 21 & MIKE 3 Flow Model FM is a general hydrodynamic flow modelling system based on a finite volume method on an unstructured mesh

The Modules of the Flexible Mesh Series

DHI's Flexible Mesh (FM) series includes the following modules:

Flow Model FM modules

- Hydrodynamic Module, HD
- Transport Module, TR
- Ecology Modules, MIKE ECO Lab/AMB Lab
- Oil Spill Module, OS
- Mud Transport Module, MT
- Particle Tracking Module, PT
- Sand Transport Module, ST
- Shoreline Morphology Module, SM

Wave module

- Spectral Wave Module, SW

The FM Series meets the increasing demand for realistic representations of nature, both with regard to 'look alike' and to its capability to model coupled processes, e.g. coupling between currents, waves and sediments. Coupling of modules is managed in the Coupled Model FM.

All modules are supported by advanced user interfaces including efficient and sophisticated tools for mesh generation, data management, 2D/3D visualization, etc. In combination with comprehensive documentation and support, the FM series forms a unique professional software tool for consultancy services related to design, operation and maintenance tasks within the marine environment.

An unstructured grid provides an optimal degree of flexibility in the representation of complex geometries and enables smooth representations of boundaries. Small elements may be used in areas where more detail is desired, and larger elements used where less detail is needed, optimising information for a given amount of computational time.

The spatial discretisation of the governing equations is performed using a cell-centred finite volume method. In the horizontal plane, an unstructured grid is used while a structured mesh is used in the vertical domain (3D).

This document provides a short description of the Hydrodynamic Module included in MIKE 21 & MIKE 3 Flow Model FM.

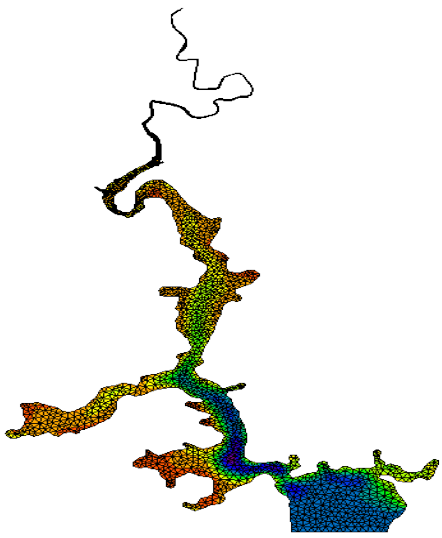

Example of computational mesh for Tamar Estuary, UK

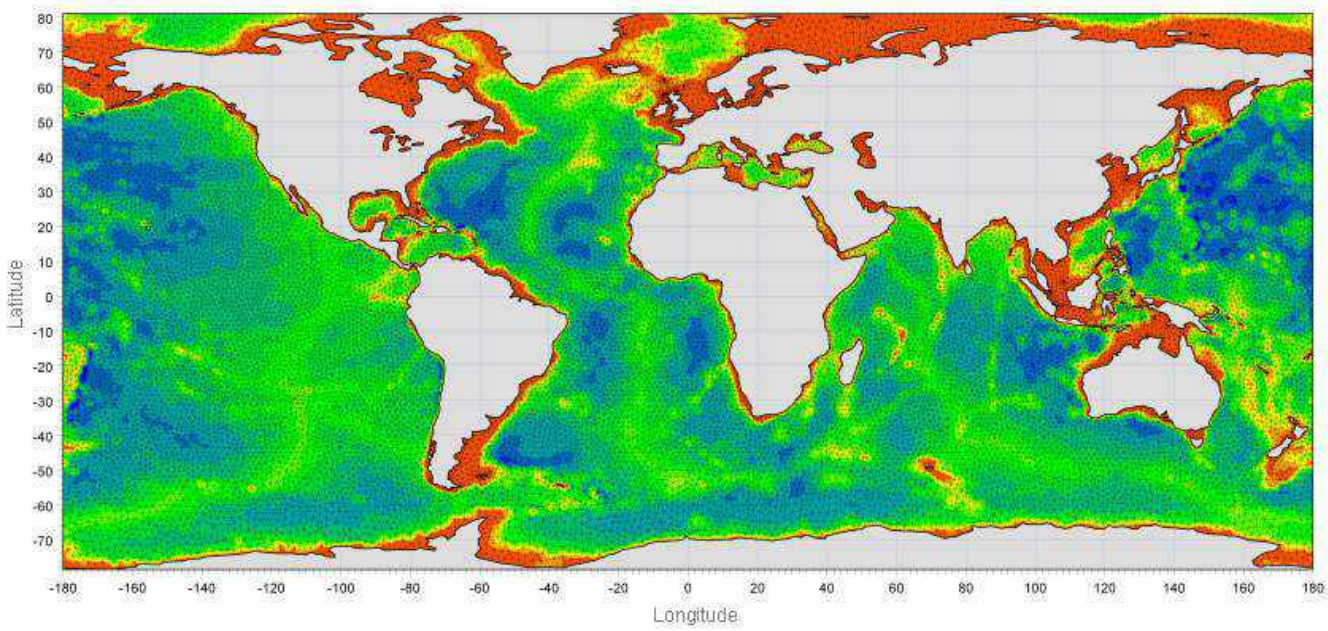

MIKE 21 & MIKE 3 FLOW MODEL FM supports both Cartesian and spherical coordinates. Spherical coordinates are usually applied for regional and global sea circulation applications. The chart shows the computational mesh and bathymetry for the planet Earth generated by the MIKE Zero Mesh Generator

MIKE 21 & MIKE 3 Flow Model FM - Hydrodynamic Module

The Hydrodynamic Module provides the basis for computations performed in many other modules, but can also be used alone. It simulates the water level variations and flows in response to a variety of forcing functions on flood plains, in lakes, estuaries and coastal areas.

Application Areas

The Hydrodynamic Module included in MIKE 21 & MIKE 3 Flow Model FM simulates unsteady flow taking into account density variations, bathymetry and external forcings.

The choice between 2D and 3D model depends on a number of factors. For example, in shallow waters, wind and tidal current are often sufficient to keep the water column well-mixed, i.e. homogeneous in salinity and temperature. In such cases a 2D model can be used. In water bodies with stratification, either by density or by species (ecology), a 3D model should be used. This is also the case for enclosed or semi-enclosed waters where wind-driven circulation occurs.

Typical application areas are

- Assessment of hydrographic conditions for design, construction and operation of structures and plants in stratified and non-stratified waters
- Environmental impact assessment studies
- Coastal and oceanographic circulation studies
- Optimization of port and coastal protection infrastructures
- Lake and reservoir hydrodynamics
- Cooling water, recirculation and desalination
- Coastal flooding and storm surge
- Inland flooding and overland flow modelling
- Forecast and warning systems

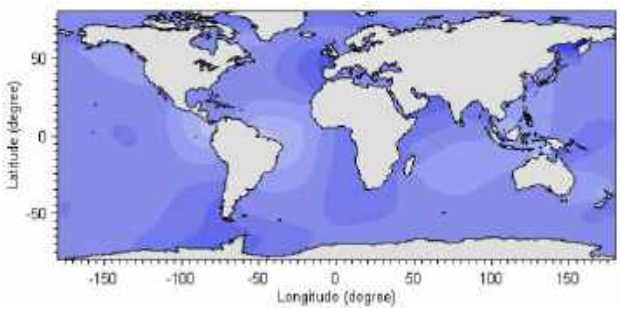

Example of a global tide application of MIKE 21 Flow Model FM. Results from such a model can be used as boundary conditions for regional scale forecast or hindcast models

The MIKE 21 & MIKE 3 Flow Model FM also support spherical coordinates, which makes both models particularly applicable for global and regional sea scale applications.

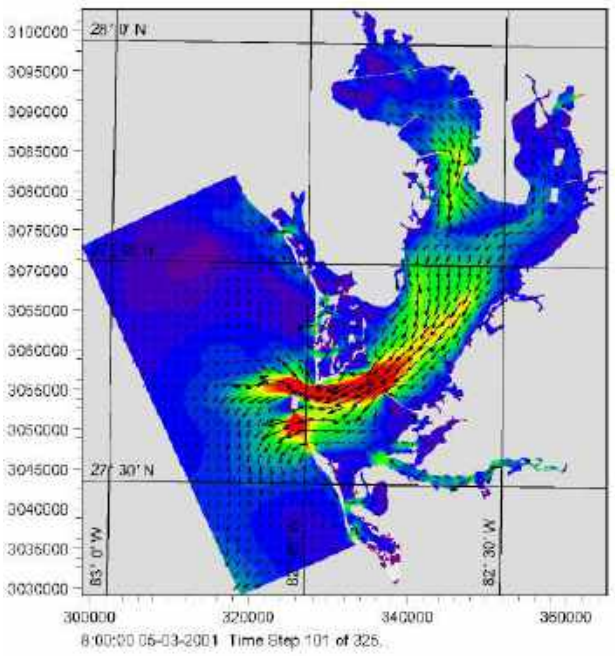

Example of a flow field in Tampa Bay, Florida, simulated by MIKE 21 Flow Model FM

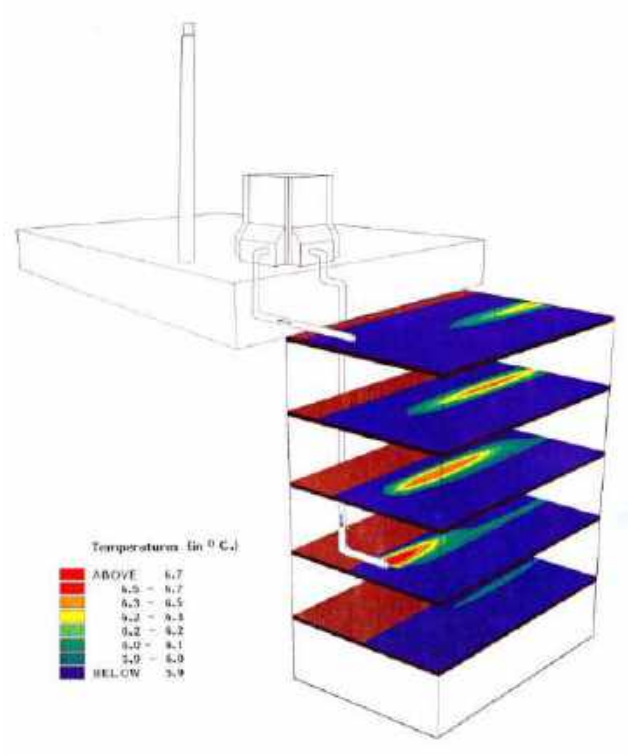

Study of thermal plume dispersion

Typical applications with the MIKE 21 & MIKE 3 Flow Model FM include cooling water recirculation and ecological impact assessment (eutrophication)

The Hydrodynamic Module is together with the Transport Module (TR) used to simulate the spreading and fate of dissolved and suspended substances. This module combination is applied in tracer simulations, flushing and simple water quality studies.

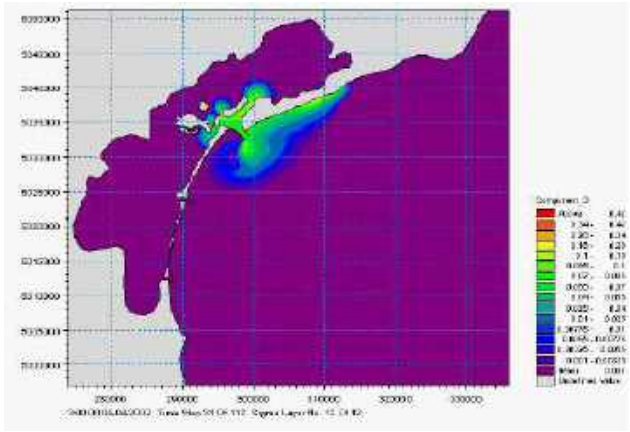

Tracer simulation of single component from outlet in the Adriatic, simulated by MIKE 21 Flow Model FM HD+TR

Prediction of ecosystem behaviour using the MIKE 21 & MIKE 3 Flow Model FM together with MIKE ECO Lab

The Hydrodynamic Module can be coupled to the Ecological Module (MIKE ECO Lab) to form the basis for environmental water quality studies comprising multiple components.

Furthermore, the Hydrodynamic Module can be coupled to sediment models for the calculation of sediment transport. The Sand Transport Module and Mud Transport Module can be applied to simulate transport of non-cohesive and cohesive sediments, respectively.

In the coastal zone the transport is mainly determined by wave conditions and associated wave-induced currents. The wave-induced currents are generated by the gradients in radiation stresses that occur in the surf zone. The Spectral Wave Module can be used to calculate the wave conditions and associated radiation stresses.

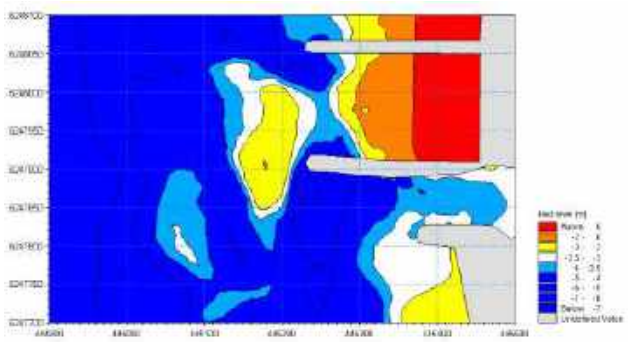

Coastal application (morphology) with coupled MIKE 21 HD, SW and ST, Torsminde harbour Denmark

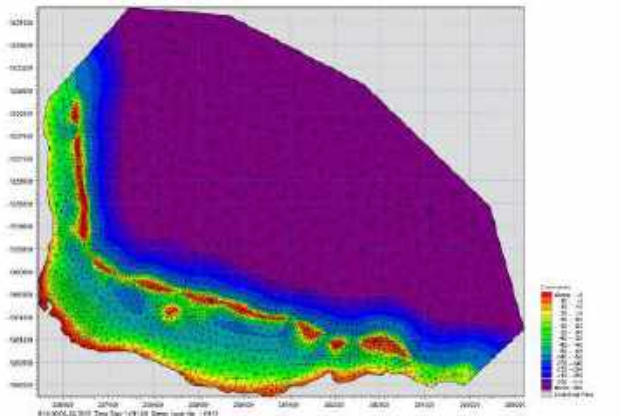

Model bathymetry of Taravao Bay, Tahiti

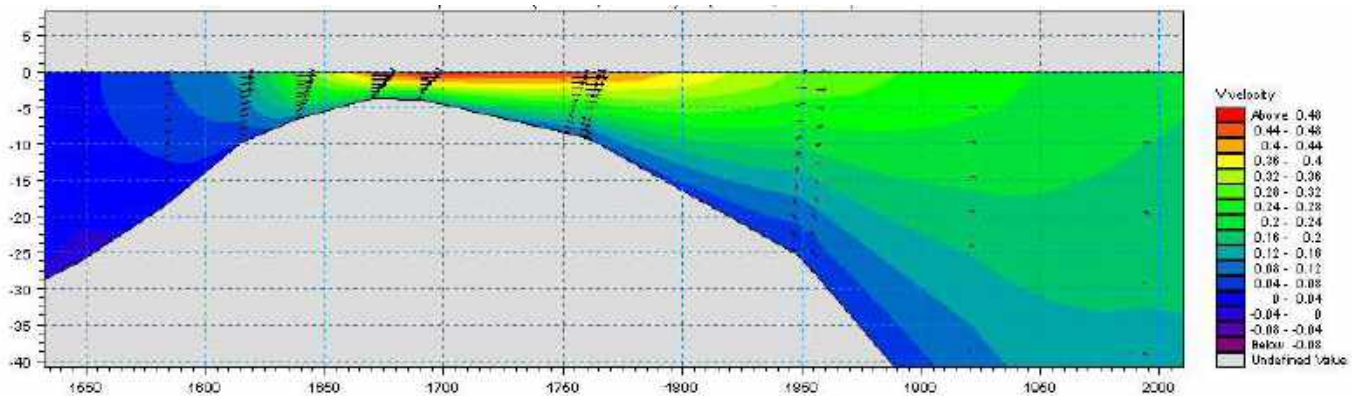

Example of vertical profile of cross reef currents in Taravao Bay, Tahiti simulated with MIKE 3 Flow Model FM. The circulation and renewal of water inside the reef is dependent on the tides, the meteorological conditions and the cross reef currents, thus the circulation model includes the effects of wave induced cross reef currents

Computational Features

The main features and effects included in simulations with the MIKE 21 & MIKE 3 Flow Model FM – Hydrodynamic Module are the following:

- Flooding and drying
- Momentum dispersion
- Bottom shear stress
- Coriolis force
- Wind shear stress
- Barometric pressure gradients
- Ice coverage
- Tidal potential
- Precipitation/evaporation
- Infiltration
- Heat exchange with atmosphere
- Wave radiation stresses
- Sources and sinks, incl. jet
- Structures

Model Equations

The modelling system is based on the numerical solution of the two/three-dimensional incompressible Reynolds averaged Navier-Stokes equations subject to the assumptions of Boussinesq and of hydrostatic pressure. Thus, the model consists of continuity, momentum, temperature, salinity and density equations and it is closed by a turbulent closure scheme. The density does not depend on the pressure, but only on the temperature and the salinity.

For the 3D model, the free surface is taken into account using a sigma-coordinate transformation approach or using a combination of a sigma and z-level coordinate system.

Below the governing equations are presented using Cartesian coordinates.

The local continuity equation is written as

$$\frac{\partial u}{\partial x}+\frac{\partial v}{\partial y}+\frac{\partial w}{\partial z}=S$$

and the two horizontal momentum equations for the x- and y-component, respectively

$$\frac{\partial u}{\partial t}+\frac{\partial u^2}{\partial x}+\frac{\partial vu}{\partial y}+\frac{\partial wu}{\partial z}=fv-g\frac{\partial \eta}{\partial x}-$$
$$\frac{1}{\rho_0}\frac{\partial p_a}{\partial x}-\frac{g}{\rho_0}\int_z^\eta \frac{\partial \rho}{\partial x}dz+F_u+\frac{\partial}{\partial z}\left(\nu_t\frac{\partial u}{\partial z}\right)+u_sS$$

$$\frac{\partial v}{\partial t}+\frac{\partial v^2}{\partial y}+\frac{\partial uv}{\partial x}+\frac{\partial wv}{\partial z}=-fu-g\frac{\partial \eta}{\partial y}-$$
$$\frac{1}{\rho_0}\frac{\partial p_a}{\partial y}-\frac{g}{\rho_0}\int_z^\eta \frac{\partial \rho}{\partial y}dz+F_v+\frac{\partial}{\partial z}\left(\nu_t\frac{\partial v}{\partial z}\right)+v_sS$$

Temperature and salinity

In the Hydrodynamic Module, calculations of the transports of temperature, *T*, and salinity, *s* follow the general transport-diffusion equations as

$$\frac{\partial T}{\partial t}+\frac{\partial uT}{\partial x}+\frac{\partial vT}{\partial y}+\frac{\partial wT}{\partial z}=F_T+\frac{\partial}{\partial z}\left(D_v\frac{\partial T}{\partial z}\right)+\hat{H}+T_sS$$

$$\frac{\partial s}{\partial t}+\frac{\partial us}{\partial x}+\frac{\partial vs}{\partial y}+\frac{\partial ws}{\partial z}=F_s+\frac{\partial}{\partial z}\left(D_v\frac{\partial s}{\partial z}\right)+s_sS$$

Unstructured mesh technique gives the maximum degree of flexibility, for example: 1) Control of node distribution allows for optimal usage of nodes 2) Adoption of mesh resolution to the relevant physical scales 3) Depth-adaptive and boundary-fitted mesh. Below is shown an example from Ho Bay, Denmark with the approach channel to the Port of Esbjerg

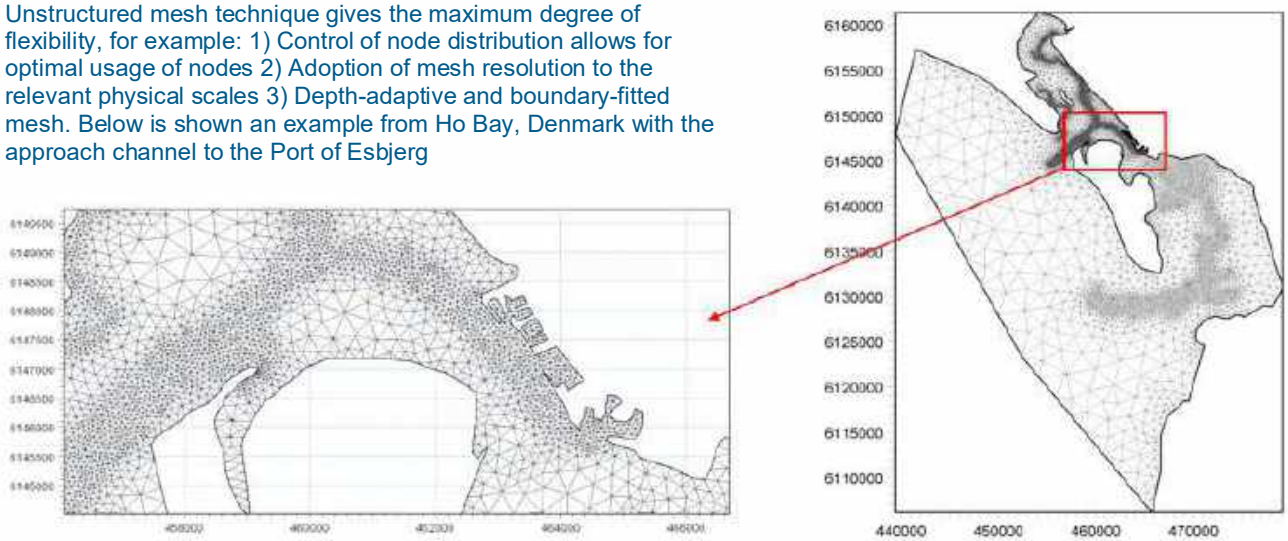

The horizontal diffusion terms are defined by

$$(F_T, F_s) = \left[\frac{\partial}{\partial x}\left(D_h \frac{\partial}{\partial x}\right) + \frac{\partial}{\partial y}\left(D_h \frac{\partial}{\partial y}\right)\right](T, s)$$

The equations for two-dimensional flow are obtained by integration of the equations over depth.

Heat exchange with the atmosphere is also included.

Symbol list

t	time
x, y, z	Cartesian coordinates
u, v, w	flow velocity components
T, s	temperature and salinity
D_v	vertical turbulent (eddy) diffusion coefficient
$\hat{H}$	source term due to heat exchange with atmosphere
S	magnitude of discharge due to point sources
T_s, s_s	temperature and salinity of source
F_T, F_s, F_c	horizontal diffusion terms
D_h	horizontal diffusion coefficient
h	depth

Solution Technique

The spatial discretisation of the primitive equations is performed using a cell-centred finite volume method. The spatial domain is discretised by subdivision of the continuum into non-overlapping elements/cells.

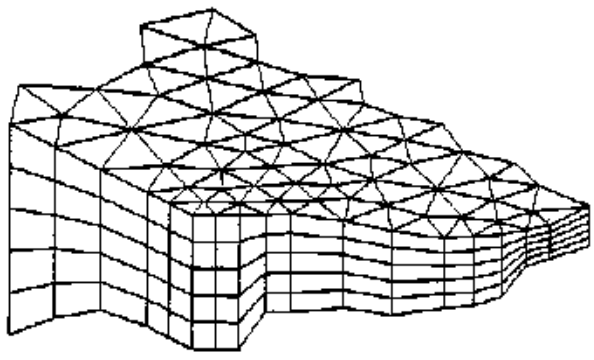

Principle of 3D mesh

In the horizontal plane an unstructured mesh is used while a structured mesh is used in the vertical domain of the 3D model. In the 2D model the elements can be triangles or quadrilateral elements. In the 3D model the elements can be prisms or bricks whose horizontal faces are triangles and quadrilateral elements, respectively.

The effect of a number of structure types (weirs, culverts, dikes, gates, piers and turbines) with a horizontal dimension which usually cannot be resolved by the computational mesh is modelled by a subgrid technique.

Model Input

Input data can be divided into the following groups:

- Domain and time parameters:
  - computational mesh (the coordinate type is defined in the computational mesh file) and bathymetry
  - simulation length and overall time step
- Calibration factors
  - bed resistance
  - momentum dispersion coefficients
  - wind friction factors
  - heat exchange coefficients
- Initial conditions
  - water surface level
  - velocity components
  - temperature and salinity
- Boundary conditions
  - closed
  - water level
  - discharge
  - temperature and salinity
- Other driving forces
  - wind speed and direction
  - tide
  - source/sink discharge
  - wave radiation stresses
- Structures
  - Structure type
  - location
  - structure data

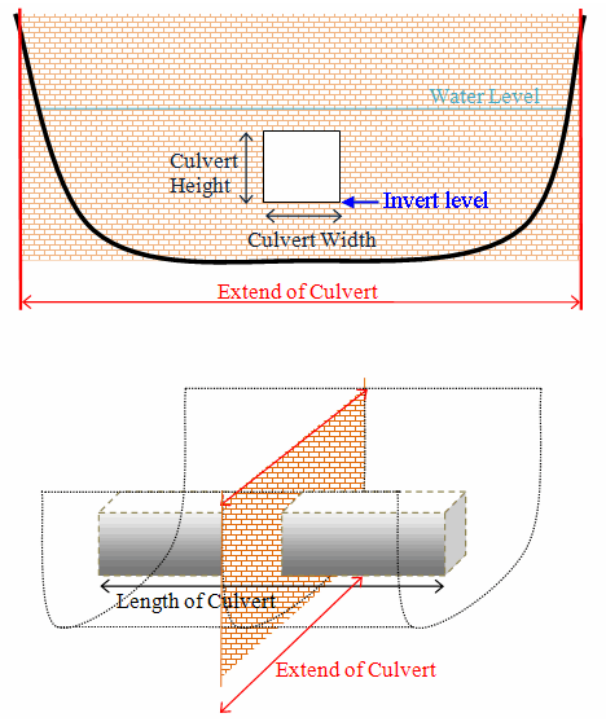

Setup definition of culvert structure

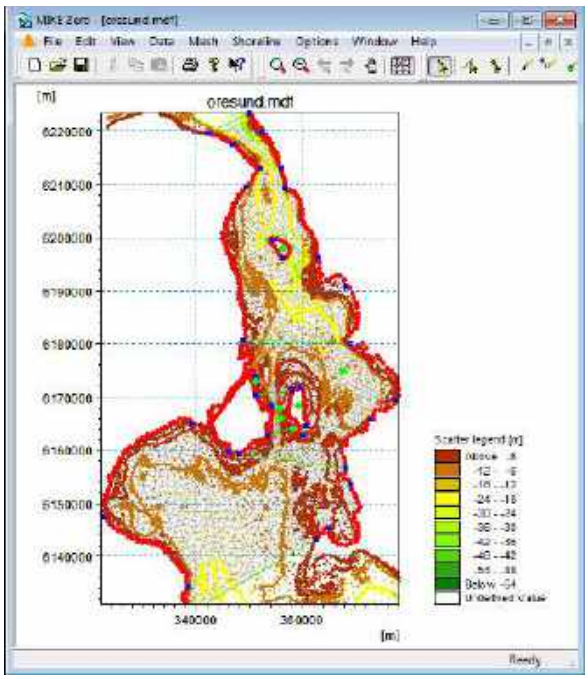

The Mesh Generator is an efficient MIKE Zero tool for the generation and handling of unstructured meshes, including the definition and editing of boundaries

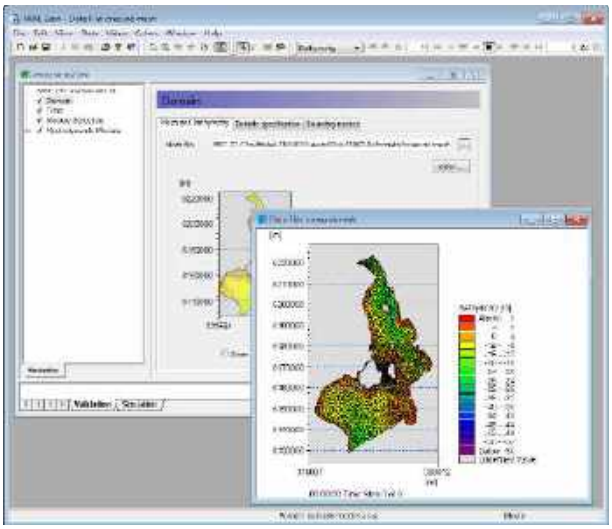

View button on all the GUIs in MIKE 21 & MIKE 3 FM HD for graphical view of input and output files

2D visualization of a computational mesh (Odense Estuary)

Providing MIKE 21 & MIKE 3 Flow Model FM with a suitable mesh is essential for obtaining reliable results from the models. Setting up the mesh includes the appropriate selection of the area to be modelled, adequate resolution of the bathymetry, flow, wind and wave fields under consideration and definition of codes for defining boundaries.

Bathymetric values for the mesh generation can e.g. be obtained from the MIKE Powered by DHI product MIKE C-Map. MIKE C-Map is an efficient tool for extracting depth data and predicted tidal elevation from the world-wide Electronic Chart Database CM-93 Edition 3.0 from C-MAP Norway.

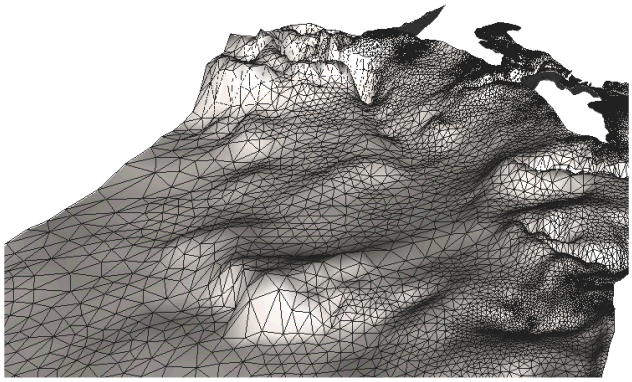

3D visualization of a computational mesh

If wind data is not available from an atmospheric meteorological model, the wind fields (e.g. cyclones) can be determined by using the wind-generating programs available in MIKE 21 Toolbox.

Global winds (pressure & wind data) can be downloaded for immediate use in your simulation. The sources of data are from GFS courtesy of NCEP, NOAA. By specifying the location, orientation and grid dimensions, the data is returned to you in the correct format as a spatial varying grid series or a time series. The link is:

http://www.waterforecast.com/hindcastdataproducts

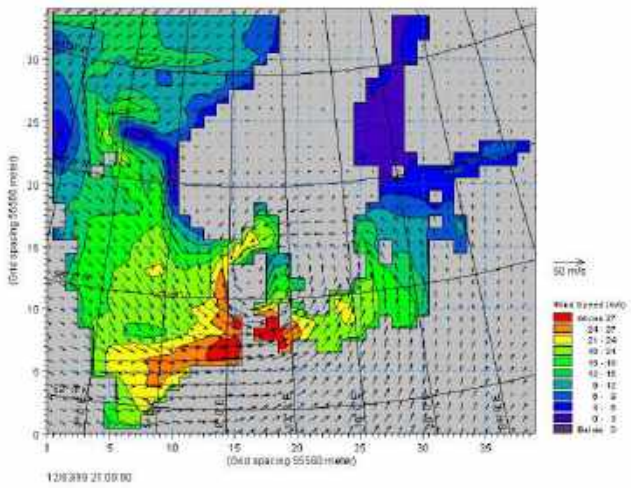

The chart shows a hindcast wind field over the North Sea and Baltic Sea as wind speed and wind direction

Model Output

Computed output results at each mesh element and for each time step consist of:

- Basic variables
  - water depths and surface elevations
  - flux densities in main directions
  - velocities in main directions
  - densities, temperatures and salinities
- Additional variables
  - Current speed and direction
  - Wind velocity
  - Air pressure
  - Drag coefficient
  - Precipitation/evaporation
  - Courant/CFL number
  - Eddy viscosity
  - Element area/volume

The output results can be saved in defined points, lines and areas. In the case of 3D calculations, the results are saved in a selection of layers.

Output from MIKE 21 & MIKE 3 Flow Model FM is typically post-processed using the Data Viewer available in the common MIKE Zero shell. The Data Viewer is a tool for analysis and visualization of unstructured data, e.g. to view meshes, spectra, bathymetries, results files of different format with graphical extraction of time series and line series from plan view and import of graphical overlays.

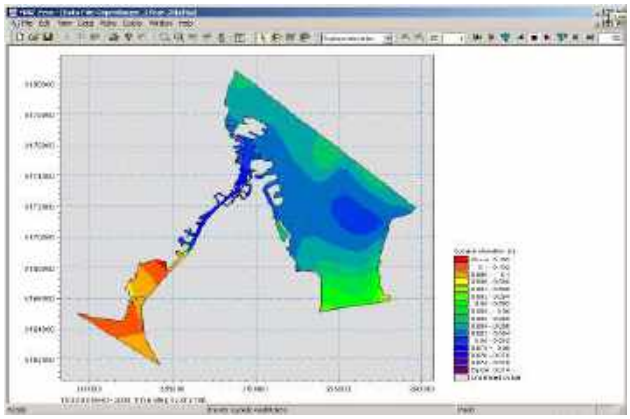

The Data Viewer in MIKE Zero – an efficient tool for analysis and visualization of unstructured data including processing of animations. Above screen dump shows surface elevations from a model setup covering Port of Copenhagen

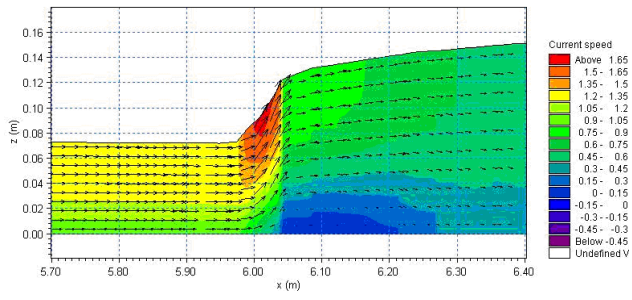

Vector and contour plot of current speed at a vertical profile defined along a line in Data Viewer in MIKE Zero

Validation

Prior to the first release of MIKE 21 & MIKE 3 Flow Model FM in year 2003 the model has successfully been applied to a number of basic idealized situations for which the results can be compared with analytical solutions or information from the literature.

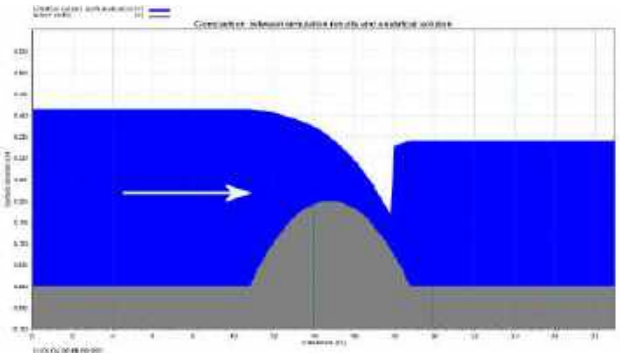

The domain is a channel with a parabola-shaped bump in the middle. The upstream (western) boundary is a constant flux and the downstream (eastern) boundary is a constant elevation. Below: the total depths for the stationary hydraulic jump at convergence. Red line: 2D setup, green line: 3D setup, black line: analytical solution

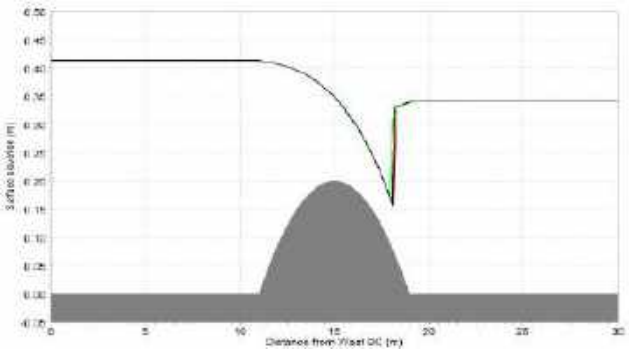

A dam-break flow in an L-shaped channel (a, b, c):

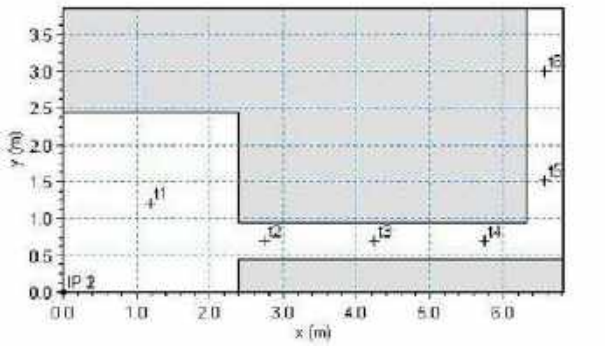

a) Outline of model setup showing the location of gauging points

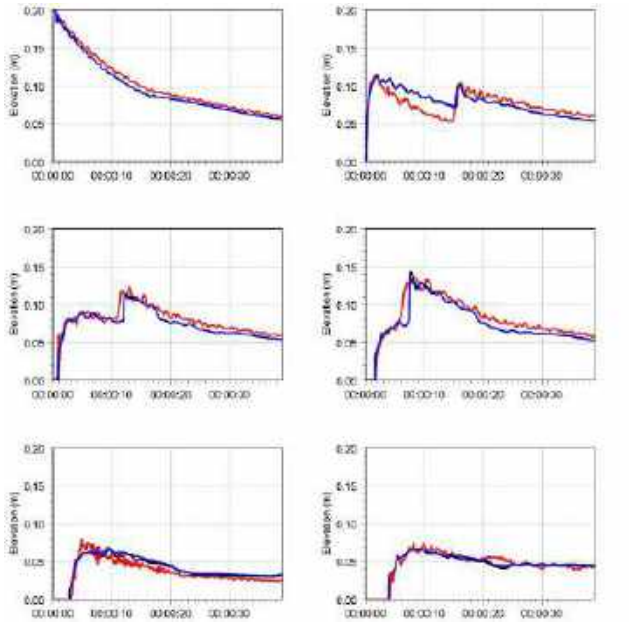

b) Comparison between simulated and measured water levels at the six gauge locations.
(Blue) coarse mesh solution (black) fine mesh solution and (red) measurements

The model has also been applied and tested in numerous natural geophysical conditions; ocean scale, inner shelves, estuaries, lakes and overland, which are more realistic and complicated than academic and laboratory tests.

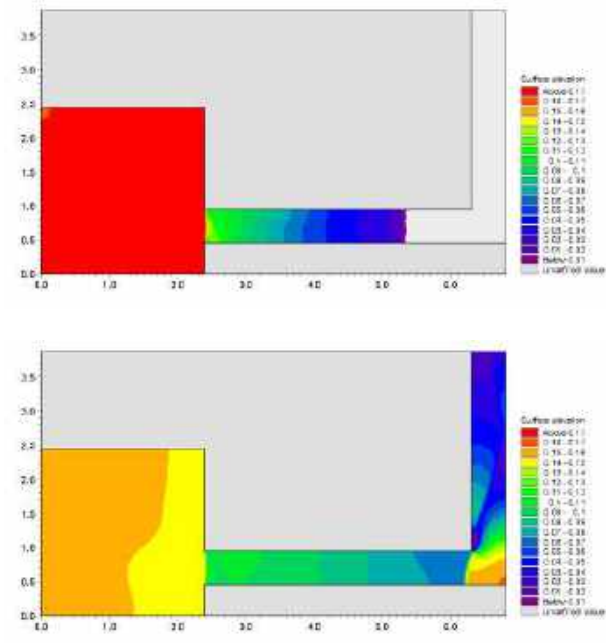

c) Contour plots of the surface elevation at T = 1.6 s (top) and T = 4.8 s (bottom)

Example from Ho Bay, a tidal estuary (barrier island coast) in South-West Denmark with access channel to the Port of Esbjerg.

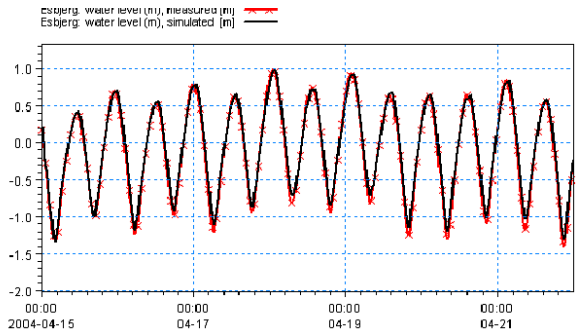

Comparison between measured and simulated water levels

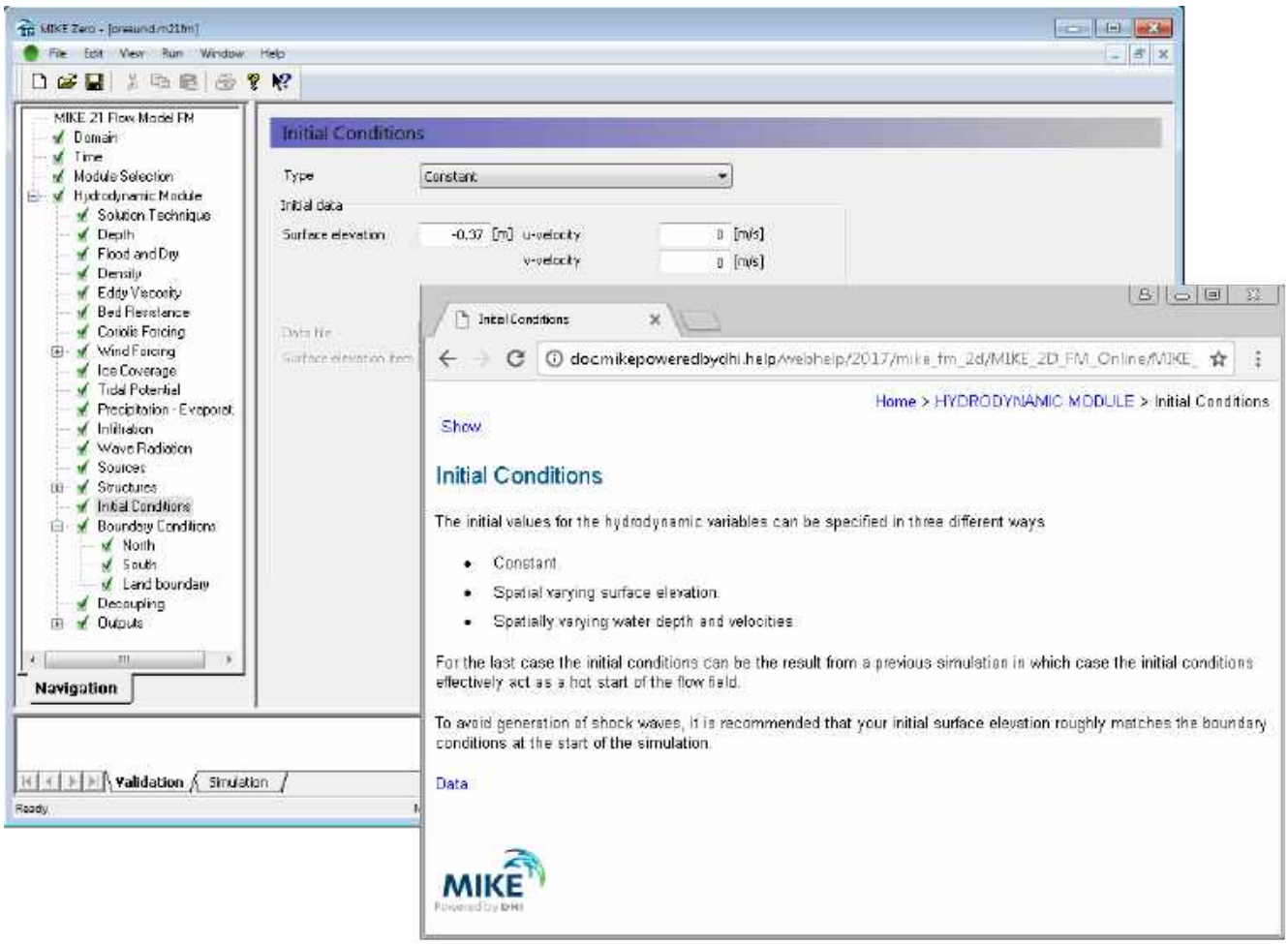

The user interface of the MIKE 21 and MIKE 3 Flow Model FM (Hydrodynamic Module), including an example of the extensive Online Help system

Graphical User Interface

The MIKE 21 & MIKE 3 Flow Model FM Hydrodynamic Module is operated through a fully Windows integrated graphical user interface (GUI). Support is provided at each stage by an Online Help system.

The common MIKE Zero shell provides entries for common data file editors, plotting facilities and utilities such as the Mesh Generator and Data Viewer.

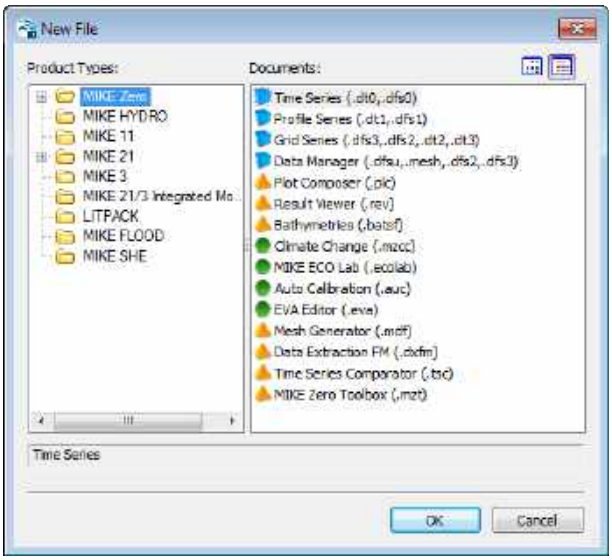

Overview of the common MIKE Zero utilities

Parallelisation

The computational engines of the MIKE 21 & MIKE 3 FM series are available in versions that have been parallelised using both shared memory as well as distributed memory architecture. The latter approach allows for domain decomposition. The result is much faster simulations on systems with multiple cores. It is also possible to use a graphics card (GPU) to perform computational intensive hydrodynamic computations.

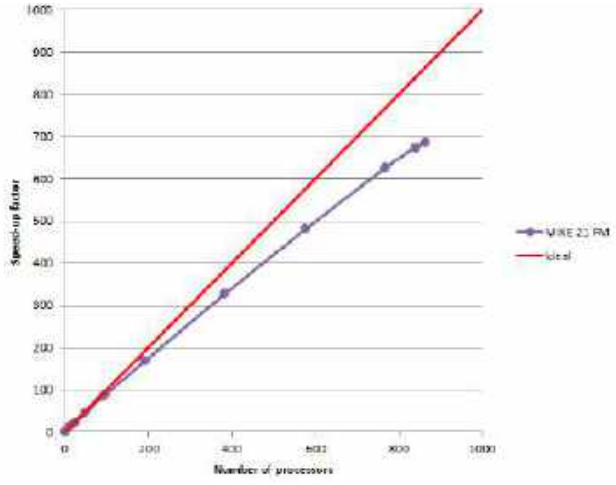

Example of MIKE 21 HD FM speed-up using a HPC Cluster with distributed memory architecture (purple)

Hardware and Operating System Requirements

The MIKE Zero Modules support Microsoft Windows 7 Professional Service Pack 1 (64 bit), Windows 10 Pro (64 bit), Windows Server 2012 R2 Standard (64 bit) and Windows Server 2016 Standard (64 bit).

Microsoft Internet Explorer 9.0 (or higher) is required for network license management. An internet browser is also required for accessing the web-based documentation and online help.

The recommended minimum hardware requirements for executing the MIKE Zero modules are:

Processor:	3 GHz PC (or higher)
Memory (RAM):	2 GB (or higher)
Hard disk:	40 GB (or higher)
Monitor:	SVGA, resolution 1024x768
Graphics card: (GUI and visualisation)	64 MB RAM (256 MB RAM or higher is recommended)
Graphics card: (for GPU computation)	1 GB RAM (or higher). requires a NVIDIA graphics card with compute capability 2.0 or higher

Support

News about new features, applications, papers, updates, patches, etc. are available here:

www.mikepoweredbydhi.com/Download/DocumentsAndTools.aspx

For further information on MIKE 21 and MIKE 3 Flow Model FM software, please contact your local DHI office or the support centre:

MIKE Powered by DHI Client Care
Agern Allé 5
DK-2970 Hørsholm
Denmark

Tel: +45 4516 9333
Fax: +45 4516 9292

mike@dhigroup.com
www.mikepoweredbydhi.com

Further Reading

Petersen, N.H., Rasch, P. “Modelling of the Asian Tsunami off the Coast of Northern Sumatra”, presented at the 3rd Asia-Pacific DHI Software Conference in Kuala Lumpur, Malaysia, 21-22 February, 2005

French, B. and Kerper, D. Salinity Control as a Mitigation Strategy for Habitat Improvement of Impacted Estuaries. 7th Annual EPA Wetlands Workshop, NJ, USA 2004.

DHI Note, “Flood Plain Modelling using unstructured Finite Volume Technique” January 2004 – download from

http://www.theacademybydhi.com/research-and-publications/scientific-publications

Documentation

The MIKE 21 & MIKE 3 Flow Model FM models are provided with comprehensive user guides, online help, scientific documentation, application examples and step-by-step training examples.

APPENDIX D
SW model short description

MIKE 21 Wave Modelling

MIKE 21 Spectral Waves FM

Short Description

DHI headquarters
Agern Allé 5
DK-2970 Hørsholm
Denmark

+45 4516 9200 Telephone
+45 4516 9333 Support
+45 4516 9292 Telefax

mike@dhigroup.com
www.mikepoweredbydhi.com

MIKE21_SW_FM_Short_Description.docx / HKH/AJS / 2017-10-03

MIKE 21 SW - SPECTRAL WAVE MODEL FM

MIKE 21 SW is a state-of-the-art third generation spectral wind-wave model developed by DHI. The model simulates the growth, decay and transformation of wind-generated waves and swells in offshore and coastal areas.

MIKE 21 SW includes two different formulations:

- Fully spectral formulation
- Directional decoupled parametric formulation

The fully spectral formulation is based on the wave action conservation equation, as described in e.g. Komen et al (1994) and Young (1999). The directional decoupled parametric formulation is based on a parameterisation of the wave action conservation equation. The parameterisation is made in the frequency domain by introducing the zeroth and first moment of the wave action spectrum. The basic conservation equations are formulated in either Cartesian co-ordinates for small-scale applications and polar spherical co-ordinates for large-scale applications.

The fully spectral model includes the following physical phenomena:

- Wave growth by action of wind
- Non-linear wave-wave interaction
- Dissipation due to white-capping
- Dissipation due to bottom friction
- Dissipation due to depth-induced wave breaking
- Refraction and shoaling due to depth variations
- Wave-current interaction
- Effect of time-varying water depth
- Effect of ice coverage on the wave field

The discretisation of the governing equation in geographical and spectral space is performed using cell-centred finite volume method. In the geographical domain, an unstructured mesh technique is used. The time integration is performed using a fractional step approach where a multi-sequence explicit method is applied for the propagation of wave action.

MIKE 21 SW is a state-of-the-art numerical modelling tool for prediction and analysis of wave climates in offshore and coastal areas. © BIOFOTO/Klaus K. Bentzen

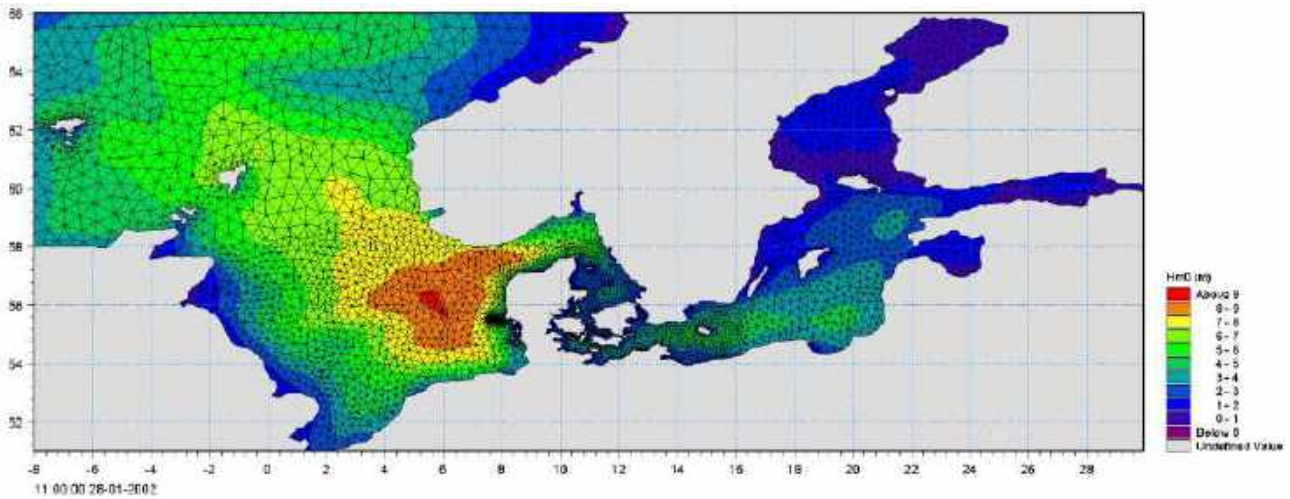

A MIKE 21 SW forecast application in the North Sea and Baltic Sea. The chart shows a wave field (from the NSBS model) illustrated by the significant wave height in top of the computational mesh. See also www.waterforecast.com

Computational Features

The main computational features of MIKE 21 SW - Spectral Wave Model FM are as follows:

- Fully spectral and directionally decoupled parametric formulations
- Source functions based on state-of-the-art 3rd generation formulations
- Instationary and quasi-stationary solutions
- Optimal degree of flexibility in describing bathymetry and ambient flow conditions using depth-adaptive and boundary-fitted unstructured mesh
- Coupling with hydrodynamic flow model for modelling of wave-current interaction and time-varying water depth
- Flooding and drying in connection with time-varying water depths
- Cell-centred finite volume technique
- Fractional step time-integration with an multi-sequence explicit method for the propagation
- Extensive range of model output parameters (wave, swell, air-sea interaction parameters, radiation stress tensor, spectra, etc.)

Application Areas

MIKE 21 SW is used for the assessment of wave climates in offshore and coastal areas - in hindcast and forecast mode.

A major application area is the design of offshore, coastal and port structures where accurate assessment of wave loads is of utmost importance to the safe and economic design of these structures.

Illustrations of typical application areas of DHI's MIKE 21 SW – Spectral Wave Model FM

Measured data are often not available during periods long enough to allow for the establishment of sufficiently accurate estimates of extreme sea states.

In this case, the measured data can then be supplemented with hindcast data through the simulation of wave conditions during historical storms using MIKE 21 SW.

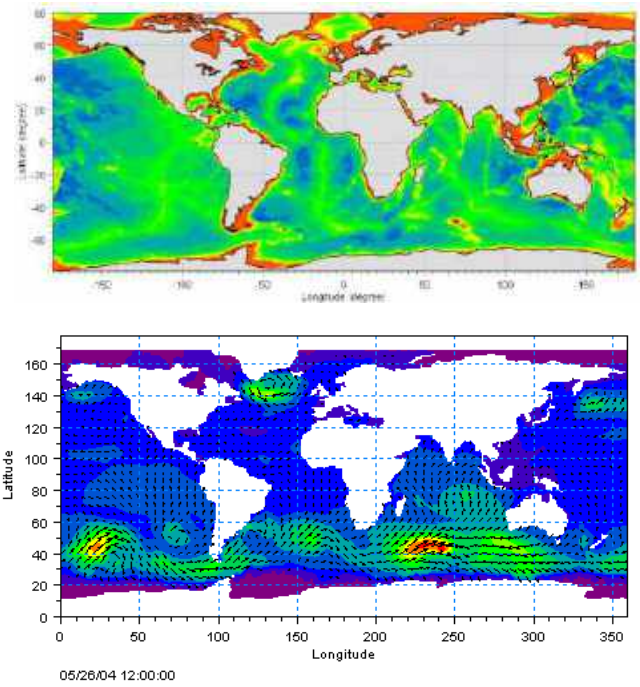

Example of a global application of MIKE 21 SW. The upper panel shows the bathymetry. Results from such a model (cf. lower panel) can be used as boundary conditions for regional scale forecast or hindcast models. See http://www.waterforecast.com for more details on regional and global modelling

MIKE 21 SW is particularly applicable for simultaneous wave prediction and analysis on regional scale and local scale. Coarse spatial and temporal resolution is used for the regional part of the mesh and a high-resolution boundary and depth-adaptive mesh is describing the shallow water environment at the coastline.

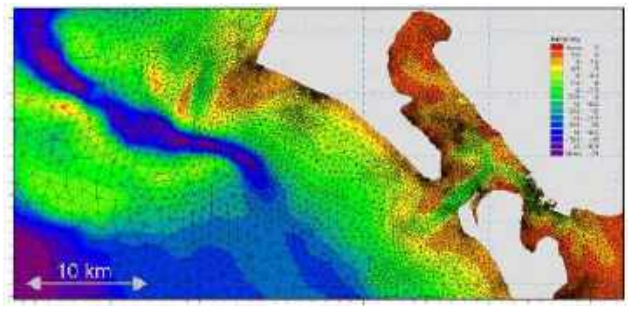

Example of a computational mesh used for transformation of offshore wave statistics using the directionally decoupled parametric formulation

MIKE 21 SW is also used for the calculation of the sediment transport, which for a large part is determined by wave conditions and associated wave-induced currents. The wave-induced current is generated by the gradients in radiation stresses that occur in the surf zone.

MIKE 21 SW can be used to calculate the wave conditions and associated radiation stresses. The long-shore currents and sediment transport are then calculated using the flow and sediment transport models available in the MIKE 21 package. For such type of applications, the directional decoupled parametric formulation of MIKE 21 SW is an excellent compromise between the computational effort and accuracy.

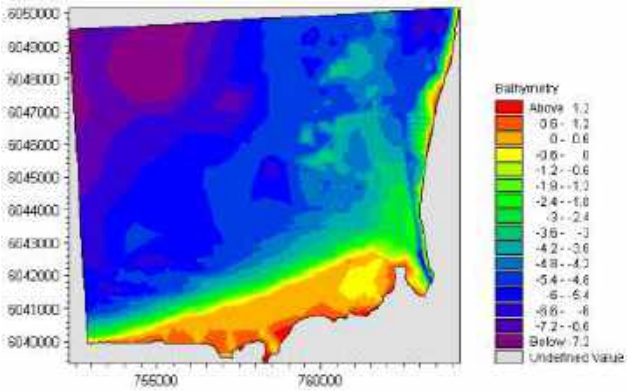

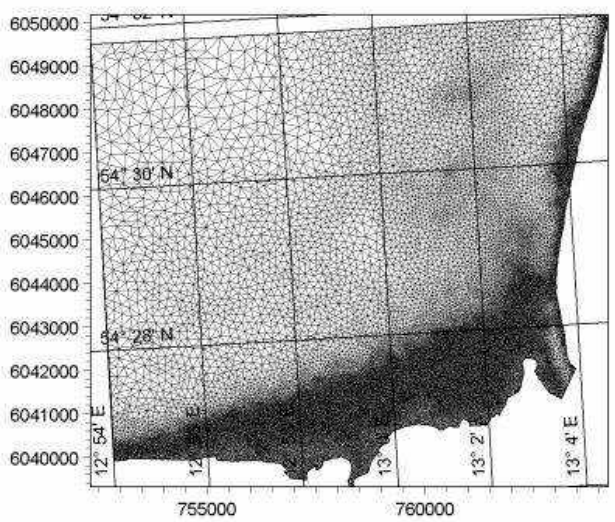

Bathymetry (upper) and computational mesh (lower) used in a MIKE 21 SW application on wave induced currents in Gellen Bay, Germany

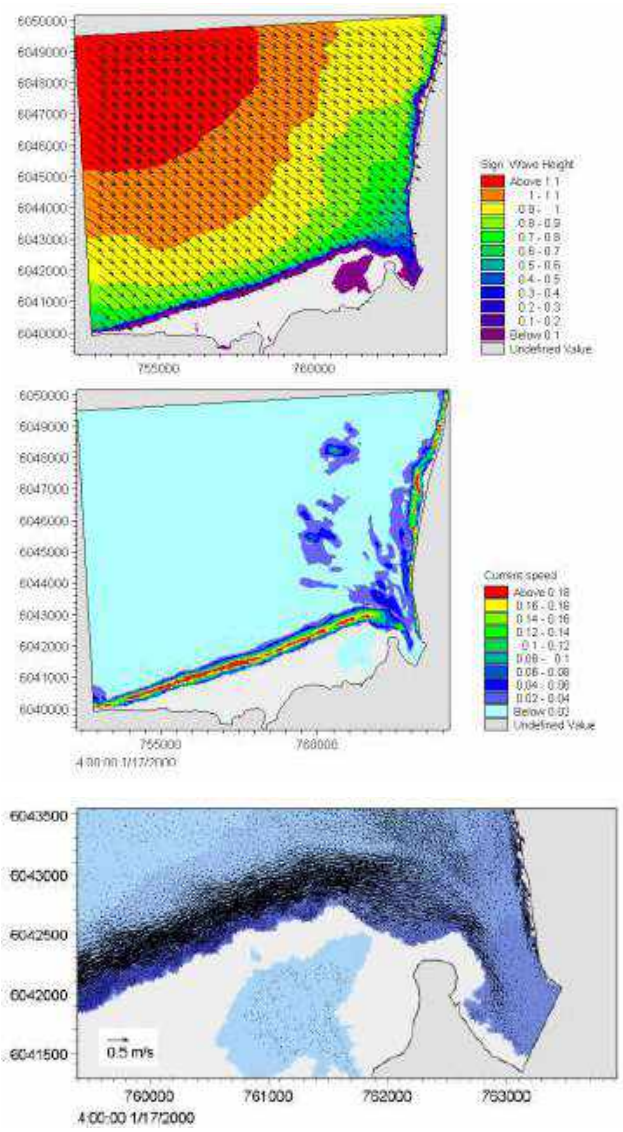

Map of significant wave height (upper), current field (middle) and vector field (lower). The flow field is simulated by DHI's MIKE 21 Flow Model FM, which is dynamically coupled to MIKE 21 SW

Model Equations

In MIKE 21 SW, the wind waves are represented by the wave action density spectrum $N(\sigma,\theta)$. The independent phase parameters have been chosen as the relative (intrinsic) angular frequency, $\sigma = 2\pi f$ and the direction of wave propagation, θ. The relation between the relative angular frequency and the absolute angular frequency, ω, is given by the linear dispersion relationship

$$\sigma = \sqrt{gk\tanh(kd)} = \omega - \bar{k}\cdot\bar{U}$$

where g is the acceleration of gravity, d is the water depth and $\bar{U}$ is the current velocity vector and $\bar{k}$ is the wave number vector with magnitude k and direction θ. The action density, $N(\sigma,\theta)$, is related to the energy density $E(\sigma,\theta)$ by

$$N = \frac{E}{\sigma}$$

Fully Spectral Formulation

The governing equation in MIKE 21 SW is the wave action balance equation formulated in either Cartesian or spherical co-ordinates. In horizontal Cartesian co-ordinates, the conservation equation for wave action reads

$$\frac{\partial N}{\partial t} + \nabla\cdot(\bar{v}N) = \frac{S}{\sigma}$$

where $N(\bar{x},\sigma,\theta,t)$ is the action density, t is the time, $\bar{x} = (x,y)$ is the Cartesian co-ordinates, $\bar{v} = (c_x, c_y, c_\sigma, c_\theta)$ is the propagation velocity of a wave group in the four-dimensional phase space $\bar{x}$, σ and θ. S is the source term for energy balance equation. ∇ is the four-dimensional differential operator in the $\bar{x}$, σ, θ-space. The characteristic propagation speeds are given by the linear kinematic relationships

$$(c_x, c_y) = \frac{d\bar{x}}{dt} = \bar{c}_g + \bar{U} = \frac{1}{2}\left(1 + \frac{2kd}{\sinh(2kd)}\right)\frac{\sigma}{k} + \bar{U}$$

$$c_\sigma = \frac{d\sigma}{dt} = \frac{\partial\sigma}{\partial d}\left[\frac{\partial d}{\partial t} + \bar{U}\cdot\nabla_{\bar{x}} d\right] - c_g\bar{k}\cdot\frac{\partial\bar{U}}{\partial s}$$

$$c_\theta = \frac{d\theta}{dt} = -\frac{1}{k}\left[\frac{\partial\sigma}{\partial d}\frac{\partial d}{\partial m} + \bar{k}\cdot\frac{\partial\bar{U}}{\partial m}\right]$$

Here, s is the space co-ordinate in wave direction θ and m is a co-ordinate perpendicular to s. $\nabla_{\bar{x}}$ is the two-dimensional differential operator in the $\bar{x}$-space.

Source Functions

The source function term, S, on the right hand side of the wave action conservation equation is given by

$$S = S_{in} + S_{nl} + S_{ds} + S_{bot} + S_{surf}$$

Here S_{in} represents the momentum transfer of wind energy to wave generation, S_{nl} the energy transfer due non-linear wave-wave interaction, S_{ds} the dissipation of wave energy due to white-capping (deep water wave breaking), S_{bot} the dissipation due to bottom friction and S_{surf} the dissipation of wave energy due to depth-induced breaking.

The default source functions S_{in}, S_{nl} and S_{ds} in MIKE 21 SW are similar to the source functions implemented in the WAM Cycle 4 model, see Komen et al (1994).

The wind input is based on Janssen's (1989, 1991) quasi-linear theory of wind-wave generation, where the momentum transfer from the wind to the sea not only depends on the wind stress, but also the sea state itself. The non-linear energy transfer (through the resonant four-wave interaction) is approximated by the DIA approach, Hasselmann et al (1985). The source function describing the dissipation due to white-capping is based on the theory of Hasselmann (1974) and Janssen (1989). The bottom friction dissipation is modelled using the approach by Johnson and Kofoed-Hansen (2000), which depends on the wave and sediment properties. The source function describing the bottom-induced wave breaking is based on the well-proven approach of Battjes and Janssen (1978) and Eldeberky and Battjes (1996).

A detailed description of the various source functions is available in Komen et al (1994) and Sørensen et al (2003), which also includes the references listed above.

Directional Decoupled Parametric Formulation

The directionally decoupled parametric formulation is based on a parameterisation of the wave action conservation equation. Following Holthuijsen et al (1989), the parameterisation is made in the frequency domain by introducing the zeroth and first moment of the wave action spectrum as dependent variables.

A similar formulation is used in the MIKE 21 NSW Near-shore Spectral Wind-Wave Model, which is one of the most popular models for wave transformation in coastal and shallow water environment. However, with MIKE 21 SW it is not necessary to set up a number of different orientated bathymetries to cover varying wind and wave directions.

The parameterisation leads to the following coupled equations

$$\frac{\partial(m_0)}{\partial t}+\frac{\partial(c_x m_0)}{\partial x}+\frac{\partial(c_y m_0)}{\partial y}+\frac{\partial(c_\theta m_0)}{\partial \theta}=T_0$$

$$\frac{\partial(m_1)}{\partial t}+\frac{\partial(c_x m_1)}{\partial x}+\frac{\partial(c_y m_1)}{\partial y}+\frac{\partial(c_\theta m_1)}{\partial \theta}=T_1$$

where $m_0(x, y, \theta)$ and $m_1(x, y, \theta)$ are the zeroth and first moment of the action spectrum $N(x, y, \sigma, \theta)$, respectively. $T_0(x, y, \theta)$ and $T_1(x, y, \theta)$ are source functions based on the action spectrum. The moments $m_n(x, y, \theta)$ are defined as

$$m_n(x,y,\theta)=\int_0^\infty \omega^n N(x,y,\omega,\theta)d\omega$$

The source functions T_0 and T_1 take into account the effect of local wind generation (stationary solution mode only) and energy dissipation due to bottom friction and wave breaking. The effects of wave-current interaction are also included. The source functions for the local wind generation are derived from empirical growth relations, see Johnson (1998) for details.

Numerical Methods

The frequency spectrum (fully spectral model only) is split into a prognostic part for frequencies lower than a cut-off frequency σ_{max} and an analytical diagnostic tail for the high-frequency part of the spectrum

$$E(\sigma,\theta)=E(\sigma_{\max},\theta)\left(\frac{\sigma}{\sigma_{\max}}\right)^{-m}$$

where m is a constant (= 5) as proposed by Komen et al (1994).

The directional decoupled parametric formulation in MIKE 21 SW is used extensively for calculation of the wave transformation from deep-water to the shoreline and for wind-wave generation in local areas

Space Discretisation

The discretisation in geographical and spectral space is performed using cell-centred finite volume method. In the geographical domain an unstructured mesh is used. The spatial domain is discretised by subdivision of the continuum into non-overlapping elements. Triangle and quadrilateral shaped polygons are presently supported in MIKE 21 SW. The action density, $N(\sigma,\theta)$ is represented as a piecewise constant over the elements and stored at the geometric centres.

In frequency space either an equidistant or a log-arithmic discretisation is used. In the directional space, an equidistant discretisation is used for both types of models. The action density is represented as piecewise constant over the discrete intervals, $\Delta\sigma$ and $\Delta\theta$, in the frequency and directional space.

Integrating the wave action conservation over an area A_i, the frequency interval $\Delta\sigma_l$ and the directional interval $\Delta\theta_m$ gives

$$\frac{\partial}{\partial t}\int_{\Delta\theta_m}\int_{\Delta\sigma_l}\int_{A_i} N d\Omega d\sigma d\theta - \int_{\Delta\theta_m}\int_{\Delta\sigma_l}\int_{A_i}\frac{S}{\sigma} d\Omega d\sigma d\theta$$
$$= \int_{\Delta\theta_m}\int_{\Delta\sigma_l}\int_{A_i} \nabla\cdot(\bar{v}N) d\Omega d\sigma d\theta$$

where Ω is the integration variable defined on A_i. Using the divergence theorem and introducing the convective flux $\bar{F} = \bar{v}N$, we obtain

$$\frac{\partial N_{i,l,m}}{\partial t} = -\frac{1}{A_i}\left[\sum_{p=1}^{NE}(F_n)_{p,l,m}\Delta l_p\right]$$
$$-\frac{1}{\Delta\sigma_l}\left[(F_\sigma)_{i,l+1/2,m} - (F_\sigma)_{i,l-1/2,m}\right]$$
$$-\frac{1}{\Delta\theta_m}\left[(F_\theta)_{i,l,m+1/2} - (F_\theta)_{i,l,m-1/2}\right] + \frac{S_{i,l,m}}{\sigma_l}$$

where NE is the total number of edges in the cell, $(F_n)_{p,l,m} = (F_x n_x + F_y n_y)_{p,l,m}$ is the normal flux trough the edge p in geographical space with length Δl_p. $(F_\sigma)_{i,l+1/2,m}$ and $(F_\theta)_{i,l,m+1/2}$ is the flux through the face in the frequency and directional space, respectively.

The convective flux is derived using a first-order upwinding scheme. In that

$$F_n = c_n\left(\frac{1}{2}(N_i + N_j) - \frac{1}{2}\frac{c}{|c|}(N_i - N_j)\right)$$

where c_n is the propagation speed normal to the element cell face.

Time Integration

The integration in time is based on a fractional step approach. Firstly, a propagation step is performed calculating an approximate solution N^* at the new time level (n+1) by solving the homogenous wave action conservation equation, i.e. without the source terms. Secondly, a source terms step is performed calculating the new solution N^{n+1} from the estimated solution taking into account only the effect of the source terms.

The propagation step is carried out by an explicit Euler scheme

$$N^*_{i,l,m} = N^n_{i,l,m} + \Delta t\left(\frac{\partial N_{i,l,m}}{\partial t}\right)^n$$

To overcome the severe stability restriction, a multi-sequence integration scheme is employed. The maximum allowed time step is increased by employing a sequence of integration steps locally, where the number of steps may vary from point to point.

A source term step is performed using an implicit method (see Komen et al, 1994)

$$N^{n+1}_{i,l,m} = N^*_{i,l,m} + \Delta t\left[\frac{(1-\alpha)S^*_{i,l,m} + \alpha S^{n+1}_{i,l,m}}{\sigma_l}\right]$$

where α is a weighting coefficient that determines the type of finite difference method. Using a Taylor series to approximate S^{n+1} and assuming the off-diagonal terms in $\partial S/\partial E = \gamma$ are negligible, this equation can be simplified as

$$N^{n+1}_{i,l,m} = N^n_{i,l,m} + \frac{(S^*_{i,l,m}/\sigma_l)\Delta t}{(1-\alpha\gamma\Delta t)}$$

For growing waves ($\gamma > 0$) an explicit forward difference is used ($\alpha = 0$), while for decaying waves ($\gamma < 0$) an implicit backward difference ($\alpha = 1$) is applied.

MIKE 21 SW is also applied for wave forecasts in ship route planning and improved service for conventional and fast ferry operators

Model Input

The necessary input data can be divided into following groups:

- Domain and time parameters:
  - computational mesh
  - co-ordinate type (Cartesian or spherical)
  - simulation length and overall time step
- Equations, discretisation and solution technique
  - formulation type
  - frequency and directional discretisation
  - number of time step groups
  - number of source time steps
- Forcing parameters
  - water level data
  - current data
  - wind data
  - ice data
- Source function parameters
  - non-linear energy transfer
  - wave breaking (shallow water)
  - bottom friction
  - white capping
- Structures
  - location and geometry
  - approach
  - structures coefficients
- Initial conditions
  - zero-spectrum (cold-start)
  - empirical data
  - data file
- Boundary conditions
  - closed boundaries
  - open boundaries (data format and type)

Providing MIKE 21 SW with a suitable mesh is essential for obtaining reliable results from the model. Setting up the mesh includes the appropriate selection of the area to be modelled, adequate resolution of the bathymetry, flow, wind and wave fields under consideration and definition of codes for essential and land boundaries.

Furthermore, the resolution in the geographical space must also be selected with respect to stability considerations.

As the wind is the main driving force in MIKE 21 SW, accurate hindcast or forecast wind fields are of utmost importance for the wave prediction.

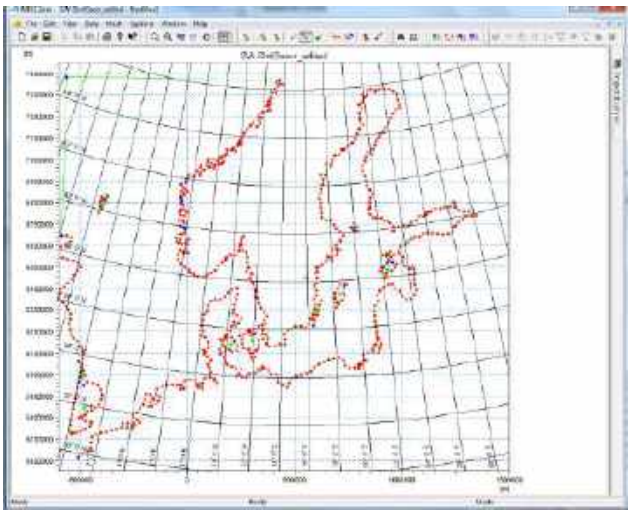

The Mesh Generator is an efficient MIKE Zero tool for the generation and handling of unstructured meshes, including the definition and editing of boundaries

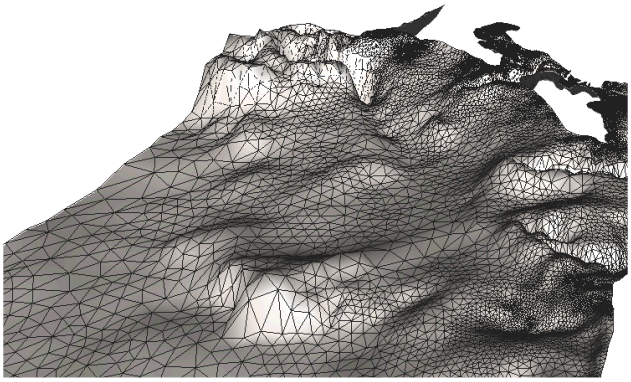

3D visualisation of a computational mesh

If wind data is not available from an atmospheric meteorological model, the wind fields (e.g. cyclones) can be determined by using the wind-generating programs available in MIKE 21 Toolbox.

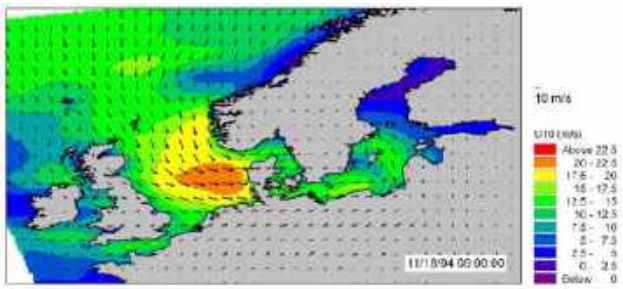

The chart shows an example of a wind field covering the North Sea and Baltic Sea as wind speed and wind direction. This is used as input to MIKE 21 SW in forecast and hindcast mode

Model Output

At each mesh point and for each time step four types of output can be obtained from MIKE 21 SW:

- Integral wave parameters divided into wind sea and swell such as
  - significant wave height, H_{m0}
  - peak wave period, T_p
  - averaged wave period, T_{01}
  - zero-crossing wave period, T_{02}
  - wave energy period, T_{-10}
  - peak wave direction, θ_p
  - mean wave direction, θ_m
  - directional standard deviation, σ
  - wave height with dir., $H_{m0} \cos\theta_m$, $H_{m0} \sin\theta_m$
  - radiation stress tensor, S_{xx}, S_{xy} and S_{yy}
  - particle velocities, *horizontal/vertical*
  - wave power, P, P_x *and* P_y

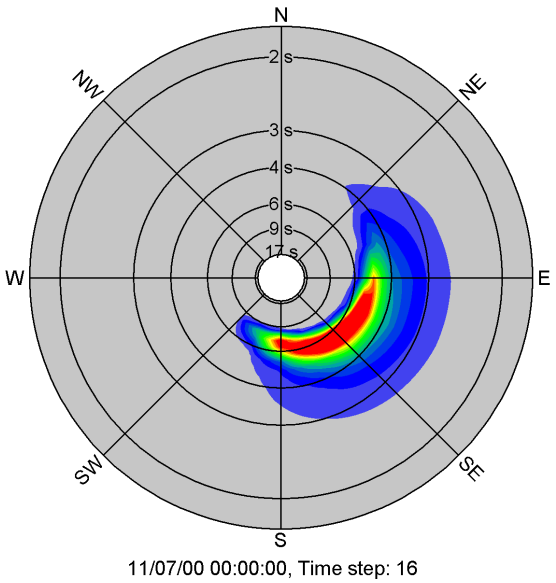

Example of model output (directional-frequency wave spectrum) processed using the Polar Plot control in the MIKE Zero Plot Composer

The distinction between wind-sea and swell can be calculated using either a constant threshold frequency or a dynamic threshold frequency with an upper frequency limit.

- Input parameters
  - water level, *WL*
  - water depth, *h*
  - current velocity, $\overline{U}$
  - wind speed, U_{10}
  - wind direction, θ_w
  - Ice concentration
- Model parameters
  - bottom friction coefficient, C_f
  - breaking parameter, γ
  - Courant number, *Cr*
  - time step factor, α
  - characteristic edge length, Δl
  - area of element, *a*
  - wind friction speed, u_*
  - roughness length, z_0
  - drag coefficient, C_D
  - Charnock parameter, z_{ch}
- Directional-frequency wave spectra at selected grid points and or areas as well as direction spectra and frequency spectra

Output from MIKE 21 SW is typically post-processed using the Data Viewer available in the common MIKE Zero shell. The Data Viewer is a tool for analysis and visualisation of unstructured data, e.g. to view meshes, spectra, bathymetries, results files of different format with graphical extraction of time series and line series from plan view and import of graphical overlays.

Various other editors and plot controls in the MIKE Zero Composer (e.g. Time Series Plot, Polar Plot, etc.) can be used for analysis and visualisation.

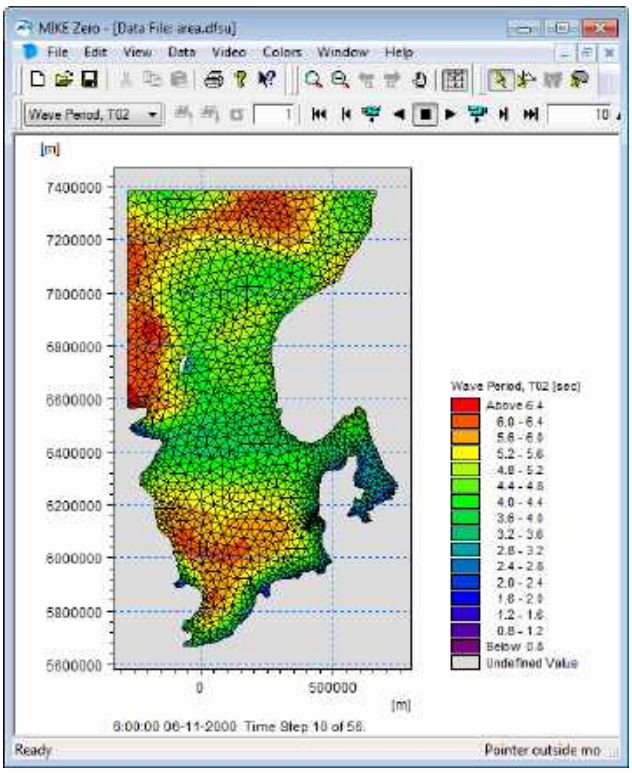

The Data Viewer in MIKE Zero – an efficient tool for analysis and visualisation of unstructured data including processing of animations

Validation

The model has successfully been applied to a number of rather basic idealised situations for which the results can be compared with analytical solutions or information from the literature. The basic tests covered fundamental processes such as wave propagation, depth-induced and current-induced shoaling and refraction, wind-wave generation and dissipation.

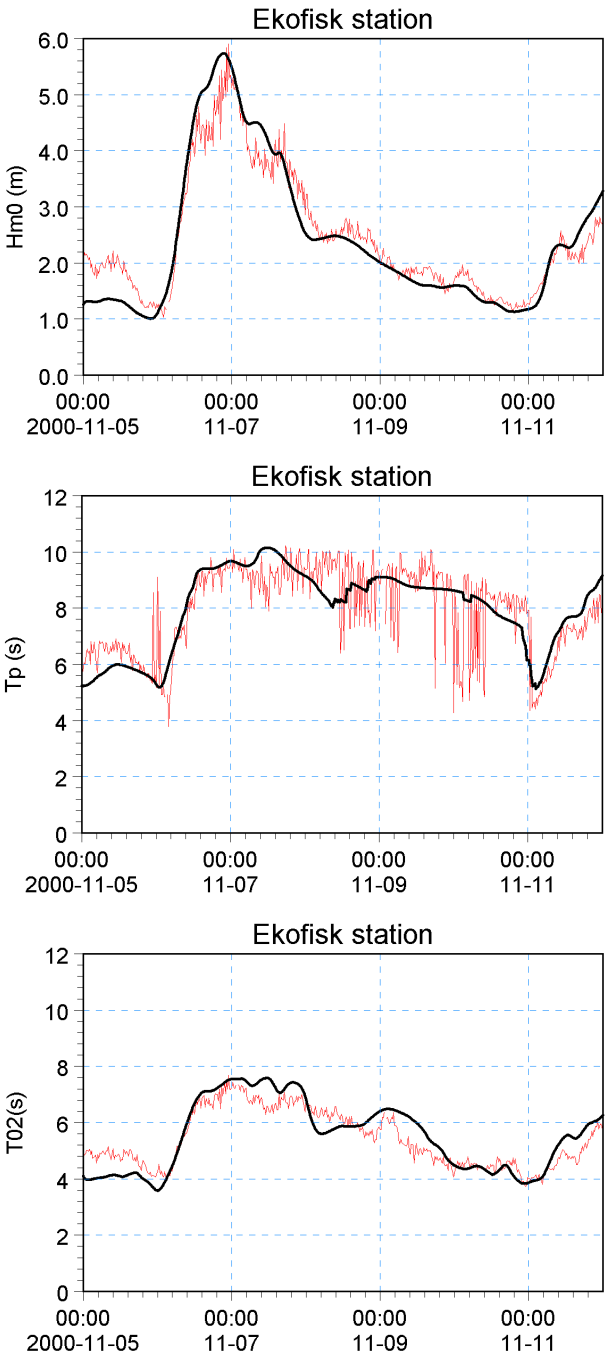

Comparison between measured and simulated significant wave height, peak wave period and mean wave period at the Ekofisk offshore platform (water depth 70 m) in the North Sea). (——) calculations and (——) measurements

A major application area of MIKE 21 SW is in connection with design and maintenance of offshore structures

The model has also been tested in natural geophysical conditions (e.g. in the North Sea, the Danish West Coast and the Baltic Sea), which are more realistic and complicated than the academic test and laboratory tests mentioned above.

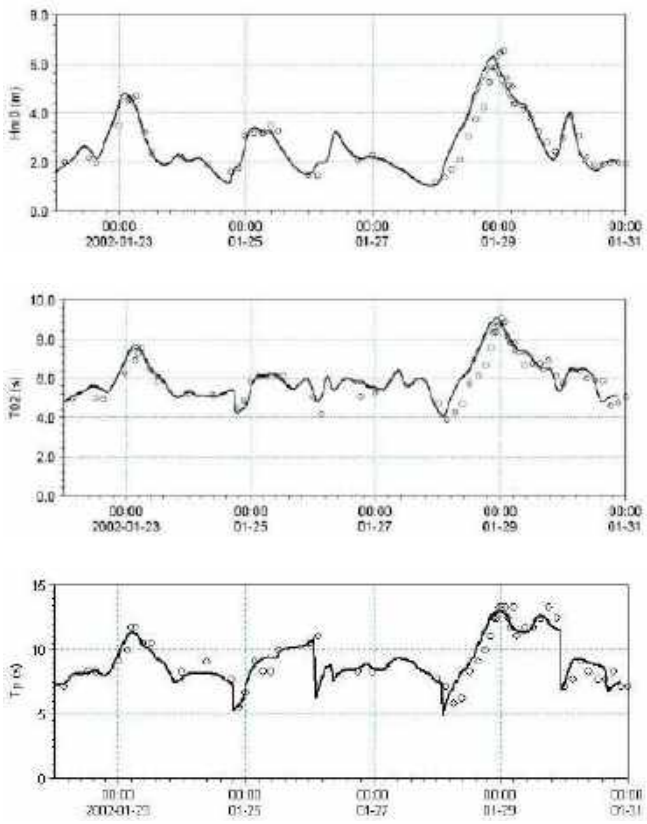

Comparison between measured and simulated significant wave height, peak wave period and mean wave period at Fjaltring located at the Danish west coast (water depth 17.5 m).(——) calculations and (o) measurements

The Fjaltring directional wave rider buoy is located offshore relative to the depicted arrow

MIKE 21 SW is used for prediction of the wave conditions at the complex Horns Rev (reef) in the southeastern part of the North Sea. At this site, a 168 MW offshore wind farm with 80 turbines has been established in water depths between 6.5 and 13.5 m.

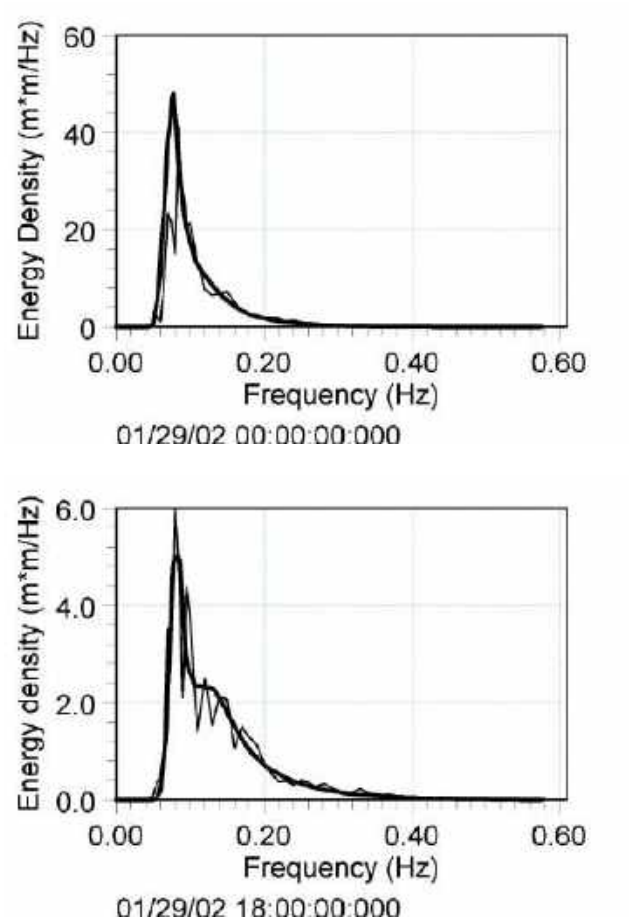

Comparison of frequency spectra at Fjaltring. (——) calculations and (——)measurements

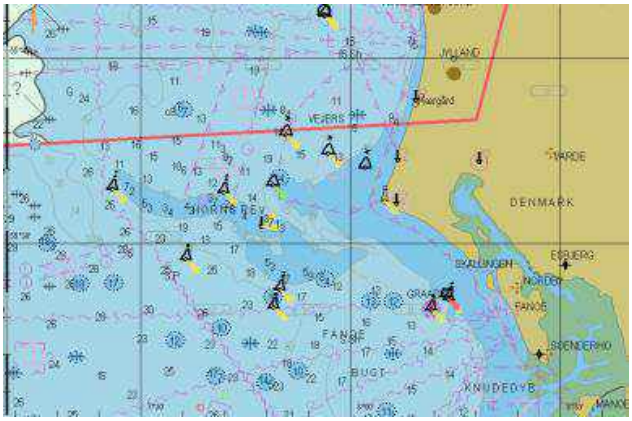

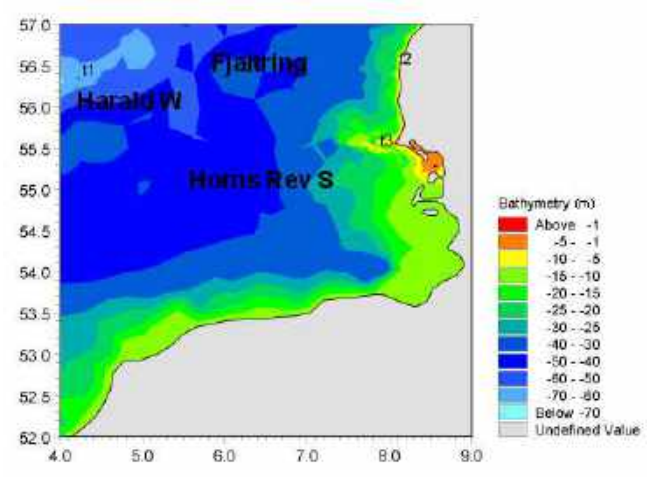

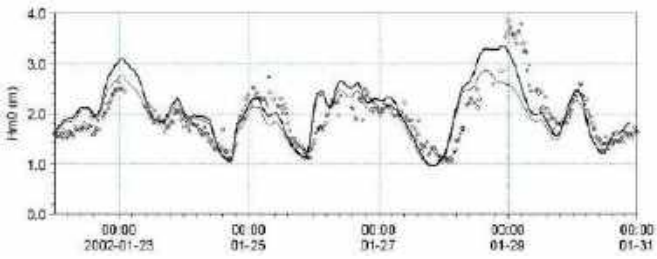

The upper panels show the Horns Rev offshore wind farm and MIKE C-map chart. 'The middle panel shows a close-up of the mesh near the Horns Rev S wave rider buoy (t3, 10 m water depth. The lower panel shows a comparison between measured and simulated significant wave height at Horns Rev S, (——) calculations including tide and surge and (——-) calculations excluding including tide and surge, (o) measurements

The predicted nearshore wave climate along the island of Hiddensee and the coastline of Zingst located in the micro-tidal Gellen Bay, Germany have been compared to field measurements (Sørensen et al, 2004) provided by the MORWIN project. From the illustrations it can be seen that the wave conditions are well reproduced both offshore and in more shallow water near the shore. The RMS values (on significant wave height) are less than 0.25m at all five stations.

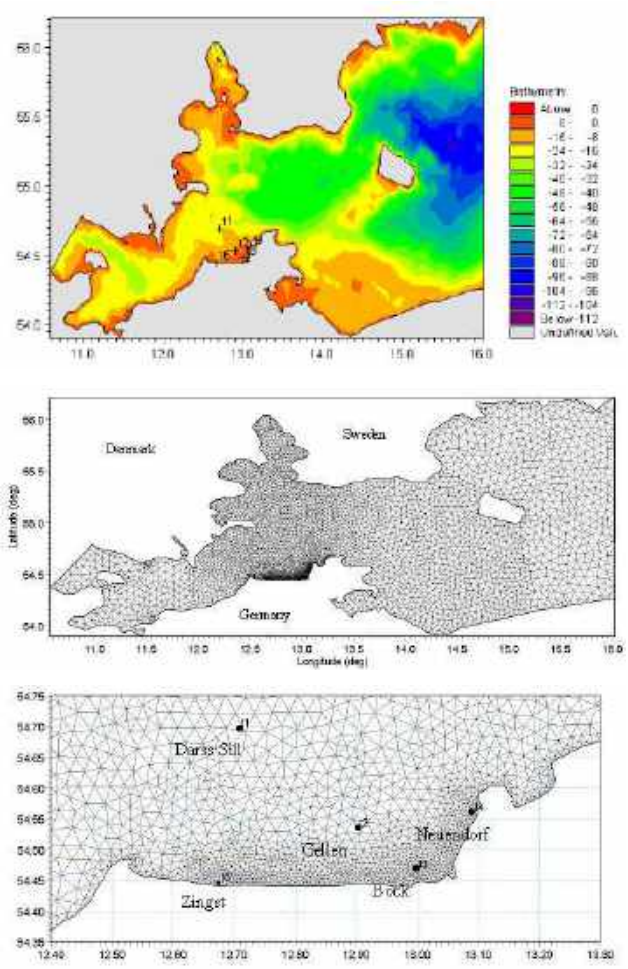

A MIKE 21 SW hindcast application in the Baltic Sea. The upper chart shows the bathymetry and the middle and lower charts show the computational mesh. The lower chart indicates the location of the measurement stations

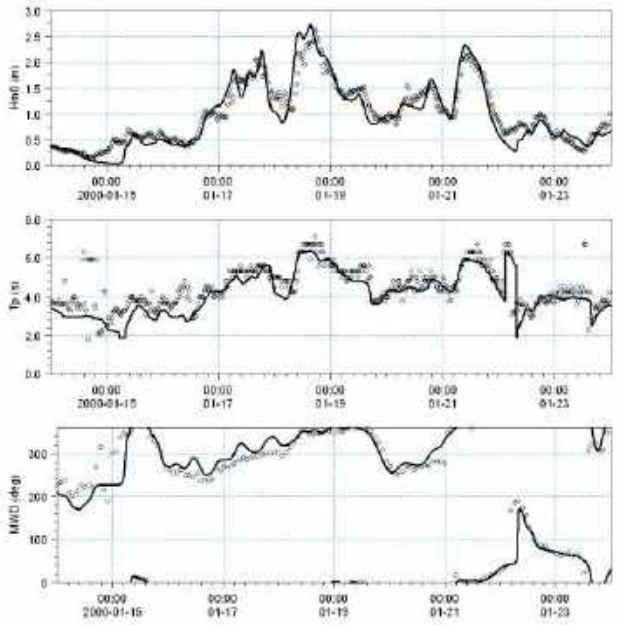

Time series of significant wave height, H_{m0}, peak wave period, T_p , and mean wave direction, MWD, at Darss sill (Offshore, depth 20.5 m). (——) Calculation and (o) measurements. The RMS value on H_{m0} is approximately 0.2 m

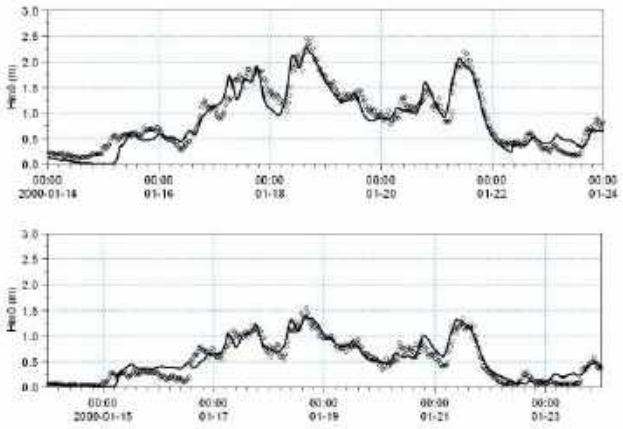

Time series of significant wave height, H_{m0}, at Gellen (upper, depth 8.3m) and Bock (lower, depth 5.5 m). (——) Calculation and (o) measurements. The RMS value on H_{m0} is approximately 0.15 m

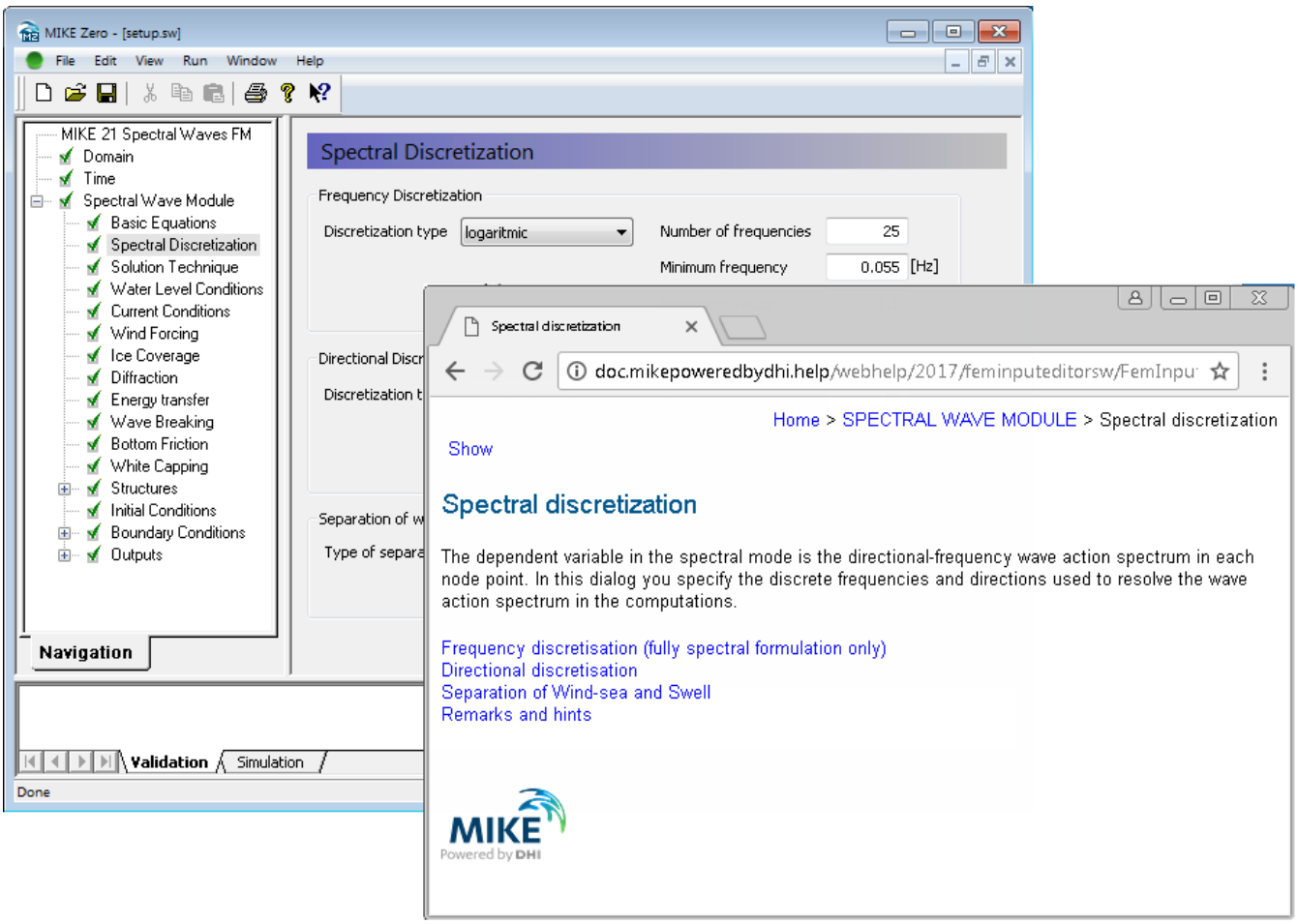

Graphical user interface of MIKE 21 SW, including an example of the Online Help System

Graphical User Interface

MIKE 21 SW is operated through a fully Windows integrated Graphical User Interface (GUI). Support is provided at each stage by an Online Help System.

The common MIKE Zero shell provides entries for common data file editors, plotting facilities and a toolbox for/utilities as the Mesh Generator and Data Viewer.

FEMA approval of the MIKE 21 package

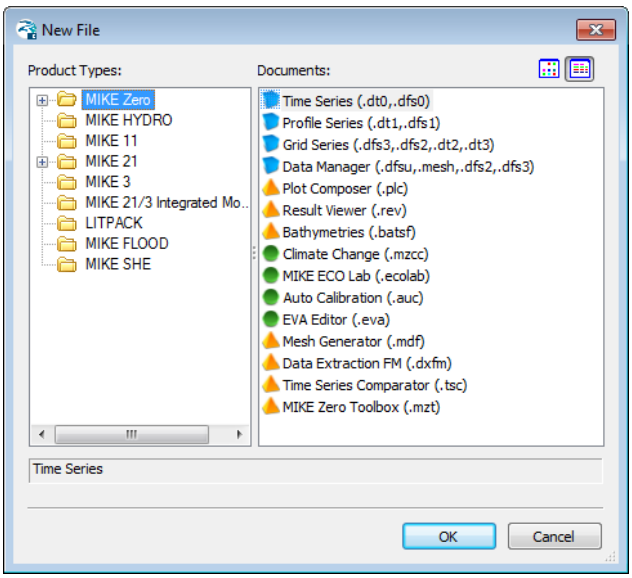

Overview of the common MIKE Zero utilities

Parallelisation

The computational engines of the MIKE 21/3 FM series are available in versions that have been parallelised using both shared memory as well as distributed memory architecture. The latter approach allows for domain decomposition. The result is much faster simulations on systems with many cores.

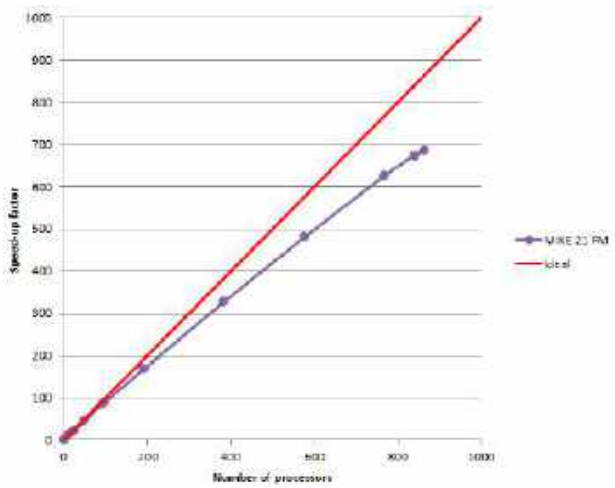

Example of MIKE 21 HD FM speed-up using a HPC Cluster with distributed memory architecture (purple)

Hardware and Operating System Requirements

The MIKE Zero Modules support Microsoft Windows 7 Professional Service Pack 1 (64 bit), Windows 10 Pro (64 bit), Windows Server 2012 R2 Standard (64 bit) and Windows Server 2016 Standard (64 bit).

Microsoft Internet Explorer 9.0 (or higher) is required for network license management. An internet browser is also required for accessing the web-based documentation and online help.

The recommended minimum hardware requirements for executing the MIKE Zero modules are:

Processor:	3 GHz PC (or higher)
Memory (RAM):	2 GB (or higher)
Hard disk:	40 GB (or higher)
Monitor:	SVGA, resolution 1024x768
Graphics card: (GUI and visualisation)	64 MB RAM (256 MB RAM or higher is recommended)

Support

News about new features, applications, papers, updates, patches, etc. are available here:

www.mikepoweredbydhi.com/Download/DocumentsAndTools.aspx

For further information on MIKE 21 SW, please contact your local DHI office or the support centre:

MIKE Powered by DHI Client Care
Agern Allé 5
DK-2970 Hørsholm
Denmark

Tel: +45 4516 9333
Fax: +45 4516 9292

mike@dhigroup.com
www.mikepoweredbydhi.com

Documentation

The MIKE 21 & MIKE 3 FM models are provided with comprehensive user guides, online help, scientific documentation, application examples and step-by-step training examples.

References

Sørensen, O. R., Kofoed-Hansen, H., Rugbjerg, M. and Sørensen, L.S., (2004): A Third Generation Spectral Wave Model Using an Unstructured Finite Volume Technique. In Proceedings of the 29th International Conference of Coastal Engineering, 19-24 September 2004, Lisbon, Portugal.

Johnson, H.K., and Kofoed-Hansen, H., (2000). Influence of bottom friction on sea surface roughness and its impact on shallow water wind wave modelling. *J. Phys. Oceanog.,* **30,** 1743-1756.

Johnson, H.K., Vested, H.J., Hersbach, H. Højstrup, J. and Larsen, S.E., (1999). On the coupling between wind and waves in the WAM model. *J. Atmos. Oceanic Technol.,* **16,** 1780-1790.

Johnson, H.K. (1998). On modeling wind-waves in shallow and fetch limited areas using the method of Holthuijsen, Booij and Herbers. *J. Coastal Research,* **14**, 3, 917-932.

Young, I.R., (1999). Wind generated ocean waves, in Elsevier Ocean Engineering Book Series, Volume 2, Eds. R. Bhattacharyya and M.E. McCormick, Elsevier.

Komen, G.J., Cavaleri, L., Doneland, M., Hasselmann, K., Hasselmann S. and Janssen, P.A.E.M., (1994). Dynamics and modelling of ocean waves. Cambridge University Press, UK, 560 pp.

Holthuijsen, L.H, Booij, N. and Herbers, T.H.C. (1989). A prediction model for stationary, short-crested waves in shallow water with ambient currents, *Coastal Engr*., **13**, 23-54.

References on Applications

Kofoed-Hansen, H., Johnson, H.K., Højstrup, J. and Lange, B., (1998). Wind-wave modelling in waters with restricted fetches. In: Proc of 5th International Workshop on Wave Hindcasting and Forecasting, 27-30 January 1998, Melbourne, FL, USA, pp. 113-127.

Kofoed-Hansen, H, Johnson, H.K., Astrup, P. and Larsen, J., (2001). Prediction of waves and sea surface roughness in restricted coastal waters. In: Proc of 27th International Conference of Coastal Engineering, pp.1169-1182.

Al-Mashouk, M.A., Kerper, D.R. and Jacobsen, V., (1998). Red Sea Hindcast study: Development of a sea state design database for the Red Sea.. *J Saudi Aramco Technology*, **1**, 10 pp.

Rugbjerg, M., Nielsen, K., Christensen, J.H. and Jacobsen, V., (2001). Wave energy in the Danish part of the North Sea. In: Proc of 4th European Wave Energy Conference, 8 pp.

APPENDIX E
MWM model description

MWM: Mediterranean Wind Wave Model

General description of the models' chain

The models and datasets used for the development of the MWM database are:

- the *CFSR* (*Climate Forecast System Reanalysis*) global re-analysis dataset, produced and freely published by NCEP (*National Centers for Environmental Prediction*) (Saha et al, 2010; http://rda.ucar.edu/datasets/ds093.0/index.html#description), hourly (re-forecast) data with a space resolution of 0.5°; these data are used as initial (IC) and boundary conditions (BC) of the *WRF-ARW model* (below);

- the atmospheric model *WRF-ARW – version 3.4.1* (*Weather Research and Forecast - Advanced Research WRF*), model developed by NCAR (*National Center for Atmospheric Research*) (Skamarock and Klemp, 2007; Michalakes et al, 2001; Michalakes et al, 2005); *WRF-ARW* is presently considered among the best state-of-the-art non-hydrostatic meteorological models; it is supported by a massive worldwide community that contributes to its local use and development (http://www.mmm.ucar.edu/wrf/OnLineTutorial/index.htm; http://www.wrf-model.org/index.php);

- the wave model MIKE 21 Spectral Waves (SW) developed by DHI (former Danish Hydraulic Institute) (Sorensen, O.R., Kofoed-Hansen, H., Rugbjerg, M. and Sorensen, L.S., 2004). MIKE 21 SW is among the state of the art wave models, widely used in thousands of offshore and coastal applications worldwide.

In the following a description of the CFSR dataset, the WRF-ARW and the MIKE 21 SW model is given, with specific interest to the implementation adopted in MWM.

CFSR Dataset

The CFSR dataset (Fig. A.1) is the result of a long and complex process performed by NCEP, an ensemble of nine weather prediction centers in the United States belonging to the NWS (*National Weather Service*) of the NOAA (*National Oceanic and Atmospheric Administration*). The simulation, completed in 2011, is based on a global atmospheric numerical model including atmosphere-ocean and sea-ice couplings, with a systematic ingestion of both conventional (point) and satellite observations with data assimilation procedures.

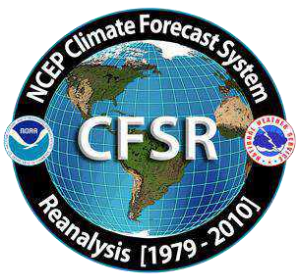

Figure A.1

The CFSR now covers a 35-year period from 1979 to 2013 (included) and is continuously updated with new recent data. The simulations were performed as 9 hours forecast simulations, initialized 4 times a day (at 00:00, 06:00, 12:00 and 18:00) between the 6-hourly re-analysis frames. The

results of these simulations, gathered in the CFSR dataset, consist in complete atmospheric data over ocean and lands with a one hour time resolution and a 0.5° horizontal resolution, while the vertical resolution changes greatly amongst the atmospheric variables, spanning from the single surface value up to values at 64 different isobaric levels.

MWM dataset ingest the 6-hourly CFSR data, specifically the *ds093.0* dataset.

Chawla et al (2013) presented a thorough analysis of the *CFSR* dataset against satellite and oceanic buoys data. The final goal of that study is the use of the U_{10} wind data from the *CFSR* dataset as the forcing term of *WWIII* to generate wave fields at global scale, without any assimilation of wave data. The analysis of the *CFSR* dataset shown in that paper includes the intrinsic performance of the model in terms of the seasonal and annual variability of the percentiles. A moving average is applied to smooth the altimeter data from the satellites and from the buoys. The normalized percentiles ("...normalized with the wind speeds at corresponding percentiles from the altimeters") computed over the satellite tracks exhibit an oscillatory behavior, never below 0.93 or 0.90 in the Northern and Southern hemisphere respectively. From that analysis, the wind and wave *CFSR* and *WWIII* data compare very well with satellite data in terms of normalized percentiles. The Q-Q plots at selected offshore buoys are generally good or very good, with some unexpected variations from case to case for some buoys close to the coast, with even a contradictory behavior between U_{10} and H_s in some locations.

The analysis of the wind field of the *CFSR* dataset is far beyond the scope of the present work but still some checks have been done in specific cases, like the event of November 1999 in Trieste (Italy). The performance of a local area model is directly related to the information contained in the global model used as boundary and initial conditions; Fig. A.2 after Contento et al (2014) shows the wind speed for the case of November 1999 in Trieste (Northern Adriatic Sea - Italy); the red dots are experimental data by NOAA (http://gis.ncdc.noaa.gov/map/viewer/#app=cdo&cfg=cdo&theme=hourly&layers=1&node=gis); the yellow line corresponds to the re-analysis data *CFSR d093.0* (Saha et al, 2010; http://rda.ucar.edu/datasets/ds093.0/index.html#description) interpolated at the same position of the station; the blue dots are related to a fully certified and verified measurement station of the Regional Agency for the Environment Protection (ARPA FVG-OSMER, http://www.osmer.fvg.it/home.php) located few meters far from the station used by NOAA (http://gis.ncdc.noaa.gov/map/viewer/#app=cdo&cfg=cdo&theme=hourly&layers=1&node=gis); the cyan line corresponds to the present hindcast dataset (model *WRF-ARW*). It is rather evident that the CFSR dataset ingests the experimental data from NOAA but there are some non-negligible discrepancies between the two experimental datasets (private communication with ARPA FVG-OSMER - Regional Agency for the Environment Protection – Friuli Venezia Giulia Region, Italy). In this case the local model *WRF-ARW* is able to develop the local wind field and matches correctly the measurement by ARPA, irrespective of the wrong assimilated data as BC and IC; this, however, cannot be always guaranteed.

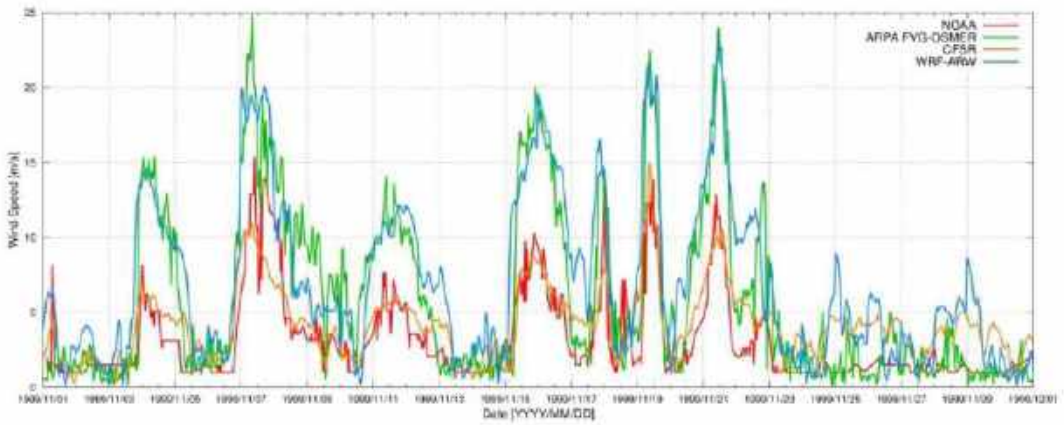

Figure A.2 Comparison between measured wind speed at two ground neighbor (few meters from each other) stations in Trieste (Italy - Northern Adriatic Sea) from the database of NOAA

(http://gis.ncdc.noaa.gov/map/viewer/#app=cdo&cfg=cdo&theme=hourly&layers=1&node=gis) (red line) and from ARPA-FVG OSMER (http://www.osmer.fvg.it/home.php) (blue line). Model data from *CFSR* (Saha et al, 2010) (yellow line) and the present simulations with *WRF-ARW* (cyan line) are overlapped.

The scope of these checks was solely to verify the sensitivity of the *CFSR* wind pattern to a complex steep geographic area facing the sea. The eastern coast of the Adriatic Sea is just an example among many others. The availability of certified wind data from the local Regional Agency for the Environment Protection – Friuli Venezia Giulia (ARPA FVG-OSMER, http://www.osmer.fvg.it/home.php) related to ground stations and to a fixed station in the middle of the Gulf of Trieste (Northern Adriatic Sea *http://www.ts.ismar.cnr.it/node/84*]), helped a lot in defining the set-up of the local area meteorological model. The aim of the set-up process was to let the model *WRF-ARW* develop mesoscale and local weather structures, thus using a domain large enough to develop these structures, but at the same time avoiding the use of too large a domain that may lead to a model drift from the experimental data. These undesired effects were observed along the entire Adriatic Sea, specifically on the eastern side (Contento et al, 2011; Contento et al, 2014).

WRF-ARW meteorological model

The WRF model is an open source mesoscale to microscale atmospheric model developed by the American atmospheric research center NCAR in cooperation with many other meteorological institutions. It is largely used worldwide for both atmospheric research and forecast or hindcast purposes due to its ability to perform atmospheric simulations over a wide range of length scales spanning from less then 1 kilometer to thousands of kilometers. This flexibility is further increased by its capability of performing two way coupled nested runs.

The WRF modelling system includes a pre-processor system (WPS), a data assimilation system (WRF-DA) and the dynamic solver. During this work the ARW dynamic solver, developed and maintained by the Mesoscale and Microscale Meteorology Division of NCAR, has been used. The ARW dynamic core is a fully compressible and non-hydrostatic model, based on a terrain-following hydrostatic pressure vertical coordinate system and on an Arakawa C-grid staggered evaluation of the vector quantities. The solver uses high order time integration and 3-D advection schemes.

The WRF model works internally with NetCDF files, a self-describing and machine-independent data format particularly suitable for the manipulation of long arrays of scientific data.

A WRF-ARW model run is a quite complex process, since it involves several different steps to be run in a precise order. First of all, WRF requires boundary and initial conditions; these conditions can be supplied by the GRIB files obtained from the CFSR dataset files described in CISL RDA: NCEP Climate Forecast System Re-analysis (CFSR) 6-hourly Products, January 1979 to December 2010." [Online] Available at http://rda.ucar.edu/datasets/ds093.0/index.html#description

GRIB files needed to cover completely the whole simulated period must be fed to the model to complete the simulation process successfully.

Moreover, since the atmosphere behaviour is strongly dependent on the soil characteristics, detailed data about these characteristics must be fed to the model too in order to let it develop the local weather phenomena correctly. However, there is no need to produce this type of data since suitable 30'' resolved geographic data are included in the default WRF pre-processing (WPS). Since these data are time-independent they need to be downloaded only once, and they remain valid for every simulation unlike the GRIB files. Actually, some of the parameters contained in the geographic data cannot be considered as completely time-independent; in fact, some of the parameters show a time dependence which, however, is limited to seasonal changes, e.g. the

reduced vegetation cover in winter. The possible seasonal variability of the geographical parameters is included in the geographical data archive of WPS.

A complete WRF-ARW simulation needs the WPS (*WRF Pre-processor System*) to be run before the numerical solver (*wrf.exe*). The WPS pre-processor system deals with both the domain set-up and the preliminary input manipulations; it is composed by three main executables carrying out different tasks:

- *geogrid.exe* is responsible for the definition of the horizontal grid as well as for the interpolation of the geographic data on the user-defined grid. When performing nested runs, the *geogrid.exe* run produces a NetCDF file *geo_em.dxx.nc* containing the grid and geographic data for each domain, where xx stands for the code of the domain (01, 02, …).

- *ungrib.exe* is responsible for the decoding of the input GRIB files used as initial and boundary conditions. The GRIB files, which need to be linked to the work directory of WPS by means of the script *link_grib.csh*, are "ungribbed" and rewritten in an intermediate format suitable for further manipulations, excluding all the fields not needed for the following model run.

- *metgrid.exe* is responsible for the horizontal interpolation of the intermediate input files produced by ungrib.exe on the grid defined by geogrid.exe. Moreover, the geographic data contained in the *geo_em* files are ingested by metgrid and written on its output files. The output of metgrid.exe is in fact composed by the NetCDF files *met_em.dxx.YYYY-MM-DD_HH:00:00.nc*, each containing the interpolated boundary conditions and geographic data for the xx domain and for every timestep of the supplied GRIB files. In the case considered, as the CFSR dataset is composed of hourly data, the produced *met_em* files are hourly spaced too.

The whole WPS process is controlled by a single external configuration file: *namelist.wps*, which contains the user specified parameters defining the time length and the domain of the simulation as well as the time and space resolutions.

An additional manipulation is needed before launching the actual solver: the NetCDF data produced by metgrid.exe must be vertically interpolated onto the user- defined vertical levels of the WRF simulation. This task is performed by the *real.exe* executable, which, despite actually being a pre-processing routine, is not included in the WPS system. The real.exe run finally produces the NetCDF files needed by the bare solver: *wrfinput_dxx* and *wrfbdy_dxx*, containing respectively, for each of the nested domains under simulation, the initial condition inclusive of the domain geographic data and the boundary conditions forcing the domain over time.

The last step of a WRF-ARW model simulation is the *wrf.exe* solver run which performs the numerical integration and produces the final output files *wrfout_dxx_YYYY-MM-DD_HH:MN:SS,* one for each simulated domain and for every temporal frame in the total simulated period. Each wrfout file contains therefore the complete atmospheric variables set calculated by the ARW solver for every point of the user defined simulation 3-D grid at a single temporal frame.

Both real.exe and wrf.exe are controlled by *namelist.input*, an external configuration file gathering the user defined parameters regarding the vertical resolution of the simulation, the atmosphere microphysical parameters and, again, the time / length scales and resolutions of the simulation.

A script that makes all steps involved automatic in a WRF-ARW simulation procedure, from the set-up of the configuration files to the archiving of output files, was developed and tested extensively.

The above depicted working scheme is summarized in Figure A.3:

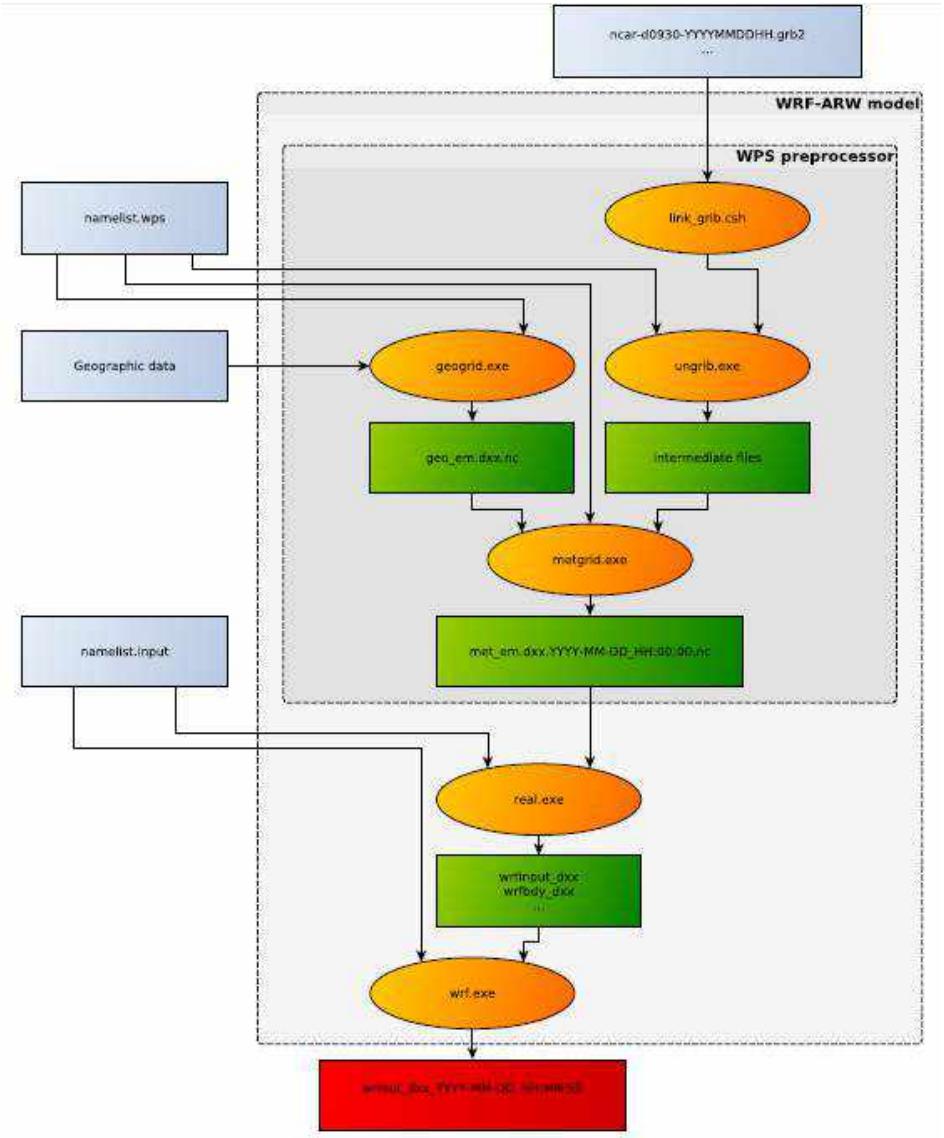

Figure A.3 Working scheme of the WRF-ARW model.

WRF-ARW domains, resolution, set-up in MWM

The preliminary set-up and tuning of the met-ocean models chain was performed simulating the month of November 1999, chosen for the remarkable number of very intense storms occurred over the Mediterranean Sea. The second step, before running the entire period 1979-2013, was done simulating one complete year, from November 1999 to October 2000, relying on 41 ground stations along the Mediterranean coast and 25 wave buoys for comparison. The results obtained in these steps are summarized in Contento et al. (2014), Contento et al. (2012-2014) and Donatini (2013).

The two-steps set-up started with the meteorological model *WRF-ARW*, adopting different configurations (domain size, resolution, run length, spin-up time) and comparing the wind speed and direction with observational data from ground stations. Since the *CFSR* (Saha et al, 2010) re-analysis dataset reproduces large scale events correctly, after several tests the final decision was to adopt three relatively small, overlapping domains, which cover respectively the Western, Eastern and Central Mediterranean Sea (Fig. A.4). Hereafter these domains will be referred as MEW, MEE and MEC respectively. The wind field obtained from the 3 domains was merged in a

single dataset by a bi-linear interpolation on a Lat-Lon grid and by a linear blending of the results inside the two overlapping zones (Fig. A.4).

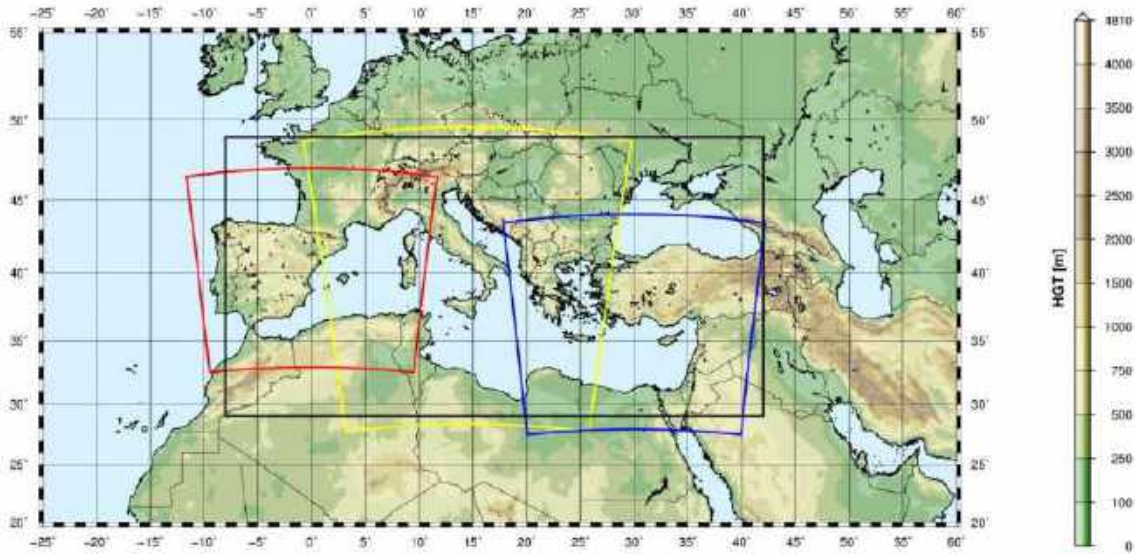

Figure A.4 WRF-ARW domains (red=domain MEW, yellow=domain MEC, blue=domain MEE) and interpolation/blending domain (black line).

The horizontal resolution of *WRF-ARW* was set to 10.53 km, with a grid ratio to the *CFSR* re-analysis data of 1:5 approximately. An additional domain (ITN) with a resolution of 3.51 km was run over Northern Italy as a nested domain of MEC.

The time length of the model run, in terms of hours simulated continuously between two consecutive model initializations with *CFSR* frames,proved to be among the most important parameters that influence the quality of the results. Keeping a small run length reduces the risk of model drift. On the other hand, shortening it excessively may lead to a too constrained behavior of the model, which prevents the correct development of the mesoscale weather structures. The problem of the model drift proved to be particularly tough over the Adriatic Sea where the orography is rather complex and the North-Eastern wind (Bora) can occasionally reach the speed of 150 km/h or more in very narrow zones.

A spin-up time window was used in order to let the model *WRF-ARW* ingest and process the coarser initial conditions from *CFSR*, thus letting it evolve and develop local weather structures. This spin-up window was overlapped with the tail of the previous run so that the data of the simulation during the spin-up window were discarded. The time length of this overlapping window is typically of few hours.

The Mediterranean Sea is a very complex basin from the meteorological point of view, with violent storms usually characterized by a short duration. The two examples given below show the importance of resolving the large space and time gradients of the variables.

Fig. A.5 shows a typical winter wind pattern (from the present simulations, 5 December 2009). The well-known 3 major narrow gates of the “Bora” wind over the Adriatic Sea are well captured by the model, i.e. Trieste (Italy), Rijeka and Sibenik (Croatia). The reference distance of these large variations is of 1° at most.

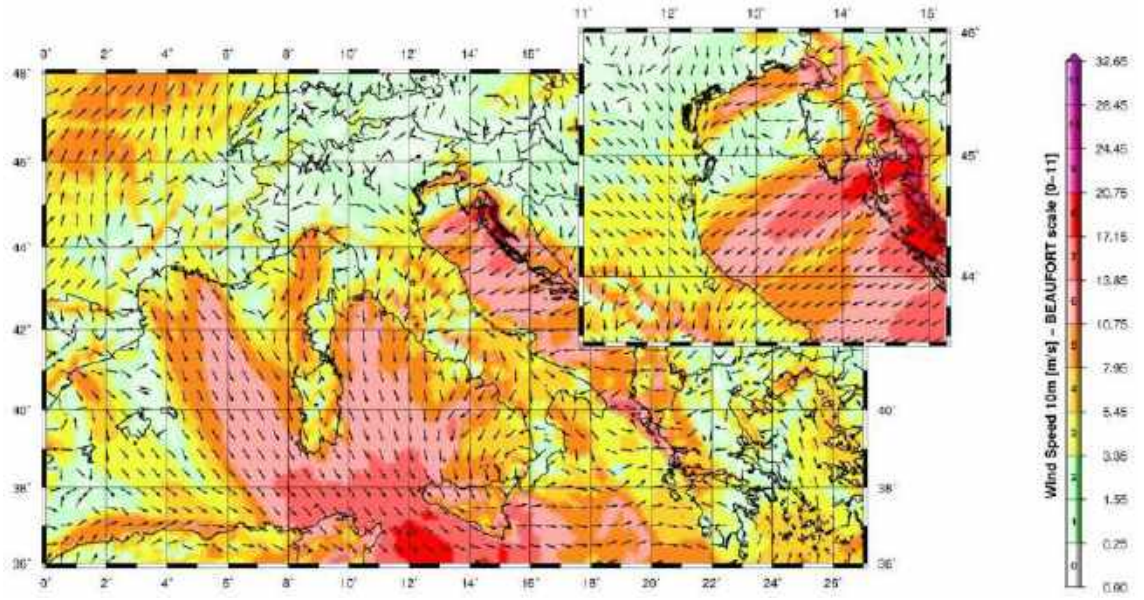

Figure A.5 A typical winter wind pattern over the Mediterranean Sea (from the present simulations, 5 December 2009). The well-known 3 major narrow gates of the "Bora" wind over the Adriatic Sea are well captured by the model, i.e. Trieste (Italy), Rijeka and Sibenik (Croatia). The upper-right figure shows a zoom over the Northern part of the Adriatic Sea (Istria peninsula).

Fig. A.6 (Contento et al., 2011) shows the time series of the wind speed during a squall event occurred on August 2008 in the Gulf of Trieste that caused the loss of two human lives and damages in the main harbor. The squall lasted about 10 min reaching more than 20 m/s from an almost calm situation. The red line corresponds to the results of the operational forecast meteorological model *WRF-ARW* run at that time by some of the authors of this work for ARPA FVG-OSMER, http://www.osmer.fvg.it/home.php. The black line corresponds to the measurement at the station PALOMA (45° 37' 06" N, 13° 33' 55" E) [*http://www.ts.ismar.cnr.it/node/84*]. The station is a fixed pole in the middle of the Gulf of Trieste. The measured wind speed is 5 min averaged with 5 min samples. The time step of the model is approximately 13 s. This situation is not uncommon in the Adriatic zone, mostly during the summer, with violent fronts from North and North-West then rotating to North-East.

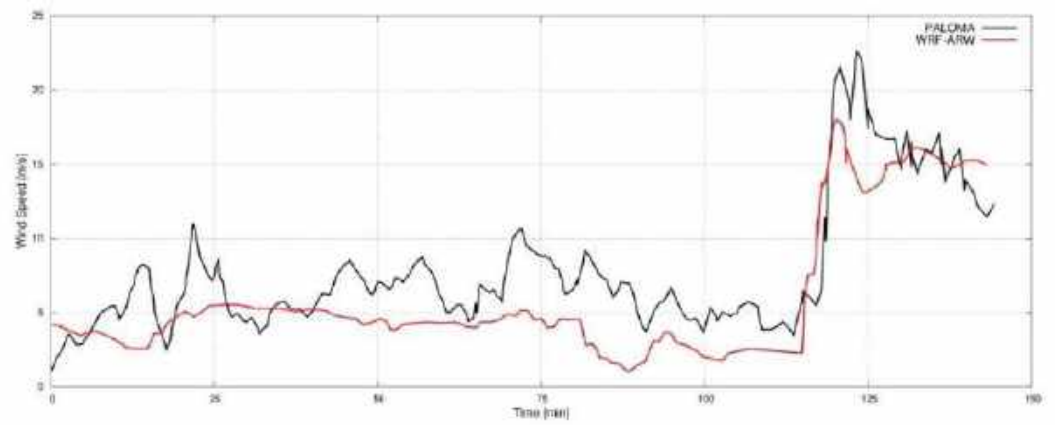

Figure A.6 Time series of the wind speed during a squall event occurred on August 2008 in the Gulf of Trieste. The squall lasts about 10 min reaching over 20 m/s from an almost calm situation. The red line corresponds to the results of the operational forecast meteorological model *WRF-ARW*. The black line corresponds to the measurement at the measurements station PALOMA (45° 37' 06" N, 13° 33' 55" E) [*http://www.ts.ismar.cnr.it/node/84*]. The measured wind speed is 5 min averaged with 5 min samples. The time step of the model is approximately 13 s.

MIKE 21 SW wave model

The wave modeling system includes the state of the art third generation spectral wind-wave model MIKE 21 SW, developed by DHI. MIKE 21 SW simulates the growth, decay and transformation of wind-generated waves and swell in offshore and coastal areas.

MIKE 21 SW includes two different formulations:

- Directional decoupled parametric formulation
- Fully spectral formulation

and includes the following physical phenomena:

- Wave growth by action of wind
- Non-linear wave-wave interaction
- Dissipation due to white-capping
- Dissipation due to bottom friction
- Dissipation due to depth-induced wave breaking
- Refraction and shoaling due to depth variations
- Wave-current interaction
- Effect of time-varying water depth

The discretization of the governing equation in geographical and spectral space is performed using cell-centered finite volume method. In the geographical domain, an unstructured mesh technique is used. The time integration is performed using a fractional step approach where a multisequence explicit method is applied for the propagation of wave action.

For the production of the MWM database, the fully spectral formulation has been adopted, based on the wave action conservation equation, as described in e.g. Komen et al. and Young where the directional-frequency wave action spectrum is the dependent variable.

The time integration of the governing equations is done by using a dynamically determined time step. The time step is determined in order to verify the stability criteria (CFL number).

The only driving force is represented by the two components of wind fields U10 and V10, (x and y component of wind at the elevation of 10m). The process by which the wind transfers energy into the water body for generating waves is controlled by a uncoupled air-sea interaction.

The spectral discretization adopted in the wave model has been deeply investigated and the final configuration is able to guarantee at the same time a high level of accuracy of the results and a reasonable computational effort.

The model domain covers the whole Mediterranean Sea but the spatial resolution is not the same everywhere: while in the offshore areas the spatial resolution is around 0.1°, when approaching the coast the spatial resolution increases up to around 0.03°.

The wave model is forced by the wind fields coming from the WRF Atmospheric models, illustrated above. The wave model generated results in terms of wave parameters (Significant Wave Height, Wave Periods, Wave Directions, etc.) over the whole domain and, in addition, spectral parameters in predefined output locations have been stored, too.

MIKE 21 SW domain, resolution, set-up in MWM

The model domain, covering the entire Mediterranean Sea, is illustrated in Figure A.7.

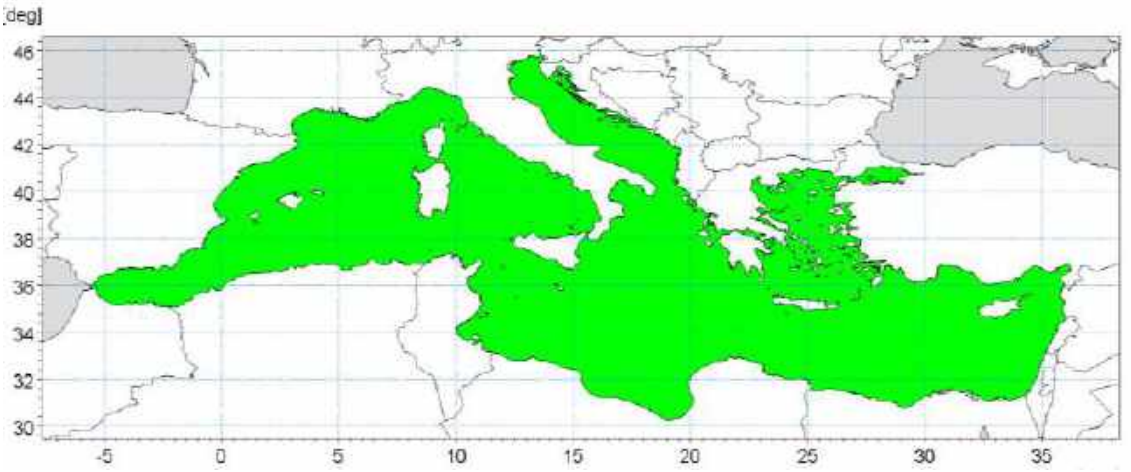

Figure A.7 Wave model domain filled in green

The unstructured mesh, generated over the entire domain by means of a specific tool included in MIKE 21 package, is characterized by different resolutions (in terms of mean length of triangle sides) over the domain. In particular the following criteria have been adopted:

- a coarser resolution of 0.1° (about 10 Km) is used for offshore areas;
- a finer resolution of 0.03° (about 3 Km) has been adopted in shallow water areas, where bathymetry is less than 100m depth or, in coastal areas characterized by very steep profiles, where the distance from the coastline is less than 5÷10 Km.

Figure A.8 illustrates the computational mesh of the Mediterranean wave model.

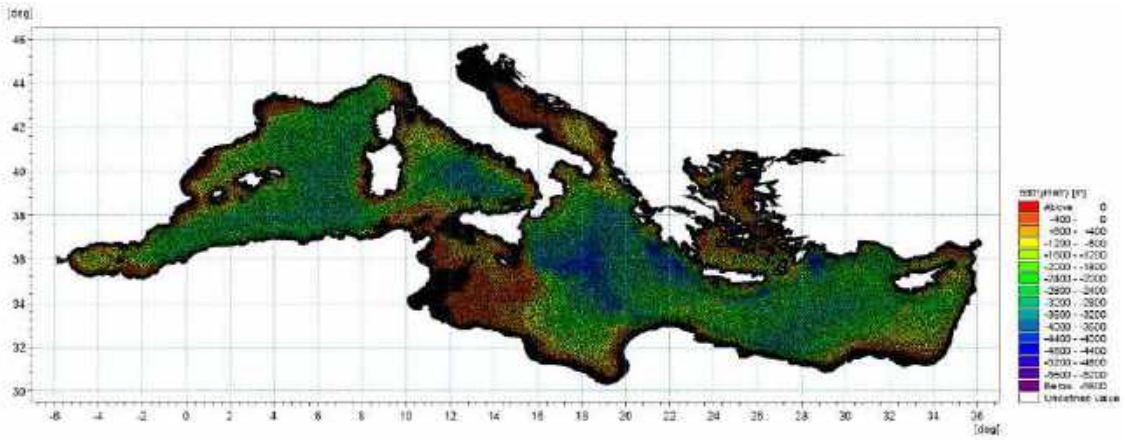

Figure A.8 - Mediterranean wave model computational mesh

Figure A.9 illustrates a detail of the above computational mesh, with special focus on the Adriatic Sea.

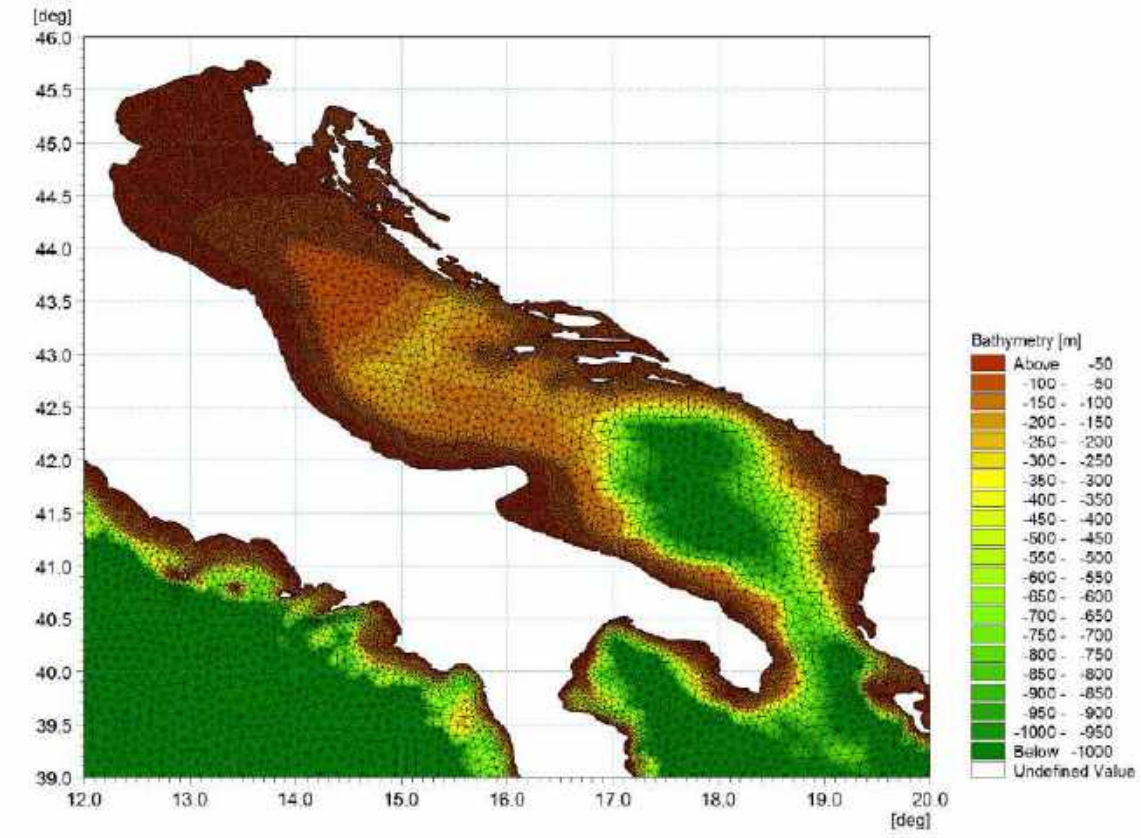

Figure A.9 - Detail of the mesh – Adriatic Sea

Scatter bathymetry data have been derived from GEBCO_08 database. The GEBCO_08 Grid is a 30 arc-second grid of global elevations and it is a continuous terrain model for ocean and land. The grid was generated by combining quality-controlled ship depth soundings with interpolation between sounding points guided by satellite-derived gravity data.

The gridded data are stored in a netCDF data file. Grids are stored as one dimensional arrays of 2-byte signed integer values. The complete data sets provide global coverage. Each data set consists of 21,600 rows x 43,200 columns, resulting in a total of 933,120,000 data points. The data start at the Northwest corner of the file, i.e. for the global file, position 89°59'45"N, 179°59'45"W, and are arranged in latitudinal bands of 360 degrees x 120 points/degree = 43,200 values. The data range eastward from 179°59'45"W to 179°59'45"E. Thus, the first band contains 43,200 values for 89°59'45"N, then followed by a band of 43,200 values at 89°59'15"N and so on at 30 arc-second latitude intervals down to 89°59'45"S. Data values are pixel centred registered, they refer to elevations at the centre of grid cells.

Figure A.10 illustrates GEBCO_08 scatter data for the entire area of the Mediterranean Sea.

GEBCO scatter data have not been used in the whole domain of the Mediterranean Sea. Following a detailed check of agreement and discrepancies between GEBCO database and nautical charts, it has been assumed to limit the use of GEBCO database for offshore areas (up to 500 m water depth) and to use nautical charts for shallower water areas (mainly coastal areas).

The nautical charts database which has been used is the CM93/3 database from CMAP.

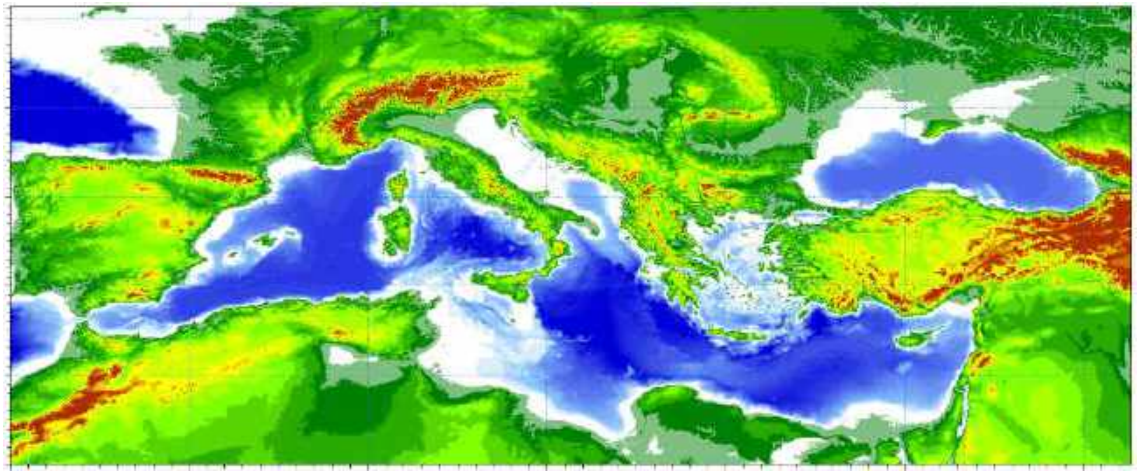

Figure A.10 - Scatter bathymetry data derived from GEBCO_08 database

The number of discrete frequencies and directions form the so called “spectral resolution”, which is a key parameter for wave models in general. The number of discrete frequencies and directions should in fact be high enough to properly represent the “real shape” of the wave spectrum and, on the other hand, it can’t be too high, since it would lead to unacceptable computational times and memory consumption.

In terms of frequency range, the minimum frequency f_{min} (which corresponds to the maximum wave period T_{max}, according to the common relation $= \frac{1}{T}$) should be able to capture the longest wave periods that can occur in the Mediterranean Sea.

The analysis of ordinary and extreme waves in the Mediterranean Sea (from available data of wave buoys) has highlighted that almost all the wave energy associated to waves in the Mediterranean Sea are associated to wave periods between 1.5 seconds and 20 seconds.

In addition, a logarithmic distribution for the discrete frequencies acts better than a simple linear distribution, since most of the wave periods are concentrated below 8-10 seconds. A number of frequencies around 30 is widely considered as adequate for a proper discretization of wave energy spectra in the Mediterranean Sea. The following formulation has therefore been adopted:

$$f_{n=}0.04 \cdot \ 1.1^{n},$$

where n goes from 0 to 29 (30 frequencies in total). The discrete frequencies range from 0.04 Hz to 0.63 Hz (from 1.6s to 25.0s of Mean Wave Period T_m).

Also the choice of the number of discrete directions (directional discretization) is the result of detailed investigations and tests. In particular, a high number of wave model tests, each one characterized by a different spectral resolution (directional), i.e. by a different number of discrete directions have been setup and run.

Few examples of the results of the above model tests are illustrated from Figure A.11 to Figure A.13 in terms of short time series of wave heights extracted at 3 different locations where also measurements were available (La Spezia wave buoy, Ponza wave buoy, Cetraro wave buoy).

In all the below test cases, it appears that the two time series of wave height characterized by 24 and 36 discrete directions are almost coincident. Higher discrepancies can be found for a much limited number of discrete directions (12). After a high number of tests, the 24 directions solution has been assumed as a very good compromise between accuracy of results and computational time (the computational time of the wave model is linearly dependent on the number of discrete directions).

Provided that wave directions can vary within the 360° rose, the directional resolution of the wave model is 360°/24 = 15°

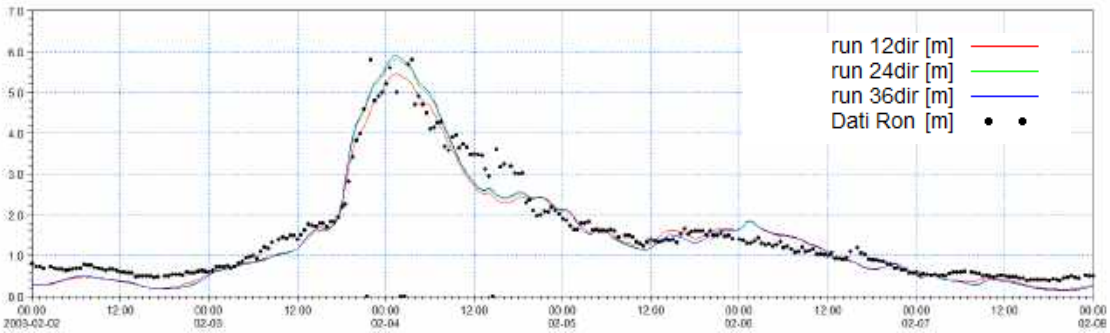

Figure A.11 - Time series of wave height at La Spezia buoy location for 3 different numbers of discrete directions

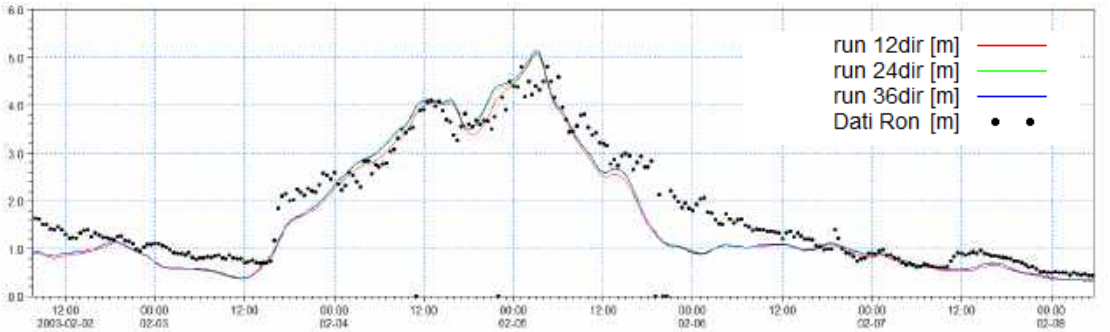

Figure A.12 - Time series of wave height at Ponza buoy location for 3 different numbers of discrete directions

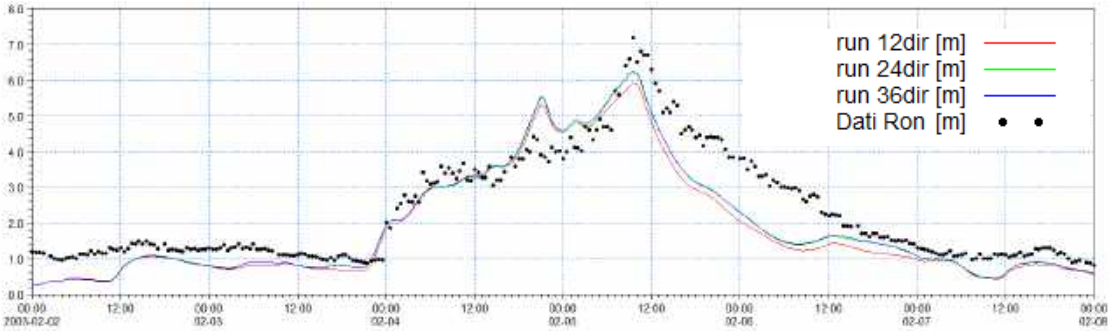

Figure A.13 - Time series of wave height at Cetraro buoy location for 3 different numbers of discrete directions

Available products of the MWM database

The results of the wind and wave model are stored, in the whole domain, in terms of wind parameters and wave parameters averaged over the wave period ("phase averaged results"). In particular, the following hourly time series are available:

- Wind speed, WS [m/s]
- Wind direction, WD [deg]
- Significant Wave height, Hs [m]
- Mean wave period, Tm [s]
- Peak wave period, Tp [s]
- Zero crossing period, Tz [s]
- Mean wave direction, MWD [deg]
- Peak wave direction, PWD [deg]
- Directional standard deviation, DSD [deg]

In addition, hourly spectral results (in terms of wave energy associated to the frequency-direction bins) are saved on a regular grid with an equidistant spatial resolution of 0.1°.

Figure A.14 and Figure A-15 illustrate respectively an example of phase averaged results over a portion of Mediterranean Sea (Hs) and an local example of spectral results.

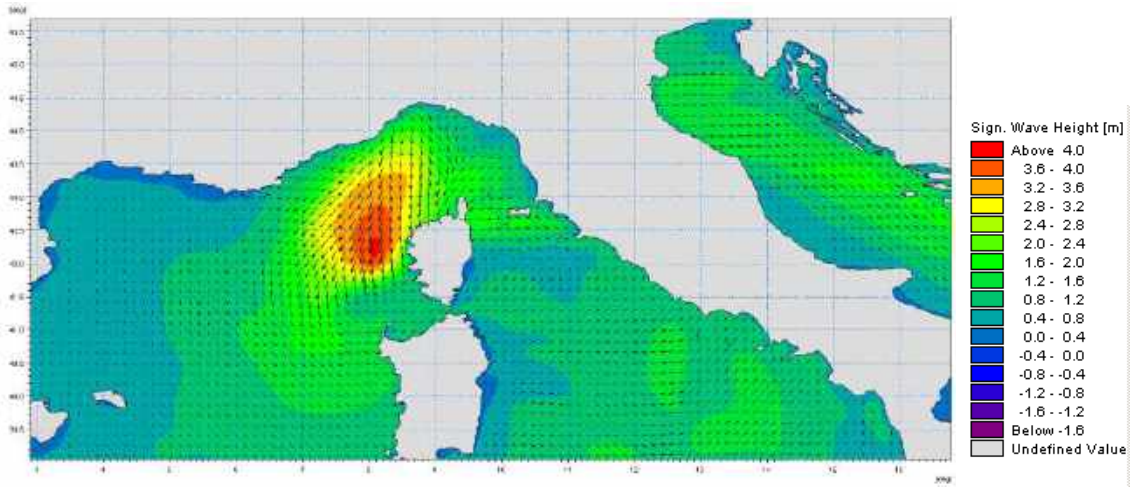

Figure A.14 Phase averaged results: Field of significant wave height and direction

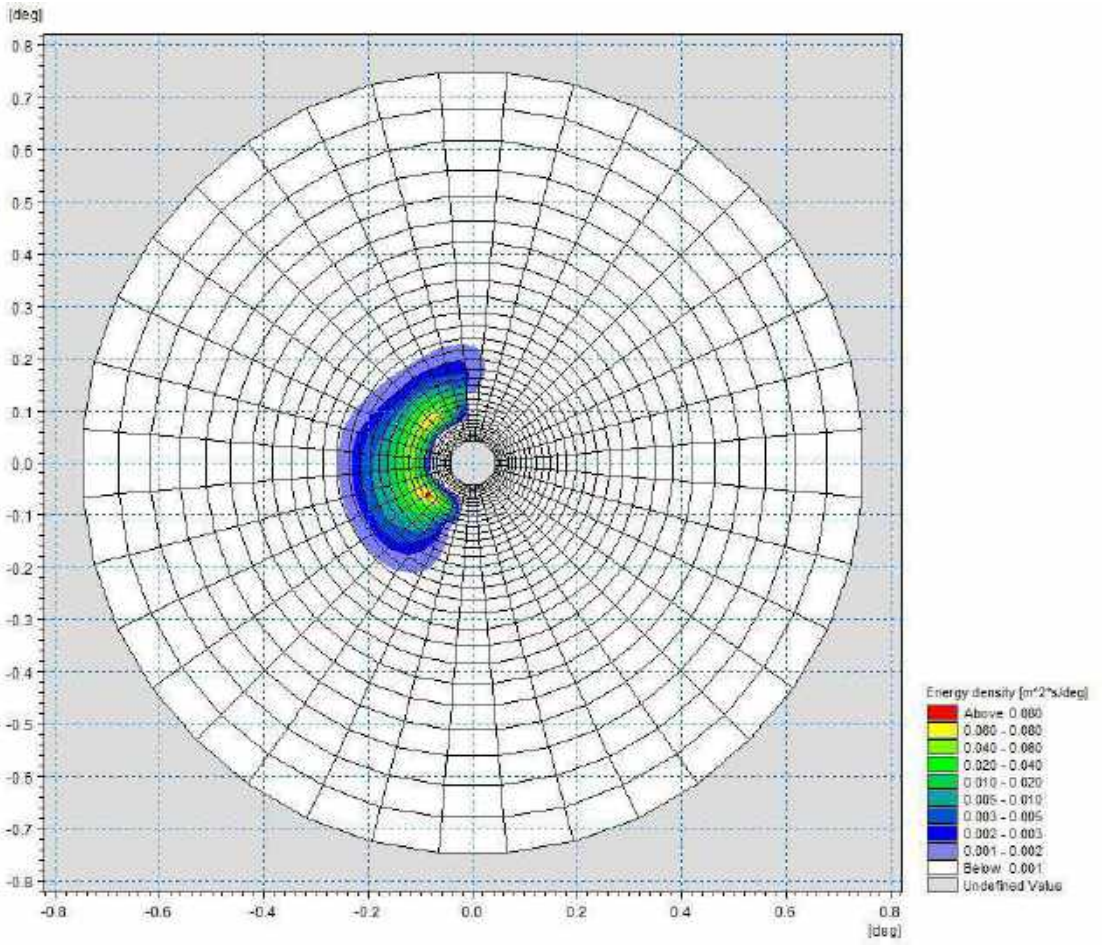

Figure A.15 Polar plot of spectral results. Wave energy density (coloured contours) as a function of directions (angular coordinate) and frequencies (radial coordinate)

References

Ardhuin, F., Bertotti, L., Bidlot, J.R., Cavaleri, L., Filipetto, V., Lefevre, J.M,, Wittmann, P., 2007, Comparison of wind and wave measurements and models in the Western Mediterranean Sea. *Ocean Engineering*, Vol. 34, pp. 526-541.

Athanassoulis, G., Stefanakos, Ch., Cavaleri, L., Ramieri, E., NoEL, C., Lefevre, J.M., Gaillard, P., 2004, RTP 10.10 / WW_MEDATLAS Scientific Report.

Battjes, J.A., Janssen, J.P.F.M., 1978, Energy loss and set-up due to breaking of random waves, Proceedings, 16th Int. Conf. Coastal Eng., ASCE, pp.569-587.

Bolaños-Sanchez, R., Sanchez-Arcilla, A., Cateura, J., 2007, Evaluation of two atmospheric models for wind-.wave modeling in the NW Mediterranean. *Journal of Marine Systems* 65:336-353.

Cavaleri, L., Bertotti, L., 2004, Accuracy of the modelled wind and wave fields in enclosed seas. Tellus, Vol. 56, pp. 167-175.

Cavaleri, L., 2005, The wind and wave atlas of the Mediterranean Sea – the calibration phase. *Advances in Geosciences*, Vol. 2, pp. 255-257.

Cavaleri, L., Sclavo., M., 2006, The calibration of wind and wave model data in the Mediterranean Sea. Coastal Engineering, Vol.53, pp. 613-627.

Chawla, A., Spindler, D.M., Tolman, H.L., 2013, Validation of a thirty year wave hindcast using the Climate Forecast System Reanalysis winds, Ocean Modelling, Vol. 70, pp. 189-206.

Contento, G., Lupieri, G., Venturi, M. Ciuffardi, T., 2011, A medium-resolution wave hindcast study over the Central and Western Mediterranean Sea, *Journal of Marine Science and Technology*, Vol. 16(2), pp. 181–201.

Contento, G., Lupieri, G., Donatini, L, Feudale, L, Pedroncini, A., Cusati, L.A., 2014, A state-of-the-art met-ocean model chain for wind&wave hindcast over the Mediterranean and Black Seas: implementation, tuning and validation against field data, accepted for presentation at the 21th Symposium Theory and Practice of Shipbuilding SORTA 2014, Oct. 2-4, 2014, Baška, Island of Krk, Croatia.

Contento, G., Lupieri, G., Donatini, L, 2012-2014, Project SEAPOL - Sistema modellistico ad Elevata risoluzione per l'Analisi storica e la Previsione del moto Ondoso nel mar Ligure, Department of Engineering and Architecture, University of Trieste, Technical Reports codes SEAPOL_UT_1.1.0 to SEAPOL_UT_5.1.0.

Donatini, L., 2013, Implementation of a state-of-art met-ocean model chain for hindcast wave simulations over the Mediterranean Sea and comparison of results with field data, Master Degree Thesis, Department of Engineering and Architecture, University of Trieste, Italy.

Donatini, L., Lupieri, G., Contento, G., 2014, A medium resolution wind&wave hindcast study for the Mediterranean Sea, Journal Paper, under review.

Hasselmann, K., Barnett, T.P., Bouws, E., Carlson, H., Cartwright, D.E., Enke, K., Ewing, J.A., Gienapp, H., Hasselmann, D.E., Krusemann, P., Meerburg, A., Mueller, P., Olbers, D.J., Richter, K., Sell, W., Walden, H., 1973, Measurements of wind-wave growth and swell decay during the Joint North Sea Wave Project (JONSWAP). Ergaenzungsheft zur Deutschen Hydrographischen Zeitschrift, Reihe, A(8), 12, 95 pp.

Hasselmann, S., Hasselmann, K., Allender, J.H., Barnett, T.P., 1985. Computations and parametrizations of the nonlinear energy transfer in a gravity-wave spectrum, Part II: Parametrizations of the nonlinear energy transfer for applications in wave models. J. Phys. Oceanogr. Vol. 15, pp. 1378–1391.

ISPRA (formerly APAT), 2004, Agenzia per la Protezione dell'Ambiente e per i servizi Tecnici, Dipartimento Tutela Acque Marine ed Interne, Servizio difesa delle coste, Analisi preliminare dei dati marini lungo le coste italiane – Atlante delle coste – Il moto ondoso al largo delle coste italiane, Technical Report (in Italian). http://www.apat.gov.it/site/_files/Atlante_coste/Introduzione.pdf.

Janssen, P.A.E.M., Abdalla, S., Hersbach, H., Bidlot, J.R., 2007: Error Estimation of Buoy, Satellite, and Model Wave Height Data. *J. Atmos. Oceanic Technol.*, Vol. **24**, pp. 1665–1677. doi: http://dx.doi.org/10.1175/JTECH2069.1

Michalakes, J., Chen, S., Dudhia, J., Hart, L., Klemp, J., Middlecoff, J., Skamarock, W., 2001, Development of a Next Generation Regional Weather Research and Forecast Model. *Developments in Teracomputing. In Proceedings of the 9th ECMWF Workshop on the Use of High Performance Computing in Meteorology.* Eds. Walter Zwieflhofer and Norbert Kreitz. World Scientific, 269-276.

Michalakes, J., Dudhia, J., Gill, D., Henderson, T., Klemp, J., Skamarock, W., Wang, W., 2005, The Weather Research and Forecast Model: Software Architecture and Performance. In *Proceedings of the 11th ECMWF Workshop on the Use of High Performance Computing in Meteorology.* Eds. Walter Zwieflhofer and George Mozdzynski. World Scientific, 56 - 168.

Ponce del León, S., Guedes Soares, C., 2008, Sensitivity of wave model predictions to wind fields in the Western Mediterranean Sea. *Coastal Engineering*, Vol. 55, pp. 920-929.

Puertos del Estado, Spain, 2009, – (http://www.puertos.es/oceanografia_y_meteorologia/), private communication.

Queffeulou, P., 2004, Long term validation of wave height measurements from altimeters. Marine Geodesy, Vol. 27, 495-510.

Queffeulou, P., Croizé-Fillon, D., 2010, Global altimeter SWH data set, version 7, Technical Report, Ifremer, ftp://ftp.ifremer.fr/cersat/products/swath/altimeters/waves/documentation/altimeter_wave_merge__7.0.pdf

Queffeulou, P., 2009, Altimeter Wave Height Measurements - Validation of Long Time Series.Poster: Ocean Surface Topography Science Team meeting, Seattle, Washington,USA.(http://www.aviso.oceanobs.com/en/courses/oststt/oststt-2009-seattle/posters/).

Saha, S., Moorthi, S., Pan, H., Wu, X., Wang, J., Nadiga, S., Tripp, P., Kistler, R., Wollen, J., Behringer, D., Liu, H., Stokes, D., Grumbine, R., Gayno, G., Wang, J., Hou, Y., Chuang, H., Juang, H., Sela, J., Iredell, M., Treadon, R., Kleist, D., VanDelst, P., Keyser, D., Derber, J., Ek, M., Meng, J., Wei, H., Yang, R., Lord, S., van den Dool, H., Kumar, A., Wang, W., Long, C., Chelliah, M., Xue, Y., Huang, B., Schemm, J., Ebisuzaki, W., Lin, R., Xie, P., Chen, M., Zhou, S., Higgins, W., Zou, C., Liu, Q., Chen,Y., Han, Y., Cucurull, L., Reynolds, R., Rutledge, G., Goldberg, M., 2010, The NCEP Climate Forecast System Reanalysis. *Bull. Amer. Meteor. Soc.*, Vol. 91, 1015–1057.

Skamarock WC, Klemp JB, 2007, A time-split nonhydrostatic atmospheric model for research and NWP applications. *J. Comp. Phys.* Special issue on environmental modeling.

Sorensen, O.R., Kofoed-Hansen, H., Rugbjerg, M. and Sorensen, L.S., 2004: A Third Generation Spectral Wave Model Using an Unstructured Finite Volume Technique. In Proceedings of the 29th International Conference of Coastal Engineering, 19-24 September 2004, Lisbon, Portugal.

Tolman, H.L., 2002a. Alleviating the garden sprinkler effect in wind wave models. Ocean Modelling, Vol. 4, pp. 269–289.

Tolman, H.L., 2002f, Validation of WAVEWATCH III, version 1.15 for a global domain. Tech. Note 213, NOAA/NWS/NCEP/OMB, 33p.

Tolman, H.L., 2008, http://cioss.coas.oregonstate.edu/CIOSS/workshops/Altimeter_workshop_08/Coastal_Alt_Presentations/18_Tolman_Sig_Wave_Ht.pdf

Sorensen, O.R., Kofoed-Hansen, H., Rugbjerg, M. and Sorensen, L.S., 2004: A Third Generation Spectral Wave Model Using an Unstructured Finite Volume Technique. In Proceedings of the 29th International Conference of Coastal Engineering, 19-24 September 2004, Lisbon, Portugal.

Komen,G.J., Cavaleri,L., Doneland,M., Hasselmann,K., Hasselmann,S. and Janssen,P.A.E.M., (1984). Dynamics and modelling of ocean waves. Cambridge University Press, UK, 560 pp.

Young,I.R., (1999). Wind generated ocean waves, in Elsevier Ocean Engineering Book Series, Volume 2, Eds. R. Bhattacharyya and M.E. McCormick, Elsevier.

WAMDI-group: S. Hasselmann, K. Hasselman, E. Bauer, P.A.E.M. Janssen, G.J. Komen, L. Bertotti, P. Lionello, A. Guillaume, V.C. Cardone, J.A. Greenwood, M. Reistad, L. Zambresky and J.A. Ewing, (1988) “The WAM model – a third generation ocean wave prediction model”, J. Phys. Oceanogr., 18, 1775-1810

General Bathymetric Chart of the Oceans (GEBCO) – www.gebco.net

CM-93 Edition 3.0, CM-93/3 - www.jeppesen.com/marine/commercial/professional/

Ole Baltazar Andersen (1995), Global ocean tides from ERS 1 and TOPEX/POSEIDON altimetry, J. of Geophys. Res., 100, C12, p. 25249-25260

Doodson, A. T., Warburg, H. D., 1941 “Admiralty manual of tides”

Web references

ARPA-FVG OSMER, [Online] http://www.osmer.fvg.it/home.php

ARW Online Tutorial.” [Online] Available at http://www.mmm.ucar.edu/wrf/OnLineTutorial/index.htm

CISL RDA: NCEP Climate Forecast System Re-analysis (CFSR) 6-hourly Products, January 1979 to December 2010.” [Online] Available at http://rda.ucar.edu/datasets/ds093.0/index.html#description

NOAA, Hourly/Sub-Hourly Observational Data.” [Online] Available at http://gis.ncdc.noaa.gov/map/viewer/#app=cdo&cfg=cdo&theme=hourly&layers=1&node=gis

The Weather Research&Forecasting Model Website.” [Online] Available at http://www.wrf-model.org/index.php